

International Conference  
**Advanced Laser Technologies**



**ALT'15**

**The 23<sup>th</sup> Annual International Conference  
on Advanced Laser Technologies  
ALT'15**

Faro, Portugal  
September 7–11, 2015

***BOOK  
of ABSTRACTS***

## Contents

Organizers and Sponsors	page 3
Program and Organizing Committees	page 4
Plenary Talks	page 5
<b>SECTION B.</b> Biophotonics	page 13
<b>SECTION D.</b> Laser Diagnostics and Spectroscopy	page 50
<b>SECTION LM.</b> Laser–Matter Interaction	page 78
<b>SECTION LS.</b> Laser Systems and Materials	page 150
<b>SECTION NL.</b> Nonlinear Optics and Photonics	page 181
<b>SECTION OC.</b> Optical Communication	page 190
<b>SECTION S.</b> Sensors	page 196
<b>SECTION TH.</b> THz Sources and Applications	page 208
Key for Authors	page 225

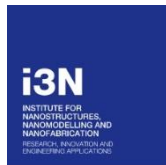
## Organizers and Sponsors



General Physics Institute  
of Russian Academy of Sciences, Russia



Centro de Electrónica, Optoelectrónica e  
Telecomunicações (CEOT), Universidade  
do Algarve, Portugal



I3N - Instituto de Nanoestruturas,  
Nanomodelação e Nanofabricação,  
Universidade de Aveiro, Portugal



IT - Instituto de Telecomunicações,  
Portugal



IST - Instituto Superior Técnico,  
Universidade de Lisboa, Portugal



Center of Laser Technology  
and Material Science, Russia



International Laser Center,  
Lomonosov Moscow State University,  
Russia



Universidade do Algarve, Portugal



National Research Nuclear University  
MEPhI, Russia



Lomonosov Moscow State University,  
Russia



Universidade de Aveiro, Portugal

## **Conference Chairman**

Ivan SHCHERBAKOV, Russia

## **Program Committee Co-Chairs**

Vitaly KONOV, Russia  
Paulo ANDRÉ (Portugal)

## **International Program Committee**

Ekaterina BORISOVA (Bulgaria)	Oleg LOUCHEV (Japan)
Jean-Louis COUTAZ (France)	Yong Feng LU (USA)
Aladar CZITROVSKY (Hungary)	Vladimir MAKAROV (Russia)
Philippe DELAPORTE (France)	Andreas MANDELIS (USA)
Boris DENKER (Russia)	Ion MIHAILESCU (Romania)
Dan DUMITRAS (Romania)	Kyung Hyun PARK (Korea)
Jose FIGUEIREDO (Portugal)	Valentin PETROV (Germany)
Costas FOTAKIS (Greece)	Alexander PRIEZZHEV (Russia)
Thomas GRAF (Germany)	Valerio ROMANO (Switzerland)
Sergey GARNOV (Russia)	Marc SENTIS (France)
Fatih HUSEYINOGLU (Turkey)	Alexander SHKURINOV (Russia)
Lan JIANG (China)	Nikolai SOBOLEV (Portugal)
Pavel KASHKAROV (Russia)	Vadim VEIKO (Russia)
Martin LEAHY (Ireland)	Ioanna ZERGIOTI (Greece)

## **Organizing Committee Co-Chairs**

Vladimir PUSTOVOY (Russia)  
José FIGUEIREDO (Portugal)  
Nikolai SOBOLEV (Portugal)

## **International Organizing Committee**

Carlos FIOLEAIS (Portugal)	José António RODRIGUES (Portugal)
Rui GUERRA (Portugal)	Bruno ROMEIRA (Portugal)
Natalia KHAKAMOVA (Russia)	Sara Martins VIEIRA (Portugal)
Vladimir LUZGIN (Russia)	Tatiana VOLYAK (Russia)

---

---

## **PLENARY TALKS**

---

---

# **Polarization and mode properties of fiber lasers and their applications**

**Byoung Yoon Kim**

*Department of Physics, KAIST  
291 Daehak-ro, Yuseong-gu, Daejeon, Korea*

*yoonkim@kaist.ac.kr*

## **ABSTRACT**

Fiber lasers based on rare-earth doped optical fibers have been actively developed for more than three decades and are currently widely used in many applications. High power fiber lasers for marking and machining applications are of great commercial interest and are replacing traditional technologies in the industry. Besides the high power lasers, other unique characteristics of fiber lasers are being utilized for their applications in optical communications and sensing. One such example is amplified spontaneous emission light sources with broad optical spectra that are deployed in sensors including optical fiber gyroscope and optical coherence tomography. However, many more interesting possibilities of fiber laser applications are still need to be extensively explored. One such application area is optical fiber sensors.

Optical fiber sensors provides high sensitivity, small size, immunity to electromagnetic interference, environmental stability and multiplexing capability. Many different forms of fiber sensors have been developed and deployed. Most of the sensors use external light source to probe physical parameters through passive optical fiber circuits such as interferometers. However, since fiber lasers are built with the same material and structure as the sensing fiber element, the fiber laser cavity itself can be used as the sensing element. In this case, the sensor signal to be monitored would be the laser signal parameters such as changes in optical frequency, polarization, amplitude and phase. This approach can lead to better performance with simpler sensor configuration compared to the more familiar passive fiber sensors. Some simple active fiber laser sensors based on fiber lasers using fiber Bragg grating cavities have been developed demonstrating much superior performance for strain and acoustic sensing. The fundamental advantage of using fiber laser cavities as sensing element comes from the fact that the lasing action provides optical means to convert physical parameter to be measured to the parameters of laser output that could be directly monitored with high accuracy. Understanding the modal and polarization characteristics of fiber lasers under different environmental parameters is important to develop such fiber laser sensors.

In this presentation, some early works on fiber laser sensors will be reviewed along with more recent developments. Focus will be made to stimulate new thoughts for the use of fiber lasers in different application areas other than fiber sensors.

## **REFERENCES**

- [1] G. A. Miller, G. A. Cranch, C. K. Kirkendall, "High performance sensing using fiber lasers", *Optics & Photonics News*, pp. 30-36 (Feb. 2012).
- [2] B. Y. Kim, "Fiber lasers in optical sensors", Chapter 3 in *Optical Fiber Sensor Technology*, Vol. 2, Edited by K. T. V. Grattan and B. T. Meggitt (Chapman and Hall, London) (1998)

## Quantum dots: Genesis, the Excitonic Zoo, and Nano-photonics

Dieter Bimberg

Institute of Solid State Physics and Center of Nanophotonics, Technical University Berlin, Germany  
and King-Abdul-Aziz University, Jeddah, Saudi-Arabia

Universal self-organization and self-ordering effects at surfaces of semiconductors lead to the formation of coherent zero-dimensional clusters called quantum dots (QDs). The electronic and optical properties of QDs, being smaller than the de-Broglie-wavelength in all three directions of space are closer to those of atoms in a dielectric cage than of solids. Their delta-function-like energy eigenstates are only twofold (spin) degenerate. All few particle excitonic states are strongly Coulomb correlated. Their energies depend on shape and size of the dots, such that positive or negative biexciton binding energies or fine-structure splitting caused by exchange interaction appear.

Consequently, single QDs present the most practical possible basis of emitters of single polarized photons (Q-bit emitters) on demand or entangled photons via the biexciton-exciton cascade for future quantum cryptography and communication systems.

Multiple QD layers, as active materials, are extremely promising for novel optoelectronic devices, like edge and surface emitting lasers, amplifiers with properties going far beyond devices based on higher dimensional systems. Semiconductor nanotechnologies transform presently to enabling technologies for new economies. It is expected that first commercialization of nanophotonic devices and systems will appear soon. High bit rate and secure quantum cryptographic systems, nano-flash memories, or ultra-high speed nanophotonic devices for future optical interconnects, the Terabus, and 100 - 160 Gbit/s Ethernet might present some of the first fields of applications of nanophotonic devices.

## What is a Photon?

O. Krokhin

*1-P.N. Lebedev Physical Institute of RAS, Leninsky pr.53, Moscow, 119991, Russia  
2- National research Nuclear University MEPhI (Moscow Engineering Physics Institute),  
Rashirskoe sh.31, Moscow, 115409, Russia*

*krokhin@sci.lebedev.ru*

In the recent years, due to the development of the techniques aimed at generation of optical high-coherent radiation, the question of the photon nature has become a topical problem again, i.e. what is a quant of electromagnetic radiation.

Historically, the photon as a particle with the finite energy was introduced by M. Planck in 1900 in order to explain the radiation spectrum of a “black body” in the high frequency range, where the intensity exponentially decreases with the frequency growth. This circumstance is very important, because it allows one to define at once the energy localization area, and, therefore, the energy material object – the electromagnetic field.

The equation can be considered as the Schrödinger equation. Here arises an important question: what does the symbol  $\psi$  mean? The field or the wave function – probability amplitude? A correct answer implies both quantities, and this is not surprising, since the photon is a purely wave structure.

We have two similar equations: one for the material medium – the field, and the second – for the  $\psi$  function, which determines the motion of the particle – the photon. One should try to find the answer in the wave-particle duality. Where one finds a symbol  $\psi$ , the equation describes the material component, i.e. the particle – photon.

What practical conclusions follow from the above discussion?

The main conclusion is the following: despite of a rather small size of the photon-elementary particle, its wave function determined by the emission process is of rather big length and significantly exceeds the wavelength, and is, actually, defined by the coherence length. This means that all the systems based on photon application (“photonics”) will be very slow.

On the other hand, the systems which use the electrons turn to be much faster. In both cases the reason is the same: the data processing and transfer rate is limited by quantum physics. For the photon, under comparable energy with the electron, it starts earlier, since the photon momentum is significantly smaller than the electron momentum because the electron has a rest mass. From this follows that, according to the uncertainty relation, under similar energies the electron has a higher degree of localization than the photon, the electron is “classical”. The known “Moore's law” describing the progress in the data processing rate in electronics will stop working, when, due to the decrease in the size of electron devices, the electron will become a quantum one. At the same time we see that the Internet, which is based on optical communication lines, is very fast. But Internet is based on a classical light!

In conclusion I would like to thank Dr. A.P. Kanavin for useful discussions and help.

# Advances in Optical Coherence Tomography for Imaging Scattering Tissues

Martin. J. Leahy

<sup>1</sup>Tissue Optics & Microcirculation Imaging Facility, National University of Ireland, Galway, Ireland and National Biophotonics & Imaging Platform, Ireland.

Optical coherence tomography (OCT) has been established as a powerful tool for diagnosis of eye diseases. It has been widely applied to imaging of scattering tissues, but despite several promising studies, especially for intravascular and skin diseases, it is yet to gain formal clinical acceptance in these areas. Gaining more traction for clinical acceptance will require advances in technology, miniaturization, (motion) artefact reduction, cost reduction and clinical trials.

This paper will discuss a number of technologies we have developed which may help advance OCT for imaging scattering tissues. These include correlation mapping optical coherence tomography (cmOCT) to render the 3D microcirculation in scattering tissues and this has been applied to biometrics, skin cancers and brain imaging [1,2]; second order correlation statistics to identify vessel wall microcirculation with intravascular OCT in the presence of severe bulk motion due to the heart[3]; since velocity and the architecture of the coronary vessel are known, we can reduce the number of catheters necessary to perform a diagnosis[4]. In order to further extend the capabilities of OCT to look at the nanostructural changes associated with cancer, we have developed nano-sensitive optical coherence tomography (nsOCT) [5] and multiple reference OCT to reduce the footprint and cost of OCT systems.

## References:

---

1. Enfield, J., Jonathan, E. and Leahy, M.J., 2011. *In vivo* imaging of the microcirculation of the volar forearm using correlation mapping optical coherence tomography (OCT). *Biomedical Optics Express* **2** (5) 1184-1193.
2. Zam, A., Dsouza, R., Subhash, H.M., O'Connell, M., Enfield, J., Larin, K., Leahy, M.J. , 2013. Feasibility of correlation mapping optical coherence tomography (cmOCT) for anti-spoof sub-surface fingerprinting. *J. Biophoton.* **6** (9), 663-667. <http://dx.doi.org/10.1002/jbio.201200231>.
3. Joseph S, Adnan A, Subhash H, Leahy M and Adlam D, 2015, Developing cross-correlation as a method for microvessel imaging using clinical intravascular optical coherence tomography systems *Biomedical Optics Express* **6**, 3, 668 <http://dx.doi.org/10.1364/BOE.6.000668>
4. Zafar, H. Leahy, M.J., and Sharif, F., 2014. Feasibility of Intracoronary Frequency Domain Optical Coherence Tomography Derived Fractional Flow Reserve for the Assessment of Coronary Artery Stenosis. *Int. Heart Journal* **55**: 307-311.
5. Alexandrov, S., Subhash, H.M., Zam, A. and Leahy M.J. 2014, Nano-sensitive optical coherence tomography, *Nanoscale*, **6**, 3545-3549, [DOI: 10.1039/C3NR06132A](https://doi.org/10.1039/C3NR06132A)

# **Laser Processing of Plasmonic Materials and Metamaterial Structures**

**Alberto Piqué<sup>1</sup>, Nicholas A. Charipar<sup>1</sup>, Heungsoo Kim<sup>1</sup>, Eric Breckenfeld<sup>2</sup>, Ray C.Y. Auyeung<sup>1</sup> and Scott Mathews<sup>1</sup>**

*1 - Materials Science and Technology Division, Naval Research Laboratory, Washington DC, USA*

*2 - National Research Council Fellow at the Naval Research Laboratory, Washington, DC 20375, USA*

*Main author email address: pique@nrl.navy.mil*

The use of plasmonic materials and metamaterials structures has been the subject of extensive discussions given their wide range of applications. However, a large fraction of the work available to date has not been able to transition from models to practical demonstrations. One reason for the limited success inserting these structures into working systems and real-world applications is the high level of complexity involved in their fabrication. In particular, non-lithographic, digital-based processes are needed for the fabrication of arbitrary periodic and aperiodic structures found in most metamaterial and plasmonic designs. For these applications, laser-based processes such as pulsed laser deposition or PLD and laser direct-write or LDW offer numerous advantages since they can be applied to virtually any surface over a wide range of scales. PLD allows the deposition of high quality conductive oxides whose lower plasma frequencies make them ideally suited for near IR plasmonic applications. In the case of LDW, this technique allows the precise deposition and/or removal of material in non-lithographic fashion, thus enabling the fabrication of novel metamaterial designs over 2D and 3D surfaces. This presentation will show examples of metamaterial and plasmonic structures developed at the Naval Research Laboratory via laser processing and discuss their benefits for various applications.

This work was sponsored by The Office of Naval Research (ONR) through the Naval Research Laboratory Basic Research Program.

# Ultrafast nonlinear optics in the mid-infrared

Aleksei Zheltikov

*Department of Physics and Astronomy, Texas A&M University  
Physics Department, International Laser Center, M.V. Lomonosov Moscow State University  
Russian Quantum Center, Skolkovo, Moscow Region, Russia*

Recent progress in the generation of high-power ultrashort pulses in the mid-infrared opens new horizons in ultrafast optical science and technologies, revealing unusual phenomena and unexpected properties of materials in the mid-infrared range and promising new, unprecedented opportunities for laser-filamentation-assisted long-range transmission of high-power laser radiation and standoff detection. With the critical power of self-focusing scaling as the laser wavelength squared, a longer-wavelength driver would radically increase the peak power and, hence, the laser energy in a single laser filament in the atmospheric air. The search for such drivers has been ongoing over two decades, during which time the available laser sources limited filamentation experiments in the atmosphere to the near-infrared and visible ranges. In our experiments, filamentation of ultrashort mid-infrared pulses in the atmosphere has been demonstrated for the first time. With the spectrum of a femtosecond laser driver centered at 3.9  $\mu\text{m}$ , right at the edge of the atmospheric transmission window, radiation energies above 20 mJ and peak powers in excess of 200 GW can be transmitted, as our experiments show, through the atmosphere in a single filament. Our studies reveal unique properties of mid-infrared filaments, where the generation of powerful mid-infrared supercontinuum is accompanied by unusual scenarios of optical harmonic generation, giving rise to remarkably broad radiation spectra, stretching from the visible to the mid-infrared. Generation of few- and even single-cycle mid-infrared field waveforms with peak powers ranging from a few megawatts to hundreds of gigawatts has been demonstrated within a broad range of central wavelengths.

A high-energy supercontinuum spanning 4.7 octaves, from 250 to 6500 nm, is generated using a 0.25-TW, 3.9- $\mu\text{m}$  output of a mid-infrared optical parametric chirped-pulse amplifier as a driver inducing a laser filament in the air. The high-frequency wing of the supercontinuum spectrum is enhanced by odd-order optical harmonics of the mid-infrared driver. Optical harmonics up to the 15th order are observed in supercontinuum spectra as overlapping, yet well-resolved peaks broadened, as verified by numerical modeling, due to spatially nonuniform ionization-induced blue shift.

A strongly coupled nonlinear spatiotemporal dynamics of ultrashort mid-infrared pulses undergoing self-focusing simultaneously with soliton self-compression in an anomalously dispersive, highly nonlinear solid semiconductor is shown to enable the generation of multioctave supercontinua with spectra spanning the entire mid-infrared range and compressible to subcycle pulse widths. With 7.9- $\mu\text{m}$ , 150-fs, 2- $\mu\text{J}$ , 1-kHz pulses used as a driver, 1.2-cycle pulses of mid-infrared supercontinuum radiation with a spectrum spanning the range of wavelengths from 3 to 18  $\mu\text{m}$  were generated in a 5-mm GaAs plate. A further compression of these pulses to subcycle pulse widths is possible through a compensation of the residual phase shift.

## **Intense Laser Pulses with a Twist**

**J. T. Mendonça**

*IPFN, Instituto Superior Técnico, Universidade de Lisboa, Av. Rovisco Pais 1, 1049-001 Lisboa, Portugal*

*Author email address: [titomend@tecnico.ulisboa.pt](mailto:titomend@tecnico.ulisboa.pt)*

We give an overview of recent work on the physics of intense laser pulses carrying a finite amount of orbital angular momentum, and their interaction with matter. These twisted laser pulses are vortical electromagnetic waves which can be described in terms of Laguerre-Gauss modes. They have been explored in optics in the last twenty years, but only recently it has been recognized that intense lasers interacting with matter can lead to interesting new phenomena. Intense lasers interacting with matter naturally lead to the formation of a dense plasmas. In plasmas, qualitative changes occur on the properties of twisted waves, because not only electromagnetic waves but also longitudinal oscillations (such as plasmons and phonons) can be excited with orbital angular momentum.

A variety of new effects, associated with Raman and Brillouin stimulated scattering [1], inverse Faraday effect with linearly polarized laser pulses[2], radiation pressure [3], high harmonic generation, photoionization and modified Landau resonances [4] have been considered. Twisted plasmons and laser wake fields can also be excited, leading to toroidal density perturbations where not only electron but also positron acceleration processes take place [5]. Finally, we discuss new perspectives for theoretical and experimental work with twisted laser light in the high intensity regime.

[1] J.T. Mendonça, B. Thidé and H. Then, Phys. Rev. Lett., 102, 185005 (2009).

[2] S. Ali, J. Davies and J.T. Mendonça, Phys. Rev. Lett., 105, 035001 (2010).

[3] J.T. Mendonça and J. Vieira, Phys. Plasmas, 21, 033107 (2014).

[4] J.T. Mendonça, Phys. Plasmas, 19, 112113 (2012).

[5] J. Vieira and J.T. Mendonça, Phys. Rev. Lett., 112, 215001 (2014).

---

---

**SECTION B**

**Biophotonics**

---

---

**COMBINING NONLINEAR LASER SCANNING MICROSCOPY AND  
BAG-OF-FEATURES IMAGE CLASSIFICATION FOR AUTOMATED  
DISEASE DIAGNOSIS**

Stefan G. Stanciu<sup>1</sup>, Denis E. Tranca<sup>1</sup>, George A. Stanciu<sup>1</sup>, Radu Hristu<sup>1</sup> and Juan M. Bueno<sup>2</sup>

<sup>1</sup>*Center for Microscopy-Microanalysis and Information Processing, University Politehnica of Bucharest, Splaiul Independentei 313, sector 6, Bucharest, Romania*

<sup>2</sup>*Laboratorio de Óptica, Universidad de Murcia, Campus Espinardo, 30100 Murcia, Spain*  
*e-mail: stefan.stanciu@cmmip-upb.org*

Nonlinear Laser Scanning Microscopy (NLSM) for Two-Photon Excitation Fluorescence (TPEF) and Second Harmonic Generation (SHG) imaging has been demonstrated in the past couple of decades as a powerful imaging tool for the qualitative and quantitative assessment of various diseases. NLSM techniques provide consistent advantages over Confocal Scanning Laser Microscopy, such as increased imaging penetration depth or reduced photobleaching and phototoxicity. TPEF & SHG microscopies can be used for imaging endogenous signals of tissue structures, thus allowing for various medically relevant aspects to be assessed based on the investigation of non-stained tissue samples. Such approaches contribute to avoiding observer errors, which are related to staining variations, or sample artifacts that may derive from the labeling procedures. Typically, when investigating non-stained tissue samples, SHG is used to image the deposition and architectural changes of collagen, which represent prominent hallmarks for a plethora of pathologies. On the other hand, TPEF is used for imaging the signals generated by endogenous fluorophores, such as NAD(P)H, flavins, keratin or elastin. TPEF data are thus equally important to SHG data in regard to diseases diagnosis, as it provides information connected to various aspects that are clinically relevant, such as cell inflammation and apoptosis or vascular architecture. Currently, the interpretation of NLSM data sets is mainly performed by trained specialists, but numerous recent experiments have demonstrated that the possibilities offered by microscopy imaging can be expanded in a spectacular manner by employing high-end computer vision techniques for support. These latter exploit texture, shape, contour and prior knowledge along with contextual information from digital images in order to replicate in an automated fashion the inspection and analysis capabilities of a trained expert. The Bag-of-Features (BoF) paradigm, inspired from the Bag-of-Words representation used in textual information retrieval, has been introduced to the field of computer vision about a decade ago. Since then, its potential usefulness with respect to image classification and retrieval tasks has been demonstrated in numerous experiments, and BoF approaches became well-established in the field because of their simplicity and performance. The potential of BoF methods for biomedical classification problems has been demonstrated so far in several experiments, but the methods reported to date rely mainly on spatial intensity information such as image gradients. Besides spatial intensity information, NLSM data sets many times embed additional information that could be exploited in sophisticated BoF scenarios, such as spectral or polarization related information. In this contribution we present our recent progresses on using BoF strategies for the automated classification of NLSM data, and discuss future strategies that we plan on developing, which simultaneously exploit multiple NLSM information categories for reliable automated disease diagnosis.

**Acknowledgments:** The presented work was partially supported by the UEFISCDI PN-II-PT-PCCA-2011-3.2-1162 Research Grant. The corresponding author, thanks the financial support of the SOP HRD, financed from the European Social Fund and the Romanian Government under the contract number POSDRU/159/1.5/S/137390/.

# **Intensified laser diagnostics and therapy at tissue optical clearing**

*Valery Tuchin*

*Research-Educational Institute of Optics and Biophotonics, National Saratov State University,  
Saratov, 410012, Russia*

*Institute of Precise Mechanics and Control of Russian Academy of Sciences, Saratov, 410028,  
Russia*

## **Abstract**

Fundamentals and advances of tissue optical clearing (TOC) in application to laser imaging, spectroscopy and treatment of tissues and organs are presented. One of the TOC technologies is based on controlling of tissue optical properties by using immersion technique via application of exogenous optical clearing agents (OCAs), another one is based on mechanical tissue compression or stretching. Impact of OCA and water transport in a tissue, caused by an action of a hyperosmotic OCA or by mechanical compression and leading to tissue reversible shrinkage and dehydration on temporal tissue optical properties, is discussed. The specific features of TOC for fibrous and cell-structured tissues are investigated using different linear and nonlinear laser probing and treatment modalities working in the visible, NIR and terahertz ranges. *In vitro*, *ex vivo*, and *in vivo* studies of a variety of human and animal tissues, including skin, fat, eye sclera, muscle, cerebral membrane, digestive tract tissue, cartilage, tendon, bone, blood vessels, and blood are presented. The technologies of delivery of OCAs are also under discussion, including hidden free diffusion, enforced tissue permeability, including laser heating and shock wave generation. Impact of different OCAs on tissue structure, free/bound water balance and microcirculation are analyzed. Experimental results on diffusivity of glucose and other biocompatible OCAs in normal and modified by cancer and diabetes tissues are presented.

**LASER-BASED TECHNOLOGIES IN AESTHETIC MEDICINE**

O. Panova<sup>1</sup>, E. Sanches<sup>1</sup>, N. Bulgakova<sup>2</sup>, S. Daue<sup>3</sup>, V. Ashmarov<sup>3</sup>, A. Batomonkuev<sup>3</sup>,  
S. Gamayunov<sup>4,5</sup>, M. Kirillin<sup>6</sup> and N. Shakhova<sup>5,6</sup>

<sup>1</sup> *Central Clinical Hospital RAS, 117593, Litovskiy boulevard, 1A, Moscow, Russia*

<sup>2</sup> *Prokhorov General Physics Institute RAS 119991, Vavilov Str., 38, Moscow, Russia*

<sup>3</sup> *Revixan Ltd 105082, Bakuninskaya St.69/1, Moscow, Russia*

<sup>4</sup> *Oncologic Clinic, 603126, Rodionov St., 190, Nizhny Novgorod, Russia*

<sup>5</sup> *State Medical Academy, 603000, Minin Sq.10/1, Nizhny Novgorod, Russia*

<sup>6</sup> *Institute of Applied Physics RAS, 603950, Uljanov St. 46, Nizhny Novgorod, Russia*  
*shakh@ufp.appl.sci-nnov.ru*

Medical aesthetic technology has advanced rapidly over the last two decades. Today there are few types of laser-based technologies used in wide range of medaesthetic treatments available [1]. Ablative resurfacing using lasers was long considered the gold standard for skin rejuvenation [2]. But it is associated with significant risk of side effects and a prolonged postoperative recovery period [3]. This required the development of new technologies, including PDT [4,5]. It was shown that photodynamic therapy (PDT) resulted in histological changes indicating restoration of aged skin [4]. This effect is due to molecular changes in the dermal matrix following PDT [5].

The aim of study is to demonstrate a new method of PDT for skin rejuvenation and to show the possibility of non-invasive monitoring of skin morphological changes in real time.

The new topical photosensitizer Revixan-derma was used. Laser irradiation was done at the wavelength of 660 nm. The measurements of skin biophysical parameters were performed before and after the treatment using corneometer and dermoscope. Real-time monitoring of internal skin structure was performed using cross-polarization OCT (CP-OCT) device.

As a result efficacy of the PDT was demonstrated, all methods showed improvement in skin properties. CP-OCT showed the ability to detect changes in characteristics of collagen.

These data suggest that new method of PDT could be effective for photorejuvenation. OCT allows to control results of procedure.

**Acknowledgements**

The authors thank the Ministry of Education and Science of Russian Federation (project 14.B25.31.0015) and Revixan Ltd. for the financial support of this work.

**References**

1. Michael H. Gold. Update on Fractional Laser Technology. *Clin Aesthet Dermatol.* V. 3(1), pp.42–50, (2010)
2. Tierney EP, Kouba DJ, Hanke CW. Review of fractional photothermolysis: treatment indications and efficacy. *Dermatol Surg.* V. 35(10), pp.1445–1461, (2009)
3. Shah S, Alam M. Laser resurfacing pearls. *Semin Plast Surg.* V. 26(3), pp.131-6, (2012)
4. Park MY, Sohn S, Lee ES, Kim YC. Photorejuvenation induced by 5-aminolevulinic acid photodynamic therapy in patients with actinic keratosis: a histologic analysis. *J Am Acad Dermatol.* V.62(1), pp. 85-95, (2010)
5. Choi JY1, Park GT, Na EY, Wi HS, Lee SC, Lee JB. Molecular changes following topical photodynamic therapy using methyl aminolaevulinate in mouse skin. *J Dermatol Sci.* 2010 Jun;58(3):198-203

## **Synchronous Fluorescence Spectroscopy of Human Neoplasia – Advanced Tool for Endogenous Fluorophores Evaluation and Cancer Detection**

**E. Borisova<sup>1</sup>, Al. Zhelyazkova<sup>1</sup>, Ts. Genova<sup>1</sup>, N. Penkov<sup>2</sup>, P. Troyanova<sup>2</sup>,  
B. Vladimirov<sup>2</sup>, L. Avramov<sup>1</sup>**

*1- Biophotonics lab., Institute of Electronics, Bulgarian Academy of Sciences,  
72, Tsarigradsko chaussee Blvd., 1784 Sofia, Bulgaria*

*2- University Hospital "Tsaritsa Yoanna – ISUL", 8, Byalo more str., Sofia, Bulgaria  
borisova@ie.bas.bg*

Biological tissues consist of different chromophores – fluorophores and absorbers that determine the optical spectral properties of each type of tissue or its health condition. Steady-state fluorescence spectroscopy is a powerful tool for investigation of complex and multicomponent fluorescent samples, including human tissues. It is one of the most prominent and widely – used tool for investigation of the spectral properties, as well as a tool for differentiation of the pathologies based on spectral discrimination. Autofluorescence, when only the signal from endogenous fluorophores would be detected is a totally non-invasive and real-time techniques that could found clinical application for initial diagnosis and monitoring of the therapy of human neoplasia.

However, the disadvantages related to application of autofluorescence spectroscopy into clinical practice are related to the low level of the detected signals, which require special technical solutions, and the complexity of the signal detected, which require difficult algorithms for the received data analysis. The last one is related to the overlapped spectra of excitation and of emission for different endogenous fluorophores, which all could have diagnostic meaning. Synchronous fluorescence spectroscopy (SFS), which is a specific modality of a steady-state fluorescence technique, could be used to solve this problem.

Analysis of the fluorescence through the SFS method is performed by maintaining constant wavelength interval between excitation wavelength and emission wavelength through the spectrum. This allows optimal excitation of the emission maxima, which result in narrower emission peaks. That is the main reason for the greater sensitivity of SFS in comparison with standard fluorescence detection [1]. Narrower peaks in the obtained fluorescence spectra allows decrease the extent of spectral overlaps and this effect is useful in investigating multi-component samples which consist mixture of fluorescence compounds, like biological tissues. [2]

Recent study presents SFS results *ex vivo* over pairs of healthy and cancerous tissues from skin and gastrointestinal tissues (GIT). The procedure of obtaining the investigated samples includes their excision during surgery for removal of neoplasia lesions. After the surgical removal biological samples are transported in isothermal conditions and safe-keeping solution from the hospital to the spectral laboratory, where their SFS is investigated. All patients received and signed written informed consent and this research is approved by Ethics committee of University Hospital "Tsaritsa Yoanna", Sofia.

SFS measurements were performed with excitation wavelength in the spectral range of 280-440 nm with increment of 10 nm and wavelength interval (offset) in the range of 10-200 nm with increment of 10 nm. Improved spectral resolution of the emission was obtained and better differentiation of the endogenous fluorophores and their alterations in the process of tumour development were observed. Optimal SFS signals of discrimination between normal and cancerous tissues would be also discussed.

**Acknowledgements:** This work is supported in part by the National Science Fund of Bulgarian Ministry of Education and Science under grant #DFNI-B02/9/2014 "Development of biophotonics methods as a basis of oncology theranostics", COST Action BM1205 "European Network for Skin Cancer Detection Using Laser Imaging" and in part under personal fellowship of E. Borisova from Foundation UNESCO/L'Oreal "Women in Science", Bulgaria - 2014.

[1] L. Liu, Y. Nie, L. Lin, W. Li, Z. Huang, S. Xie, B. Li, "Pattern recognition of multiple excitation autofluorescence spectra for colon tissue classification.", *Photodiagn Photodyn* 10(2), 111-119 (2012).

[2] A. Frank, E. Wehry, „Handbook of Instrumental Techniques for Analytical Chemistry.“, Prentice Hall PTR (ECS Professional), Molecular Fluorescence and Phosphorescence Spectrometry (1997).

## Transcutaneous drug delivery with laser ablation

**E.A. Genina<sup>1,2,3</sup>, A.N. Bashkatov<sup>1,2,3</sup>, L.E. Dolotov<sup>1</sup>, I.Yu. Yanina<sup>1,2</sup>, E.A. Kolesnikova<sup>1</sup>, G.S. Terentyuk<sup>1,2</sup>, Yu.I. Svenskaya<sup>2</sup>, D.A. Gorin<sup>2</sup>, G.B. Sukhorukov<sup>2,4</sup>, V.V. Tuchin<sup>1,2,4,5</sup>**

<sup>1</sup>Research-Educational Institute of Optics and Biophotonics, Saratov State University, Saratov, Russia

<sup>2</sup>Remote Controlled Theranostic System Lab, Saratov State University, Saratov, Russia

<sup>3</sup>Interdisciplinary Laboratory of Biophotonics, Tomsk State University, Tomsk, Russia

<sup>4</sup>The Queen Mary University of London, London, UK

<sup>5</sup>Institute of Precise Mechanics and Control of RAS, Saratov, Russia

*e-mail of corresponding author: [eagenina@yandex.ru](mailto:eagenina@yandex.ru)*

Fractional laser microablation (FLMA) is one of the relatively safe and effective methods of drug delivery into the skin at sufficiently large depth. Fractional devices create thermally induced microchannels of damage in the skin. The variation in laser radiation parameters allows for control the depth of the microchannels [1, 2].

In this study we are presenting the results of transcutaneous delivery of optical clearing agent (OCA) and microparticles. The experiments were carried out with rat skin *in vivo*. Polyethylene glycol with molecular weight 300 dalton and refractive index 1.457 (930 nm) was used as OCA. The suspension of CaCO<sub>3</sub> particles with average size 2 μm in water with concentration 0.5 g/mL was used. FLMA of skin was provided by a system based on a pulsed Er:YAG laser (Palomar Medical Technologies Inc., Burlington, MA). The laser emission beam (2940 nm) was split into micro-beams using an array of micro-lenslets. Three laser modes with the following parameters were used: mode I with pulse energy 3.0 J and pulse duration 15 ms; mode II with pulse energy 1.0 J and pulse duration 5 ms; and mode III with pulse energy 0.8 J and pulse duration 5 ms. In both I and II modes 64 vertical micro-channels on the area 8×8 mm<sup>2</sup> were created; and in III mode skin upper layer on the area 6×6 mm<sup>2</sup> was ablated. The skin after FLMA with I mode was used for the particles delivery. The skin after FLMA with II mode and surface ablation (III mode) was used for the OCA delivery. Delivery of the particles and OCA was monitored with optical coherence tomography (OCT) (~930 nm). Figure 1 shows result of rat skin ablation with different modes.

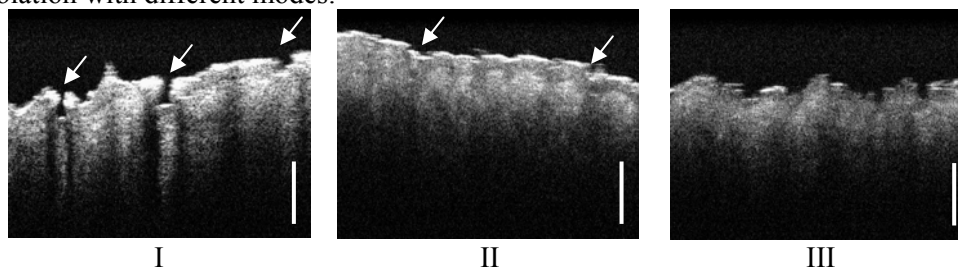


Figure 1. OCT images of the rat skin areas *in vivo* after fractional laser micro-ablation with different modes: I - pulse energy 3.0 J and pulse duration 15 ms; II - pulse energy 1.0 J and pulse duration 5 ms (micro-channels are marked with arrows); III - pulse energy 0.8 J and pulse duration 5 ms (ablation of the skin surface). Bars correspond to 300 μm.

Optical depth of the particle visualization inside skin has fallen within the range 150-250 μm. Optical probing depth during 60 min has increased from 180±10 μm for intact skin to 350±10 μm for skin after the complex action of FLMA (II mode) and OCA, and to 240±10 μm for skin after FLMA (III mode) and OCA. For skin after OCA alone the optical probing depth during the same period has increased only up to 205±10 μm. Results of the study have shown that the FLMA increases the depth of drug delivery in skin significantly.

The work was supported by Russian Federation Governmental No. 11.G.34.31.0030 designed to support scientific research projects implemented under the supervision of leading scientists at Russian institutions of higher education and the Tomsk State University Academic D.I. Mendeleev Fund Program.

[1] B.D. Zelickson, S.E. Walgrave, M.Y.H. Al-Arashi, G.B. Altshuler, I.V. Yaroslavsky, J.J. Childs, R.H. Cohen, A.V. Erofeev, E.F. Depina, M.Z. Smirnov, D.A. Kist, D.R. Tabatadze, *Lasers Surg. Med.*, vol. 41, pp. 634-642, (2009).

[2] E.A. Genina, A.N. Bashkatov, L.E. Dolotov, G.N. Maslyakova, V.I. Kochubey, I.V. Yaroslavsky, G.B. Altshuler, V.V. Tuchin, *J. Biomed. Opt.*, vol. 18, pp. 111406-1 - 111406-9, (2013).

# Optical Coherence Elastography of the Eye

K.V. Larin

University of Houston, Houston, TX 77204, USA

[klarin@uh.edu](mailto:klarin@uh.edu)

In this talk I will discuss the capability of a novel combined focused ultrasound/air-puff and phase-sensitive optical coherence elastography (OCE)

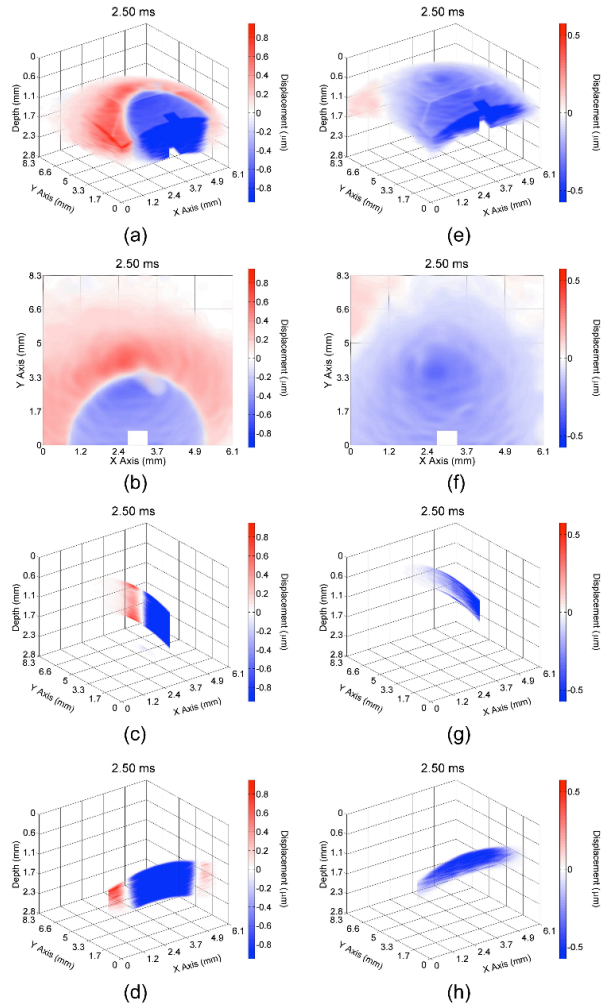


**Fig 1:** Propagation of the elastic wave in the porcine cornea (a-d) before and (e-h) after CXL treatment. Multiple views are shown, corresponding to (a,e) 3D, (b,f) en-face, (c,g) single longitudinal plane aligned with the excitation, and (d,h) single transverse plane near the excitation.

and quantification of cornea and lens biomechanical properties in 2D (lens) and in 3D (cornea) and as a function of age or therapy (e.g. CLX procedures).

system to assess biomechanical properties of ocular tissues (such as cornea and the lens) *in situ* and *in vivo* in 3D. Low-amplitude elastic deformations in mice and rabbit ocular tissues were measured by the OCE system consisting of a spectral-domain optical coherence tomography (OCT) combined with focused ultrasound (lens excitation) and air-puff (cornea excitation) systems used to produce a transient force on the tissue surface. The amplitude, temporal profile, and the speed of the deformations were used to reconstruct tissue biomechanical properties using novel analytical models. Gold standard uniaxial compressional tests were used to validate the OCE data.

The OCE measurements in rabbit lens showed that the amplitude and the relaxation rate of the displacements (and, thus, Young's modulus and shear viscosity) of the young lenses were significantly larger than those of the mature lenses, indicating a gradual increase of the lens stiffness with age (2.5 kPa and 7.4 kPa, respectively). 3D visualization of the elastic wave propagating in rabbit corneas shows the obvious velocity difference in normal ( $1.3 \pm 0.1$  m/s) and CLX ( $3.5 \pm 0.1$  m/s) corneas (Figure 1). Then, the frequency analysis allowed depth-resolved analysis of cornea biomechanical properties clearly demonstrating the biomechanical differences of the corneal layers. Finally, the stress-strain measurements using uniaxial mechanical tests confirmed the results obtained by the OCE system.

These results demonstrate that the OCE system can be used for noninvasive analysis

# **Laser Modification of Eye Sclera Structure as a Novel Approach for Normalization of Intraocular Pressure**

**E. Sobol<sup>1</sup>, O. Baum<sup>1</sup>, A. Bolshunov<sup>2</sup>, O. Chomchik<sup>2</sup>**

*1-Institute on laser and information technologies, Russian Academy of Sciences, Troitsk, Russia,*

*2- Institute on eye diseases, Russian academy of medical sciences, Moscow, Russia*

*esobol@rambler.ru*

Intraocular pressure (IOP) is non-uniqueness, but a key characteristic in glaucoma diagnostics and its normalization is a main target for therapeutic or surgical treatments. Although a number of pharmacologic and surgical techniques to decrease IOP are employed in clinical practice, none resolve the disease completely and permanently. In mammalian eyes, two aqueous outflow pathways are recognized. In the conventional pathway, aqueous flows from the anterior chamber into the trabecular meshwork, through Schlemm's canal. In the unconventional pathway, aqueous flows from the anterior chamber into scleral pores and out of the eye through episcleral structures. The uveoscleral transport pathway contributes to aqueous outflow and accounts for up to fifty percent of aqueous outflow in the eyes of youth and diminishes with increasing age to a value of about three percent.

We develop a novel and innovative technique for IOP normalization which is based on enhancing role of sclera outflow. The technique creates permeable pathways for water transport as a result of formation of nano- and micro-pores under nondestructive thermo-mechanical effect of pulsed laser irradiation [1]. The results of in –vivo experiments in rabbit eye sclera have shown that laser irradiation leads to substantial increase of water permeability trough sclera. Histological investigations of tissue structure of the pig eyes were performed using optical microscope and before and after laser treatment. Histological and Atomic Force Microscopy examinations have clearly recognized laser-assisted stable structural alterations: rarefication of the collagen structure in the laser affected zone and formation of sub-micron pores. Mechanism of stabilization of pore system arisen as a result of laser irradiation is due to formation of small stable gas bubbles in the sclera tissue.

Dynamics of laser-induced structural alterations in the sclera was studied using light scattering technique. When irradiating the sclera for improving its hydraulic permeability, the optical characteristics of the tissue showed definite changes that can be used as a basis of control system for novel laser medical technology of glaucoma treatment [2]. Pre-clinical trials performed for 49 patients with open angle glaucoma have demonstrated stable normalization of the IOP with one year follow-up observations [3]. The advantages and prospects of the novel approach for glaucoma treatment have been demonstrated.

[1] O. Baum, E. Sobol, A. Bolshunov, A. Fedorov, A. Omelchenko, O. Chomchik, E. Shcherbakov, Microstructural changes in sclera under thermo-mechanical effect of 1.56  $\mu\text{m}$  laser radiation increasing transscleral humour outflow, *Lasers in Surgery & Medicine*, vol.46, pp. 46–53, (2014).

[2] A. Yuzhakov, A. Sviridov, O. Baum, E. Shcherbakov, E. Sobol, Optical characteristics of the cornea and sclera and their alterations under the effect of nondestructive 1.56  $\mu\text{m}$  laser radiation, *Journal of Biomedical Optics*, vol.18, pp. 1-6, (2013).

[3] S. Avetisov, A. Bolshunov, O. Chomchik, A. Fedorov, V. Siplivj, O. Baum, A. Omelchenko, E. Shcherbakov, V. Panchenko, E. Sobol, Laser-induced increase of sclera hydro-permeability in treating resistant forms of open-angle glaucoma, *Glaucoma*, vol.14, 3, (2015).

# **New perspectives with light-responsive nano-gold and graphene in therapy and sensing**

**Roberto Pini<sup>1</sup>, Paolo Matteini<sup>1</sup>, Fulvio Ratto<sup>1</sup>, Francesca Rossi<sup>1</sup>, Marella de Angelis<sup>1</sup>,  
Martina Banchelli<sup>1</sup>, Lucia Cavigli<sup>1</sup>, Sonia Centi<sup>1</sup>, Francesca Tatini<sup>1</sup>**

<sup>1</sup>*Institute of Applied Physics “Nello Carrara”, National Research Council,  
via Madonna del Piano 10, 50019 Sesto Fiorentino (Italy)*

*r.pini@ifac.cnr.it*

Nanophotonics solutions are providing new answers to topical biomedical challenges. A relevant example is the use of laser-activated plasmonic nanoparticles and graphene for generating heat or for enhancing the local electric field. These processes are being exploited for a variety of biomedical applications including cancer therapy, tissue repair, drug delivery and biosensing. Here we will present into more details some light-activated materials, which we have recently developed and proposed as viable solutions to critical issues in therapy and sensing applications.

A first example is the development of an implantable device for on demand chemical release in the form of a light-activated sponge-like scaffold. The photothermal response of the nanoparticles contained inside the sponge triggers a contraction in proximal drug-loaded thermosensitive micelles, thus promoting the expulsion of the drug from the sponge [1,2]. An advanced version of this devices consists in a dispersion of graphene nanosheets in a biopolymer matrix, which is activated by millisecond-long light pulses for confined and precisely dosed drug release [3].

The potential of organized bidimensional assemblies of gold and silver nanocubes decorated with a graphene film was instead exploited for the direct Surface Enhanced Raman Scattering (SERS) analysis of proteins and biomarkers [4]. We will finally introduce a SERS sensor we engineered for the rapid and reproducible quali-quantitative detection of toxic amyloid oligomers associated with neurodegenerative diseases.

[1] Paolo Matteini, Maria Raffaella Martina, Giuliano Giambastiani, Francesca Tatini, Roberta Cascella, Fulvio Ratto, Cristina Cecchi, Gabriella Caminati, Luigi Dei and Roberto Pini. Light-responsive nanocomposite sponges for on demand chemical release with high spatial and dosage control. *J Mater Chem B* 1, 1096-1100 (2013)

[2] Paolo Matteini, Francesca Tatini, Lapo Luconi, Fulvio Ratto, Francesca Rossi, Giuliano Giambastiani, Roberto Pini. Photothermally Activated Hybrid Films for Quantitative Confined Release of Chemical Species. *Angew Chem Int Edit* 52 (23) 5956–5960 (2013)

[3] Paolo Matteini, Francesca Tatini, Lucia Cavigli, Stefania Ottaviano, Giacomo Ghini and Roberto Pini. Graphene as photothermal switch for controlled drug release. *Nanoscale* 6(14), 7947-7953 (2014)

[4] Paolo Matteini, Marella de Angelis, Lorenzo Ulivi, Sonia Centi, Roberto Pini. Concave gold nanocubes assemblies as nanotraps for surface-enhanced Raman scattering-based detection of proteins. *Nanoscale* 8, 3374-3380 (2015)

## Parametric extensions of optical coherence tomography can improve contrast in highly scattering tissues

D. D. Sampson<sup>1,2</sup>, L. Chin<sup>1</sup>, P. Gong<sup>1</sup>, P. Wijesinghe<sup>1</sup>, S. Es'haghian<sup>1</sup>,  
W. M. Allen<sup>1</sup>, B. R. Klyen<sup>1</sup>, B. F. Kennedy<sup>1</sup>, R. A. McLaughlin<sup>1</sup>

1- Optical+Biomedical Engineering Laboratory, School of Electrical, Electronic & Computer Engineering,  
The University of Western Australia

2- Centre for Microscopy, Characterisation & Analysis,  
The University of Western Australia

Email: David.Sampson@uwa.edu.au

Parametric optical coherence tomography<sup>1</sup> (OCT) is a promising approach to extracting additional information from three-dimensional OCT scans of tissue, beyond simple imaging by the measurement of backscatter. The parametric approach uses models parameterised with the property, or properties, of interest, and signal processing to fit these models to the acquired data. Such properties are generally optical, for example, axial attenuation (extinction)<sup>2-4</sup> or birefringence,<sup>5-7</sup> but may not necessarily be. We have been exploring mechanical contrast,<sup>8</sup> for example, performing parametric imaging based on mechanical properties:<sup>9</sup> either strain<sup>10</sup> or elasticity.

In all cases we have explored to date, the parameter of interest is determined in the axial direction only and, in order to do so, some sacrifice is made in axial resolution, that is, compared to the native OCT axial resolution (although this loss of resolution is not intrinsic to the concept). The natural mode of display of such images is in the *en face* dimension, as maps of the parameter.

Figure 1 shows an example of a parameter map of birefringence of mouse muscle afflicted with muscular dystrophy. Our work is demonstrating enhanced contrast between different soft tissue constituents in tissues across applications in muscular dystrophy, burn scars to breast cancer.

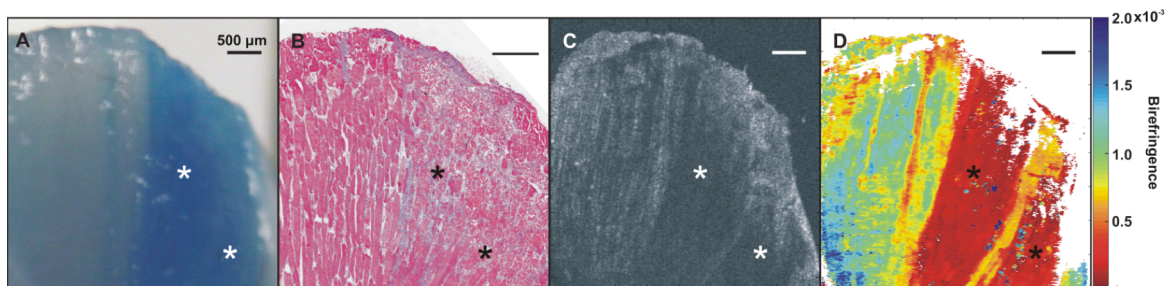


Figure 1: Example of parametric OCT of muscle birefringence. (a) Photo, damaged region dyed blue; (b) Histology; (c) En face OCT, and (d) parametric map of birefringence showing enhanced contrast between normal and damaged tissue. [6]

- [1] R. A. McLaughlin, L. Scolaro, P. Robbins, C. Saunders, S. L. Jacques, and D. D. Sampson, "Parametric imaging of cancer with optical coherence tomography," *Journal of Biomedical Optics*, vol. 15, no. 4, art. 046029, 2010.
- [2] L. Scolaro, R. A. McLaughlin, B. R. Klyen, B. A. Wood, P. D. Robbins, C. M. Saunders, S. L. Jacques, and D. D. Sampson, "Parametric imaging of the local attenuation coefficient in human axillary lymph nodes assessed using optical coherence tomography," *Biomedical Optics Express*, vol. 3, no. 2, pp. 366-379, 2012.
- [3] P. J. Gong, R. A. McLaughlin, Y. M. Liew, P. R. T. Munro, F. M. Wood, and D. D. Sampson, "Assessment of human burn scars with optical coherence tomography by imaging the attenuation coefficient of tissue after vascular masking," *Journal of Biomedical Optics*, vol. 19, no. 2, art. 021111, 2014.
- [4] B. R. Klyen, L. Scolaro, T. Shavlakadze, M. D. Grounds, and D. D. Sampson, "Optical coherence tomography can assess skeletal muscle tissue from mouse models of muscular dystrophy by parametric imaging of the attenuation coefficient," *Biomedical Optics Express*, vol. 5, no. 4, pp. 1217-1232, 2014.
- [5] L. X. Chin, X. J. Yang, R. A. McLaughlin, P. B. Noble, and D. D. Sampson, "En face parametric imaging of tissue birefringence using polarization-sensitive optical coherence tomography," *Journal of Biomedical Optics*, vol. 18, no. 6, 2013.
- [6] X. J. Yang, L. X. Chin, B. R. Klyen, T. Shavlakadze, R. A. McLaughlin, M. D. Grounds, and D. D. Sampson, "Quantitative assessment of muscle damage in the mdx mouse model of Duchenne muscular dystrophy using polarization-sensitive optical coherence tomography," *Journal of Applied Physiology*, vol. 115, no. 9, pp. 1393-1401, 2013.
- [7] P. Gong, L. X. Chin, S. Es'haghian, Y. M. Liew, F. M. Wood, D. D. Sampson, and R. A. McLaughlin, "Imaging of skin birefringence for human scar assessment using polarization-sensitive optical coherence tomography aided by vascular masking," *Journal of Biomedical Optics*, vol. 19, no. 12, p. 126014, 2014.
- [8] B. F. Kennedy, K. M. Kennedy, and D. D. Sampson, "Optical coherence elastography," *Optics & Photonics News*, pp. 32-39, April 2015.
- [9] B. F. Kennedy, K. M. Kennedy, and D. D. Sampson, "A review of optical coherence elastography: Fundamentals, techniques and prospects," *IEEE Journal of Selected Topics in Quantum Electronics*, vol. 20, no. 2, p. 7101217, 2014.
- [10] B. F. Kennedy, R. A. McLaughlin, K. M. Kennedy, L. X. Chin, A. Curatolo, A. Tien, B. Latham, C. M. Saunders, and D. D. Sampson, "Optical coherence micro-elastography: mechanical-contrast imaging of tissue microstructure," *Biomedical Optics Express*, vol. 5, no. 7, pp. 2113-2124, 2014.

## **Modular 3D Microscopy for Biomedicine**

**Herbert Schneckenburger, Sarah Schickinger, Verena Richter, Petra Weber, Michael Wagner,  
Thomas Bruns**

*Aalen University, Institute of Applied Research, Beethovenstr. 1, 73430 Aalen, Germany*

*corresponding author: [herbert.schneckenburger@htw-aalen.de](mailto:herbert.schneckenburger@htw-aalen.de)*

Various modules for 3D imaging, which can be adapted to an upright or an inverted microscope, are commercially available. These modules include laser scanning heads, structured illumination devices or special units for illumination under total internal reflection (TIR) using high aperture microscope objective lenses.

Further modules, as presently reported, represent individual solutions for

- TIR fluorescence microscopy with a special microscope condenser for variable-angle illumination, as required for measurements of cell surface topology, e.g. in tumour cell recognition [1];
- Light sheet fluorescence microscopy with a miniaturized add-on unit to excite selective planes of a 3D sample with a minimum of light exposure and phototoxic cell damage. The positions of the light sheet and the detection lens have, therefore, been synchronized [2];
- Axial rotation of individual samples located in micro-capillaries, so that they can be observed from different sides [3]. This appears most essential for larger and strongly scattering samples, e.g. 3D cell cultures or small organisms;
- Devices for illumination and detection under variable angles in light scattering experiments to distinguish between samples of different morphology [4];
- Adaptation of a micro-fluidic system in order to apply small amounts of fluorescent dyes, drugs or pharmacological agents [2].

This modular concept permits almost simultaneous use of all these techniques as well as combination with spectral imaging, fluorescence lifetime imaging (FLIM), Förster resonance energy transfer (FRET) [5] or nanosecond ratio imaging [6]. For example, apoptosis is detected by FRET experiments of a specific sensor expressed in 3D cell cultures upon light sheet illumination (biochemical response), as well as by light scattering experiments with high angular resolution (morphological response).

Projects are funded by Land Baden-Württemberg, European Union (Europäischer Fonds für die regionale Entwicklung), Bundesministerium für Wirtschaft und Energie (BMW, ZIM project) and financed by Baden-Württemberg-Stiftung gGmbH.

- [1] M. Wagner, P. Weber, H. Baumann, H. Schneckenburger: Nanotopology of cell adhesion upon variable-angle total internal reflection fluorescence microscopy (VA-TIRFM), *J. Vis. Exp.* 68 (2012) e4133.
- [2] T. Bruns, S. Schickinger, H. Schneckenburger: Single plane illumination module and micro-capillary approach for a wide-field microscope, *J. Vis. Exp.* 90 (2014) e51993.
- [3] T. Bruns, S. Schickinger, H. Schneckenburger: Sample holder for axial rotation of specimens in 3D Microscopy, *J. Microsc.* (2015); doi: 10.1111/jmi.12263.
- [4] V. Richter, F. Voit, A. Kienle, H. Schneckenburger: Light scattering microscopy with angular resolution and its possible application to apoptosis, *J. Microsc.* 257 (1) (2015) 1–7;
- [5] P. Weber, S. Schickinger, M. Wagner, B. Angres, T. Bruns, H. Schneckenburger: Monitoring of apoptosis in 3d cell cultures by FRET and light sheet fluorescence microscopy, *Int. J. Mol. Sci.* 16(3) (2015) 5375–5385.
- [6] S. Schickinger, T. Bruns, R. Wittig, P. Weber, M. Wagner, H. Schneckenburger: Nanosecond ratio imaging of redox states in tumour cell spheroids using light sheet based fluorescence microscopy, *J. Biomed. Opt.* 18(12) (2013) 126007.

# **Holographic beam shaping in light sheet microscopy**

**T. Vettenburg<sup>1,2</sup> and K. Dholakia<sup>1</sup>**

*1- School of Physics and Astronomy, University of St Andrews, St Andrews, UK.*

*2 - Dept. of Bioeng. and Aerospace Eng., University Charles 3<sup>th</sup> of Madrid, Leganés (Madrid), Spain.*

*kd1@st-andrews.ac.uk*

Light sheet microscopy is quickly establishing itself as a fundamental tool for many biologists. By illuminating one plane at time, a light sheet microscope captures high contrast images of large samples whilst keeping photo-bleaching and damage to a minimum. High frame rates can be achieved since a single one-dimensional scan of the sample records a three-dimensional volume. Although it is possible to focus the light-sheet to sub-micron widths, the field-of-view with optimal resolution is limited because diffraction restricts the propagation distance over which the light sheet illumination is confined to sub-cellular features. Furthermore, sample-induced aberrations often prevent diffraction limited resolution. Recently it was demonstrated that the field-of-view of a light sheet microscope can be extended by employing the propagation invariant Bessel beam to form the planar illumination. While this is deemed an excellent solution for multi-photon fluorescence excitation, linear fluorescence excitation is often preferred due to the lower irradiation levels associated and the practicality of multi-colour imaging. Unfortunately, the large transversal structure of the Bessel beam leads to a reduction in contrast and unnecessarily increases the sample irradiance. Even if contrast can be reclaimed by deviating from the single one-dimensional scan principle and by incorporating concepts from confocal scanning or structured illumination, the excess irradiation by the outer structure of the Bessel beam is unavoidable. We employed holographic beam shaping to penetrate deeper into the sample [1], and image a 10-fold larger area in a single scan [2]. Furthermore, we demonstrate that most useful wavefront modulations can be achieved using off-the-shelf components [3]. A single Airy light sheet scan, without further modification of existing instrumentation, uses the fluorescence of the entire transversal structure to yield high contrast over an extended field-of-view. Here we explore the potential of beam shaping in light sheet microscopy to enhance contrast, resolution, and optical manipulation abilities.

[1] Dalgarno et al., "Wavefront corrected light sheet microscopy in turbid media," *Applied Physics Letters* 100(19), pp. 191108 (2012).

[2] Vettenburg et al., "Light-sheet microscopy using an Airy beam," *Nature Methods* 11, pp. 541–544 (2014).

[3] Yang et al., "A compact Airy beam light sheet microscope with a tilted cylindrical lens," *Biomedical Optics Express* 5(10), pp. 3434–3442 (2014).

## Alterations of optically measured characteristics of blood as bio-optical markers of diseases

**A.V. Priezzhev<sup>1,2,\*</sup>, A.E. Lugovtsov<sup>2</sup>, S.Yu. Nikitin<sup>1,2</sup>, K. Lee<sup>1</sup>, T. Tikhonova<sup>1,2</sup>, E. Shirshin<sup>1,2</sup>,  
V.B. Koshelev<sup>2,3</sup>, O.E. Fadyukova<sup>3</sup>, M.D. Lin<sup>2</sup>, Yu.I. Gurfinkel<sup>4</sup>**

*1- Faculty of Physics, Lomonosov Moscow State University, Moscow 119991 Russia*

*2- International Laser Center, Lomonosov Moscow State University, Moscow 119991 Russia*

*3- Faculty of Fundamental Medicine, Lomonosov Moscow State University, Moscow 119991 Russia*

*4- Research Clinical Center of JSC "Russian Railways", Moscow, 125315 Russia.*

E-mail : \* [avp2@mail.ru](mailto:avp2@mail.ru)

Search and identification of biomarkers of socially important diseases is one of hot problems of contemporary science. Fast development of laser-optic and biophotonic technologies, in particular, new optical measurement techniques on cellular and molecular levels, recently obtained understanding of tissue optics and fundamental aspects of laser-tissue interactions, allow for introducing new bio-optical markers, as optically measured characteristics of biological structures constituting human organism, which measurable alterations from normal values designate an advent of disease.

This paper focuses at the characteristics of blood that can be measured in-vitro and/or in-vivo by laser-optic techniques, and which alterations can be considered as an indication of disease. The techniques to be discussed are: laser diffractometry of erythrocytes [1, 2], laser scattering aggregometry of erythrocytes and platelets, digital optical capillaroscopy and measurement of the microcirculation parameters [3], erythrocytes trapping and manipulation with laser tweezers [4, 5], fluorescence spectroscopy of blood plasma [6], etc. Experimental protocols and results of measurements performed in-vitro with the samples of whole human and rat blood and blood components will be outlined. Blood for the experiments in-vitro was drawn from clinically healthy human volunteers (control) and from patients suffering from diabetes mellitus, hypertension and other diseases. In-vivo measurements of the microcirculation parameters were conducted with control human subjects and patients suffering hypertension. For the in-vitro experiments with rat blood, the samples were drawn from healthy (control) and sham operated animals, those with experimentally induced diabetes mellitus and/or hypertension. Samples of human and rat blood plasma separated from blood cells were used to study the aggregation of plasma proteins that leads to the loss of their functional properties and is one of the causes of such socially important diseases as the Parkinson and Alzheimer diseases. Fluorescence spectroscopy allows also for identifying other alterations at the molecular level in blood plasma caused by proteins conformational changes that may induce pathological changes at the cellular level and so on up to the level of the whole organism.

The obtained results allow us to conclude that the overviewed laser-optic techniques comprise a powerful tool for efficiently identifying and assessing a set of clinically informative bio-optical markers of diseases.

The work was financially supported by the Russian Scientific Foundation, grant No14-15-00602.

[1] S. Nikitin, A. Priezzhev, A. Lugovtsov, V. Ustinov, A. Razgulin. Laser ektacytometry and evaluation of statistical characteristics of inhomogeneous ensembles of red blood cells. *JQSRT* 146, pp. 365-375 (2014). DOI: 10.1016/j.jqsrt.2014.05.012.

[2] S. Nikitin, A. Priezzhev and A. Lugovtsov., Diffraction by the erythrocytes and deformability measurements. In: *Advanced Optical Flow Cytometry: Methods and Disease Diagnoses*. Edited by V. Tuchin. *Wiley-VCH Verlag GmbH & Co*, ISBN 978-3-527-40934-1, 24 (2011) DOI: 10.1002/9783527634286.

[3] Yu. Gurfinkel, M. Sasonko and A. Priezzhev, Digital capillaroscopy as important tool for early diagnostics of arterial hypertension, *Proc. SPIE* 9448, 944804 (2015). DOI:10.1117/12.2180259.

[4] K. Lee, M. Kinnunen, A. Lugovtsov, A. Priezzhev, and A. Karmenian, Optical study of the dynamics and deformation of erythrocytes in the flow. *Optoelectronics, Instrumentation and Data Processing*. 50(5), 519–524 (2014). DOI: 10.3103/S8756699014050112.

[5] K. Lee, M. Kinnunen, M. D. Khokhlova, E. V. Lyubin, A. V. Priezzhev, I. Meglinski, A. A. Fedyanin, Optical tweezers study of red blood cells aggregation and disaggregation in plasma and protein solutions. *Biomed. Optics Express* (2015) (Submitted).

[6] E. Shirshin, O. Cherkasova, T. Tikhonova, A. Priezzhev, and V. Fadeev, Native fluorescence spectroscopy of blood plasma of rats with experimental diabetes: identifying fingerprints of glucose-related metabolic pathways, *J. Biomed. Opt.* 20(5), 051033 (2015). DOI:10.1117/1.JBO.20.5.051033.

# **Investigation of the penetration into the skin *in vivo/ex vivo* using confocal Raman microscopy**

**M. E. Darwin<sup>1</sup>, S. Mujica Ascencio<sup>1,2</sup>, C-S. Choe<sup>1,3</sup>, J. Lademann<sup>1</sup>**

*1- Center of Experimental and Applied Cutaneous Physiology, Department of Dermatology, Venerology and Allergology, Charité – Universitätsmedizin Berlin, Charitéplatz 1, 10117 Berlin, Germany*

*2- Centro de Investigación e Innovación Tecnológica (CIITEC) del Instituto Politécnico Nacional (IPN). Cerrada de Cecati S/N. Col. Santa Catarina Azcapotzalco México D. F. CP:02250, Mexico*

*3- Kim Il Sung University, Ryongnam-Dong, Taesong District, Pyongyang, DPR Korea*

*Main author email address: maxim.darvin@charite.de*

The penetration of topically applied substances into the skin is a topic of intense non-invasive investigations in dermatology. In this context, confocal Raman microscopy is widely used.

The penetration of “low-penetrating” substances, such as oils, and of “high-penetrating” substances, such as propylene glycol and a phospholipid-contained formulation, applied topically onto the skin were analyzed using four different methods of confocal Raman microscopy: (1) The non-restricted multiple least square fit method in the whole fingerprint region; (2) The specific Raman peak tracking in the fingerprint region; (3) The perpendicular drop down cut-off procedure of lipid-keratin Raman peak (2820 – 3030 cm<sup>-1</sup>) in the high wavenumber region; (4) The deconvolution method of lipid-keratin Raman peak (2820 – 3030 cm<sup>-1</sup>) in the high wavenumber region. To increase the sensitivity of these methods, multivariate statistical methods, such as the principal component analysis and the linear discriminant analysis, were employed to distinguish the small Raman peak intensities in the inner layers of the stratum corneum where the signal-to-noise ratio is low. The advantages, shortcomings and limitations of these methods are discussed in the present paper.

The results confirm that oils do not penetrate through the stratum corneum, while propylene glycol and a phospholipid-contained formulation are able to pass through the stratum corneum barrier and reach the living cells of the stratum spinosum. The multivariate statistical methods are well suited to increase the sensitivity of analytical methods used for analyses of Raman spectra.

## **Imaging technologies in stem cell research and tissue bioengineering**

**E.V. Zagaynova<sup>1,2</sup>, A.V. Meleshina<sup>1,2</sup>, D.S. Kuznetsova<sup>1,2</sup>, V.V. Dudenkova<sup>2</sup>, A.S. Bystrova<sup>2</sup>,  
E.I. Cherkasova<sup>1,2</sup>, P.S. Timashev<sup>3</sup>, V.N. Bagratashvili<sup>3</sup>**

<sup>1</sup> *Nizhny Novgorod State Medical Academy, Russia*

<sup>2</sup> *Lobachevsky State University of Nizhni Novgorod, Russia*

<sup>3</sup> *Institute of Laser and Information Technologies, Troitsk, Russia*

[ezagaynova@gmail.com](mailto:ezagaynova@gmail.com)

The main stream studies in stem cell research are devoted to monitoring differentiation process, to analysis of the role of stem cells in tumor development, to creating new tissue constructions. In all these fields the researchers need high resolution, safe and high quality imaging techniques and approaches. In our studies we combined fluorescent proteins, genetically encoded in different stem cell lines, and fluorescence imaging in vitro and in vivo (laser scanning microscopy, FLIM, whole body imaging).

We investigated the effect of mesenchymal stem cells (MSCs) on the breast cancer metastases formation. Human bone marrow MSC were genetically labeled with luciferase. To establish lung metastases model, human breast cancer cells, stably expressing red fluorescent protein Turbo FP650, were injected intravenously into nude mice. Development of metastases in the lung was monitored by the appearance of red fluorescence on the in vivo images. The metastasis formation in animals from the group with MSC-luc administration was delayed in the time as compared with those in animals group without MSC-luc. During the whole period of observation luminescence signal was observed in the lungs and abdomen of animals.

The purpose of the another part of work was to obtain the polylactide scaffolds with and without nanoscale hydroxyapatite (HA) by surface selective laser sintering and study the proliferation and viability of mesenchymal stromal cells expressing the fluorescence protein TurboFP635 on the derived scaffolds. According to a newly developed protocol of data processing based on the fluorescence signal of TurboFP635 the scaffolds with HA had more cells than those without HA. Moreover, MSC penetrated deeper from the surface of all samples into the pores. By day 20 MSC colonized all volume of both scaffold types. The scaffolds with HA had more cells and can be considered as more perspective material for bone regeneration.

The non-invasive imaging of cell metabolism within tissues to assess the efficacy of stem cell therapy and understanding the tissue development is of great interest. In this study we investigated metabolic trajectory of the mesenchymal stem cell (MSC) differentiation on the change of the fluorescence lifetime of free and bound forms of the nicotinamide adenine dinucleotide (NADH) and flavin adenine dinucleotides (FAD) using Fluorescence Lifetime Microscopy. Undifferentiated, adipogenically and osteogenically differentiated human MSCs were imaged with a Zeiss 710 microscope coupled to a FLIM system. Short and long NADH, FAD lifetime fluorescence and ratio of free and bound NADH and FAD were shown to increase in differentiated cells.

## **Optical coherence tomography of reproductive and developmental events**

Irina V. Larina, PhD

Department of Molecular Physiology and Biophysics, Baylor College of Medicine,  
One Baylor Plaza, Houston, Texas 77030, USA  
Contact email: [larina@bcm.edu](mailto:larina@bcm.edu)

The mouse model is essential for our understanding of normal human reproduction, development and congenital defects. Live dynamic imaging of mouse developmental events is a challenging task; imaging depth and resolution are interdependent, and a significant improvement in one of these parameters usually comes at the expense of the other. Because early mouse embryos go through rapid and dramatic morphological changes, there is no single imaging modality, which would allow for visualization of all these events at high resolution. Our research focuses on developing methods for live imaging and dynamic characterization of reproductive and early embryonic developmental events and using them in mouse models of human diseases. Using multidisciplinary methods: optical coherence tomography (OCT), fluorescence microscopy, live mouse embryo manipulations and static embryo culture, molecular biology, advanced image processing and computational modeling we aim to understand developmental processes. We have developed a series of OCT based approaches to live analysis of reproductive and developmental processes including (1) three-dimensional imaging and tracking of murine oocytes as they exit the ovary and migrate through the oviduct to the uterus; (2) live imaging of early mouse embryos (E8.5 – E9.5) cultured on an imaging stage and visualization of developmental events with a spatial resolution of a few micrometers (less than the size of an individual cell) and a frame rate of up to hundreds of frames per second; (3) reconstruction of cardiodynamics in 4D (3D+time), and (4) *in utero* embryonic imaging of different organ systems including limbs, brain and eye. We are now using these methods to study how specific mutations affect organogenesis.

## **Label free polarization microscopy for diagnosis applications**

Honghui He,<sup>1</sup> Ye Wang,<sup>1,2</sup> Jintao Chang,<sup>1,2</sup> Hui Ma<sup>1,2\*</sup>

<sup>1</sup> Shenzhen Key Laboratory for Minimal Invasive Medical Technologies, Institute of Optical Imaging and Sensing, Graduate School at Shenzhen, Tsinghua University, Shenzhen 518055, China

<sup>2</sup>Department of Physics, Tsinghua University, Beijing 100084, China

\*mahui@tsinghua.edu.cn

### **ABSTRACT**

Polarization imaging can be used to probe the micro structural and optical properties of various samples, such as rocks and minerals, mural pigment, and textiles. Recently, as label-free, non-destructive methods, polarization imaging techniques have been widely applied to biomedical studies and clinical practices including cancerous tissues detection. Polarization imaging methods are compatible in optical layout with the corresponding none polarized optical techniques, but can provide abundant information, especially the sub-wavelength scale structural characteristic features of tissue samples. In this work, we design a polarized light microscope based on Mueller matrix imaging method by adding a set of polarization states generator and analyzer (PSG and PSA) to an ordinary commercial transmission optical microscope. In this polarized light microscope all the Mueller matrix elements can be simultaneously determined by using the dual-rotating quarter-wave plate measurement scheme. Through the proper calibrations and subsequent processing of the received polarization images, the error of the measurement can be reduced and the micro structural information of the samples can be obtained. We apply the Mueller matrix microscope to different kinds of cancerous tissues, such as the liver cancer, cervical cancer and thyroid cancer. By analyzing the Mueller matrix elements and transformation parameters of the non-stained slices of the cancerous tissues, we verify the reliability of the Mueller matrix microscope to extract structural features of the pathological tissues. With the advantages of simple structure, rapid imaging speed and high measurement precision, the Mueller matrix microscope shows good potential for diagnostic applications.

**Keywords:** Mueller matrix, microscope, polarization, cancerous tissues

## **Enabling polarization based technologies for cancer detection and tissue characterization**

**Igor Meglinski**

Laboratory of Opto-Electronics and Measurement Techniques,  
University of Oulu, Oulu, FI-90014 Finland

E-mail: [igor.meglinski@oulu.fi](mailto:igor.meglinski@oulu.fi)

The field of cancer diagnostics is rapidly expanding, and as diagnostic technology improves so does the ability to detect and identify the many different types and sub-types of cancer. For the successful treatment the early detection of cancer is extremely important. However, during early cancer onset it is quite difficult for pathologist to differentiate between tissues that may be neoplastic versus normal tissue undergoing dysplastic changes that is unlikely to become neoplastic. Currently, the most widely used methodology for cancer diagnosis is histological analysis with further microscopy investigation. Despite the best laboratory practice the rate of conclusive diagnosis by histological analysis for a range of cancers, including cervical, bladder, skin and oral cancer, is only 65-75%. We demonstrated that circular and/or elliptical polarized light scattered within the biological tissues is highly sensitive to the presence of cancer cells and their aggressiveness in tissues. Moreover, we found that the position of Stokes vector of scattered light on the Poincaré sphere displays the successive stages of colorectal cancer. We use the sphere as a convenient tool for analysis the state of polarization of light scattered within biological tissue; navigating by Poincaré sphere (similar as by terrestrial globe, using longitude and latitude as in GPS navigator) to monitor/determine polarisation properties and condition of biological tissues. We envisage that this research will enable the development of a new revolutionary diagnostic tool. For example, this technique could help in confirming the presence of early stages of prostate, melanoma or colon cancer *in situ* in doubtful cases.

## **NIR-triggered photodynamic therapy of human cancer with vitamin B2 photosensitised by upconversion nanoparticles**

**E.V. Khaydukov<sup>1</sup>, K.E. Mironova<sup>1,2</sup>, V.A. Semchishen<sup>1</sup>, A.N. Generalova<sup>1,2</sup>,  
A.V. Nechaev<sup>1,3</sup>, D.A. Khochenkov<sup>1,4</sup>, E.V. Stepanova<sup>4</sup>, O. Lebedev<sup>5</sup>,  
A.V. Zvyagin<sup>1,6</sup>, S.M. Deev<sup>2</sup>, V.Ya. Panchenko<sup>1</sup>**

*1- Institute on Laser and Information Technologies of the Russian Academy of Sciences,  
1 Svyatoozerskaya, Shatura 140700, Russia*

*2- Shemyakin-Ovchinnikov Institute of Bioorganic Chemistry of the Russian Academy of Sciences,  
16/10 Miklukho-Maklaya, Moscow 117997, Russia*

*3 - Lomonosov Moscow University of Fine Chemical Technology,  
86 Prospect Vernadskogo, 119571 Moscow, Russia*

*4 - Federal State Scientific Institution Russian Cancer Research Center them. Blokhin,  
23 Kashirskoye, Moscow, 115478, Russia*

*5 - Université de Caen, 6Bd Marechal Juin, 14050 Caen, France*

*6 - Macquarie University, MQ Biofocus Research Centre, NSW 2109, Australia*

*khaydukov@mail.ru*

Riboflavin (vitamin B2) is a micronutrient vital for maintaining the cell homeostasis by regulating flavoprotein enzyme reactions owing to its charge-separation property. This property coupled with a high optical absorption cross-section in the broad ultraviolet-visible spectral band makes it a serendipitous endogenous photosensitiser capable to generate singlet oxygen and reactive oxygen species. Its reportedly high uptake in mammary cancers was intriguing to test the feasibility of salutary photodynamic therapy (PDT) based on riboflavin and its hydrophilic derivatives (Rf). We found that the Rf concentration in excess of 30  $\mu\text{M}$  in the tumour interstitium was achievable *in vivo*, exhibited optical contrast of 5 on the background of the healthy tissue, and sufficed to induce sustainable apoptosis in human breast adenocarcinoma cells SK-BR-3 under ultraviolet irradiation at 365 nm. In addition, SK-BR-3 xenograft tumoricidal regression in immunodeficient mice was observed, following peritumoural Rf injection and PDT treatment. In order to extend the PDT treatment depth in biological tissue from the demonstrated  $\sim 0.5$  mm typical for many potent photosensitisers to 3 mm, we introduced a new type of upconversion nanoparticles (UCNPs,  $\text{NaYF}_4:\text{Yb}^{3+}:\text{Tm}^{3+}$ ) capable to convert deeply-penetrating infrared radiation at 975 nm to ultraviolet-visible light with an unprecedentedly high conversion efficiency measured as 0.5%. A highly efficient (17%) Förster resonance energy transfer (FRET) from the purpose-designed UCNP hybrid assemblies to Rf facilitated production of cytotoxic singlet oxygen. Selective PDT treatment of SK-BR-3 cells incubated with Rf and UCNPs was demonstrated, and also a considerable sustainable suppression of the human breast adenocarcinoma xenografts in a nude mouse model treated with clinically acceptable doses of infrared light ( $3 \text{ W/cm}^2$ ) after administering Rf-UCNP formulation peritumourally.

The work was supported by RSF grant 14-13-01421.

## **Laser-optic techniques for the assessment of erythrocyte hyperaggregation syndrome in diabetes mellitus**

**A.E. Lugovtsov<sup>1</sup>, A.V. Priezzhev<sup>1,2</sup>, V.D. Ustinov<sup>3</sup>, V.B. Koshelev<sup>4</sup>, O.E. Fadyukova<sup>4</sup>, M.D. Lin<sup>4</sup>**

*1 - International Laser Centre,*

*2 - Faculty of Physics,*

*3 - Faculty of Computational Mathematics and Cybernetics,*

*4 - Faculty of Basic Medicine,*

*M.V. Lomonosov Moscow State University,*

*Leninskiye Gory 1, Moscow, 119991, Russia*

*e-mail: [anlug@bmp.ilc.edu.ru](mailto:anlug@bmp.ilc.edu.ru)*

Nowadays the number of people suffering from diabetes mellitus (DM) increases rapidly due to unhealthy eating and lifestyle. DM is a group of metabolic diseases characterized by high blood sugar levels over a prolonged period. DM occurs due to either the pancreas not producing enough insulin or the cells of the body not responding properly to the insulin produced. This can lead to severe alterations of vitally important systems of the organism including the cardiovascular system. Some of the major DM complications are related to the damage to blood vessels and capillaries, impairment of blood rheological properties. Enhanced aggregation of erythrocytes and platelets is one of key factors, which determines the blood flow and thereby affects the blood rheology. Therefore, controlling and monitoring the blood cells aggregation in DM patients is very important.

There are several instruments currently available for the assessment of erythrocyte aggregation *in vitro*. In this work, we used two commercially available aggregometers – LADE-6 (RheoMedLab, Russia) and Rheoscan-D300 (Rheomeditech, Korea). Operation of these devices is based on laser scattering aggregometry technique [1]. Laser aggregometry allows to study the kinetics of spontaneous aggregation (time dependence of the intensity of light backscattered from a sample of whole blood at rest) and shear-induced disaggregation (shear stress dependence of the intensity of light backscattered from a sample of whole blood under controlled shear flow conditions) [2].

Experiments with LADE are carried out with samples of whole blood placed in a Couette chamber where uniform shear rate is induced. Shear flow arising in the chamber destroys the aggregates. Computer processing the obtained aggregation and disaggregation kinetics yields the characteristic times of linear and three-dimensional aggregates formation as well as the hydrodynamic strength of the aggregates.

The Rheoscan operates with a disposable plastic units having a disc-shaped chamber for the sample containing a metal bar. The metal bar can be rotated in the sample chamber to achieve erythrocyte disaggregation. The obtained aggregation kinetics (dependence of light transmitted through the blood sample on time) is analyzed and the characteristic time of aggregation is calculated.

All measurements were performed with human blood samples drawn from patients with diabetes mellitus and normal individuals (control) as well as with rat blood drawn from healthy animals and from rats with experimentally induced DM.

The experimental results obtained using LADE shows that DM is characterized by about 30% increase in time of the formation of linear aggregates that, however, have close to normal hydrodynamic strength. Time of 3D aggregates formation decreases by about 10-25 % in comparison with that in the control group. Alterations of the related parameters obtained with Rheoscan are quantitatively different and more pronounced. These differences are discussed.

This work was partially supported by RFBR grant № 13-02-01373a.

[1] A.V. Priezzhev, N.N. Firsov, J. Lademann, [Light backscattering diagnostics of RBC aggregation in whole blood samples], Chapter 11 in Handbook of Optical Biomedical Diagnostics, Editor V. Tuchin, Washington: SPIE Press, pp. 651 – 674 (2002).

[2] V.N. Lopatin, A.V. Priezzhev et al. Light Scattering Methods in the Analysis of Aqueous Disperse Biological Media. Published by "Fizmatlit", Moscow (2004) (in Russian).

## Assessment of fibrillar structures in blood plasma using the fluorescent probe Thioflavin T

T. Tikhonova<sup>1</sup>, E. Shirshin<sup>2</sup>, N. Rovnyagina<sup>2</sup>, V. Fadeev<sup>2</sup>, A. Priezzhev<sup>1,2</sup>

1- International Laser Center of M.V.Lomonosov Moscow State University, 119991, Leninskie gory 1/62, Moscow, Russia

2- M.V. Lomonosov Moscow State University, Department of Physics, 119991, Leninskie gory 1/2, Moscow, Russia

shirshin@lid.phys.msu.ru

A number of diseases is accompanied by conformational changes of proteins, caused by its misfolding, which can induce the changes in binding affinities, aggregation, loss of functionality etc. The most typical example includes Parkinson and Alzheimer diseases, the neurodegenerative disorders, which are associated with the formation and accumulation in brain of compact plaques –  $\beta$ -sheet-rich amyloid fibrils. However, it is known that not only special amyloidogenic proteins may induce fibrils formation in the human organism – for instance, some molecular pathways which are involved in the pathogenesis of diabetes mellitus also result in fibril formation. Namely, glycation of albumin, the major protein in human blood plasma, also may lead to its fibrillation. Albumin fibrils, in its turn, can be sorbed on the surface of red blood cells, leading to its aggregation and rheological complications. Summarizing, changes at the molecular level, caused by proteins conformational changes, may induce pathological changes at the cellular level and so on, up to the level of the whole organism. Among the problems associated with the pathological processes associated with conformational changes of proteins, fibril formation is one of the most intriguing ones. At the same time, the majority of work, devoted to fibrils assessment, deal with fibrils in tissues and *in vitro* model experiment, while the investigation of fibrils in blood remains a promising task for optical spectroscopy.

One of the most common markers for the detection of amyloid fibrils is the fluorescent dye – Thioflavin T (ThT), which act as a molecular rotor. There is a large number of works devoted to the investigation of Thioflavin T binding by fibrils [1], including albumin fibrils [2], however, there is no detailed investigation of interaction between Thioflavin T and albumin, which is crucial for ThT application for quantitative assessment of fibrils in blood plasma.

Here, we investigated the process of albumin binding by Thioflavin T in order to develop a protocol for separation of the impacts from ThT-albumin and ThT-fibril complexes in blood plasma. The fluorescence of Thioflavin T was used to determine the major parameters of binding process – the binding constant  $K_a$  and the number of binding sites for the albumin-ThT and albumin fibril-ThT systems. The use of laser fluorescence spectroscopy (time-resolved fluorescence spectroscopy in the picosecond domain), allowed us to perform detailed investigation of ThT-albumin binding kinetics, moreover the localization of ThT-albumin binding sites was studied. Time-resolved fluorescence anisotropy was also studied here and provided information about the Thioflavin T rotational mobility and the change of its microenvironment during its binding with protein. Using the data, obtained by TRFA technique, it was possible to select between two possible mechanisms of ThT binding – non-specific binding by albumin and incorporation into the albumin aggregates, which are always present even in pure albumin solution. The obtained result were applied for the assessment of fibrils in blood plasma of patients with diabetes mellitus. This pilot study allowed to confirm that the use of ThT-based fluorescence assay could be a promising tool for prediction of complications, connected with fibril formation in blood plasma.

[1] I. Kuznetsova et al., Analyzing thioflavin T binding to amyloid fibrils by an equilibrium microdialysis-based technique, *PLoS one*, vol. 7(2), e30724 (2012).

[2] M. Bhattacharya, J. Neha and S. Mukhopadhyay, Insights into the mechanism of aggregation and fibril formation from bovine serum albumin, *The Journal of Physical Chemistry B*, vol. 115(14), pp. 4195-4205, (2011).

## **High-resolution noncitotoxic photopolymerization process of biocompatible compositions using IR light**

**A.G. Savelyev, E.V. Khaydukov, V.A. Semchishen**

*Institute on Laser and Information Technologies, Russian Academy of Sciences, Shatura, 140700, Russia*

*a.g.savelyev@gmail.com*

Fabrication of 3D biocompatible polymer structures is one of the key problems in modern regenerative medicine. The specificity of application is demanding to the utilized materials. The general requirements are sufficient mechanical strength, nontoxicity of polymer and its decomposition products. The methacrylated hyaluronic acid meets requirements and may be utilized for biological applications, e.g. scaffolding for tissue engineering. [1] In this paper we present a new noncitotoxic polymerization method implemented for fabrication 3D structures on the basis of methacrylated hyaluronic acid.

The realization of method is based on embedding core/shell upconverting nanoparticles (UCNPs)  $\text{NaYF}_4/\text{NaYF}_4:\text{Yb}^{3+},\text{Tm}^{3+}$  [2] into the photocurable composition consisted of methacrylated hyaluronic acid dissolved in distilled water with flavin mononucleotide (FMN) as a photoinitiator. It must be emphasized that all the above mentioned components are biocompatible and do not produce any cytotoxic products as a result of decomposition. UCNP and FMN in the composition construct a nanocomplex capable to activate the polymerization process under IR irradiation. In the present work we have implemented 975 nm laser light source to expose the composition. In this case, UCNP  $\text{NaYF}_4/\text{NaYF}_4:\text{Yb}^{3+},\text{Tm}^{3+}$  absorbs IR light and transfers energy to the FMN molecule via Förster Resonance Energy Transfer (FRET) mechanism. Excited FMN molecule generates the radicals in the monomer composition. Therefore, the complexes UCNP – FMN become the centers of polymerization.

The method is promising for producing high resolution structures for biological applications. The upconversion process in comparison with multiphoton process [1] allows operating at much lower intensities avoiding temperature overheating, with resolution of the method remaining high. On the other hand, the nonradiative energy transfer from upconverting nanoparticles to riboflavin mononucleotide makes possible fabrication process with minimized phototoxicity to live cells, enabling photopolymerization of the initial monomer composition directly with embedded live cells. This work has been supported under Grant RFBR 14-02-00875A and 14-29-10211.

[1] O. Kufelt, A. El-Tamer, C. Sehring, S. Schlie-Wolter, and B.N. Chichkov, Hyaluronic Acid Based Materials for Scaffolding via Two-Photon Polymerization, *Biomacromolecules*, **15**(2), pp. 650-659 (2014).

[2] E.V. Khaydukov, V.A. Semchishen, V.N. Seminogov, A.V. Nechaev, A.V. Zvyagin, V.I. Sokolov, A.S. Akhmanov, and V.Ya. Panchenko, Visualization of upconverting nanoparticles in strongly scattering media, *Biomedical Optics Express*, **5**(6), pp. 1952-1964 (2014).

## Silicon Nanoparticles Formed by Means of Laser Ablation as Potential Biomarkers and Contrasting Agents

**S.V. Zobotnov<sup>1</sup>, F.V. Kashaev<sup>1</sup>, D.M. Zhigunov<sup>1</sup>, I.A. Kamenskikh<sup>1</sup>, P.A. Forsh<sup>1</sup>,  
L.A. Golovan<sup>1</sup>, P.D. Agrba<sup>2</sup>, M.Yu. Kirillin<sup>2</sup>, P.K. Kashkarov<sup>1,3</sup>**

*1- Lomonosov Moscow State University, 1/2 Leninskie Gory, Moscow, 119991 Russia*

*2- Institute of Applied Physics RAS, 46 Uljanov str., Nizhny Novgorod, 603950 Russia*

*3- Russian Research Center "Kurchatov Institute", 1 Kurchatov square, Moscow, 123182 Russia*

*E-mail: zobotnov@physics.msu.ru*

Silicon nanostructures in biophotonics attract attention of researchers owing to good biocompatibility and biodegradation of this material [1]. By now silicon nanocrystal suspensions prepared via laser ablation in liquids have been suggested to serve as molecular oxygen photosensitizers for photodynamic cancer therapy [2] and photoluminescent (PL) markers for drug delivery and bioimaging [3]. In our work we show a possibility to form the PL silicon nanoparticles by femtosecond laser ablation in gases. Also we demonstrate that the picosecond laser ablation of silicon in liquid yields silicon-based suspensions for optical coherence tomography (OCT) applications.

To obtain the PL nanoparticles we realized ablation regimes in air and helium when the silicon nanoparticles with size smaller 5 nm in crystalline phase are formed. The existence of such structures are verified by the atomic force microscopy and Raman spectroscopy methods. The PL peaks are located near 540 nm and 760 nm for the cases of ablation in air and helium correspondingly. In both cases the PL lifetimes in order of 10  $\mu$ s. The examined nanocrystals are promising as photoluminescent markers in biotissues and similar objects.

The nanoparticles suspension for use in OCT was produced by picosecond laser irradiation of monocrystalline silicon wafers in water. According to transmission electron microscopy and small-angle X-ray scattering analysis the silicon nanoparticles in obtained suspension vary in size from 2 to 200 nm while concentration of the particles is estimated as  $10^{13}$  cm<sup>-3</sup>. Optical properties of the suspension in the range from 400 to 1000 nm were studied by spectrophotometry measurements revealing scattering coefficient of about 0.1 mm<sup>-1</sup> and scattering anisotropy factor in the range of 0.2–0.4. In OCT study a system with central wavelength of 910 nm was employed. Potential of the silicon nanoparticles as contrasting agent for OCT was studied in experiments with agarose gel phantoms. Topical application of the nanoparticles suspension allowed to obtain the contrast of structural features of phantom up to 14 dB in the OCT image.

Thus, the new prospects for silicon nanoparticle fabrication by means of laser ablation in air, helium and water were offered: such particles may be used as PL markers in bioimaging or contrasting agents in OCT.

This work was financially supported by the Russian Foundation for Basic Research (project 15-32-20227 – PL and spectrophotometry measurements, 14-22-01086 – small-angle X-ray scattering technique).

[1] J.R. Henstock, L.T. Canham, S.I. Anderson, Silicon: The evolution of its use in biomaterials, *Acta Biomaterialia*, vol. 11, pp. 17-26, (2015).

[2] D. Rioux, M. Laferriere, A. Douplik, et al., Silicon nanoparticles produced by femtosecond laser ablation in water as novel contamination-free photosensitizers, *J. Biomed. Opt.*, vol. 14, art. 021010, (2009).

[3] P. Blandin, K.A. Maximova, M.B. Gongalsky, et al., Femtosecond laser fragmentation from water-dispersed microcolloids: Toward fast controllable growth of ultrapure Si-based nanomaterials for biological applications, *J. Mater. Chem. B*, vol. 1, pp. 2489-2495, (2013).

## **Sculpting light for new biophotonics applications**

**J. Glückstad<sup>o\*</sup>, D. Palima\*, M. Villangca\* and A. Bañas<sup>o\*</sup>**

*\*DTU Fotonik, Programmable Phase Optics, Techn. Univ. Denmark*

*<sup>o</sup>GPC Photonics ApS, [www.GPCphotonics.com](http://www.GPCphotonics.com)*

*[jesper.gluckstad@fotonik.dtu.dk](mailto:jesper.gluckstad@fotonik.dtu.dk) [www.ppo.dk](http://www.ppo.dk)*

Generalized Phase Contrast (GPC) is a power efficient approach for generating speckle-free contiguous optical distributions using spatial phase-only light modulation. GPC has been demonstrated in a variety of applications such as optical micro-manipulation [1], active microscopy [2], structured illumination, optical phase encryption, and recently in contemporary biophotonics applications such as for real-time parallel two-photon optogenetics and neurophotonics [3]. Our most recent GPC light sculpting developments will be presented. These include both static and dynamic GPC Light Shapers where lasers have to be actively shaped into particular light patterns [4]. We show the potential of GPC for biomedical and multispectral applications where we demonstrate phase-only light shaping of a supercontinuum laser over most of its visible wavelength range [5].

- [1] J. Glückstad, "Optical manipulation: sculpting the object", *Nature Photonics*, Vol. 5, 7-8 (2011).
- [2] D. Palima, and J. Glückstad, "Gearing up for optical microrobotics: micromanipulation and actuation of synthetic microstructures by optical forces," *Laser & Photon. Rev.* 7, 478-494 (2013).
- [3] E. Papagiakoumou, F. Anselmi, A. Bègue, V. de Sars, J. Glückstad, E. Y. Isacoff, and V. Emiliani, "Scanless two-photon excitation of channelrhodopsin-2," *Nature Methods* 7, 848–854 (2010).
- [4] A. Bañas, O. Kopylov, M. Villangca, D. Palima and J. Glückstad, "GPC Light Shaper: static and dynamic experimental demonstrations," *Opt. Express* 22, 23759-23769 (2014).
- [5] O. Kopylov, A. Bañas, M. Villangca, and D. Palima, "GPC light shaping a supercontinuum source," *Opt. Express* 23, 1894–1905 (2015).

# **The effect of optical clearing in the optical properties of skeletal muscle**

**L. Oliveira<sup>1</sup>, M. I. Carvalho<sup>2</sup>, E. Nogueira<sup>1</sup>, V. V. Tuchin<sup>3</sup>**

*1- CIETI/ISEP – Physics Department, Rua Dr. António Bernardino de Almeida N°431, 4249-015 Porto, Portugal*

*2- INEST-TEC/DEEC, Rua Dr. Roberto Frias s/n, 4200-465 Porto, Portugal*

*3- Saratov State University, Research-Educational Institute of Optics and Biophotonics, 83, Astrakhanskaya Street, Saratov 410012, Russia*

*Main author email address: lmo@isep.ipp.pt*

Many biological tissues present significant light scattering. Such fact is presented in literature for many tissues that have significantly high scattering coefficients [1]. One of the reasons for such high scattering is the refractive index mismatch verified between tissue components [2, 3]. Water in the interstitial and intra-cellular fluids plays a major role, since its refractive index is considerably smaller than the one from the other tissue components [3]. Water content in many tissues is also significant. To reduce the scattering coefficient in biological tissues, the optical immersion method can be used [3-5]. In this method, part of the water in the tissue is replaced by an agent with higher refractive index, better approximated to the index of the other tissue components [2, 6]. During such a treatment, the magnitude of the refractive index mismatch decreases due to the water loss and its replacement by the agent [3, 6]. Such variations are directly connected to the variations of the scattering coefficient of the tissue. Due to the difference of magnitudes between the scattering and absorption coefficients, the absorption coefficient can be considered unchanged during the treatment since the agents used have low absorption in the visible and NIR regions [2, 7]. By measuring muscle transmittance, reflectance and thickness during treatments with glucose and ethylene glycol (EG), we have estimated the time dependence of these measurements and of the optical properties of the muscle at different wavelengths for those treatments. Time dependencies of the optical properties were obtained through inverse Adding-Doubling simulations [8] and they have confirmed a decrease in the scattering and reduced scattering coefficients and an increase in anisotropy and refractive index of the muscle. These behaviors were observed in both treatments.

From experimental measurements we have observed an increase in tissue transmittance and a decrease in tissue reflectance [9]. Thickness has presented a major decrease at early treatment, due to tissue dehydration and after that a smooth increase that corresponds to the entry of agent in the muscle [3]. Such smooth increase precedes the saturation regime, which was observed to have no changes in sample thickness for the treatment with glucose 40%. In opposition the treatment with EG 99% shows increasing thickness during saturation, indicating that EG diffuses into muscle for a longer time [3, 6]. Using collimated transmittance measurements during treatments with different concentrations of these agents we could estimate the diffusion time and diffusion coefficient values for glucose and EG in the muscle [1, 3, 6].

[1] V. V. Tuchin, *Tissue Optics: Light Scattering Methods and Instruments for Medical Diagnosis – 3<sup>rd</sup> Ed.* (Bellingham, WA: SPIE Press), Chapter 9, (2015).

[2] V. V. Tuchin, *Optical Clearing of Tissues and Blood* (Bellingham, WA: SPIE Press), Chapters 1 and 2, (2006).

[3] L. Oliveira, M. I. Carvalho, E. Nogueira, V. V. Tuchin, Diffusion characteristics of ethylene glycol in skeletal muscle, *J. of Biomedical Optics*, vol. 20, pp. 051019-1-10, (2015).

[4] E. A. Genina, A. B. Bashkatov, V. V. Tuchin, Tissue optical immersion clearing, *Expert. Rev. Med. Devices*, Vol. 7, pp. 825-842, (2010).

[5] D. Zhu, K. V. Larin, Q. Luo, V. V. Tuchin, Recent progress in tissue optical clearing, *Laser Photonics Rev.*, vol. 7, pp. 732-757, (2013).

[6] L. Oliveira, M. I. Carvalho, E. Nogueira, V. V. Tuchin, The characteristic time of glucose diffusion measured for muscle tissue at optical clearing, *Laser Physics*, vol. 23, pp. 075606-1-6, (2013).

[7] S. L. Jacques, Optical properties of biological tissues: a review, *Phys. Med. Biol.*, vol. 58, pp. R37-R61, (2013).

[8] S. A. Prahl, M. J. C. van Gemert, A. J. Welch, Determining the optical properties of turbid media by using the adding-doubling method, *Appl. Opt.* vol. 32, pp. 559-568, (1993).

[9] L. Oliveira, M. I. Carvalho, E. Nogueira, V. V. Tuchin, Optical measurements of rat muscle samples under treatment with ethylene glycol and glucose, *j. Innovative Opt. Health. Sci.*, vol. 6, 1350012-1-15, (2013).

# Combinatorial Matrix - Assisted Pulsed Laser Evaporation of organic materials for biomedical applications

C. Ristoscu<sup>1</sup>, F. Sima<sup>1</sup>, E. Axente<sup>1</sup>, L. E. Sima<sup>2</sup>, N. Mihailescu<sup>1</sup>, I. Negut<sup>1</sup>, A. Visan<sup>1</sup>, E. Toksoy Oner<sup>3</sup>, A. Bigi<sup>4</sup>, I. N. Mihailescu<sup>1</sup>

<sup>1</sup> National Institute for Lasers, Plasma and Radiation Physics, POBox MG-36, Magurele, Ilfov, Romania

<sup>2</sup> Department of Molecular Cell Biology, Institute of Biochemistry, Romanian Academy, Bucharest, Romania

<sup>3</sup> Marmara University, Turkey

<sup>4</sup> Department of Chemistry "G. Ciamician", University of Bologna, Bologna, Italy

e-mail: [carmen.ristoscu@inflpr.ro](mailto:carmen.ristoscu@inflpr.ro)

We introduce Combinatorial Matrix-Assisted Pulsed Laser Evaporation (C-MAPLE) for the fabrication of organic biopolymer thin films [1]. Structures with compositional gradient are obtained by the simultaneous laser vaporization of two distinct targets. Synchronized MAPLE of levan and oxidized levan cryogenic targets was applied in order to transfer under protection and assemble a two-compound biopolymer film structure. FTIR micro-spectroscopy confirmed the existence of a composition gradient along the length of the sample. Modification of chemical composition from L to OL and the physical texture stayed at the origin of the improved accumulation of cells on discrete film regions (different from the two ends) as compared with all other film areas. *In-vitro* cell culture assays illustrated characteristic responses of cells to specific surface regions [2]. The cell response induced by the compositional gradient using imaging of early osteoblast attachment and analysis of signaling phosphoprotein expression was investigated. Cells attached along the gradient in direct proportion with oxidized levan concentration. Cell signalling response to the surface composition gradient and roughness has shown that combinations of OL and L (OL-L and L-OL) increase ERK activation as compared to OL or L alone. The analyses revealed a structure-function relationship and beneficial design guidelines. This basically refers to the existence of an optimum mixture between OL and L constituents, and more or less hydrophilic areas. Once identified, the optimum region could be recognized by rapid fluorescence microscopy scanning. The generation of smart discrete materials with desired properties such as the rate of coating dissolution is a prospective, challenging task. We demonstrated the use of C-MAPLE to the *in-situ* synthesis of Poly-dl-lactide (PDLLA) and fibronectin (FN) [3]. Confocal and FTIR microscopy evidenced FN packages embedded in the polymeric matrix. The composition of PDLLA and FN was preserved after C-MAPLE as supported by protein staining and FTIR.

C-MAPLE was applied to synthesize crystalline gradient thin films with variable composition of Sr-substituted hydroxyapatite (SrHA) and Zolendronate modified hydroxyapatite (ZOLHA) on Titanium substrates [4]. The inhibitory action of ZOL on osteoclast viability and activity is more efficient than that of Sr, which plays a greater beneficial role on osteoblast proliferation and viability. The deposition method allows to modulate the composition of the thin films and hence the promotion of bone growth and the inhibition of bone resorption.

C-MAPLE opens the possibility to both combine and immobilize two or more organic materials on a solid substrate in a well defined manner by laser evaporation under protection.

[1] F. Sima, E. Axente, L. E. Sima, U. Tuyel, M. S. Eroglu, N. Serban, C. Ristoscu, S. M. Petrescu, E. Toksoy Oner, I. N. Mihailescu, "Combinatorial Matrix-Assisted Pulsed Laser Evaporation: Single-step synthesis of biopolymer compositional gradient thin film assemblies", *Applied Physics Letters* **101**, 233705 (2012)

[2] E. Axente, F. Sima, L. E. Sima, M. Erginer, M. S. Eroglu, N. Serban, C. Ristoscu, S. M. Petrescu, E. Toksoy Oner, I. N. Mihailescu, "Combinatorial MAPLE gradient thin film assemblies signalling to human osteoblasts", *Biofabrication* **6**, 035010 (2014)

[3] F. Sima, E. Axente, I. Iordache, C. Luculescu, O. Gallet, K. Anselme, I.N. Mihailescu, "Combinatorial Matrix Assisted Pulsed Laser Evaporation of a biodegradable polymer and fibronectin for protein immobilization and controlled release" *Applied Surface Science* **306**, 75–79 (2014)

[4] P. Torricelli; F. Sima; E. Axente; M. Fini; I. N. Mihailescu; A. Bigi; "Strontium and Zoledronate Hydroxyapatites Graded Composite Coatings for Bone Prostheses; *Journal of Colloid & Interface Science*, Volume 448, 15 June 2015, Pages 1-7

## **Laser plasmonic photothermal therapy of transplanted liver tumors**

**A.B. Bucharskaya,<sup>1\*</sup> G.N. Maslyakova,<sup>1</sup> N.A. Navolokin,<sup>1</sup> G.S. Terentyuk,<sup>1,2</sup> A.N. Bashkatov,<sup>2,3</sup>  
E.A. Genina,<sup>2,3</sup> B.N. Khlebtsov,<sup>4</sup> N.G. Khlebtsov,<sup>4</sup> and V.V. Tuchin<sup>2,3,5</sup>**

<sup>1</sup>*Saratov State Medical University, Russia*

<sup>2</sup>*Research-Educational Institute of Optics and Biophotonics, Saratov State University, Russia*

<sup>3</sup>*Interdisciplinary Laboratory on Biophotonics, Tomsk State University, Russia*

<sup>4</sup>*Institute of Biochemistry and Physiology of Plants and Microorganisms, RAS, Russia*

<sup>5</sup>*Institute of Precision Mechanics and Control, RAS, Russia*

\*E-mail: [allaalla\\_72@mail.ru](mailto:allaalla_72@mail.ru)

The aim of the study was to evaluate the efficiency of plasmonic photothermal therapy (PPTT) of transplanted liver tumor. Thirty male outbred albino rats with transplanted liver cancer PC-1 were used in the experiment. The gold nanorods (length  $41 \pm 8$  nm, diameter  $10.2 \pm 2$  nm, gold concentration 400  $\mu\text{g/ml}$ ) were synthesized using early designed protocol [1]. To prevent nanoparticles aggregation in tissues and enhance their biocompatibility, nanorods were functionalized using thiolated polyethylene glycol (MW=5000, Nektar, USA) [2]. Prior some medical procedure or treatment, the rats were anaesthetized with Zoletil 50 (Virbac, France) in dose of 0.05 mg/kg. An hour before laser irradiation, the animals were injected intratumorally by the solution of gold nanorods in the amount of 30% of the tumor volume. The injection of the gold nanoparticles directly into the tumor was conducted according the protocol presented by of Xie and co-workers [3], which provided a prolonged retention of nanoparticles in tumor tissue. The tumor was irradiated during 15 min with the infrared 808-nm diode laser at a power density of 2.3 W/cm<sup>2</sup>. The IR imager (IRI4010, Infrared Integrated System (IRYSYS, UK)) allowed for monitoring of the heated tumor temperature. The withdrawal of the animal from the experiment was performed in 24 hrs after the laser exposure. The standard histological and immunohistochemical staining with antibodies for Ki-67, p53, FAS-receptor, FAS-ligand, EGFR were used for morphological study of transplanted tumors. After PPTT the pronounced necrotic changes in the tumor tissue, accompanied by the observation of decreased expression of proliferation marker Ki-67 and the increased expression of apoptosis markers - p53, FAS-receptor and FAS-ligand, were revealed.

1. A.V. Alekseeva, V.A. Bogatyrev, B.N. Khlebtsov, A.G. Melnikov, L.A. Dykman, N.G. Khlebtsov, Gold nanorods: synthesis and optical properties, *Colloid Journal*, 68(6), 661–678 (2006).
2. B. N. Khlebtsov, E. S. Tuchina, V. A. Khanadeev, E. V. Panfilova, P.O. Petrov, V.V. Tuchin, N. G. Khlebtsov, Enhanced photoinactivation of *Staphylococcus aureus* with nanocomposites containing plasmon particles and hematoporphyrin, *J. Biophotonics*, 6(4), 338-351 (2013).
3. H. Xie, B. Goins, A. Bao, Z.J. Wang, W.T. Philips, Effect of intratumoral administration on biodistribution of 64 Cu-labeled nanoshells, *Int. J. Nanomedicine*. 7, 2227–2238 (2012).

# COMPUTER SIMULATION OF PHOTON DENSITY NORMALIZED MAXIMUM MOVEMENT IN TURBID MEDIA

**A.Yu. Potlov, S.V. Frolov, S.G. Proskurin**

*Tambov State Technical University  
Sovetskaya 106, Tambov, Russia  
[spros@tamb.ru](mailto:spros@tamb.ru)*

The investigated approach is based on numerical solution of the radiative transfer equation in the diffusion approximation for the light pulse with a fixed number of photons [1,2]. It allows describing experimentally acquired time point spread functions (TPSF) obtained for homogeneous and inhomogeneous cases with different scattering and absorption of the main cylinder imbedded cylindrical inhomogeneities [3,4]. For monitoring the ultra-short pulse of irradiation in a strongly scattering object we show the Photon Density Normalized Maximum (PDNM) taken at a chosen level of the photon density current maximum and its trajectories.

As a result of the computer simulation [3] we were able to demonstrate regularities of PDNM movement in cylindrical objects:

1. In all homogeneous cases, the regardless of the values of absorption and scattering coefficients PDNM moves in the geometric center of the object [3].
2. In the case of an absorbing inhomogeneity PDNM moves towards the point which is symmetrical to the geometric center of it with respect to the center of the cylindrical object [3]. Fig. 1a) shows the photon density in the cross-section at the half-height of the inhomogeneous phantom with absorbing inhomogeneity at a time  $t=3.75$  ns.
3. In the case of a scattering inhomogeneity PDNM moves toward the geometric center of it [3]. Fig. 1b) shows the photon density in the cross-section at the half-height of the simulated phantom with single scattering inhomogeneity at a time  $t=4.5$  ns.

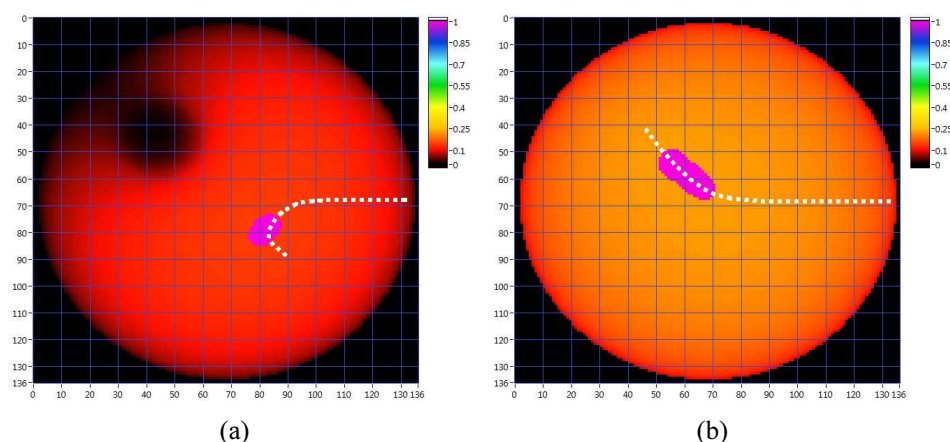


Figure 1 Photon density distributions and PDNM movement trajectories for the case of an absorbing inhomogeneity (a) and the case of a scattering inhomogeneity (b)

Note that the rate of decay of radiation intensity in the simulated cases with absorbing inhomogeneities is significantly higher than in those with scattering inhomogeneities [3].

The revealed PDNM behavior allow estimating the influence of optical properties distribution to the propagation and attenuation of infrared irradiation in biological objects. Presented results will be useful in developing more effective methods for solving Diffuse Optical Tomography (DOT) inverse problems by using Late Arriving Photons (LAP) and all shape of TPSF.

[1] M.S. Patterson, B.Chance, B.C. Wilson Time resolved reflectance and transmittance for the noninvasive measurement of tissue optical properties, *Applied Optics*, Vol. 28, №. 12, p 2331 (1989)

[2] A.E. Profio Light transport in tissue, *Applied Optics*, Vol. 28, №. 12, p 2216 (1989)

[3] A.Yu. Potlov, S.V. Frolov, S.G. Proskurin Movement of the photon density normalized maximum in homogeneous and inhomogeneous media with tissue-like optical properties, *Laser Physics*, Vol.25, №3, p. 035601 (2015)

[4] A.Yu. Potlov, S.V. Frolov, S.G. Proskurin Inhomogeneity Detection in Diffuse Optical Imaging using Conformal Mapping, *Proceedings of SPIE*, Vol. 9448, p.944805.1-8 (2015)

## **OCA diffusion in biological tissues**

**L. Oliveira<sup>1</sup>, M. I. Carvalho<sup>2</sup>, E. Nogueira<sup>1</sup>, V. V. Tuchin<sup>3</sup>**

*1- CIETI/ISEP – Physics Department, Rua Dr. António Bernardino de Almeida N°431, 4249-015 Porto, Portugal*

*2- INEST-TEC/DEEC, Rua Dr. Roberto Frias s/n, 4200-465 Porto, Portugal*

*3- Saratov State University, Research-Educational Institute of Optics and Biophotonics, 83, Astrakhanskaya Street, Saratov 410012, Russia*

*Main author email address: lmo@isep.ipp.pt*

The study of chemical diffusion in biological tissues is very important for clinical applications, therapeutics, cosmetics and research [1]. Different techniques have been used to determine the characteristic diffusion time or the diffusion coefficient of some chemicals in different tissues [2-6]. Glucose diffusion has been studied recently in normal and cancerous tissues as a possible way to establish a diagnosis [7]. In optical clearing procedures, where the mechanisms of tissue dehydration and refractive index matching cooperate to create tissue transparency, the study of water and agent diffusion allows to distinguish and characterize between both mechanisms [8]. Using collimated transmittance measurements made from muscle samples under optical clearing with glucose and ethylene glycol solutions, we were able to calculate the characteristic diffusion time values for these fluids [8-9]. These values were used with thickness measurements made under the same treatments from samples with adequate geometry to calculate the diffusion coefficients for water, glucose and ethylene glycol [7-8]. Such results are adequate to characterize the dehydration and refractive index matching mechanisms and the method used also allowed identifying the amount of free water content on tissues. Such method can now be used to make similar analysis regarding the diffusion of medications and cosmetics.

[1] V. V. Tuchin, *Optical Clearing of Tissues and Blood* (Bellingham, WA: SPIE Press), Chapters 1 and 2, (2006).

[2] G. Vargas, E. K. Chan, J. K. Barton, H. G. Rylander and A. J. Welch, Use of an agent to reduce scattering in skin, *Lasers in Surgery and Medicine*, vol. 24, pp. 133-141, (1999).

[3] G. Vargas, J. K. Barton and A. J. Welch, Use of hyperosmotic chemical agent to improve the laser treatment of cutaneous vascular lesions, *J. Biomedical Optics*, vol. 13, pp. 021114-1-8, (2008).

[4] H. Zeng, J. Wang, Q. Ye, Z. Deng, J. Mai, W. Zhou, C. Zhang and J. Tian, Study on the refractive index matching effect of ultrasound on optical clearing of bio-tissues based on the derivative total reflection method, *Biomedical Optics Express*, vol. 5, pp. 3482-3493, (2014).

[5] E. A. Genina, A. B. Bashkatov, V. V. Tuchin, Tissue optical immersion clearing, *Expert. Rev. Med. Devices*, Vol. 7, pp. 825-842, (2010).

[6] D. Zhu, K. V. Larin, Q. Luo, V. V. Tuchin, Recent progress in tissue optical clearing, *Laser Photonics Rev.*, vol. 7, pp. 732-757, (2013).

[7] H. Q. Zhong, Z. Y. Guo, H. J. Wei, C. C. Zeng, H. L. Xiong, Y. H. He and S. H. Liu, Quantification of glycerol diffusion in human normal and cancer breast tissues in vitro with optical coherence tomography, *Laser Physics Letters* vol. 7, pp. 315-320, (2010).

[8] L. Oliveira, M. I. Carvalho, E. Nogueira, V. V. Tuchin, Diffusion characteristics of ethylene glycol in skeletal muscle, *J. of Biomedical Optics*, vol. 20, pp. 051019-1-10, (2015).

[9] L. Oliveira, M. I. Carvalho, E. Nogueira, V. V. Tuchin, The characteristic time of glucose diffusion measured for muscle tissue at optical clearing, *Laser Physics*, vol. 23, pp. 075606-1-6, (2013).

# Nanoparticles Effects on Optical Properties of Biological Tissues

**E. Perevedentseva<sup>1,2</sup>, A. Karmenyan<sup>1</sup>, O. Bibikova<sup>3</sup>, A. Bykov<sup>3</sup>, I. Skovorodkin<sup>4</sup>,  
R. Prunskaitė-Hyyryläinen<sup>4</sup>, S. Vainio<sup>4</sup>, C.L. Cheng<sup>1</sup>, M. Kinnunen<sup>3</sup>, I. Meglinski<sup>3</sup>**

*1- National Dong Hwa University, 1 Sec. 2 Da Hsueh Rd, Shoufeng, Hualien 974 Taiwan*

*2- P.N. Lebedev Physics Institute, 53 Leninskii pr-t, Moscow 199911 Russia*

*3- Department of Electrical Engineering, University of Oulu, P.O.Box 8000 Oulu FI-90014, Finland*

*4- Biocenter Oulu, University of Oulu, P.O.Box 5000, Oulu FI-90014, Finland*

*elena@mail.ndhu.edu.tw*

Recent wide development of nanotechnologies and use of nanostructures in various applications requires analysis of their interaction with living systems in wide range of problems from bioapplications to nanosafety. In presented work the methods of 2-photon imaging and fluorescence lifetime imaging (FLIM), optical coherence tomography (OCT), fluorescence confocal imaging have been used for analysis of nanoparticles (NP) penetration into mice skin, biodistribution and influence on the tissue morphology.

Nanodiamonds (ND) of different average sizes in range from 5-10 nm for detonation nanodiamond (DND) to 100 nm prepared to the investigation and characterized by methods described somewhere else [1], with various structure and optical-spectroscopic properties, and Au NP of size 100 nm [2], have been used. The selection of the nanoparticles for this study was due to their applicability in biomedical researches. Number of diamond NP bio-imaging, bio-labeling, drug delivery and delivery tracing applications are suggested and developed, based on their fluorescence, surface and biocompatible properties [3]. Au NP together with their unique optical properties, related to the localized plasmon resonance resulting in an enhanced electromagnetic field at the metal nanoparticle surface, and attractive for imaging and sensing applications also have low toxicity, convenient surface for bioconjugation, stability in solvents and ideal size for delivery within the body [4].

Albino mice of CD1 strain were used in all experiments. The skin was shaved but no hair follicles were removed. The NP suspensions in physiological solution were applied on the skin surface and the samples were incubated for 48 h at 37°C and 5% CO<sub>2</sub>. After that the samples were fixed with 4% PFA. Using the method of optical coherence tomography (spectral-domain OCT, Thorlabs) the effect of the nanoparticles on optical (scattering) properties of the skin is discussed. Tissue-mimicking phantoms on base of PVC have been used to analyze 3D distribution of studied NP in 3D matrix for comparison with the skin model. For this comparison also an optical clearing was applied with benzyl benzoate and benzyl alcohol mixture (2:1) as clearing agent. As the ND reveal its fluorescence originated from defect color centers in diamond lattice [3] fluorescence confocal images were obtained using Zeiss LSM 780 Laser scanning confocal microscope (Zeiss) and confocal scanning microscope TCS SP5 (Leica) to observe the distribution of NP in the skin and to analyse the penetration and interaction mechanisms. Fluorescence lifetime imaging has been used both to visualise the NP in the skin and to analyse the skin conditions using the tissue autofluorescence. For FLIM an excitation has been used with Ti-sapphire laser (Chameleon Ultra, Coherent, USA), with excitation wavelength 800 nm; pulse duration 150 fs; repetition rate 80 MHz. The imaging has been performed with 2D scanner (EINST Technology). The registration was done with single photon counting system PicoHarp 300 (PicoQuant) and cooled PMT.

The penetration and effects of nanoparticles of different sizes and origin on tissues as well as a possibility to use these nanoparticles as potential imaging agent for applied imaging applications are discussed.

[1] P.H. Chung, E. Perevedentseva, J.S. Tu, C.C. Chang, C.L. Cheng, Spectroscopic study of bio-functionalized nanodiamonds, *Diam Relat Mater* 15, 622–625 (2006).

[2] O. Bibikova, A. Popov, A. Bykov, A. Prilepskii, M. Kinnunen, K. Kordas, V. Bogatyrevb, N. Khlebtsov, V Tuchin, Gold nanostructures for OCT imaging of capillary flow, *Proc. of SPIE*, 9129, 912930-9 (2014).

[3] E. Perevedentseva, Y.C. Lin, Mona Jani, C.L. Cheng, Biomedical Applications of Nanodiamond in Imaging and Therapy, *Future Medicine. Nanomedicine*, 8(12), 2041-2060 (2013)

[4] L.A. Dykman, N.G. Khlebtsov, Gold nanoparticles in biomedical applications: recent advances and perspectives, *Chem. Soc. Rev.* 41(6), 2256–2282 (2012).

## **PARTICULAR ASPECTS OF LASER-BASED PROCEDURES IN ENT**

M.A.Shakhova<sup>1</sup>, A.E.Meller<sup>2</sup>, D.Sapunov<sup>3</sup>, S.Gamayunov<sup>4</sup>, Yu.A.Rylkin<sup>1</sup>, A.V.Shakhov<sup>1</sup> and  
M.Yu.Kirillin<sup>5</sup>

<sup>1</sup>*State Medical Academy, 603000, Minin Sq.10/1, Nizhny Novgorod, Russia*

<sup>2</sup>*Volga District Medical Centre, 603001, Nizhnevolgskaya Emb., 2, Nizhny Novgorod, Russia*

<sup>3</sup>*Regional Hospital, 603126, Rodionov St., 190, Nizhny Novgorod, Russia*

<sup>4</sup>*Regional Oncologic Clinic, 603126, Rodionov St., 190, Nizhny Novgorod, Russia*

<sup>5</sup>*Institute of Applied Physics RAS, 603950, Uljanov St. 46, Nizhny Novgorod, Russia*  
*maha-shakh@yandex.ru*

Laser-based procedures (laser surgery and PDT) are the methods of choice in wide range of ENT pathologies. Laser surgery is applicable for treatment of several pathologies, in particular, early forms of malignant tumors. This choice is governed by the following features of laser application: minimizing intraoperative blood loss, prevention of secondary infection and adherence to the basic principle of oncology - ablastics [1]. Development and improvement of laser techniques allows to design new laser-based medical technologies. In recent decades, photodynamic therapy (PDT) was introduced into ENT. PDT is used in different clinical situations (tumor and non-tumor pathologies) in ENT area and it may substitute laser surgery [2]. Morphological and functional features of ENT determine the possibility of complications in case of improper choice of laser surgery and PDT mode [3]. This requires the development of monitoring techniques. In this study we demonstrate cases of complications of laser-based procedures and capability of optical coherence tomography (OCT) to real-time control and prediction of an undesirable outcomes.

Clinical cases of laser surgery and PDT are demonstrated, complications cases are analyzed. For laser surgery Alta®-ST at 0.98 μm (Dental Photonics, Inc) was employed. For PDT in this study the chlorine photosensitizers (PS) was used. Laser irradiation was done at the wavelength of 662 nm. OCT monitoring was performed with "OCT-1300U" modality (IAP RAS, BioMedTech Ltd., Nizhny Novgorod, Russia). OCT device specifications are following: probing wavelength is 1280 nm, in-depth resolution is 15 μm, lateral resolution is 30 μm, imaging rate is 8-10 frames per second, probing depth is up to 2 mm, replaceable endoscopic probe has 2.4 mm in diameter.

In results it is shown that:

- the greatest impact to the development of complications of laser-based procedures in ENT makes the presence of such morphological substrate as cartilage;
- OCT enables the detection of morphological and functional features of ENT area that may be predictors of complications;
- OCT allows in real time monitoring of the morphological and functional tissue changes during the procedure.

This phase of the study leads to the following conclusions:

- the proper choice of laser surgery and PDT regimes is the key for optimal clinical outcomes;
- real-time noninvasive control of laser-based procedures allows optimization and personification of treatment;
- the application of monitoring techniques requires further development and investigation.

### **Acknowledgements**

The authors thank the Russian Foundation for Basic Research (project 15-32-20250) for the financial support of this work and the hospital staff and management for the possibility to conduct this study.

### **References**

1. Zeitels SM, Burns JA, Lopez-Guerra G, Anderson RR, Hillman RE. Photoangiolytic laser treatment of early glottic cancer: a new management strategy. *Ann Otol Rhinol Laryngol Suppl.* V.199, pp. 3–24, (2008)
2. Bredell MG, Besic E, Maake C, Walt H. J Photochem Photobiol. The application and challenges of clinical PD-PDT in the head and neck region: a short review, V. 101(3), pp. 185-90, (2010)
3. Yan Yan, Aleksandra E. Olszewski, Matthew R. Hoffman, Peiyun Zhuang, Charles N. Ford, Seth H. Dailey, and Jack J. Jiang. Use of lasers in laryngeal surgery, *J Voice.* V. 24(1), pp. 102–109, (2010)

## **Multimodal optical coherence tomography for individualization cancer therapy**

N. Gladkova, M. Sirotkina, N. Buyanova, V. Elagin, M. Karabut, G. Gelikonov,  
M. Matveev, V. Zaitsev, F. Feldchtein, E. Zagaynova, and A. Vitkin

Despite considerable progress and impressive effectiveness of various non-invasive cancer treatments such as radiotherapy (RT) and chemotherapy (ChT), the clinical outcomes are quite variable because of the variation in individual patient responses [1]. If some convenient measurements from specific patients undergoing specific treatments could be made that report on treatment progress and response, these could be used to select responders from non-responders, alter ‘the doses’ for the remaining treatment, and in general optimize the therapies based on individual treatment feedback. Optical coherence tomography (OCT) is a promising novel bioimaging technique for detecting early treatment responses *in vivo* based on photonic technologies. Microscopy-like subsurface images of tissue microstructure and microvasculature are possible in living tissues using OCT. In the project, we are developing of OCT imaging technologies and performing preclinical and selected clinical studies to come up with quantifiable metrics of tumor and normal tissue responses to a variety of minimally invasive therapies.

Specifically, the OCT imaging platform consist of multiple modes of operation, including direct structural, polarization-sensitive (CP-OCT), angiographic (MA OCT), and elastographic regimes [2]. These will let obtain unique high-resolution images on tissue grade organization, connective tissue compartment, blood microcirculation, and tissue stiffness, respectively. The abilities of multimodal OCT will be tested preclinically on a series of normal and tumor-bearing mice undergoing ChT, RT, and photodynamic therapy (PDT) [3].

For example, the blood vessels network with abnormal shape and significant tortuosity was visualized by OCT angiographic on the 9 days after cancer cells inoculation. Immediately after PDT no changes in the vessels network were observed. But in 24 hours and 48 hours vessels network partly disappeared on the images. It was a reaction of blood vessels or microcirculation on PDT treatment. Histological analysis confirmed that the tumors had a good response to PDT. Among cellular component there were about 75% of irreversibly damaged cancer cells. On the other hand no visible tumor damage (burn, hyperemia) was observed during or after treatment. Unfortunately, we did not detect any visible changes in the OCT signal intensity or penetration depth on the initial and orthogonal polarization images after PDT. We suppose that quantitative analysis of CP-OCT images can help to reveal the differences between treated and untreated tumors.

**Conclusions** A series of treatment-specific multimodal OCT response metrics will be derived, and then tested in a series of further clinical pilot studies of PDT, RT and ChT in the oral cavity and skin of patients with cancers in these clinical sites. Initial results of this research will be highlighted in this presentation. It is hoped that the multimodal OCT technologies and treatment response metrics thus developed will help usher in the era of “personalized cancer medicine” of the 21<sup>st</sup> century.

### **Acknowledgements**

The design and manufacturing of multi-functional OCT scanner used in this study was supported by the grant no. 14.B25.31.0015 of the Russian Federation Government and the development of MA algorithm by RFBR grant 15-42-02513.

### **References**

1. S.Y. Yoo, J-S Kim, K.W. Sung, et al, *Cancer*, 119, 656-664 (2013)
2. V.Y. Zaitsev, V.M. Gelikonov, L.A. Matveev, et al, *Radiophysics and Quantum Electronics*, 57, 52–66 (2014);
3. B. Davoudi, M. Morrison, K. Bizheva, et al, *Journal of Biomedical Optics*, 2013, 18(7), 076008 (2013).

## TiO<sub>2</sub> and ZnO – Phthalocyanine Nanoparticles for Photodynamic Inactivation of Waste Water Bacterial Strains

**E. Borisova<sup>1</sup>, I. Angelov<sup>2</sup>, V. Mantareva<sup>2</sup>, V. Kussovski<sup>3</sup>, L. Avramov<sup>1</sup>**

*1 - Institute of Electronics, Bulgarian Academy of Sciences*

*72, Tzarigradsko chaussee Blvd., 1784, Sofia, Bulgaria*

*2 - Institute of Organic Chemistry with Centre of Phytochemistry, BAS*

*Acad. G. Bonchev, str., Bl. 9, 1113 Sofia, Bulgaria*

*3 - The St. Angeloff Institute of Microbiology, Bulgarian Academy of Sciences*

*Acad. G. Bonchev str., Bl. 26, 1113 Sofia, Bulgaria*

*e-mail: [borisova@ie.bas.bg](mailto:borisova@ie.bas.bg)*

The light exposure on a daily basis has been well accepted as a competitive method for decontamination of wastewater. The catalytic properties of TiO<sub>2</sub> and ZnO offer a great potential to reduce the transmission of pathogens in the environment. Although these oxides show a high activity against pathogens, their general usage in water cleaning is limited due to the insufficient excitation using natural light irradiation (few percents of the whole solar spectrum could be used for these two materials).

A hydrophobic dodecylpyridyloxy Zn(II)-phthalocyanine with four peripheral hydrocarbon chains of C12 (ZnPcDo) was immobilized on a photocatalyst TiO<sub>2</sub> and on ZnO particles. The resulted nanoparticles were characterized by the means of absorption, fluorescence and infrared spectroscopy. The laser scanning confocal fluorescence microscopy was used to visualize the phthalocyanine dye by the red fluorescence emission (650 – 740 nm). The intensive Q-band in the far red visible spectral region (~ 690 nm) suggested a monomeric state of phthalocyanine on the TiO<sub>2</sub> and ZnO nanoparticles. The water suspensions of the ZnPcDo-TiO<sub>2</sub> and ZnPcDo-ZnO were studied for photoinactivation of pathogenic bacteria associated with wastewater.

Two pathogenic bacterial strains (*methicillin-resistant Staphylococcus aureus - MRSA* and *Salmonella enteritidis*) associated with wastewater were photoinactivated with the suspension of the particles. The effective photoinactivation was observed with 1 g.L<sup>-1</sup> concentration of the materials at irradiation with UVA irradiation at 364 nm, as well with irradiation at 364 nm and 643 nm. The photodynamic inactivation efficiency is not cumulative from the effectiveness of the two compounds separately and a synergetic effect is observed. The proposed conjugates appear as useful composite materials for antibacterial disinfection.

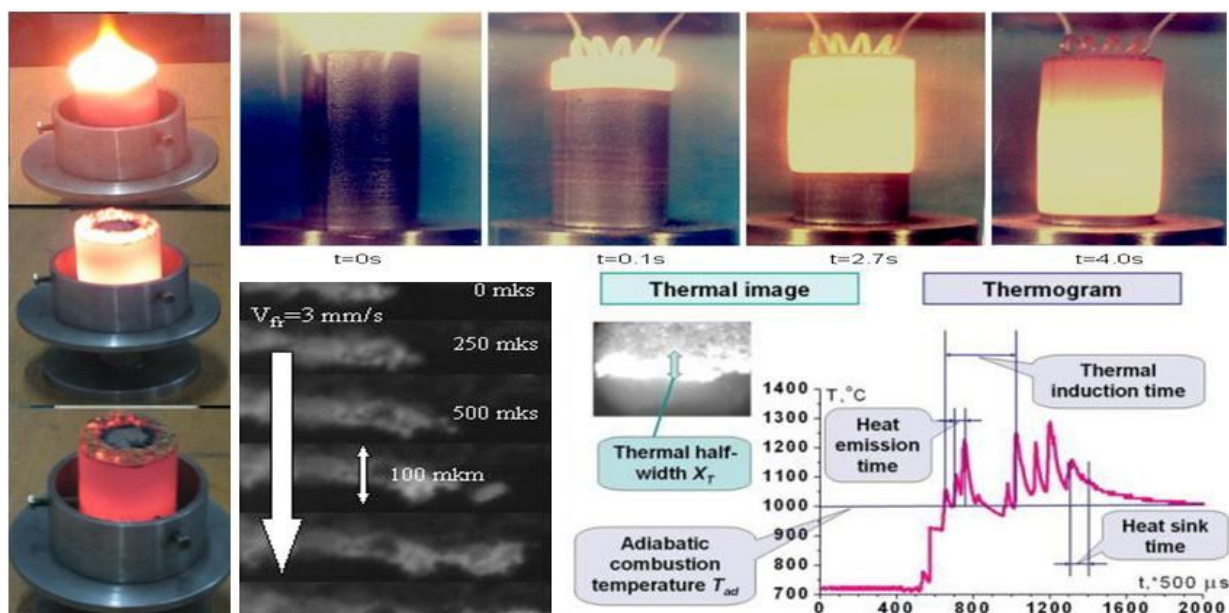
**Acknowledgements:** This work is supported in part by the National Science Fund of Bulgarian Ministry of Education and Science under grant #DFNI-B02/9/2014 “Development of biophotonics methods as a basis of oncology theranostics”, and in part under COST Action MP1302 “NanoSpectroscopy”.

## SHT-synthesis and application of biofunctional nanoparticles used high photo-thermal effect for laser heating of biotissues

Gulyaev P.Yu., Kotvanova M.K., Omelchenko A.I., Sobol E.N.

Optical properties of a number of the metal oxides of the transition group of elements are still interested for many applications. Metal oxide nanoparticles are widely used in the many electronic devices. Besides, these nanoparticles can be properly used in medicine. First of all, these are an absorber of EM radiation in thermal therapy, the carriers in targeted drug delivery, and contrast agents in diagnostics.

As shown [1], these nanoparticles demonstrate high absorption of laser radiation in the near IR spectral region. It opens a perspective for their use as biofunctional nanoparticles in laser diagnostics and healing of a damaged articular cartilage [2] and others hydrated biotissues. Selfpropagating–high-temperature–synthesis (SHT-synthesis) of biofunctional nanoparticles of a high photo-thermal laser effect on the hydrated biotissues has been presented. With use of super fast TV camera filming through a microscope registration of a burning wave has been made by video, and new results about evolution of thermal structure are shown on the following illustration.



Oxide bronzes of the composition:  $A_xO \cdot BO_y$ , where  $A=K, H, Na, B=Ti, Mo, W, 0 < x < 2, y=2, 3$  were prepared from the ultra dispersed metals by SHT-synthesis.

Iron oxide nanoparticles were synthesized in a high temperature oxidation of metallic iron in air. Ultra dispersed suspensions of iron oxide with oxide bronzes used for the biofunctional composite nanoparticles preparation by the method of mechanical activation in the planetary mill. Nano dispersed products were washed in distilled water and separated by size in centrifuge and aqueous chromatographic column.

Laser treatment of the nanoparticles in starch aqueous solution resulted in formation composite of magnet-controlled nanoparticles. These composite nanoparticles are stable in water relating to agglomeration and sedimentation.

Biofunctional nanoparticle aqueous solution has been used for impregnation in pig skin. These animals are filling well in the sun one month after our experiments.

Authors thanks Russian Foundation for Basic Research for financial aid in this work. Grant RFBR- 15-48-00106, 15-29-03811.

1. Gulyaev P.Yu., Kotvanova M.K., Pavlova S.S., Sobol E.N., Omelchenko A.I. *Nanotechnologies in Russia*, 2012, Vol. 7, № 3-4, pp.127-131.
2. Baum O.I., Golubev V.V., Omelchenko A.I., Sobol E.N., Shekhter A.B. *In: Materials of 3th Eurasian Congress on Medical Physics and Engineering «Medical Physics-2010», Moscow, 21-25 June 2010*. Vol.3, pp.222-224

## ***In vivo* assessment of components involved in signaling pathway responsible for non-photochemical quenching in cyanobacteria**

**E. Shirshin<sup>1</sup>, F. Kuzminov<sup>1,2</sup>, E. Maksimov<sup>3</sup>, V. Fadeev<sup>1</sup>**

1- *M.V. Lomonosov Moscow State University, Department of Physics, 119991, Leninskie gory 1/2, Moscow, Russia*

2- *Department of Marine and Coastal Sciences, Rutgers University, New Brunswick, NJ, 08901 USA*

3 - *M.V. Lomonosov Moscow State University, Department of Biology, 119991, Leninskie gory 1/12, Moscow, Russia*

*shirshin@lid.phys.msu.ru*

Non-photochemical quenching in cyanobacteria is an example of a self-regulating system responsible for high light tolerance. *In vitro* experiments [1] confirmed that the minimum set of components required for the proper functioning of this system includes (i) a sensor of light – molecules of photoactive Orange Carotenoid Protein (OCP), (ii) the target (an object of quenching) – light harvesting antennae, phycobilisomes (PBs), and (iii) a protein responsible for the OCP cycling (detachment of OCP from PBs) – Fluorescence Recovery Protein (FRP). Briefly, upon the absorption of a blue-green light quantum, OCP is converted to the active (signaling) conformational state, which is capable of binding to PBs. As a result, the excess excitation energy is effectively transferred from PBs to OCP preventing overexcitation of the photosynthetic reaction center of photosystem II in cyanobacteria and, consequently, reducing formation of the reactive oxygen species. In darkness, OCP detaches from PBs, hence, fluorescence recovery of PBs takes place. This process is significantly accelerated by FRP molecules that are involved in both detachment of OCP from the PBs and its conversion to the stable (non-signaling/non-active) form.

Here, we present a detailed study of the kinetics of fluorescence recovery of the phycobilisomes. We demonstrate that the fluorescence recovery process is nonlinear and shows enzyme catalysis-like behavior, where FRP serves as an enzyme, PBs-OCP complex as a substrate and the stable non-active OCP form as a product. The analysis of the recovery kinetics with the presented mathematical model suggests that the functioning of the system involves product inhibition. Using kinetics of the fluorescence recovery, we also developed an approach to determine relative concentrations of the components involved in NPQ *in vivo*. The obtained results allow for better understanding of the regulatory mechanisms responsible for the proper cycling of the molecular elements involved in NPQ in cyanobacteria.

[1] M. Gwizdala, A. Wilson and D. Kirilovsly, *In vitro* reconstitution of the cyanobacterial photoprotective mechanism mediated by the Orange Carotenoid Protein in *Synechocystis* PCC 6803, *The Plant Cell*, vol. 23(7), pp. 2631-2643, (2011).

## **Keratin fluorescence in ecological monitoring of house dust**

**O.V. Proskurina, E.A. Shirshin**

*M.V. Lomonosov Moscow State University, Department of Physics, 119992, Leninskie gory 1/2, Moscow, Russia*

*E-mail address: [olgavproskurina@gmail.com](mailto:olgavproskurina@gmail.com)*

Respirable dust is one of the sources of pathogenic bacteria and toxic compounds. As reported [1], one of the main sources of dust in occupied rooms is shed human skin. Human skin flakes are often responsible for contamination and infection spreading because of microorganisms attached to them. On the other hand, human skin flakes are digested by fungi and dust mites that may be a cause of allergy and asthma [2]. So, monitoring of skin cell content in house dust is a necessary step in ecology control of dwellings and health care.

Skin cells consist of more than 80% keratins cross linked to other cornified proteins. Keratin from human skin cells is the major protein component of indoor airborne dust [3]. So, keratin concentration in dust can be used as an indicator of indoor bacterial contamination. The main goal of the current research was to develop a rapid express method for the determination of keratin content in house dust for detection of bacterial or allergen indoor contamination or dust state in occupied rooms. From the numerous works which deal with fluorescence of human skin, it is known that keratin exhibits fluorescence when excited in the UV region of spectrum (at ca 350 nm). However, this fluorescence is different from the tryptophan fluorescence and is due to the presence of specific fluorophores, e.g., fluorescent cross-linkings in the protein structure. Here, we made an attempt to separate the contribution of keratin fluorescence to the overall signal of house dust.

Dust from volunteers' Moscow homes and office rooms was used for the investigation. Water extracts of sieved fine dust were used to measure fluorescence signal and protein concentration.

Dust extract fluorescence spectra obtained upon 275 nm excitation exhibited two major peaks with its maxima near 350 nm and 420 nm, neither of which correlated with total protein concentration in the samples determined using Lowry assay. At the same time, we observed that the spectral band shape of fluorescence emission of house dust obtained at 350 nm excitation was similar for all the samples under investigation. Further investigation showed that this band shape was typical for keratins from different sources. Moreover, the fluorescence intensity obtained upon 350 nm excitation exhibited linear correlation with the total protein content in dust. As for keratin is an insoluble fibrillar protein, in order to increase its concentration in dust extract proteinase K was used. When dust samples and human keratin were treated with proteinase K with mercaptoethanol, the increase of fluorescence intensity of extracts was found, while the spectral band shape remained similar. It was also shown that the peak of dust fluorescence at 275 nm excitation was due to the impacts of raw keratin and hydrolyzed keratin.

As a result, it was shown that dust fluorescence may be used to measure keratin content, hence, it could be a promising indicator of indoor microbial and allergen exposure.

[1] A. Fox, W. Harley, C. Feigley, D. Salzberg, C. Toole, A. Sebastian, & L. Larsson, Large particles are responsible for elevated bacterial marker levels in school air upon occupation. *Journal of Environmental Monitoring*, 7(5), 450-456, (2005).

[2] Colloff, Matthew J. "Dust mites." (2009).

[3] K. Fox, E. Castanha, A. Fox, C. Feigley, & D. Salzberg, Human K10 epithelial keratin is the most abundant protein in airborne dust of both occupied and unoccupied school rooms. *Journal of Environmental Monitoring*, 10(1), 55-59, (2008).

## **SDS binding as a tool for indication of albumin conformational changes in human blood plasma**

**N. Zhdanova<sup>1</sup>, E. Shirshin<sup>1</sup>, V. Fadeev<sup>1</sup>, A. Priezzhev<sup>1,2</sup>**

*1- M.V. Lomonosov Moscow State University, Department of Physics, 119991, Leninskie gory 1/2, Moscow, Russia*

*2- International Laser Center of M.V. Lomonosov Moscow State University, 119991, Leninskie gory 1/62, Moscow, Russia*

*zhdanova@physics.msu.ru*

Conformational changes of blood plasma proteins may cause a failure of its functional properties and lead to different diseases. Among all plasma proteins human serum albumin (HSA) is the most studied one as it is the major transport protein capable of binding a wide variety of ligands, especially fatty acids. Conformational changes of albumin can be revealed in structural changes in the vicinity of binding sites, that allows one to use binding parameters as an indicator of conformational changes of protein macromolecule (e.g. metal binding assay in case of ischemic disease [1]). To achieve better results, the chosen ligand should have several specific binding sites that are located uniformly in protein structure.

In the case of albumin, fatty acids (FAs) can be used for this purpose as there are from 6 to 9 binding sites (depending on the type of FA) in albumin structure [2]. It should be noted that the binding parameters of spin-labeled FAs in human blood plasma are used to indicate different pathologies using the ESR technique [3]. This method is based on the fact that spin-labeled FAs binds specifically (with a high binding affinity) to HSA and other types of proteins (e.g., immunoglobulin gamma (IgG)) don't interact with it.

Another ligand which induces a wide range of conformational changes in HSA and can simulate binding of FAs to HSA is sodium dodecyl sulfate (SDS) [4]. Alterations in parameters of SDS-HSA binding were chosen in this work to indicate HSA conformation in blood plasma.

In this paper, SDS binding properties in blood plasma samples as well as in model solutions (HSA aqueous solution, IgG aqueous solution, mixed HSA and IgG aqueous solution – the so-called synthetic plasma) were determined by means of tyrosine (Tyr) fluorescence contribution to the whole intrinsic fluorescence of the investigated samples. In contrast to tryptophan (Trp), Tyr is distributed more uniformly in the HSA structure that allows one to detect its conformational changes far from the single Trp residue [5]. We showed [5] that Tyr fluorescence allows detection of SDS binding to the specific FA sites, whereas Trp fluorescence is constant in the corresponding range of SDS concentrations.

Here, we compared Tyr fluorescence of blood samples as a function of SDS concentration with that of aqueous solution of the main plasma proteins (HSA and IgG) as well as that of artificial plasma. Based on the obtained results, we concluded that at low SDS concentrations (less than critical micelle concentration) the changes in Tyr fluorescence can be explained by binding SDS to the specific binding sites of HSA, while IgG seems not to contribute the observed signal. This fact allows one to use the dependence of Tyr fluorescence on SDS concentration as a tool for monitoring albumin conformational changes in blood plasma.

[1] G. Fanali, A. di Masi, V. Trezza, M. Marino, M. Fasano, and P. Ascenzi, Human serum albumin: from bench to bedside, *Molecular aspects of medicine*, 33(3), 209-290 (2012).

[2] A. A. Bhattacharya, T. Grüne, and S. Curry, Crystallographic analysis reveals common modes of binding of medium and long-chain fatty acids to human serum albumin. *Journal of molecular biology*, 303(5), 721-732, (2000).

[3] V. Muravsky, T. Gurachevskaya, S. Berezenko, K. Schnurr, and A. Gurachevsky, Fatty acid binding sites of human and bovine albumins: Differences observed by spin probe ESR. *Spectrochimica Acta - Part A: Molecular and Biomolecular Spectroscopy*, 74(1), 42-47, (2009).

[4] E. L. Gelamo, C. H. T. P. Silva, H. Imasato, and M. Tabak, Interaction of bovine (BSA) and human (HSA) serum albumins with ionic surfactants: spectroscopy and modelling. *Biochimica et Biophysica Acta (BBA)-Protein Structure and Molecular Enzymology*, 1594(1), 84-99 (2002).

[5] N.G. Zhdanova, E.A. Shirshin, E.G. Maksimov, I.M. Panchishin, A.M. Saletsky, and V.V. Fadeev, Tyrosine fluorescence probing of the surfactant-induced conformational changes of albumin. *Photochemical & Photobiological Sciences*, 14(5), 897-908, (2015).

---

---

**SECTION D**

**Laser Diagnostics and Spectroscopy**

---

---

## Raman scattering and time-resolved measurements: a review of recent applications with a nanosecond laser

P. Simon<sup>1</sup>, A. Canizarès<sup>1</sup>, M.R. Ammar<sup>1</sup>, G. Guimbretière<sup>1</sup>, Y. Tobon<sup>1</sup>,  
E.S Fotso Gueutue<sup>1</sup>, M. Dutreilh-Colas<sup>2</sup>, O.A. Maslova<sup>1,3</sup>, N. Raimboux<sup>1</sup>, F. Duval<sup>1</sup>,  
Y.I. Yuzyuk<sup>3</sup>, R. Mohun<sup>4</sup>, L. Desgranges<sup>4</sup>, M. Magnin<sup>5</sup>, C. Jégou<sup>5</sup>

1- CNRS UPR 3079 CEMHTI, and Université d'Orléans, 45071 Orléans Cedex 2, France

2- Centre Européen de la Céramique, SPCTS-UMR CNRS6638, 87068 Limoges Cedex,

France 3- Faculty of Physics and Research Institute of Physics, Southern Federal University, 5,

Rostov-on-Don, 344090, Russia

4- CEA/DEN/DEC Cadarache, 13108 Saint-Paul-lez-Durance Cedex, France

5- CEA/DEN/DTCD Marcoule, 30207 Bagnols-sur-Cèze Cedex, France

simon@cnrs-orleans.fr

Raman scattering spectroscopy is well-known to be a powerful experimental method for investigating matter under its various states, solid, liquid or gaseous. The most often Raman analyses are performed in continuous mode, with a continuous-wave laser and a detector (generally a CCD camera) able to give time resolution limited down to  $10^{-1}$  -  $10^{-2}$ s. The availability of intensified CCD cameras, for some fifteen years now, has opened a new field of investigations in Raman scattering, giving access to time resolution down to the nanosecond range with adapted pulsed lasers. In this time range only relatively limited modifications of a continuous Raman device are needed, compared to more specific setups in the picosecond range. The interest of time-resolved Raman spectroscopy is mainly to probe transient species (reactive molecules or excited electronic states), but it can also separate optical phenomena of very different time scales and then allow to obtain Raman data in conditions where continuous Raman is unsuccessful. These potentialities will be shown through a review of some recent studies, after a detailed presentation of the experimental set-up.

The first example deals with Raman scattering on excited electronic states of ruby ( $\text{Al}_2\text{O}_3:\text{Cr}^{3+}$ ), where it was possible to measure the time constant of Raman emission from the electronic doublet responsible from the red emission characteristic of Ruby [1].

Luminescence is often a difficulty for acquiring Raman data as its intensity is generally much higher. But fortunately the time characteristics of Raman (<ns range) and luminescence (from ns to very long times, up to some hours sometimes) can allow to separate them. The cases of ruby and zirconia will be presented.

Besides luminescence, other long-lasting optical emissions can also be a problem for Raman acquisition. The case of high temperatures, where thermal emission can be some orders of magnitude greater than Raman, will be discussed in details. Continuous Raman spectroscopy becomes delicate above 1000-1200°C; examples will be shown on zirconia above 2000°C, and on ageing effects of silica around its glass temperature (1000-1400°C) [2,3].

Other case of long-lasting light is the stray light in field measurements, outside the laboratory, with major interest in Earth sciences.

As perspectives, we intend to apply these methods of time-resolved spectroscopy for detecting transient phenomena on an *in situ* Raman device recently instrumented on a cyclotron accelerator [4-5], mainly devoted to materials for nuclear applications. The ion beam can be pulsed, and then one can access to transient molecular or electronic species created by irradiation. First results on time-resolved ionoluminescence on silica will be presented.

[1] Y.A Tobon, D. Bormann, A. Canizarès, N. Raimboux, P. Simon, Time-resolved Raman studies on  $\text{Al}_2\text{O}_3:\text{Cr}^{3+}$ : lifetime measurements of the excited-state transition  $\tilde{E} \rightarrow 2\tilde{A}$ , *J. Raman Spectr.*, 42, pp. 1109-1113 (2011).

[2] P. Simon, B. Moulin, E. Buixaderas, N. Raimboux, E. Herault, B. Chazallon, H. Cattey, N. Magneron, J. Oswald, D. Hocrelle, High temperatures and Raman scattering through pulsed spectroscopy and CCD detection, *J. Raman Spectr.*, 34, pp. 497-504 (2003).

[3] M. Dutreilh-Colas, A. Canizarès, A. Blin, S. Ory, P. Simon, *In situ* Raman diagnostic of structural relaxation times of silica glasses, *J. Am. Ceram. Soc.*, 94, pp. 2087-2091 (2011).

[4] A. Canizarès et al., *In situ* Raman monitoring of materials under irradiation: study of uranium dioxide alteration by water radiolysis, *J. Raman Spectr.*, 43, pp. 1492-1497 (2012).

[5] G. Guimbretière, L. Desgranges, A. Canizarès, R. Caraballo, F. Duval, N. Raimboux, R. Omnée, M. R. Ammar, C. Jégou, P. Simon, *In situ* Raman monitoring of  $\text{He}^{2+}$  irradiation-induced damage in a  $\text{UO}_2$  ceramic, *Appl. Phys. Lett.*, 103, pp. 041904/1-4 (2013).

## **Nano-composite materials and their applications in energy harvesting**

**S. Christiansen<sup>1,2,3</sup>, G. Sarau<sup>1,3</sup>, S. Schmitt<sup>1,3</sup>, M. Latzel<sup>3</sup>, M. Bashouti<sup>3</sup>, M. Heilmann<sup>3</sup>,  
Ch. Tessarek<sup>1,3</sup>, S. Jäckle<sup>1,3</sup>, M. Kulmas<sup>3</sup>, Th. Feichtner<sup>1,3</sup>, K. Höflich<sup>1,3</sup>, B. Rech<sup>1</sup>**

*1- Helmholtz-Zentrum for Materials and Energy, Berlin, Germany*

*2- Free University, Berlin, Germany*

*3 - Max Planck Institute for the science of light, Erlangen, Germany*

[silke.christiansen@mpl.mpg.de](mailto:silke.christiansen@mpl.mpg.de)  
[silke.christiansen@helmholtz-berlin.de](mailto:silke.christiansen@helmholtz-berlin.de)

We will report on novel nano-patterned composite materials for energy harvesting and their characterization based on correlated microscopies / spectroscopies. We rely on a wealth of nano-composites composed of silicon (Si) as well as GaN nanowires (NWs) or nanocones (NCs), complex gold and silver plasmonic nano-particles, few layer graphene and transparent conductive oxide layers all realized by a combination of wet chemical solution processing and vapor phase deposition methods. NWs and particles show a large surface area that can chemically be functionalized to account for surface passivation or functionality. Examples of how nano-composites will be formed and utilized in energy harvesting applications will be provided. The backbone of our devices are Si and GaN NWs and NCs for which optical modes can be controlled and efficient absorption of solar light can as much be tuned as light emission in light emitting diodes (LEDs) or laser devices. The integration of NWs or NCs in thin film solarcell concepts and LEDs will be demonstrated together with novel graphene or AgNW webs based electrodes. Correlated electron microscopy and spectroscopy techniques will be used to optimize device performance and to infer from properties of individual 3D nanoarchitectures properties of large area devices.

- [1] G. Shalev, S.W. Schmitt, G. Brönstrup, S.H. Christiansen, Enhanced photovoltaics inspired by the Fovea Centralis, Nature Scientific Reports 5, 8570 (2015). doi:10.1038/srep08570
- [2] G. Shalev, S.W. Schmitt, G. Brönstrup, S.H. Christiansen, Maximizing the ultimate absorption efficiency of vertically-aligned semiconductor nanowire arrays with wires of a low absorption cross-section photovoltaics, nano energy 12, 801 (2015).

# **Optical characterization of nanostructures and thin films for solar cells applications**

**J. P. Leitão**

*Department of Physics and I3N, University of Aveiro, Campus Universitário de Santiago, Aveiro, 3810-193 Aveiro, Portugal*

The improvement of the performance of solar cells requires the continuous search for new materials as well as the investigation of its fundamental properties. The analysis of optical properties is relevant since it contributes decisively to the understanding of the electronic energy levels structure of the semiconductor. Photoluminescence is well suited for that purpose because it allows the investigation of radiative and non-radiative recombination channels. In particular, these studies allow us to evaluate the role of defects of structural origin or created by intentional doping.

GaAs nanowires and Cu<sub>2</sub>ZnSnS<sub>4</sub> based thin films are very promising materials for solar cells applications due to their high absorption coefficients and bandgap energy values close to the optimal value for this type of devices. In the first case, we will discuss how the occurrence of structural defects determines the radiative recombination mechanisms [1,2]. The parameters that characterize the luminescence, like activation energies and rate shift of the luminescence under the increase of the excitation power, is related with the structural properties of the nanowires. The type-II radiative recombination involving electrons and holes in segments with different crystalline phases is shown. The influence of the substrate, GaAs(111)B or Si(111), is observed on both structural and optical properties. Concerning the case of Cu<sub>2</sub>ZnSnS<sub>4</sub> based thin films, the huge influence on the electronic energy levels structure of the semiconductor of the increase of the doping level, is discussed. For heavily doped materials, electrons are free or bound to large donor agglomerates which hinder the involvement of single donors in the radiative recombination channels. This lead us to a quite different description of the electronic properties commonly observed for lightly doped semiconductors where the occurrence of fluctuating potentials along the film must be considered [3,4]. The radiative recombination channels can involve tails states in the forbidden gap as well as acceptor defects.

[1] B. P. Falcão, J. P. Leitão, M. R. Correia, M. R. Soares, F. M. Morales, J. M. Manuel, R. Garcia, A. Gustafsson, M. V. B. Moreira, A. G. de Oliveira and J. C. González, Structural and optical characterization of Mg-doped GaAs nanowires grown on GaAs and Si substrates, *J. Appl. Phys.* vol. 114, pp. 183508 (12 pages) (2013).

[2] B. P. Falcão, J. P. Leitão, M. R. Correia, M. P. Leitão, M. R. Soares, M. V. B. Moreira, A. G. de Oliveira, F. M. Matinaga and J. C. González, New insights into the temperature-dependent photoluminescence of Mg-doped GaAs nanowires and thin films, *J. Mater. Chem. C*, vol. 2, pp. 7104-7110 (2014).

[3] J. P. Teixeira, R. A. Sousa, M. G. Sousa, A. F. da Cunha, P. A. Fernandes, P. M. P. Salomé and J. P. Leitão, Radiative transitions in highly doped and compensated chalcopyrites and kesterites: The case of Cu<sub>2</sub>ZnSnS<sub>4</sub>, *Phys. Rev. B*, vol. 90, pp. 235202 (10 pages) (2014).

[4] J. P. Teixeira, R. A. Sousa, M. G. Sousa, A. F. da Cunha, P. A. Fernandes, P. M. P. Salomé, J. C. González and J. P. Leitão, Comparison of fluctuating potentials and DAP transitions in a Cu-poor Cu<sub>2</sub>ZnSnS<sub>4</sub> based solar cell, *Appl. Phys. Lett.*, vol. 105, pp. 163901 (4 pages) (2014).

## Laser spectroscopy of QW-based low dimensional structures for optoelectronic applications

**N. Ben Sedrine<sup>1</sup>, J. Rodrigues<sup>1</sup>, L. Rino<sup>1</sup>, A. J. Neves<sup>1</sup>, M. C. Sequeira<sup>2</sup>, K. Lorenz<sup>2</sup>, E. Alves<sup>2</sup>, P. R. Edwards<sup>3</sup>, K. P. O'Donnell<sup>3</sup>, M. Bockowski<sup>4</sup>, O. Mauguin<sup>5</sup>, J.-M. Jancu<sup>6</sup>, J. C. Harmand<sup>5</sup>, P. Voisin<sup>5</sup>, M. R. Correia<sup>1</sup>, and T. Monteiro<sup>1</sup>**

<sup>1</sup>*Departamento de Física e I3N, Universidade de Aveiro, 3810-193 Aveiro, Portugal*

<sup>2</sup>*IPFN, Instituto Superior Técnico, Campus Tecnológico e Nuclear, Bobadela LRS, Portugal*

<sup>3</sup>*SUPA Department of Physics, University of Strathclyde, Glasgow, G4 0NG, Scotland, UK*

<sup>4</sup>*Institute of High Pressure Physics, Polish Academy of Sciences, 01-142 Warsaw, Poland*

<sup>5</sup>*CNRS-LPN Laboratory of Photonic & Nanostructures, F-91460 Marcoussis, France*

<sup>6</sup>*Université Européenne Bretagne, CNRS, FOTON INSA Rennes, F-35708 Rennes, France*

*nbensedrine@ua.pt*

Since the successful development of quantum well lasers in the 1970s, one of the richest areas of application of semiconductor nanostructures has been in the area of optoelectronic devices, with the two most important areas being semiconductor lasers and detectors [1]. The most widely used semiconductors for optoelectronic applications are the compounds formed by group III and group V elements. Thanks to the nowadays-reached expertise in growth and in post-growth techniques, tailoring the semiconductors properties has become possible for achieving the desired applications. More specifically, quantum well (QW) III-V semiconductor heterostructures are playing a major role in such applications. For instance, GaAs and related compounds are mostly used for optical fiber communications, near infra-red and visible light emitting diodes (LEDs) as well as laser diodes (LDs). In the short wavelength range, the GaN and their alloys are important for light emitters in solid state lighting systems. In this work, we present our recent results, obtained by photoluminescence (PL) and micro-Raman spectroscopy on low dimensional QW structures grown by *i*) molecular beam epitaxy (MBE) material engineering for the Ultrashort-period superlattices (USPSL) InGaAs/AIP, and *ii*) metalorganic chemical vapour deposition (MOCVD) for the InGaN/GaN multi-QWs and subject to post-growth treatments by thermal annealing.

USPSL zinc-blende materials sharing no-common atom are good candidates for cubic semiconductor-based frequency conversion devices due to their interesting potential for phase matching over long distances. Successful growth of high quality In<sub>0.5</sub>Ga<sub>0.5</sub>As/AIP USPSL structures on GaAs substrate was achieved by MBE [2]. The knowledge of the optical and vibrational properties of these structures is of utmost importance for such applications; however, no information exists so far. We have found that the USPSL still obeys to first order Raman selection rules, and does not contain a high level of structural disorder, in addition the different optical phonons: disorder-activated, GaAs-, InP-, GaP-, and AIP-like LO phonons were identified.

The invention of efficient blue LEDs has led to white light sources for illumination [3]: when exciting a phosphor material with a blue LED, light is emitted in the green and red spectral ranges, which, combined with the blue light, appears as white. Here we demonstrate laser-induced white light emission from a single monolithic InGaN/GaN quantum well-based LED structure grown by MOCVD. As-grown and thermally annealed samples at HTHP were analysed by spectroscopic techniques, and the annealing effect on photoluminescence is deeply explored. Moreover, the control of the yellow/blue bands intensity ratio, responsible for the white emission, could be achieved after annealing at 1000 °C.

[1] Semiconductor Nanostructures for Optoelectronic Applications, Todd Steiner ARTECH HOUSE, INC, Chapter 1 (2004).

[2] J.-M. Jancu, A. Vasanelli, R. Magri and P. Voisin, Phys. Rev. B, 69, 241303(R) (2004).

[3] The Nobel Prize in Physics 2014 [http://www.nobelprize.org/nobel\\_prizes/physics/laureates/2014/](http://www.nobelprize.org/nobel_prizes/physics/laureates/2014/).

# Enhanced photon lifetime in silicon nanowire arrays and increased efficiency of optical processes in them

A. Efimova, A. Eliseev, L. Golovan, M. Kholodov, D. Presnov, A. Tkachev, S. Zobotnov, and P. Kashkarov

Lomonosov Moscow State University, Moscow, 119991, Russia  
efimova@vega.phys.msu.ru

Arrays of silicon nanowires (SiNW) are of great interest due to their unique optical properties and enhanced optical interactions in them [1]. The arrays formed by means of metal-assisted chemical etching consist of columnar silicon (Si) structures of 100–2000 nm in diameter and length ranging from 0.5 to 50  $\mu\text{m}$  (Fig.1).

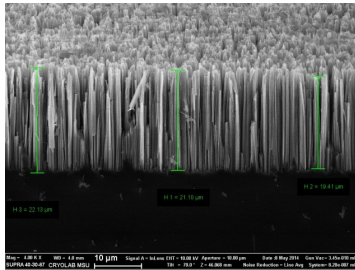


Fig. 1. SEM image of a 23  $\mu\text{m}$  thick SiNW layer

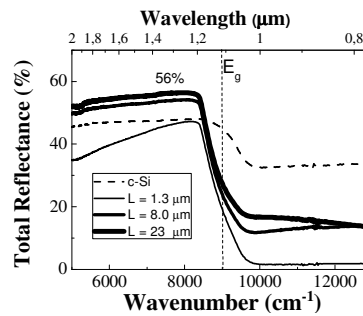


Fig. 2. Total reflectance spectra of SiNW layers of different thickness. Vertical dashed line indicates the band gap of c-Si

The SiNW arrays demonstrate effective light scattering. Below the Si band gap, the thick layers exhibit total reflection exceeding the one of crystalline silicon, whereas above the Si band gap the thin SiNW layers have properties of black silicon [1] (Fig.2). The light propagation in SiNW arrays is described in the frames of diffusion approximation with proper account of inner reflection on the interfaces [2].

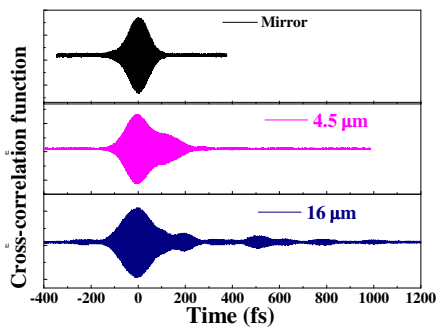


Fig. 3. Cross-correlation function in reflection

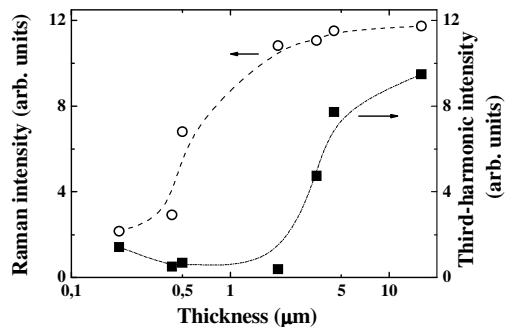


Fig. 4. Raman and third harmonic intensities vs SiNW layer thickness

Along with diffuse reflectance, cross-correlation of the scattered radiation function duration (Fig.3), Raman and third harmonic (TH) signals (Fig.4) grow up with SiNW length increase in the region under study. The second effect can be explained by weak light localization inside mesoscopic structure of SiNW arrays due to multiple scattering. In its turn this phenomenon leads to an order of magnitude increase in Raman and TH signals. Hence we observe the correlation between the photon life-time and Raman and TH efficiency in SiNWs.

The work was supported by the RFBR Grant 15-29-01185.

[1] L. Osminkina, K. Gonchar, V. Marshov, et al, Optical Properties of Silicon Nanowire Arrays Formed by Metal-Assisted Chemical Etching: Evidences for Light Localization Effect, *Nanoscale Research Letters*, vol. 7, pp. 524-530, (2012).

[2] O.L. Muskens, J.G. Rivas, R.E. Algra, et al, Design of Light Scattering in Nanowire Materials for Photovoltaic Applications, *Nano Letters*, vol. 8, N. 9, pp. 2638-2642, (2008).

# Measurement of $^{13}\text{CO}_2/^{12}\text{CO}_2$ ratio in the natural air by means of diode laser spectrometer with external optical cavity

I.V.Nikolaev<sup>1</sup>, V.N.Ochkin<sup>1</sup>, S.N.Tskhai<sup>1</sup>, A.A.Zaytsev<sup>1,2</sup>

<sup>1</sup>*P. N. Lebedev Physical Institute, Russian Academy of Sciences, Leninsky pr. 53, 119991 Moscow, Russia*

<sup>2</sup>*Institute of Physics and Technology (State University), Institutskii per. 9, 141700 Dolgoprudnyi, Moscow region, Russia*

e-mail: [ochkin@lebedev.ru](mailto:ochkin@lebedev.ru)

The knowledge of stable carbon  $^{13}\text{C}/^{12}\text{C}$  isotope ratio is needed in many areas of nature, life and technology. In most cases of practical measurements this ratio strictly follows the ratio  $\gamma = ^{13}\text{CO}_2/^{12}\text{CO}_2$  with  $^{16}\text{O}$  in the form of  $\delta^{13}\text{C} = ((\gamma/0.011237) - 1) \cdot 1000 \text{‰}$  [1].

Traditionally this information can be obtained with the help of high resolution mass-spectrometry in some cases combined with gas chromatography. Because of the complexity of such technique, its costs, low mobility, necessity to manage the special technique of probe preparation and some other specific features motivated the alternative trend with the use of laser spectroscopy.

The most of studies and developments have been concentrated at the problem of the human breath isotopic analysis. According to the medical standards the accuracy of  $\delta$  measurements has to be not more than  $\Delta\delta \leq 0.5\text{‰}$ . In some works on laser absorption spectrometry this accuracy has been improved (0.07‰ [2]).

When talking about this success it is necessary to mention that in the specific case of human breath the exhaled gas contain a large amount of  $\text{CO}_2$  molecules about 3% which is a lucky factor for the absorption measurements. In [2] the simple Herriott cell provided the enough optical pass  $\sim 20\text{m}$  for the optical transitions near  $2 \mu\text{m}$ .

The same time in the open atmosphere this fraction is of two order less  $\sim 0.03\%$  so much less absorption has to be measured. There are a lot of practical problems related to the isotopic analysis of the open atmosphere (environment, food control, agriculture technologies...). To our knowledge we perform such optical measurements at a first time. Taking into account the experience of work [2] we implemented the following main points:

- we kept the scheme of measurements based on the comparison of the measured and simulated absorption spectra include the temperature and gas pressure control (regression scheme);
- we used much weaker (2 orders) molecular optical transitions near  $1.6 \mu\text{m}$  to get the absorption coefficients for different isotopes more comparable in the range of laser frequency tuning;
- we used the fiber based optical scheme and high quality optical cavity with effective optical lengths  $\sim 5\text{km}$  to enhance the weak absorption.

The approach above justified itself. Fig.1 shows the detected and simulated adsorption spectra in open atmosphere. Due to the system stability and statistics the accuracy of isotopic ratio measurements is high enough. In our laboratory air  $\delta^{13}\text{C} = -8.2 \pm 0.3\text{‰}$ . To get this accuracy the 1h signal acquisition time is needed.

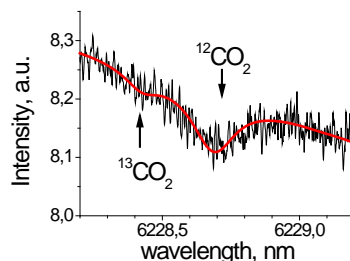


Fig.1. Measured and simulated absorption spectra

The work was supported by the Russian Scientific Foundation (project 14-12-00784).

[1] В.Н.Очкин. Задачи и методы оптики для диагностики объектов по относительному содержанию стабильных изотопов. М.:ФИАН, 84с., (2012)

[2] S.N. Andreev, E.S. Mironchuk, I.V. Nikolaev, V.N. Ochkin, M.V. Spiridonov, S.N. Tskhai, High precision measurements of the  $^{13}\text{CO}_2/^{12}\text{CO}_2$  isotope ratio at atmospheric pressure in human breath using a  $2 \mu\text{m}$  diode laser, Appl Phys B 104, pp.73–79, (2011)

## **Self-organization and crystallization of dust plasma**

**Vladislav I.Pustovoit**

*Scientific and Technological Centre of Unique Instrumentation of RAS, 15 str., Butlerova, 117342 Moscow  
(vladpustovoit@gmail.com)*

The physical base of self-organization and appearance of ordered structures (crystallization) in dust bounded plasma was built-up. It is considered that dust plasma in stationary i.e. in a state non-dependent on time, is described by hydrodynamic equations, in which time derivatives are omitted, and besides all processes of electrons capture and ejection from dust particle came to stationary state, and that is why continuity equation does not contain them. Under these suggestions from hydrodynamic equations of charged medium three-dimension equations for electrostatic potential (inhomogeneous Helmholtz equation) were obtained. Right part of the obtained equation contains source, which is determined by plasma hydrodynamic properties (flows character, laminar or vortex flow, availability of flow, collisions etc.). Further, solutions obtained from Helmholtz equation for electrostatic potential, in which considerable role is played by boundary conditions on plasma outer boundary (Dirichlet or Neumann), were found. The obtained particular expressions for electrostatic potential, which under certain conditions, pointed out in the work, contain extrema, in which according to laws of electrostatics charged dust particles are located. Spatial position of electrostatic potential extrema form 3D, 2D or 1D structure, that means appearance of ordering or occurrence of crystal structure in plasma. General expressions for spatial position of extrema were obtained and criterion of such structure destruction was suggested. The essence of this adds up to the following. Visible structure will be destroyed if energy depth or height of extremum, in which charged particle of dust is located, will be substantially smaller of thermal energy of the particle of dust itself. Asymptotic expressions for potential both for plasma with small and large dimensions were found.

There are many experiments' in which by scanner laser illuminate observe self-organization dust plasma. The created theory allows to explain this many phenomena of self-organization, being observed in experiments and opens possibility of their theoretical description.

creating the conditions for managed self-managed. The latter is important to create technology a meta-materials for optics and electronics

## **Measurements of aerosol drug deposition using optical methods**

**M. Veres, I. Rigó, L. Himics, T. Verebélyi, S. Tóth, M. Koós, A. Nagy, A. Kerekes, D. Oszetzky, Sz. Kugler, A. Czitrovszky**

*Wigner Research Centre for Physics of the Hungarian Academy of Sciences, PO Box 49., Budapest, Hungary*

*veres.miklos@wigner.mta.hu*

The more precise targeted delivery of inhaled medications requires detailed understanding of the properties of aerosol drugs. The size distribution and other characteristics of the inhaled particles, as well as the inhalation itself strongly affect, in which tracts of the respiratory system the deposition will take place. While the distribution of inhaled drugs in airways is of great importance, its determination, especially *in vivo* is not so trivial. The methods presented so far gave a rather integrated view on the particle deposition, had poor resolution and utilized procedures influencing the drug deposition process itself.

Recently we have developed a new system to characterize the inhalation drugs and other aerosols, and to study their spatial distribution in human respiratory system. The main setup consists of a chamber where airway tracts can be placed for deposition experiments; a respiration simulator that is able to reproduce different breathing patterns and is connected to the above mentioned chamber; a holder for metered dose inhaler with pneumatic actuator that can be synchronised with the respiration simulator. Realistic airway tracts can be obtained by 3D printing of models obtained by reconstruction of computer tomographic data recorded on patients. Beside this system a Copley Next Generation Impactor is used to measure the size distribution of the aerosol drugs.

Several optical methods have been developed to study the amount and the characteristics of the deposited medications in both the impactor and the inhalation drug testing setup. We use Raman spectroscopy, optical microscopy and interferometry to investigate the coverage of the introduced medication. All of the three methods have their own advantages in terms of speed and precision of the measurement. The velocity profile of the aerosol drug particles during their introduction into the artificial lung model is determined by Laser Doppler anemometry.

Different medications were tested and compared in terms of particle size distribution and deposition characteristics in 3D airway models.

This work was supported by the National Research and Technology Innovation Fund under grant KTIA\_AIK\_12-1-2012-0019.

**MULTI-WAVELENGTH, NANOSECOND, HIGH-PEAK POWER LASER DIODE  
SYSTEM FOR OPTOACOUSTIC MONITORING, SENSING, AND IMAGING**

Rinat O. Esenaliev

*Laboratory for Optical Sensing and Monitoring,  
Center for Biomedical Engineering,  
Department of Neuroscience and Cell Biology,  
Department of Anesthesiology  
University of Texas Medical Branch,  
301 University Blvd., Galveston, Texas 77555-1156, USA*

[riesenal@utmb.edu](mailto:riesenal@utmb.edu)

Optoacoustic (photoacoustic) technique is a novel diagnostic modality which combines high optical contrast and ultrasound spatial resolution. It is based on time-resolved detection of thermoelastic waves generated in tissues by short (typically nanosecond) optical pulses. We proposed to use the optoacoustic technique for noninvasive sensing and monitoring applications. One of the most important optoacoustic applications is noninvasive monitoring of blood oxygenation, in particular cerebral blood oxygenation in patients with traumatic brain injury, neonatal patients, and fetuses during late stage labor. We developed and built a number of tunable optical parametric oscillator (OPO)-based systems operating in the near infrared spectral range from 700 and up to 2400 nm. Recently, we built a multi-wavelength, highly-compact, laser diode-based system for optoacoustic applications. The system has nanosecond pulse duration, high peak power, and high pulse repetition rate. One of the most challenging tasks in laser diode system applications is efficient fiber coupling. We designed and built a fiber-optic system with high coupling efficacy. The fiber-optic system was incorporated in ultra-sensitive, wide-band optoacoustic probes specially designed for monitoring of blood oxygenation in important blood vessels in adults, neonates, and fetuses. We performed clinical tests of the system using the optoacoustic probes that were designed for backward (reflection) mode or forward (transmission) mode. In the backward mode, both optical irradiation and ultrasound detection are performed from the same hemisphere, while in the forward mode ultrasound detection is performed from the opposite hemisphere. Both modes were used in the clinical tests. The high peak power and repetition rate allowed for rapid data acquisition with high signal-to-noise ratio from cerebral blood vessels such as the superior sagittal sinus (SSS), central veins such as the internal jugular vein (IJV) as well as from peripheral veins and arteries. The system was capable of automatic, real-time, continuous measurements of blood oxygenation in these blood vessels. Because of the high peak power and pulse repetition rate, the system can also be used for rapid optoacoustic imaging and sensing.

The authors acknowledge support of these studies by the NIH (Grants # U54EB007954, R01EB00763, R01NS044345, R41HL103095, R43HD075551, and R41HD076568), Noninvasix, Inc., John Sealy Memorial Endowment Fund for Biomedical Research, Moody Center for Traumatic Brain Injury Research, 2 DOD grants, UTMB Business Acceleration Program, and Texas Emerging Technology Fund. Drs. Esenaliev and Prough are co-owners of Noninvasix, Inc., a UTMB-based startup that has licensed the rights to optoacoustic monitoring, sensing, and imaging technology.

## **Non-invasive evaluation of breath biomarkers in oxidative stress using photoacoustic spectroscopy**

**D. C. Dumitras<sup>1,2</sup>, M. Petrus<sup>1</sup>, A. M. Bratu<sup>1</sup>, M. Patachia<sup>1</sup>, S. Banita<sup>1</sup>, C. Achim (Popa)<sup>1,2</sup>**

*1- National Institute for Laser, Plasma and Radiation Physics, Laser Department, 409 Atomistilor St., PO Box MG-36, 077125 Bucharest, Romania*

*2- University Politehnica of Bucharest, Faculty of Applied Sciences, Physics Department, 313 Splaiul Independentei, Bucharest - 060042, Romania*

*Main author email address: dan.dumitras@inflpr.ro, cristina.achim@inflpr.ro*

Breath analysis is an attractive field for noninvasive diagnosis of serious illnesses. Collecting/analyzing breath samples is preferred to direct measurement of blood samples, because it is extremely simple (in the gas phase than in a complex biological media such as blood), painless, non-invasive and contamination is easily avoided [1, 2].

Biomarker analysis in exhaled breath may be the most simple, rapid and safest way to accurately determine the stage or the severity of a disease. Although numerous biomarkers have been identified so far, very little is known about their origin, if they are metabolic or not (e.g. ethylene biomarker is a product of oxidative stress of linoleic acid and can assess free radical damage) [1,2].

Exhaled breath contains hundreds of VOCs (volatile organic compounds) that can be attributed to either exogenous or endogenous volatiles.

The determination of the ethylene gas compound was investigated using a CO<sub>2</sub> laser photoacoustic system (LPAS), a well known method in the field of trace gas detection, used in our study for quantitative determination of biomarkers [3].

The first objective was to investigate the ethylene biomarker in diaphragmatic breath (deep breathing activities) with ethylene biomarker from normal breath. Analysis of ethylene concentrations at deep breathing subjects indicated that diaphragmatic breathing can help with stress reduction and can be correlated with a lower ethylene level in the exhaled breath.

The second objective was to analyze oxidative stress marker in breath samples of patients with autism compared with breath samples of healthy subjects. The breath ethylene biomarker in the exhalation of autism patients exhibited differences with the breath biomarkers in the exhalation of healthy controls.

Another objective of the present study was to investigate exhaled ethylene breath via both mouth and nose before and after brushing with toothpaste/baking soda, to identify the better rout for breath analysis and detect the important endogenous biomarkers without contaminant sources [4].

To diagnose metabolic diseases, the volunteers should be instructed to use toothpaste before each breath test sampling, to avoid oral bacteria. Contamination of breath exhaled via the mouth can occur and measurements should be carried out of both mouth and nasal breath to identify the sources of different trace gases.

In conclusion, the data from this study support the hypothesis of the oxidant/antioxidant balance as a key component that may contribute to different pathologies.

Based on a non-invasive sampling method, stable in biological materials, and easy to measure, we conclude that CO<sub>2</sub> LPAS analyses of breath ethylene in oxidative stress appeared to distinguish subjects with different pathologies from healthy controls.

### *Acknowledgements*

We acknowledge the financial support of the Sectoral Operational Programme Human Resources Development 2007-2013 of the Ministry of European Funds through the Financial Agreement POSDRU/159/1.5/S/132395.

[1] C. Popa, IR spectroscopy study of the influence of inhaled vapors/smoke produced by cigarettes at active smokers, Journal of Biomedical Optics 20(5), 051003, [DOI: 10.1117/1.JBO.20.5.051003] (May 2015).

[2] C. Popa, A. M. Bratu, C. Matei, R. Cernat, A. Popescu, and D.C. Dumitras, Qualitative and quantitative determination of human biomarkers by laser photoacoustic spectroscopy methods, Laser Physics, Vol. 21, No. 7, pp: 1336-1342, (2011).

[3] D.C. Dumitras, S. Banita, A.M. Bratu, R. Cernat, D.C.A. Dutu, C. Matei, M. Patachia, M. Petrus and C. Popa, Ultrasensitive CO<sub>2</sub> laser photoacoustic system, Infrared Physics & Technology Journal, Vol. 53, nr. 5, pp. 308-314, (2010).

[4] C. Popa, D. C. Dumitras, A. M. Bratu, Mouth vs. nasal breathing biomarker analysis using photoacoustic spectroscopy method, under review at Laser Physics 2014LP0529 (2015).

## **Quartz-enhanced photoacoustic trace gas technique: recent advances and new developments**

**V. Spagnolo<sup>1</sup>, P. Patimisco<sup>1</sup>, A. Sampaolo<sup>1,2</sup>, G. Scamarcio<sup>1</sup>, Frank K. Tittel<sup>2</sup>**

*1- Dipartimento Interateneo di Fisica, Università e Politecnico di Bari, CNR-IFN UOS BARI, Via Amendola 173, Bari, Italy*

*2- Department of Electrical and Computer Engineering, Rice University, 6100 Main Street, Houston, TX 77005, USA*

*vincenzo.spagnolo@uniba.it*

We will report on the latest new developments and results of quartz-enhanced photoacoustic (QEPAS) trace-gas sensor technology, employing quantum cascade lasers (QCLs) source operating in the mid-IR and THz spectral ranges. QEPAS is an alternative approach to photoacoustic detection of trace gas utilizing a quartz tuning fork (QTF) as a sharply resonant opto-acoustic transducer to detect weak photoacoustic excitation signals and allowing the use of extremely small volumes<sup>1</sup>. We will review our latest scientific breakthroughs such as the realization of mid-IR fiber coupled QEPAS sensors with sensitivity down to the part per trillion concentration range<sup>2,3</sup>, the development of the first QEPAS sensors operating in the THz spectral range<sup>4,5</sup>, and the realization of the first intracavity-QEPAS sensors<sup>6</sup>, by coupling to a QTF in a build-up optical cavity. Furthermore, we will report details of recent accomplishments of a new QEPAS systems, specifically the design and realization of new QTFs with different geometries in terms of the spacing between the QTF prongs, their length, width and thickness, providing a significant enhancement of optoacoustic generation efficiency.

[1] P. Patimisco, G. Scamarcio, F.K. Tittel, V. Spagnolo, *Sensors*, 14, 6165-6205, (2014).

[2] V. Spagnolo, P. Patimisco, S. Borri, G. Scamarcio, B.E. Bernacki, J. Kriesel, *Opt. Lett.*, 37, 4461-4463, (2012).

[3] M. Siciliani de Cumis, S. Viciani, S. Borri, P. Patimisco, A. Sampaolo, G. Scamarcio, P. De Natale, F. D'Amato, V. Spagnolo, *Opt. Express* 22, 28222-28231, (2014).

[4] S. Borri, P. Patimisco, A. Sampaolo, M.S. Vitiello, H.E. Beere, D.A. Ritchie, G. Scamarcio and V. Spagnolo, *Appl. Phys. Lett.* 103, 0211021, (2013).

[5] V. Spagnolo, P. Patimisco, R. Pennetta, A. Sampaolo, G. Scamarcio, M.S. Vitiello, F.K. Tittel, *Opt. Express*, 23,7574-7582, (2015).

[6] S. Borri, P. Patimisco, I. Galli, D. Mazzotti, G. Giusfredi, N. Akikusa, M. Yamanishi, G. Scamarcio, P. De Natale and V. Spagnolo, *Appl. Phys. Lett.* 104, 091114 (2014).

## **Spectroscopic analysis of humans breath in subjects with type 2 diabetes**

**M. Petrus<sup>1</sup>, A.M. Bratu<sup>1</sup>, C. Popa<sup>1,2</sup>, S. Banita<sup>1</sup>, M. Patachia<sup>1</sup>,  
C. Matei<sup>1,2</sup> and D.C. Dumitras<sup>1,2</sup>**

*1- Department of Lasers, National Institute for Laser, Plasma and Radiation Physics, 409 Atomistilor St.,  
PO BOX MG-36, 077125, Bucharest, Romania*

*2- University POLITEHNICA of Bucharest, 313 Splaiul Independentei St., Bucharest, Romania*

*Email: mioara.petrus@inflpr.ro*

Type 2 diabetes, called non-insulin dependent diabetes is a severe health problem that is increasing rapidly nowadays [1-4]. Diabetes is distinguished by a very high level of glucose in the body that causes deregulation of the metabolism. It has been estimated that the number of people affected with diabetes in the world will increase to 300 million by 2025 [1-4]. Diabetes is a devastating disease throughout the world. It is associated with several mechanisms, one of which is oxidative stress. Oxidative stress plays an important role in the pathogenesis and the complications of diabetes. Hyperglycemia results in overproduction of oxygen free radicals, which contributes to the progression of diabetes [1,2,4,5].

Breath test is noninvasive, easily repeated, and does not have the discomfort or associated with blood tests [6]. Several compounds in the human breath have been associated with different diseases and pathological states of disorders. Breath biomarkers can provide important information about a given illness and will have significant implications in clinical diagnosis. In our study ethylene (C<sub>2</sub>H<sub>4</sub>) and ammonia (NH<sub>3</sub>) breath concentrations were determined using CO<sub>2</sub> laser photoacoustic spectroscopy (LPAS) [7] to determine the level of oxidative stress and protein metabolism associated with complications (due to oxidative stress). We measured breath biomarkers of oxidative stress on two groups: in patients with type 2 diabetes (n = 16) and in non-diabetic (control group, n = 9). Oxidative stress has been implicated in the major complications of diabetes disease and plays a pivotal role in the development of the illness complications. Our measurements demonstrated a significantly increase of ethylene concentration in the exhaled breath (owing to the oxidative stress) and of ammonia concentration in the exhaled breath (due to protein catabolism) at diabetic subjects compared to healthy subjects. Diabetics due to hyperglycemia and complications present an increase oxidative stress, ethylene being a product of reactive oxygen species (ROS)-induced lipid peroxidation of polyunsaturated fatty acids. High ammonia concentrations is due to protein catabolism as a consequence hyperglycemia but also is associated with oxidative stress because proteins are also a target to oxidative attack. So, ethylene and ammonia as breath biomarkers provide informations about the oxidative stress level in subjects with type 2 diabetes.

LPAS system is a fast and sensitive trace gas detector and will play an important role in exhaled breath analysis. LPAS is a technique capable of detecting specific molecular species at low concentrations with measurements made in real time without the need for sample treatment or preparation.

[1] Yi-Cheng Chang, Lee-Ming Chuang, The role of oxidative stress in the pathogenesis of type 2 diabetes: from molecular mechanism to clinical implication, *Am J Transl Res* 2(3):316-331 (2010).

[2] F. Giacco and M. Brownlee, Oxidative stress and diabetic complications, *Circ Res.*,107(9):1058–1070(2010). doi:10.1161/CIRCRESAHA.110.223545.

[3] J. E. Shaw, R. A. Sicree, P. Z. Zimmet, Global estimates of the prevalence of diabetes for 2010 and 2030. *Diabetes Res Clin Pract*, 87(1): 4-14 (2010).

[4] M. Phillips, R. N. Cataneo, T. Cheema, J. Greenberg, Increased breath biomarkers of oxidative stress in diabetes mellitus, *Clinica Chimica Acta* 344:189 – 194 (2004).

[5] T.H. Risby, Volatile organic compounds as markers in normal and diseased states, *Disease markers in exhaled breath: basic mechanisms and clinical applications*, Series I: Alife and Behavioural Sciences vol. 346, N. Marczin, M. Yacoub (Eds.), IOP Press, pp. (2002),pp 113-122.

[6] D. Hill, and R. Binions, "Breath Analysis for Medical Diagnosis," *Intern. J. on Smart Sensing and Intelligent Systems*, 5(2): 401-440 (2012).

[7] C.A. Dutu, R. Cernat, C. Matei, A.M. Bratu, S. Banita, D.C. Dumitras, Ethylene and ammonia traces measurements from the patients' breath with renal failure via LPAS method, *Appl Phys B*, 105:669–674 (2011).

## Nanosecond optical parametric oscillator for biomedical applications in spectral range from 4.2 to 10.73 $\mu\text{m}$

N. Kostyukova<sup>1</sup>, K. Zenov<sup>1</sup>, D. Kolker<sup>1,2</sup>, M. Starikova<sup>1</sup>, A. Karapuzikov<sup>1</sup>

1- Special technologies Ltd., Zeljonaja gorka str. 1/3, Novosibirsk, Russia, 630060

2 - Novosibirsk State University, 2 Pirogova Str., Novosibirsk, Russia, 630090

We demonstrate nanosecond optical parametric oscillator (OPO) based on  $\text{HgGa}_2\text{S}_4$  (HGS) crystal [1]. HGS crystal is very promising material for parametric frequency conversion because of relatively high nonlinear coefficient  $d_{36} = 31.5 \text{ pm/V}$  [2] and high surface damage threshold  $40 \text{ MW/cm}^2$  ( $1.2 \text{ J/cm}^2$ ,  $1.064 \mu\text{m}$ ,  $30 \text{ ns}$ ) [3]. Also HGS can be pumped near  $1 \mu\text{m}$  by a commercially available laser (e. g. Nd:YAG, Nd:YLF) without two-photon absorption due to its wide band-gap ( $2.79 \text{ eV}$ ) [4]. The developed OPO is pumped by nanosecond Q-switched  $1.053 \mu\text{m}$  Nd:YLF laser and provides continuous wavelength tuning from  $4.2 \mu\text{m}$  to  $10.73 \mu\text{m}$ . OPO covers the major part of mid-IR range including absorption bands of different bonds like C=O, C-H and N-H, as well as carbonyl, amide of I and II bands. OPO combined with resonant photo-acoustic detector allows developing gas analyzer for biomedical applications [5]. For example, bronchial asthma exacerbation is characterized by ammonia ( $\text{NH}_3$ ) concentration increasing [6, 7]. The study described in [8] demonstrates that acetone ( $\text{C}_3\text{H}_6\text{O}$ ) can be used as a biomarker of lung cancer.

To demonstrate the feasibility of the developed source for gas analysis applications we present absorption spectra of acetone with distinct rotational–vibrational features in the mid IR.

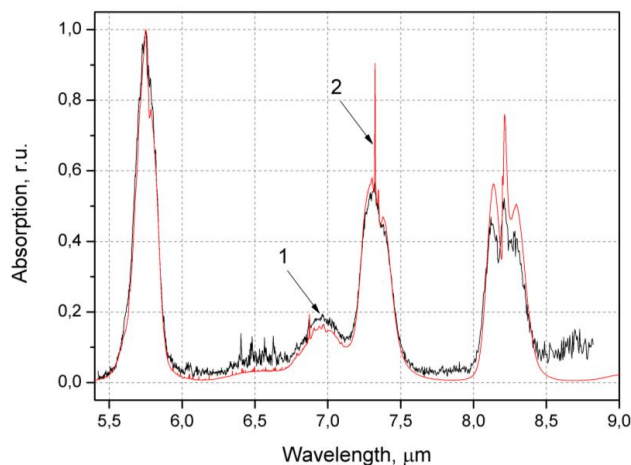


Figure 1. Absorption spectra of acetone (gas mixture of 0.2%  $\text{C}_3\text{H}_6\text{O}$  in  $\text{N}_2$ ): 1 (black line) - experimental data, 2 (red line) - data from NIST.

Figure 1 demonstrates comparison of acetone absorption spectrum obtained with developed HGS OPO system and NIST data (resolution  $2 \text{ cm}^{-1}$ ) [9]. The experimental absorption spectra and NIST data agree with each other, thus confirming a high degree of reliability of the obtained results.

[1] N. Kostyukova, D. Kolker, K. Zenov, A. Boyko, M. Starikova, I. Sherstov, A. Karapuzikov, Mercury thiogallate nanosecond optical parametric oscillator continuously tunable from 4.2 to 10.8  $\mu\text{m}$ , Laser Physics Letters (in print)

[2] F. Rotermund and V. Petrov, Mercury thiogallate mid-infrared femtosecond optical parametric generator pumped at 1.25  $\mu\text{m}$  by a Cr:forsterite regenerative amplifier, Opt. Lett., vol. 25, pp. 746-748, (2000).

[3] V. V. Badikov, N. V. Kuzmin, V. B. Laptev, A. L. Malinovsky, K. V. Mitin, G. S. Nazarov, E. A. Ryabov, A. M. Seryogin and N. I. Schebetova, A study of the optical and thermal properties of nonlinear mercury thiogallate crystals, Quantum Electron, vol. 34, pp. 451-456, (2004).

[4] A. Tyazhev, G. Marchev, V. Badikov, A. Esteban-Martin, D. Badikov, V. Panyutin, G. Shevyrdavaeva, S. Sheina, A. Fintisova and V. Petrov, High-power  $\text{HgGa}_2\text{S}_4$  optical parametric oscillator pumped at 1064 nm and operating at 100 Hz, Laser Photonics Rev., vol. 7, L21-L24, (2013).

[5] Y. Kistenev, A. Karapuzikov, N. Kostyukova, M. Starikova, A. Boyko, E. Bukreeva, A. Bulanova, D. Kolker, D. Kuzmin, K. Zenov, A. Karapuzikov, Screening of patients with bronchopulmonary diseases using methods of IR laser photo-acoustic spectroscopy and principal component analysis, J. Biomed. Opt., vol. 20(6), pp. 065001, (2015).

[6] S.A. Kharitonov and P.J. Barnes, Exhaled markers of pulmonary disease, Am. J. Respir. Crit. Care Med., vol. 163, 1693-1722, (2001).

[7] M. Yamara, Exhaled carbon monoxide levels during treatment of acute asthma, Eur. Respir. J., vol. 13, 757-760, (1999).

[8] S. M. Gordon, J. P. Szidon, B. K. Krotoszynski, R. D. Gibbons and H. J. O'Neill., Volatile organic compounds in exhaled air from patients with lung cancer, Clin Chem., vol. 31, 1272-1282, (1985).

[9] <http://webbook.nist.gov>

## **Trapping of a gas bubble in water by nanosecond laser beam**

**V.Yu. Khomich, T.V. Malinsky**

*Institute for Electrophysics and Electric Power of the Russian Acad. Sci.,  
18 Dvorzovaya nab., 191186 Sankt-Peterburg, Russia  
e-mail: tm2@newmail.ru*

We have experimentally observed the trapping of a gas bubble in water by nanosecond laser beam. Unlike the optical tweezers[1], where the force tends to push the bubble out of the laser beam, in our experiments the holding force directed to the beam's axis. This makes the trap process more convenient, reliable and predictable.

The trap was provided by 10 ns 355 nm (3-d harmonic) Nd:YAG laser with 100 Hz repetition rate and 2mJ pulse energy. The radiation was focused by a lens with 35 mm focal length in a quartz cuvette with  $K_2Cr_2O_7$  water solution. The target (a copper wire with 200  $\mu$  diameter) was used as bubble seed. It was placed near the lens focal area in cuvette.

During the copper ablation in water we observed many gas bubbles with radius from several micrometers to several tens of micrometers. They moves from the ablation zone in different directions. Some bubbles crossed the laser beam axis. This leads to change the bubble's trajectory: the bubble begin to move horizontally near the beam's axis in the direction of laser radiation entrance into the cuvette.

A typical bubble trajectory was shown in Figure 1. The trajectory was plotted from recorded by camera image sequence by ImageJ program[2]. After the bubble (dark spot in the circle) has been captured it begin to move horizontally from left to right along the laser beam axis.



Fig. 1. A typical trajectory of the bubble trapped by nanosecond laser beam.

The similar trajectories were observed for the bubbles up to 40  $\mu$  diameter. The length of the horizontal path of the trajectory in some cases exceeds 2 mm. The larger the bubble's diameter was the more horizontal distance it passed before it's "breakup" from a laser beam.

The proposed bubble trap can be used in different microtechnologies. It's used simple low-aperture optical system and may be easily conjugated with microscope.

The reported study was partially supported by Russian Foundation for Basic Research, research project № 13-08-01146.

1. A. Ashkin, J. M. Dziedzic, T. Yamane, "Optical trapping and manipulation of single cells using infrared laser beams", *Nature*, vol. 330, no. 6150, pp. 769-771, 1987.
2. C. A. Schneider, W. S. Rasband, K. W. Eliceiri, "NIH Image to ImageJ: 25 years of image analysis", *Nat Meth*, vol. 9, no. 7, pp. 671-675, 2012.

## **Skin neoplasms analysis by laser emitted fluorescence in visible and NIR regions**

**V.P. Zakharov<sup>1</sup>, I.A. Bratchenko<sup>1</sup>, D.N. Artemyev<sup>1</sup>, Yu.A. Khristophorova<sup>1</sup>,  
O.O. Myakinin<sup>1</sup>, A.A. Moryatov<sup>2</sup>, S.N. Kozlov<sup>2</sup>**

**(List of authors in 11 point, centred and bold: the presenting author underlined)**

*1- Laser and Biotechnical Systems Dept. of Samara State Aerospace University,  
443086, Russia, Samara, Moskovskoe shosse 34*

*2- Oncology Dept. of Samara State Medical University, 443099, Russia, Samara, Chapayevskaya str. 89*

*zakharov@ssau.ru*

Problem of increased incidence of cancer is known worldwide. For instance yearly in Russia more than 500000 cases of cancer are registered and the largest amount of deaths caused by cancer are due to skin cancers [1]. This situation arise a problem of cancer diagnosis on early stages. In this regard optical methods may be very useful for tissues analysis. They allow one to find chemical composition of tested tissues *in vivo* and in real time mode. In this paper we present a method of skin neoplasms analysis based on an effect of tissues autofluorescence.

Experimental registration of autofluorescence spectrums was performed in identical external conditions after tissues resection in Samara Regional Clinical Oncological Dispensary. All experiments were approved by the ethical committee of Samara State Medical University. More than 60 tissue samples were tested. Autofluorescence spectrums were registered for neoplasms and surrounding normal skin. Autofluorescence was stimulated in visible and NIR regions by two lasers 457nm and 785 nm. Stimulated fluorescence was observed in 520 – 750 nm and 800 – 925 nm areas. For autofluorescence spectrums registration spectrograph Sharmrock SR-500i-D1-R with integrated CCD camera ANDOR DU 416 A-LDC-DD was used.

Shape of autofluorescence spectra in visible region is caused by porphyrins, keratins and flavins [2, 3] and in NIR region by melanin [4]. For determination of tissue type three criteria were used. First is the intensity of fluorescence maxima in 530 – 650 nm area, second is the position of intensities maxima in visible region (around 560 and 635 nm) and the third is the incline of autofluorescence curve in NIR region. For melanoma detection these three criteria demonstrates accuracy of 71%, 60% and 79% correspondently. Combined applying of these three criteria allows to reach 89% accuracy in melanoma detection and more than 80% accuracy in basal cell carcinomas detection.

First results of combined autofluorescence method applying for skin neoplasms diagnosis seems to be very effective. Adding this result to other optical techniques of cancer control may increase overall accuracy of neoplasms determination. For example autofluorescence control may be added to the optical coherence tomography and Raman spectroscopy data to reach a higher level of cancer diagnosis [5].

[1] P.E. Goss, K. Strasser-Weippl et. al., Challenges to effective cancer control in China, India, and Russia, *Lancet Oncol*, vol. 15., pp. 489–538, (2014).

[2] I. Bliznakova, E. Borisova, L. Avramov, Laser- and Light-Induced Autofluorescence Spectroscopy of Human skin in dependence on excitation wavelengths, *Proceedings of the International School and Conference on Optics and Optical Materials, ISCOM07*, vol. 112, pp. 1131-1136, (2007).

[3] I. Seo, S.H. Tseng, G.O. Cula, P.R. Bargo, N. Kollias, Fluorescence spectroscopy for endogenous porphyrins in human facial skin, *Photonic Therapeutics and Diagnostics V, Proc. of SPIE* vol. 7161, 716103, (2009).

[4] Z. Huang and H. Zeng, Cutaneous melanin exhibiting fluorescence emission under near-infrared light excitation, *Journal of Biomedical Optics*, vol. 11(3), 034010, (2006).

[5] V.P. Zakharov, I.A. Bratchenko, D.N. Artemyev, O.O. Myakinin, D.V. Kornilin, S.V. Kozlov, A.A. Moryatov, Comparative analysis of combined spectral and optical tomography methods for detection of skin and lung cancers, *Journal of Biomedical Optics*, vol. 20(2), 025003 (2015).

# **Dual-channel lock-in thermometry with thermographic phosphors**

**A. Vetter<sup>1,2</sup>, A. Hashemi<sup>2,3</sup>, G. Jovicic<sup>1,2</sup>, M. Batentschuk<sup>1</sup>, C. J Brabec<sup>1,3</sup>**

*1- Friedrich Alexander Universität Erlangen-Nürnberg, Dept of Material Science, i-MEET, Germany*

*2- Energie Campus Nürnberg, Germany*

*3- Bavarian Center of Applied Energy Research (ZAE-Bayern), Erlangen, Germany*

*andreas.vetter@fau.de*

The determination of temperature is a common task for several applications, in particular in the field of basic science, engineering and medicine. Precise temperature measurement is a challenge due to diverse issues. During “classic” temperature determination with thermocouples, for example, contacting the thermocouple onto sample-surface plays an essential role for correct measurements. Contactless infrared (IR) measurements can replace such invasive measurement methods. Unfortunately, IR-radiation depends strongly on the surface geometry and emissivity. The emissivity is rarely precisely known and tends to depend on temperature. Temperature determination via temperature-dependent behaviour of thermographic phosphors offers another possibility to measure temperature in a contactless way and additionally offers advantages in particular for applications at high temperatures and in a wide temperature range [1, 2]. For such measurements, a thin layer of phosphor powder is coated onto the sample surface and the surface is illuminated by a light source. The surface temperature might be deduced by applying phosphors exhibiting a defined temperature dependent luminescence. For example, the intensity of two emission peaks of the phosphor may change due to temperature. This measurement technique uses in general UV-lasers for excitation. However, these lasers are often very robust and expensive. This is one reason why we follow an approach to use diode lasers using blue light for excitation [3]. Next to the lower costs, this approach also offers advantages by yielding lower safety issues. One of our aims is to improve the luminescence properties of the phosphors, for example by adjusting the morphology. Another aim is to improve the detection limit of this measurement technique by applying the lock-in method.

To do so, we have established a comprehensive, semi-automatic measurement setup. First, we characterize the luminescence of different phosphors, and in particular, we acquire temperature dependent spectra under continuous illumination. Accordingly, we can identify suitable phosphors with two emission peaks most sensitive to temperature change. In a second step, we can calibrate the temperature luminescence response of selected phosphors using the dual-channel lock-in system. The system consists of two fiber-coupled photodiodes with selectable band pass filters and notch filters to block the laser wavelength. Each diode collects the intensity of one identified emission peak. The two signals are detected by a sophisticated dual channel lock-in amplifier, which also triggers the excitation source (in our case: diode laser at 405 nm). This method enables us to detect the temperature dependent signal even under strong background noise. We tested our lock-in phosphor thermometry approach with a common phosphor (YAG:Dy), which is often used for high temperature applications (e. g. combustion science). We coupled light from a Xenon lamp into the detection channels to introduce well defined noise (noise level was ten times higher than the luminescence signal). The results show, that this approach can be successfully applied in a wide temperature range. We may utilize this innovative measurement system to measure contactless the temperature of solar receiver structures under working conditions (highly concentrated sun light, which results in strong background noise). However, the approach can be used in many other applications with a significant background noise to measure temperature via phosphor thermometry.

[1] Thermographic Phosphors for High Temperature Measurements: Principles, Current State of the Art and Recent Applications. A. H. Khalid and K. Kontis, *Sensors* 2008, 8, 5673-5744

[2] On surface temperature measurements with thermographic phosphors: A review. J. Brubach, C. Pflitsch, A. Dreizler, B. Atakan, *Progress in energy and combustion science* 2013, 39, 37-60

[3] Temperature measurements using YAG:Dy and YAG:Sm under diode laser excitation (405 nm). A. Hashemi, A. Vetter, G. Jovicic, M. Batentschuk, C. J. Brabec, *Measurement Science and Technology*, published online

## **The effects of air pollution and UV-B radiation on fruits using LPAS method**

**S. Banita, M. Patachia, D. C. Dumitras, C. Achim, M. Bercu, A.M. Bratu, C.Matei**

*Department of Lasers, National Institute for Laser, Plasma and Radiation Physics, 409 Atomistilor St., PO Box MG-36, 077125, Bucharest, ROMANIA*

[stefan.banita@inflpr.ro](mailto:stefan.banita@inflpr.ro)

Laser photoacoustic spectroscopy (LPAS) is a very powerful technique capable of measuring trace gas concentration from multicomponent mixtures with high accuracy. The near real-time analyses, high selectivity and sensitivity of LPAS detection allow the investigation of gases at low concentrations.

The purpose of our research was to distinguish and measure the effects of air pollution and UV-B radiation on fresh fruits.

Traces of gases released by various fruit samples absorb laser radiation inside the cell and the gas concentration is calculated from a comparison of the photoacoustic signals on various laser emission frequencies. The CO<sub>2</sub> laser based instrument allows detection of gas emission in a continuous-flow system down to 1 ppb and the sensitivity of the technique is such that absorptions of 10-7 cm<sup>-1</sup> can be measured over path lengths of a few tens of centimeters.

We compared the response of trace gas concentration from fresh fruits in a controlled environment: polluted air (collected from the exhaust of cars and atmosphere) and UV-B radiation (with an UV lamp in the range of 270-320 nm).

The topic addressed in this paper is one of the most important ones in Life Sciences at the international and global level, namely the effects of plant pollution on human health and the environment.

- [1] D. C. Dumitras, **Ş. Băniţă**, A. M. Bratu, R. Cernat, D. C. A. Duţu, C. Matei, M. Paţachia, M. Petruş and C. Popa, "Ultrasensitive CO<sub>2</sub> laser photoacoustic system", *Infrared Phys. Technol.*, Vol. 53, No. 5, pp. 308-314 (2010)
- [2] **Ş. Băniţă**, C. Popa, M. Paţachia and D. C. Dumitras, "Ethylene concentration at fruits under aerobic vs. anaerobic conditions", *U.P.B. Sci. Bull., Series A*, Vol. 75, No. 3, pp. 217-226 (2013)
- [3] C. Popa, D. C. Dumitras, A. M. Bratu, M. Paţachia and **Ş. Băniţă**, "Ethylene production of organic and nonorganic mature mushrooms measured by LPAS", *Rom. Rep. Phys.*, Vol. 66, No. 3 (2014)
- [4] C. Popa, A. M. Bratu, D. C. Dumitras, M. Paţachia, and **Ş. Băniţă**, "Photoacoustic detection of ethylene concentration in cherry tomatoes", *Journal of Optoelectronics and Advanced Materials*, Vol. 16, No.1-2, (2014)

# **New Optical Imaging System for Intraoperative Detection of Tumors Margins**

**M. Patachia, S. Banita, C. Matei, M. Petrus, C. Achim, A. Bratu and D.C. Dumitras**

*Department of Lasers, National Institute for Laser, Plasma and Radiation Physics,  
409 Atomistilor St., PO Box MG-36, 077125 Magurele, Ilfov, Romania*

*mihai.patachia@infpr.ro*

Patients with invasive lobular carcinoma undergoing breast conserving surgery have a particularly high risk of tumor-positive excision margins, which is usually caused by the larger and non-uniform spreading of cancer foci. Surgical removal of invasive lobular carcinoma is not fully successful in controlling breast cancer because a small number of tumor cells can be left at the surgical area, and the cancer recurrence probability is very high. Intraoperative assessment of margins using usually techniques is minimal in reducing the positive margins rate. Therefore, a technology capable of highlighting the presence of the positive margins could provide very useful information for surgery guidance and therefore could potentially eliminate cancer recurrence. The margin is defined as the distance from the tumor to the cut surface of the specimen.

The main objective of this research studies is to develop and to validate a new imaging technology for breast cancer. Very efficient cancer localization during surgery is the only way to remove cancer in its entirety. A high sensitivity and specificity dual modality imaging platform will provide the surgeon with real-time information about cancer spreading, allowing for complete removal of cancer foci, which otherwise cannot be identified with current clinical instrumentation.

This technology, based on a multimodality imaging approach combining reflectance spectral imaging with structural optical coherence tomography imaging, will provide the surgeon with real-time feedback with the exact location and amount of tissue that has to be removed.

This OCT/reflectance imaging systems share a common path optical probe. Our efforts are focused on the development of a dual imaging system and common path probe, as well as on preliminary testing of the system on excised surgical specimens.

This system uses the spectral-domain approach, which has already proved to offer superior speed and sensitivity to the traditional time-domain approach.

The development of a common path imaging probe permits the co-registration of the OCT and spectroscopic (fluorescence/reflectance) images. Diffuse reflectance spectral imaging provided by low the coherent interferometry - LCI subsystem runs simultaneously with SD-OCT imaging.

Since the hyperspectral camera analyses the sample through a linear aperture, the system requires a dynamic approach in order to cover sampling areas of few cm<sup>2</sup>. Starting from the sample, the optical path of the image is separated by a dichroic mirror. The first segment enters directly the OCT detection system, while the second path is further oriented onto a mirror controlled by a galvanometer.

The galvanometer assures the scanning of the sample line by line. Each line is focused by a lens onto the aperture of the spectrometer, then forms a complete image on the camera sensor, which transmits the result (the spectral “hypercube”) to PC by FireWire interface.

Selecting a point of interest, belonging to a tumor for example, the whole image will be changed by marking with the case color, all the points that have the same spectral characteristics. In this way, a map of the extensions of the tumor will be obtained, indicating for surgeon the safe limits of the intervention.

## References:

- [1]D.C. Dumitras, D.C. Duțu, C. Matei, A.M. Măgureanu, M. Pațachia, “Diffuse optical tomography (DOT) with serial approach”, J. Optoelectron. Adv. Mater., 747-753 (2009).
- [2]M. Pațachia, D.C.A. Duțu, D. C. Dumitras, “Blood oxygenation monitoring by diffuse optical tomography”, Quantum Electronics 40, 1062-1066 (2010).
- [3]M. Pațachia, „A simple continuous-wave diffuse optical tomography system for parametric investigation of different tissue phantoms”, Journal of Optoelectronics and Advanced Material, Vol. 15, No.3 - 4, March –2013, p. 155 – 163
- [4]M. Pațachia „Calibration and artefact minimization in a two wavelength cw diffuse optical tomography system” U.P.B. Sci. Bull., Series A, Vol. 75, Iss. 2, 2013.

## Resonant Raman spectroscopy for diagnostics of individual few-layer multi-walled carbon nanotubes

**D.I. Levshov<sup>1</sup>, M.V. Avramenko<sup>1</sup>, Yu. I. Yuzyuk<sup>1</sup>, Thierry Michel<sup>2</sup>, R. Arenal<sup>3</sup>,  
M. Paillet<sup>2</sup>, J.-L. Sauvajol<sup>2</sup>**

*1-Faculty of Physics, Southern Federal University, Rostov-on-Don, Russia*

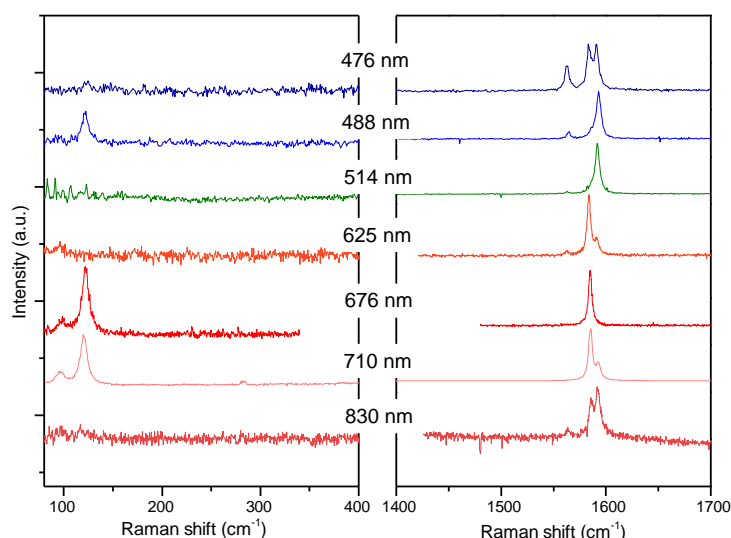
*2-University Montpellier 2, Laboratoire Charles Coulomb, Montpellier, France*

*3-Laboratorio de Microscopias Avanzadas, Instituto de Nanociencia de Aragon, Universidad de Zaragoza, Zaragoza, Spain*

*[dmitry.levshov@gmail.com](mailto:dmitry.levshov@gmail.com)*

We report the study of atomic structure and physical properties of individual suspended few-layer (double- and triple-walled) carbon nanotubes (CNTs) by means of Resonant Raman spectroscopy (RRS). The ultra-long horizontally-aligned individual tubes were synthesized by CCVD method on the perforated Si<sub>3</sub>N<sub>4</sub> membranes and structure-identified by Electron diffraction and High-resolution electron microscopy. Raman spectra of these individual CNTs were measured in a wide variety of excitation wavelengths: 458, 488, 514, 530, 568-633, 647, 676, 700-1000 nm (see Figure). The complementarity of information provided by electron and optical techniques allowed to unambiguously evidence the role of Resonant Raman spectroscopy in diagnostics of few-layer multi-walled CNTs.

The distinctive features of radial breathing-like (RBLM) and tangential (G) modes in few-layer multi-walled CNTs are discussed. We show that the index-assignment of few-layer multi-walled carbon nanotubes on the basis of Raman spectra should only be done by taking into account possible van der Waals coupling between the layers [1, 2]. We argue that the combination of electron diffraction and RRS (including the measurement of resonant excitation profiles of RBM and G-modes) is one of the most accurate approach for the CNT index-assignment.



Raman spectra of the (22,11)@(27,17) individual double-walled carbon nanotube measured at different laser excitation wavelengths

[1] Levshov, D.; Michel, T.; Paillet, M.; Than, X. T.; Tran, H. N.; Arenal, R.; Rahmani, A.; Boutahir, M.; Zahab, A.A.; Sauvajol, J.-L. MRS Proceedings, 1700, 2014

[2] Levshov, D.; Than, T. X.; Arenal, R.; Popov, V. N.; Parret, R.; Paillet, M.; Jourdain, V.; Zahab, A. A.; Michel, T.; Yuzyuk, Yu. I.; Sauvajol, J.-L. Nano Lett. 2011, 11, 4800.

## Apparatus for diagnostics and treatment of fundus diseases with monitoring of the state of biological tissues and control of laser radiation dose

**Sergey S. Model<sup>1</sup>, Tatiana A. Savelieva<sup>1,2</sup>, Kirill G. Linkov<sup>1</sup>, Victor B. Loschenov<sup>1,2</sup>**

<sup>1</sup>*A.M. Prokhorov General Physics Institute, Russian Academy of Sciences, 38 Vavilov str., Moscow, Russian Federation*

<sup>2</sup>*National Research Nuclear University MEPhI (Moscow Engineering Physics Institute), 31 Kashirskoe highway, Moscow, Russian Federation*

*modelserg@gmail.com*

In modern ophthalmology there are a number of diseases whose treatment is difficult. One of them is senile macular degeneration (SMD) with neovascularization, which has a devastating effect on the central vision. The probability of vision loss due to SMD varies greatly and depends on the stage of disease, age, race, and sex. Currently the most successful method of treatment SMD with subfoveal neovascularization is photodynamic therapy (PDT) [1]. Thus, the development of equipment for the PDT is the current trends in modern medicine.

For effective treatment and diagnosis of diseases of the eye fundus an appropriate photosensitizer (PS) must be selected. Its absorption and fluorescence spectra must be agreed with the appropriate spectra of chromophores and fluorophores in the eye tissues [2]. Also non-trivial task is the formation of a light spot on the retina with specific geometric parameters and accurate control of light dose.

We have improved a system (fig. 1) developed in our laboratory earlier [3] to analyze the spatial distribution of the concentration of PS "Photosense" in the fundus, which allows controlling the accumulation of PS in the pathologically changed and healthy tissues. Combination of micro spectral fluorimetric confocal method, implemented in one of the receiving channels of the system, with analysis of video images, implemented in the other channel, allows precise determination of the boundaries of the affected area and makes it possible to study the interaction of PS with biological tissue at the molecular level [4, 5]. The system is easy to operate and can be used in routine medical practice, to speed up diagnosis and improve the safety of photodynamic treatment.

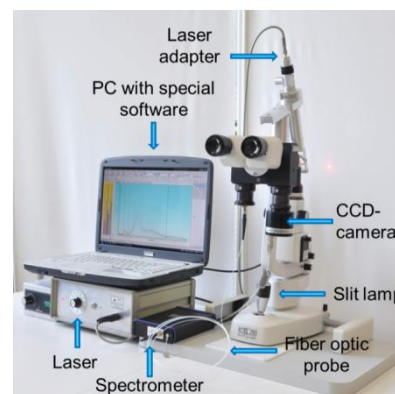


Figure 1. System set-up.

1. Sergey E. Avetisov, Maria V. Budzinskaja, Tatyana N. Kiseleva, Natalia V. Balatskaya, Irina V. Gurova, Viktor B. Loschenov, Sergey A. Shevchik, Sergey G. Kuzmin, Georgy N. Vorozhtsov, Photodynamic therapy for treatment subretinal neovascularization, Proc. SPIE 6632, Therapeutic Laser Applications and Laser-Tissue Interactions III, 663212, July 03, 2007.
2. Delori F.C., Spectrophotometer for noninvasive measurement of intrinsic fluorescence and reflectance of the ocular fundus // Arch. Biochem. — 2004. — Vol. 430, N 2. — P. 156—162.
3. Shevchik S.A., Loschenov M.V., Meerovitch G.A. et. al. The device for fluorescent diagnostics and photodynamic therapy of fundus diseases with «Photosense», Ophthalmology Journal, 2005, N 5 p. 25-28. [Article in Russian]
4. Strattonnikov A.A., Edinac N.E., Klimov D.V. et al. The control of photosensitizer in tissue during photodynamic therapy by means of absorption spectroscopy. //Proc. SPIE. 1996. - V.2924. - P.49-60.
5. Alexander A. Strattonnikov ; Natalia V. Ermishova ; Gennadii A. Meerovich ; Boris V. Kudashev ; Elena G. Vakoulovskaya ; Victor B. Loschenov; Simultaneous measurement of photosensitizer absorption and fluorescence in patients undergoing photodynamic therapy. Proc. SPIE 4613, Optical Biopsy IV, 162, May 7, 2002.

# Photoluminescence properties of silicon oxide and silicon nitride multilayer structures with silicon nanocrystals

**D.V. Shuleiko<sup>1</sup>, S.V. Zobotnov<sup>1</sup>, D.M. Zhigunov<sup>1</sup>, A. Zelenina<sup>2</sup>, P.K. Kashkarov<sup>1</sup>**

1- Faculty of Physics, Lomonosov Moscow State University, Leninskie Gory 1, Moscow 119991, Russia  
2- Faculty of Engineering, IMTEK, Albert-Ludwigs-University Freiburg, Georges-Köhler-Allee 103, Freiburg 79110, Germany

E-mail: Dmitriy1815@gmail.com

Silicon nanocrystals (SiNCs) with defined sizes embedded in a dielectric matrix are often discussed to be used in optoelectronics and photovoltaics. For example, such substance is proposed as a material for third-generation “all-silicon” tandem solar cells [1]. For this purpose the precise control of SiNC concentration, as well as their size and shape is required since the band gap of a quantum dot is mainly determined by its spatial dimensions. SiNCs can be produced by several techniques such as chemical vapor deposition (CVD), reactive evaporation, and magnetron cosputtering [2]. Control over all three parameters (size, density, spherical shape) can be achieved by depositing thin alternating layers of stoichiometric and Si-rich dielectrics in the form of a superlattice [3].

In this work, superlattices of Si<sub>3</sub>N<sub>4</sub>/Si-rich Si<sub>3</sub>N<sub>4</sub> and SiO<sub>2</sub>/Si-rich SiO<sub>2</sub> thin layers with varying thickness were prepared by plasma enhanced chemical vapor deposition [3]. Photoluminescence (PL) properties of prepared structures were studied. It was shown that silicon nanocrystals embedded in silicon oxide and silicon nitride films are efficient light emitters and demonstrate quantum-confinement properties (for example, see Figure 1).

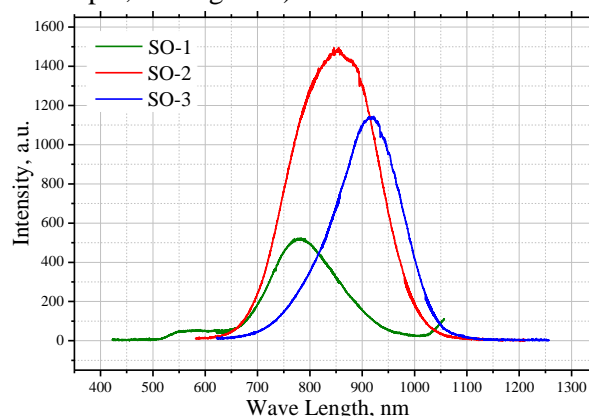


Figure 1. PL spectra of samples SO-1 – SO-3 (composed of SiO<sub>0.93</sub>/SiO<sub>2</sub> alternating layers), pump wavelength 488nm

Due to quantum-confinement effect, the possibility of control of embedded in the bulk of the film Si nanocrystals size via varying of SiN<sub>x</sub> or SiO<sub>x</sub> layer thickness can be confirmed by analysis of PL spectra of the structures, as shown in Table 1.

Table 1. Nanocrystal size and PL relaxation time in silicon oxide samples

Sample name	Active layer thickness, nm	PL peak maximum, nm	Nanocrystal mean size defined from PL spectra, nm	Relaxation time, μs
SO1	1.5	770	2	10
SO2	3	850	3.5	15
SO3	5	920	5	22

However, the origin of photoluminescence of SiNCs in silicon nitride is still unclear: radiative defects, band tail edges, as well as amorphous silicon nanoparticles might be responsible for the luminescence. Thus, PL properties of such silicon-based multilayer structures demand further research.

This work was financially supported by the Russian Foundation for Basic Research (project 14-22-01086).

[1] M. A. Green, Third generation photovoltaics: Ultra-high conversion efficiency at low cost, Prog. Photovoltaics, 9, pp. 123-135, (2001).

[2] Y.-H. So, S. Huang, G. Conibeer, M. A. Green, Formation and photoluminescence of Si nanocrystals in controlled multilayer structure comprising of Si-rich nitride and ultrathin silicon nitride barrier layers, Thin Solid Films, 519, pp. 5408-5412, (2011).

[3] M. Zacharias, J. Heitmann, R. Scholz, U. Kahler, M. Schmidt, J. Blaessing, Size-controlled highly luminescent silicon nanocrystals: A SiO/SiO<sub>2</sub> superlattice approach, Appl. Phys. Lett., 80, 661-663, (2002).

## **Optical spectroscopy diagnosis and photodynamic therapy on superficial skin malignancies**

E.Drakaki<sup>1</sup>, C. Dessinioti<sup>2</sup>, I.Stefanaki<sup>2</sup>, I.A.Sianoudis<sup>3</sup>, M. Makropoulou<sup>1</sup>,  
A.A. Serafetinides<sup>1</sup>, E. Christofidou<sup>2</sup>, A.J. Stratigos<sup>2</sup>, A.D. Katsambas<sup>2</sup>, and Ch. Antoniou<sup>2</sup>

<sup>1</sup>*National Technical University of Athens, School of Applied Mathematics and Physical Sciences, Athens 15780, Greece,*

<sup>2</sup>*University of Athens, Dept of Dermatology, Hospital A. Syggros, Athens 16121, Greece,*

<sup>3</sup>*Technological Educational Institute (TEI) of Athens, Dept of Optics & Optometry, Egaleo 12210, Greece*

*Main author email address: edrakaki@gmail.com*

### **Abstract**

Photodynamic therapy is a noninvasive therapy for non-melanoma skin cancer. Photodynamic therapy involves the activation of a photosensitizing drug by visible light to produce activated oxygen species within target cells, resulting in their destruction. In addition to its therapeutic uses, optical spectroscopy is a helpful tool to prove the efficacy of PDT. It provides information on the distribution and degradation of sensitizers at the tumor's treatment area, the formation of fluorescent photoproducts, changes in tissue autofluorescence, light absorption and scattering in tissue induced by photodynamic treatment [1-3]. In this project photodynamic therapy (PDT) with topical application of methyl 5-aminolevulinate was used to treat non-melanoma skin cancer and actinic keratosis. The interval between the photosensitizer application and illumination was 3 h. The incident light dose was mostly  $75 \text{ J cm}^{-2}$ , at  $\sim 635 \text{ nm}$  wavelength. An imaging system was used to monitor spectroscopic signals during the PDT of tumors to display the localization and extension of skin tumors and to check therapy effectiveness. The spectra were classified and compared to histopathology to evaluate the efficiency in diagnostic discrimination employing optical spectroscopic techniques. Our findings indicate the potential of combination of PDT and spectroscopy as a reporter of treatment outcome. Further work is under way, in order to establish optimal treatment schemes.

- [1] Drakaki E., Dessinioti C., Stratigos A.J., Salavastru C., and Antoniou C., "Laser-induced fluorescence made simple: implications for the diagnosis and follow-up monitoring of basal cell carcinoma," *J Biomed Opt.* 19(3), 030901 (2014).
- [2] Drakaki E., Vergou T., Dessinioti C., Stratigos A.J., Salavastru C., Antoniou C., "Spectroscopic methods for the photodiagnosis of nonmelanoma skin cancer" *J Biomed Opt.* 1, 18(6), 61221 (2013).
- [3] Alvanopoulos, K., Antoniou, C., Melpo, P., Vareltzidis, A. and Katsambas, A., "Photodynamic therapy of superficial basal cell carcinomas using exogenous 5-aminolevulinic acid and 514-nm light" *J EADV* 9, 134–136, (1997)

## Control of human serum albumin concentration using Raman spectroscopy setup

**Dmitry N. Artemyev<sup>1</sup>, Valery P. Zakharov<sup>1</sup>, Julia A. Khristoforova<sup>1</sup>,  
Anastasia A. Lykina<sup>1</sup>, Vadim N. Konyukhov<sup>1</sup>, Igor L. Davydkin<sup>2</sup>, Tatiana P. Kuzmina<sup>2</sup>**

1. Samara State Aerospace University, Laser and biotechnical systems department, 443086, Samara, Russia
2. Samara State Medical University, Department of hospital therapy and transfusion, 443099, Samara, Russia

Dmitry N. Artemyev [artemyevdn@gmail.com](mailto:artemyevdn@gmail.com)

Blood analysis is frequently performed for medical diagnosis. Approximately 600 million cholesterol tests are performed annually worldwide to assess the risk and severity of cardiovascular disease. There is a significant interest in optical measurement that would permit simultaneous analysis of multiple components in whole blood without the need for conventional sample processing, such as centrifuging and adding reagents. The major challenge in an analysis of whole blood samples lies in the presence of numerous low-concentration components. This work studied the possibility of plasma proteins (human serum albumin, globulin) concentration control using Raman spectroscopy (RS) setup. The RS method was used successfully to the study of blood proteins [1-3].

Serum albumin accounts for 55% of blood proteins, and is a major contributor to maintaining the osmotic pressure of plasma to assist in the transport of lipids and steroid hormones. Globulins make up 38% of blood proteins and transport ions, hormones, and lipids assisting in immune function.

Human albumin solution is available for medical use, usually at concentrations of 5-25% (50-250 g/L). The reference range for albumin concentrations in serum is approximately 35 - 50 g/L. Human serum albumin solution - 10% was investigated using Raman spectroscopy method.

For Raman spectrums registration thermally stabilized semiconductor laser module LML-785.0RB-04 (power of 200 mW, wavelength of 785 nm) was used. Diffusely scattered light from the sample was registered by spectrograph (Shamrock SR-303i) with integrated NIR-optimized CCD camera (ANDOR DV-420A-OE). Use of this spectrograph provided a resolution of 0.05 nm at a low noise level. Raman scattering was obtained with a narrow-band filter to cut off fluorescent contribution of fiber, and broadband filters and a dichroic mirror for prevention of excitation laser radiation registration. For autofluorescence removal from raw data and pure Raman spectrum acquiring the method of polynomial approximation was used.

In this work, research was associated with the determination of albumin concentration in the solution with water. Various volumes and concentrations of different types of protein compounds were studied. The obtained spectra with different concentrations of albumin showed significant differences in the intensities in certain spectral bands (1005, 1100, 1330, 1450 and 1650  $\text{cm}^{-1}$ ). The error and confidence interval were calculated for albumin concentration control.

[1] N.C. Dingari, G.L. Horowitz, J.W. Kang, R.R. Dasari, I. Barman, Raman Spectroscopy Provides a Powerful Diagnostic Tool for Accurate Determination of Albumin Glycation, 7(2): e32406. doi:10.1371/journal.pone.0032406, (2012).

[2] A.J. Berger, T.W. Koo, I. Itzkan, G. Horowitz, M.S. Feld, Multicomponent blood analysis by near-infrared Raman spectroscopy, Appl Opt., 38(13). 2916-26 (1999).

[3] A.M. Enejder, T.W. Koo, J. Oh, M. Hunter, S. Sasic, M.S. Feld, G.L. Horowitz, Blood analysis by Raman spectroscopy, Opt Lett., 27(22), 2004-6 (2002).

## **Experimental system for estimation of blood hemoglobin concentration in vivo**

**Valery P. Zakharov<sup>1</sup>, Igor L. Davydkin<sup>2</sup>, Vadim N. Konyukhov<sup>1</sup>, Natalya S. Kozlova<sup>2</sup>,  
Pavel I. Bakhtinov<sup>1</sup>, Dmitry N. Artemyev<sup>1</sup>, Evgeny V. Molchkov<sup>1</sup>**

1. *Samara State Aerospace University, Laser and biotechnical systems department, 443086, Samara, Russia*
2. *Samara State Medical University, Department of hospital therapy and transfusion, 443099, Samara, Russia*  
[zakharov@ssau.ru](mailto:zakharov@ssau.ru)

Non-invasive methods of hemoglobin measurement are very useful for many medical applications, particularly for anemia screening. Pulse co-oximetry is one of these methods widely used in practice. However, some clinical studies [1, 2] showed a poor correlation between laboratory hemoglobin estimations (LHbC) and co-oximetry results.

The aim of our study was to investigate the possibility and ways of accuracy increasing of hemoglobin measurement by co-oximetry method. To realize this purpose the experimental system has been developed. The system implements a co-oximetry method and includes a multi-wavelength optical sensor, an electronic unit and the necessary software. The optical sensor is located on a finger and registers the absorbance at seven wavelengths. The variable component of the absorption at each wavelength is analyzed in the electronic unit. The ratio of the normalized amplitudes of the absorption variable components is used to measure the concentration of hemoglobin (SHbC). A basic principle of the system was to provide flexibility in changing the parameters and algorithms. The design of the system makes it relatively easy to change the set wavelengths of the probe radiation. The software makes it possible to test various algorithms for estimating the parameters of both absorption and hemoglobin determination.

The developed system was tested on a group of patients with different hematological diseases such as anemia, leukemia, myeloma and others. The study involved 124 patients. Five different algorithms have been used for evaluation of hemoglobin concentration. The results compared with LHbC. The difference more than 10 percent between LHbC and SHbC has been observed in 60 percent of the patients for all algorithms and all diseases. On the other hand, for each specific group of diseases estimation accuracy of the hemoglobin concentration was higher for one of the five algorithms. In this case difference between SHbC and LHbC not exceed 7 percent on an average.

Thus, one of the possible ways for increasing of precision measurement of hemoglobin concentration is an adaptation of the algorithm and its parameters in depends on species of disease. The criterion for automatic choice of required algorithm could be based on the analysis of a pulse wave form.

[1] L. J. Moore, C. E. Wade et al, Evaluation of noninvasive hemoglobin measurements in trauma patients, *The American Journal of Surgery*, vol.206, pp.1041-1047, 2013.

[2] J. Coquin, A. Dewitte et al, Precision of noninvasive hemoglobin-level measurement by pulse co-oximetry in patients admitted to intensive care units for severe gastrointestinal bleeds, *Critical Care Medicine*, vol.40, pp.2576-2582, 2012.

# **Effects of varying refractive index on combined refractometry and displacement interferometry**

**M. Holá, J. Lazar, M. Šarbort and Z. Buchta**

*Institute of Scientific Instruments of the CAS, v. v. i. Královopolská 147, 612 64 Brno, Czech Republic*

*hola@isibrno.cz*

We report on an evaluation of the influence that fast changes of the refractive index has on the uncertainty of interferometric displacement measurement. The concept is derived from a tracking refractometry evaluating the refractive index of air in the beam axis coinciding with the positioning interferometer. Application of this approach in multi-axis positioning and measurement mean to compromise the principle of spatial unity of the displacement measuring laser beam and the beam of the tracking refractometer. In this contribution we evaluate the level of uncertainty associated with the spatial shift of these two beams. Consequently the nature of the fluctuations of the refractive index of air in laser interferometry is investigated and discussed with the focus on potential applications in coordinate measuring systems and long-range metrological scanning probe microscopy systems.

**Acknowledgements:** The authors wish to express thanks for support to the infrastructure for the research was funded by Ministry of Education, Youth and Sports CR, projects LO1212, CZ.1.05/2.1.00/01.0017, and by Academy of Sciences CR, project RVO:68081731. Technology agency of the Czech Republic, project no. TA02010711, TE01020233.

## **References**

- 1 Leach R. K., Boyd R., Burke T. et al. (2011) The European nanometrology landscape. *Nanotechnology* 22, 6
- 2 Neuschaefer-Rube U., Neugebauer M., Dziomba T. et al. (2011) Recent Developments of Standards for 3D Micro- and Nanometrology. *Tm-Tech Mess* 78, 118-126
- 3 Meli, F., Thalmann, R. (1998) Long-range AFM profiler used for accurate pitch measurements. *Meas. Sci. Technol.*, 9, 1087-1092
- 4 Dai, G L., Pohlenz, F, Xu, M., Koenders, L, Danzebrink, H. U., Wilkening, G (2006) Accurate and traceable measurement of nano- and microstructures. *Meas. Sci. Technol.* 17, 545-552
- 5 Korpelainen, V., Seppä, J., Lasilla, A. (2010) Design and characterization of MIKES metrological atomic force microscope. *Prec. Eng.* 34, 735-744
- 6 Haycocks J., and Jackson K. (2005) Traceable calibration of transfer standards for scanning probe microscopy. *Precis Eng* 29, 168-175
- 7 Lazar, J., Číp, O., Čížek, M., Hrabina, J., Buchta, Z. (2011) Suppression of air refractive index variations in high-resolution interferometry. *Sensors* 11, 7644–7655
- 8 Lazar, J., Holá, M., Číp, O., Čížek, M., Hrabina, J., and Buchta Z. (2012) Refractive Index Compensation in Over-Determined Interferometric Systems. *Sensors* 12, 14084-14094
- 9 Lazar, J., Holá, M., Číp, O., Čížek, M., Hrabina, J., and Buchta Z. (2012) Displacement interferometry with stabilization of wavelength in air. *Opt. Express*, 20, 25, 27830
- 10 Ishige, M., Aketagawa, M., Quoc, T. B., Hoshino, Y. (2009) Measurement of air-refractive-index fluctuation from frequency change using a phase modulation homodyne interferometer and an external cavity laser diode. *Meas. Sci. Technol.*, 20, 8, 084019
- 11 Joo, K.-N., Ellis, J. D., Spronck, J. W., and Schmidt, R. H. M. (2011) Real-time wavelength corrected heterodyne laser interferometry. *Precis. Eng.* 35, 1, 38–43
- 12 Fox, R. W., Washburn, B. R., Newbury, N. R., and Hollberg, L. (2005) Wavelength references for interferometry in air. *Appl. Opt.* 44, 36, 7793–7801

## **Raman Study of Porous Polymers Prepared by Radiation Initiated Polymerization**

**M. Veres<sup>1</sup>, L. Himics<sup>1</sup>, I. Rigó<sup>1</sup>, S. Tóth<sup>1</sup>, M. Koós, T. Verebélyi<sup>1</sup>, B. Beiler, Á. Sáfrány<sup>2</sup>**

*1 - Wigner Research Centre for Physics, Hungarian Academy of Sciences, PO Box 49, H-1525, Budapest, Hungary*

*2 - International Atomic Energy Agency, Division of Nuclear Sciences and Applications, Department of Physical and Chemical Sciences, Section of Industrial Applications and Chemistry, Vienna International Centre, POB: 100, A-1400, Vienna, A2371 Austria*

*veres.miklos@wigner.mta.hu*

Due to their advantageous properties porous polymers (monoliths) are widely used in many areas of modern technology [1,2]. The possibility of simple modification of the porous structure, surface chemistry and other properties allows preparation of materials with the required characteristics easily. Porous polymers can be obtained using many different methods, but the use of gamma radiation initiation has several advantages over the traditional thermal or UV-initiation methods: the process is independent of the temperature, no need for initiators and other additives, and molds of almost any shape and size can be used. In order to exploit the possibilities of the method, the effect of the preparation conditions on the properties of the formed monoliths has to be studied in detail. In this work Raman spectroscopy was used to investigate the polymerization process and properties of monoliths prepared by gamma-radiation initiated polymerization from a mixture of diethylene glycol dimethacrylate (DEGDMA) and different solvents.

The samples were prepared by an in situ radiation polymerization method. Deoxygenated solutions of DEGDMA in different solvents (methanol, ethanol, 2-propanol, ethyl acetate and acetone) were placed in plastic bags, sealed under nitrogen and irradiated in a <sup>60</sup>Co  $\gamma$ -source with doses of 1-40 kGy. The conversion of the monomer into cross-linked polymer was calculated from the weight of the cross-linked polymer as compared to the weight of the monomer in the feed solution. The morphology of the monoliths was characterized by scanning electron microscopy. The Raman spectra were taken on a Renishaw 1000 Raman spectrometer using a 785 nm diode laser for the excitation with excitation spot size of 1 micron. The spectra were normalized to the 1455 cm<sup>-1</sup> peak after baseline correction. The C=C and C=O peaks were fitted using Lorentzians.

The evolution of the bonding configuration of the structure with dose and composition of the monomer mixture was investigated. Changes of characteristic Raman peaks with the applied dose revealed well the differences of the polymerization process in different solvents. The polymerization rates were determined from Raman data, and the correlations between the porous properties and the polymerization kinetics were established as well. Intact C=C bonds were found in the matrix even after 100% conversion, indicating the presence of trapped or partially polymerized monomer molecules in the structure.

M. Veres is grateful for the support of the Bolyai János Research Scholarship of the Hungarian Academy of Sciences.

[1] F. Svec, New Developments in the Field of Monoliths for Chromatography, LC GC Eur. 23, pp. 689854 (2010).

[2] F. Svec, Porous polymer monoliths: amazingly wide variety of techniques enabling their preparation, J Chromatogr A. 1217 pp. 902-24 (2009).

# Diagnosics of a polarization state in LiTaO<sub>3</sub> crystals by modulated IR laser radiation

A. Bogomolov, A. Solnyshkin, O. Sergeeva

Laboratory of Ferroelectrics Tver State University. 170002 Tver, Russia

e-mail: [o\\_n\\_sergeeva@mail.ru](mailto:o_n_sergeeva@mail.ru)

Polar dielectrics with high pyroelectric activity are functional materials for their use as IR detectors [1]. Among such materials, the crystals of triglycine sulphate (TGS) group and lithium tantalate LiTaO<sub>3</sub> are outstanding materials for pyroelectric sensors and detectors. LiTaO<sub>3</sub> is preferable because of the wider temperature region of polarization stability. However, the important problem is a uniformity of polarization distribution through a thickness of crystal samples [2 – 4]. In this work, diagnostics of the polarized state of the LiTaO<sub>3</sub> samples (10×10×1 mm<sup>3</sup>) was carried out on the base of a frequency dependence of pyroelectric response under a heat flux modulated by rectangular pulses. As a source of heat radiation, the infrared laser was used (laser module CLM-18451R-980 with a wavelength  $\lambda = 980$  nm and the emission power  $P = 220$  mW). Kinetics of pyroelectric response induced by the periodic heating / cooling (off/on) of LiTaO<sub>3</sub> crystal is presented on Fig. 1. According to a frequency dependence of pyroelectric current (Fig. 2, a), the pyroelectric coefficient distribution via the sample thickness (Fig. 2, b) was calculated on the base of procedure described in [5].

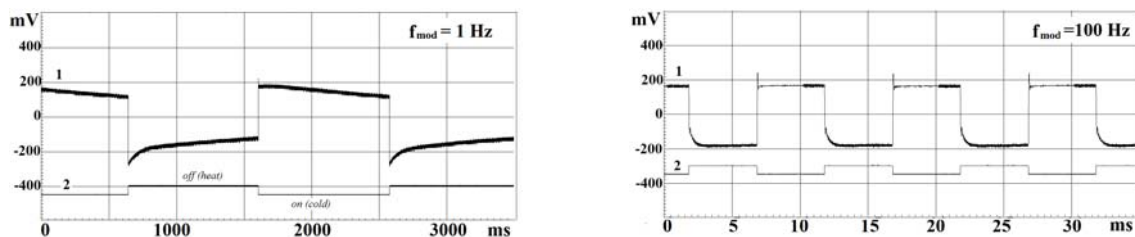


Fig. 1. Pyroelectric response of the crystal LiTaO<sub>3</sub> (1) under the IR laser beam modulated by rectangular pulses (2).

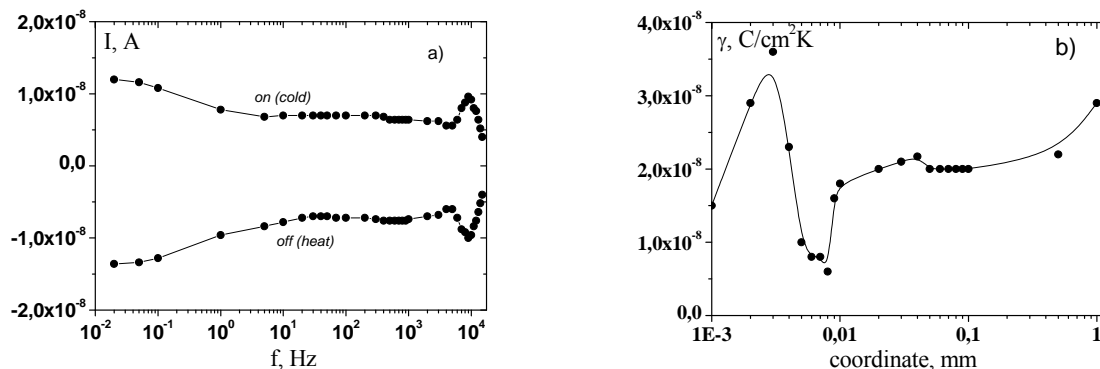


Fig. 2. The frequency dependence of the pyroelectric response amplitude (a) and recovered polarization profile (b) in LiTaO<sub>3</sub> crystal.

The inhomogeneous distribution of the polarization in the surface layers ( $\sim 10$   $\mu\text{m}$ ) crystal LiTaO<sub>3</sub> (fig. 2, b) is discussed.

- [1] Косоротов В.Ф., Кременчугский Л.С., Самойлов В.Б., Щедрина Л.В. Pyroelectric effect and its practical application. Kiev. Naukova Dumka. 1989.
- [2] Ploss B., Emmerich R., Bauer S. Thermal wave probing of pyroelectric distributions in surface region of ferroelectric materials: a new method for the analysis, J. Appl. Phys. V. 72, № 11. P. 5363 – 5370 (1992).
- [3] Bezdetny N.M., Khutorsky V.E., Zeinally A.Kh. Polarization distribution in ferroelectrics by regularization method from pyroelectric measurements, Ferroelectrics. V. 46, № 3-4. P. 267 – 273. (1983).
- [4] Lang S.B. New theoretical analysis for the laser intensity modulation method (LIMM) // Ferroelectrics. V. 106. P. 269 – 274. (1990).
- [5] Bogomolov A.A., Solnyshkin A.V., Kalgin A.V., Gorshkov A.G., Gridnev S.A. The pyroelectric effect in magnetoelectric 0.8 PZT-0.2 MZF and 0.8 PZT-0.2 NZF composites Bulletin of the Russian Academy of Sciences: Physics. T. 75. № 10. C. 1367-1370. (2011).

---

---

**SECTION LM**

**Laser–Matter Interaction**

---

---

## Laser damage of optical components in ultra-short regime for PW class lasers

O. Utéza, C. Pasquier, R. Clady, N. Sanner, M. Sentis

*Aix Marseille Université, CNRS, LP3 UMR 7341, 13288, Marseille, France.*

[Sentis@LP3.univ-mrs.fr](mailto:Sentis@LP3.univ-mrs.fr)

Nowadays laser source development for ultrahigh intensity science is a fast growing area, with huge efforts for scaling up the laser energy and scaling down the pulse duration and size of the focused beam. The perspective is here to open a route to explore the physics in the ultra-relativistic regime with expected breakthroughs in numerous topics of high field and ultrafast science from nuclear physics and engineering to medicine or astrophysics [1]. In that context, one critical issue for safe development and operation of emerging laser infrastructures of Petawatt class, combining hundreds of J and sub-15 femtoseconds pulses [2], must address the problem of damage of the optical materials and components devoted to the transport and delivery of the ultrahigh intensity beam to the target. Such damage evaluation shall be ideally conducted in vacuum to provide the exact conditions of operation for the optical components and materials under test. Laser-induced damage threshold (LIDT) is expected to vary depending on the ambience (air/vacuum) that may affect the energy exchange between the surrounding gas and the surface of the material. For instance, considering metals, smaller ablation thresholds have been measured in air with respect to vacuum [3]. Nevertheless, performing damage tests in air will provide LIDT data from which one can define important fluence parameters for safe and reliable operation of optical components and laser systems. Such quantitative evaluation of performance of optics is of high interest for laser manufacturers and optics suppliers, since it enables rapid feedback and comparative assessments for optimization of optical components. Measuring and improving the knowledge of laser – matter interaction thus appears to be essential to the development of any controlled and optimized laser systems and processes [4-6].

In that context, we will present in a first part the design and operation in air of a laser test-bench able to measure the laser-induced damage and ablation thresholds of optical materials and components with ultrashort pulses down to nearly 10 fs pulse duration. Working in air environment brings the advantage of convenience and rapid diagnostics, provided that the laser beam is properly handled. As a preliminary step, a careful analysis of the spatial, spectral and temporal properties of the ultrashort laser beam is performed to characterize its propagation till the focal plane where the target is located. The results allow us to determine an upper limit of the incident energy below which the beam propagation is not affected by nonlinear effects, like Kerr effect or air ionization, which could skew the determination of laser-induced damage and ablation thresholds.

In a second part we will demonstrate the capability of the laser test-bench by measuring the damage and ablation thresholds of fused silica irradiated by single ultrashort pulses of nearly 10 fs pulse duration. Finally, LIDT measurements of optical components designed for future multi Petawatt laser sources like mirrors and gratings will be presented.

[1] T. Tajima, D. Habs, G.A. Mourou, *Optik & Photonik* 4 (2010) 24.

[2] J. P. Chambaret, F. Mathieu, and K. Osvay, *ELI Courier* 2(2) (2010).

[3] E. G. Gamaly, N. R. Madsen, M. Duering, A. V. Rode, V. Z. Kolev, and B. Luther-Davies, *Phys. Rev. B* 71 (2005) 174405.

[4] M. Lebugle, N. Sanner, O. Utéza, M. Sentis, *Appl. Phys. A* 114 (2014) 129.

[5] M. Lenzner, J. Krüger, S. Sartania, Z. Cheng, Ch. Spielmann, G. Mourou, W. Kautek, F. Krausz, *Phys. Rev. B* 80 (1998) 4076.

[6] B. Chimier, O. Utéza, N. Sanner, M. Sentis, T. Itina, P. Lassonde, F. Lédaré, J.C. Kieffer, *Phys. Rev. B* 84 (2011) 094104.

**DIAMOND DEPOSITION IN OPEN AIR USING LASER RESONANT VIBRATIONAL  
EXCITATION OF PRECURSOR MOLECULES**

Y.F. Lu

*Department of Electrical Engineering, University of Nebraska-Lincoln, Lincoln,  
NE 68588-0511, USA*

*[\\*ylu2@unl.edu](mailto:ylu2@unl.edu)*

**Abstract**

In this study, we explored laser resonant vibrational excitations for promotion of energy efficiency in chemical reactions, for enhancement of diamond deposition, and for control of chemical reactions. The research mainly focused on resonant vibrational excitations of precursor molecules using lasers in combustion flame deposition of diamond, which led to: 1) promotion of chemical reactions; 2) enhancement of diamond growth with higher growth rate and better crystallizations; 3) steering of chemical reactions which lead to preferential growth of {100}-oriented diamond films and crystals; and 4) mode-selective excitations of precursor molecules toward bond-selective control of chemical reactions.

Diamond films and crystals were deposited in open air by combustion flame deposition through resonant vibrational excitations of precursor molecules, including ethylene (C<sub>2</sub>H<sub>4</sub>) and propylene (C<sub>3</sub>H<sub>6</sub>). A kilowatt wavelength-tunable CO<sub>2</sub> laser with spectral range from 9.2 to 10.9 μm was tuned to match vibrational modes of the precursor molecules. Resonant vibrational excitations of these molecules were achieved with high energy efficiency as compared with excitations using a common CO<sub>2</sub> laser (fixed wavelength at 10.591 μm). With resonant vibrational excitations, the diamond growth rate was increased; diamond quality was promoted; diamond crystals with lengths up to 5 mm were deposited in open air; preferential growth of {100}-oriented diamond films and single crystals was achieved; mode-selective excitations of precursor molecules were investigated toward control of chemical reactions.

## Control of agglomeration-fusion process of colloidal particles using laser processes in liquids

T. Tsuji<sup>1</sup>, I. Takade<sup>1</sup>, M. Tsuji<sup>2</sup>, Y. Ishimawa<sup>3</sup>, N. Koshizaki<sup>4</sup>

1- Interdisciplinary Graduate School of Science and Engineering, Shimane University, 1060 Nishikawatsu-Cho, Matsue 690-8504 Japan

2- Institute of Materials Chemistry and Engineering, Kyushu University, Kasuga 816-8580, Japan

3- Nanosystem Research Institute, National Institute of Advanced Industrial Science and Technology, Tsukuba 305-8565, Japan

4- Interdisciplinary Graduate School of Engineering, Hokkaido University, Kita13 Nishi8, Kita-Ku, Sapporo 060-8623, Japan

tktsuji@riko.shimane-u.ac.jp

The size control of metal nanoparticles is important in colloid science, because various properties of nanoparticles strongly depends on their size. Laser irradiation for colloidal nanoparticles is one of promising size control techniques.

Recently, laser melting in liquids (LML), in which non-focused laser irradiation at moderate fluence is conducted for colloidal nanoparticles to induce the nanoparticle fusion, attracts much attention as a novel technique to prepare submicron-sized spherical particles (SMPs).[1] The previous works showed that the nanoparticles agglomeration is necessary to prepare SMPs.[2,3] It was also found that when nanoparticles stabilized by ligands is used, the nanoparticles agglomeration is controlled not only by ligands statically, but also by laser irradiation dynamically. Such dynamic agglomeration process should be attributed to the reduction of the excess agglomeration and the sedimentation of the nanoparticles, suggesting that using nanoparticles stabilized by ligands is an efficient protocol to prepare SMPs.

So far we have conducted LML using nanoparticles stabilized by various ligands such as citrate and inorganic salts. The results showed that ligands affects both on the formation process of SMPs and on the SMPs size (Figure 1).

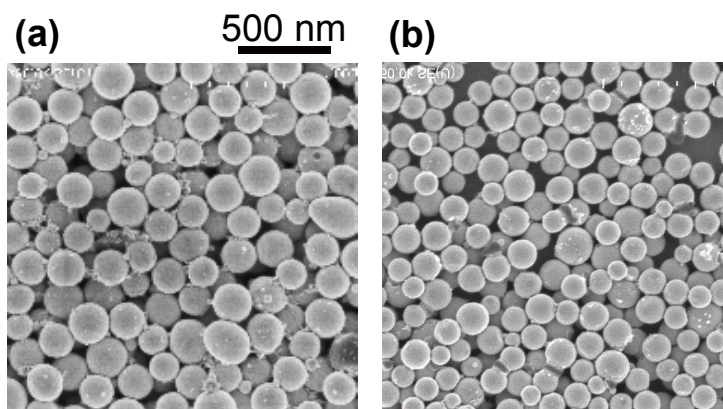


Figure.1: Gold SMPs prepared using LML conducted in a (a) 0.005 mM citrate solution and in a (b) 0.01 mM NaCl solution. The average diameter of the SMPs are (a) 230 and (b) 150 nm. The laser fluence was 60 mJ/cm<sup>2</sup>.

[1] H.Q. Wang, A. Pyatenko, K. Kawaguchi, X. Li, Z. Swiatkowska-Warkocka, N. Koshizaki, *Angew. Chem. Int. Ed.*, 49 (2010) 6361.

[2] T. Tsuji, T. Yahata, M. Yasutomo, K. Igawa, M. Tsuji, Y. Ishikawa, N. Koshizaki, *Phys. Chem. Chem. Phys.*, 15 (2013) 3099.

[3] Y. Ishikawa, Y. Katou, N. Koshizaki, Q. Feng, *Chem. Lett.*, 42 (2013) 530.

## Laser metal nanoparticles fragmentation processes

**I. Zvestovskaya<sup>1,2</sup>**

1- P.N. Lebedev Physical Institute of RAS, Leninsky pr.53, Moscow, 119991, Russia

2- National research Nuclear University MEPHI (Moscow Engineering Physics Institute),  
Rashirskoe sh.31, Moscow, 115409, Russia

INZvestovskaya@mephi.ru

Laser nanostructuring of materials is important in many scientific, technological and medical applications [1-4]. Of special interest are the metal nanoparticles, in particular the gold ones. Their unique optical properties stimulate the research of possible applications in optics, photonics, and biomedicine. All the methods of producing nanoparticles may be conventionally divided into two groups: wet chemistry i.e., the chemistry using liquid components and dry processes i.e., the processes with the use of plasma discharge or those that make use of the synthesis of the needed product in flame, as well as the material evaporation under the action of a laser pulse.

Laser ablation has manifested itself as one of most effective physical methods of nanofabrication. However, the laser methods form rather large-sized nanoparticles with a wide size spectrum. In this connection, in order to reduce the size of nanoparticles their colloids are additionally treated by ultra-short laser pulses. The mechanism of laser nanoparticles fragmentation in liquids has not been much studied and there is no consensus on this problem. They name the following possible mechanisms: the hydrodynamic instability of the melted metal drop arising due to its interaction with the liquid vapor; the evaporation of gold atoms under heating the nanoparticles by laser radiation; the Coulomb explosion.

A physical model of gold nanoparticles fragmentation in water under the action of femtosecond laser pulses is presented in this paper. When the colloids of relatively large gold nanoparticles (several tens of nm) are irradiated by femtosecond laser pulses, one can observe their fragmentation into smaller nanoparticles (up to several nm). In the process the particle is heated up to the melting temperature and turns into a drop of liquid. The heating is accompanied by thermionic emission from the drop surface. The emitted electrons take away the negative charge, and the drop of melted metal turns to be positively charged. Thus the model of fragmentation is based on the electrolyzation of metal nanoparticles heated by a laser pulse, and their division under the development of instability of a charged drop of liquid metal. As a mechanism of electrolyzation we have considered the emission of hot electrons from the surface of a nanoparticle with further solvation in liquid.

Theoretical modeling of metal nanoparticles fragmentation in water under the action of femtosecond laser pulses is discussed [3]. The problem of heating a gold nanoparticle by laser pulses of femtosecond duration has been solved. The value and typical time of the drop of thermionic emission current from the nanoparticle surface due to the heating of the particle by the laser radiation field has been found. On the basis of the Rayleigh drop model the criterion of nanoparticle fragmentation has been found. The estimates of the charge gained by the nanoparticle due to the electron thermionic emission and their further solvation have been obtained. It was shown that the charge exceeds the threshold value given by the Rayleigh criterion. It is possible to conclude that as a result of the influence of laser radiation the particle becomes unstable and the nanoparticles fragmentation takes place.

The results of theoretical modeling may be used to optimize the laser operation regime destined to produce the nanoparticles of the given size.

[1] I.N. Zvestovskaya, Laser-assisted metal surface micro- and nanostructurization, *Laser and Particle Beams*, vol. 28, pp.437 (2010).

[2] I.N. Zvestovskaya, Laser Nanostructurization of metal surfaces, *Quantum Electronics*, vol.40, pp. 942 (2010).

[3] I.N. Zvestovskaya, A.P. Kanavin, S.D. Makhlysheva Theoretical modeling of laser fragmentation of nanoparticles in liquid media. *Bulletin of the Lebedev Physics Institute*, vol. 40, pp.335 (2013)

[4] I.N. Zvestovskaya, *Fundamentals of Laser-Assisted Micro- and Nanotechnologies* (Springer), Chapter 3, pp.51-75 (2014).

# **From slow light to single-photon lasing and neutral-atom acceleration in a plasmonic crystal**

**Igor V. Melnikov**

*Department of Electronic Materials, National Research University of Electronic Technology, proezd 4806,  
Zelenograd, Moscow 124498, Russian Federation and*

*Department of Electrical and Computer Engineering, University of Illinois, 306 N Wright Street, Urbana, IL 61801*

In the recent years, quantum plasmonics has quickly become a major research field in nanoscale optics. In future integrated nanoscale plasmonic circuits quantum sources of light will provide the input signal which then will be used to channel along plasmonic waveguides and the propagating plasmons will be used as carriers of information. Integration of quantum and classical plasmonic units in a single device is projected to be a driving force in the development of next generation optoelectronic devices. Photoluminescence (PL) from silver nanoparticles is a poorly understood phenomenon and requires thorough investigation from both classical (such as local field enhancement and coupling to the LSPR) and quantum mechanical description, such as interband electronic transitions, size-dependent electronic band structure or grains effects in a single nanoparticle.

Quantum photonics integrated metamaterials will require multi-functionality in a single device. For example, quantum emitters embedded in a hyperbolic metamaterial with a gradient of the effective dielectric permittivity. Organic dyes can be used as quantum emitters integrated close to the metamaterial. However, organic dyes suffer from photobleaching degradation. Silver nanoparticles, with or without surface functionalization, are more photostable and are reported to exhibit photoluminescence with a quantum yield comparable to organic dyes. Integrating silver nanoparticles in a layered or graded metamaterial is a promising route to develop novel multi-functional quantum plasmonic metamaterials. These novel quantum plasmonic metamaterials might be used for photovoltaic, quantum computing, near-field sub-diffraction optics, super-lensing, and optical cloaking.

In this Report, we explore the population, polarization, and optical field dynamics that is the excitation transport inside both a plasmonic crystal and continuous medium of quantum emitters where isotropic spontaneous decay organizes itself into a correlated high-gain process. The objective is to develop a model that includes (i) both the spatiotemporal dynamics of the radiation field and the dynamic properties of two-level atoms; (ii) is applicable to a plasmonic crystal where excitation (LSPR) is initially localized inside a narrow area; and (iii) can be extended onto a two-dimensional geometry in a physically transparent way.

We add up this Report with a theoretical model that drives plasmonic crystal into a totally novel area of exploitation – laser acceleration of neutral atoms. Indeed, recent technological advances in coupling atoms to photonic crystal fibers and nanophotonic waveguides have been accompanied by tremendous success in single-atom trapping, self-organization, and neutral-atom transport. However, to the best of our knowledge no one has addressed issues as to whether or not basic concepts like the principle of Macmillan phase stability could be exploited in accelerating neutral atoms by an optical field that, in turn, propagates inside (or in the vicinity) of a specially tailored plasmonic structure.

Our aim here is to make a qualitative analytical assessment of neutral-atom acceleration problem and to provide direct physical insight to an otherwise complicated problem. In particular, our goal in this presentation is to show that the mechanism of continuously varying recoil, which may be implemented by the engineered dispersion, provides an effective acceleration tool. Introduction a dipole-dipole interaction into the model will provide a better connection, and hence understanding, on how to balance between atom bunching and repulsion can be created and applied to atom beam acceleration inside a photonic crystal.

Our method is based on the two-level density-matrix equation modified to include dipole-dipole interaction which has the advantage of providing a semi-analytical result without resorting to cumbersome numerical simulations. Specifically, we find conditions at which distribution function collapses and examine bounds for dispersion tailoring that provides corresponding gradual increase of the speed of light. Additionally, we simulate density-matrix equations for the plasmonic crystal made of metal/semiconductor nanowires that provide an additional tool to keep the atom bunching.

## 3D double wave-length lasers-induced reversible phase-structure modification inside photostructurable glass

V. P. Veiko, E. I. Sergeev

ITMO University, 197101, Kronverkskiy Pr., 49, St. Petersburg, Russia

veiko@lastech.ifmo.ru

3D modification inside a photostructurable glass (PhG) is of great interest for the micromachining of different components, systems and devices of photonics, microfluidic etc. Unfortunately, known techniques such laser crystallization consist from two stages—a photoactivation by femtosecond laser pulses and a heat treatment in a furnace that takes long enough time (4 – 8 h.) for 3D structures formation [1, 2]. The other limitation of this technique is irreversibility which significantly reduces an area of its possible applications. Thus, the development of direct laser crystallization process without the stage of annealing in a furnace seems to be quite important.

The purpose of this work is to find new solutions for realization of direct and reversible phase - structure transformation inside PhG by laser irradiation.

The direct laser writing at this technique was implemented with the simultaneous use of two different lasers. The first of them is the picosecond Nd:YAG laser (532 nm, 30 ps, 10 mJ) was used to realize a photoactivation process [3]. The local area was formed by the interaction of picosecond laser pulses with PhG and consisted of defects in the form of dots, lines or curves. At the annealing process these laser produced defects acted as centers of crystallization. The other wavelength was in the region of high absorption of silica glasses -10.6 μm of CO<sub>2</sub> laser (10.6 μm, 190 ns, 5 kJ) and it was used for final formation of crystalline phase (or amorphous phase at reverse process) which was initiated by CO<sub>2</sub> laser-induced fast annealing (LIFA). Also, the CO<sub>2</sub> laser annealing was used to eliminate the rough distortion of topology (fig.).

As a result of experiments multiple phase transformation in the bulk of PhG plates by direct laser writing were demonstrated. The visualization of crystallization and reversible amorphization processes was implemented. This fact allowed exploring the kinetic of phase transformation inside glass in real time. The temperature ranges and durations of LIFA within these ranges which initiated crystallization and reversible amorphization were experimentally determined. Finally two types of crystalline phases was revealed, which compositions corresponded to lithium metasilicate (Li<sub>2</sub>SiO<sub>3</sub>) and lithium disilicate (Li<sub>2</sub>Si<sub>2</sub>O<sub>5</sub>) crystalline phase that was confirmed by Raman microspectroscopy.

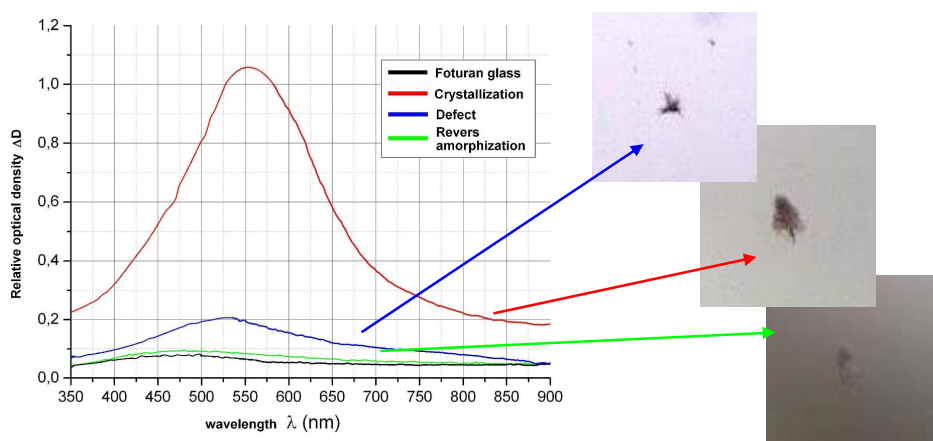


Fig. Spectral dependence of relative optical density of PhG plate, crystallization area, defect and area of reversible amorphization.

**Acknowledgements**—The presented work was completed under financial support due to Russian Federation Government grant 074-U01, RSF agreement № 14-12-00351 and by the Leading State Universities of Russian Federation subsidy NS 1364.2014.2.

- [1] V. P. Veiko, Q. K. Kieu, N. V. Nikonov, and P. A. Skiba, On the Reversibility of Laser – induced Phase-structure Modification of Glass – ceramics, *J. Laser Micro/Nanoeng.*, Vol. 1, No 2., pp 149–154 (2006).  
 [2] F. Ye, Q. Liao, J. Lin, J. Song, L. Qiao, Q. Cheng, K. Sugioka, Femtosecond Laser Fabrication of Monolithically Integrated Microfluidic Sensors in Glass, *Sensors*, Vol. 14, pp 19402-19440 (2014).  
 [3] V. P. Veiko, M. M. Sergeev, E. I. Ageev, A. A. Petrov, 3D express crystallization of Foturan glass at CO<sub>2</sub> laser annealing on the defects produced by picosecond laser, *Proc. of SPIE.*, Vol. 9065 (33), pp 90650M–90650M-7 (2013).

**Tailoring properties in materials for energy by laser processing**

F.M. Costa<sup>1</sup>, M.R. Soares<sup>1</sup>, J. Rodrigues<sup>1</sup>, N.M. Ferreira<sup>1</sup>, Sh. Rasekh<sup>2</sup>, R.G. Carvalho<sup>1</sup>,  
T. Holz<sup>1</sup>, N.F. Santos<sup>1</sup>, A.J.S. Fernandes<sup>1</sup>, M.A. Madre<sup>2</sup>, J.C. Diez<sup>2</sup>, F.M. Figueiredo<sup>3</sup>,  
R.F. Silva<sup>3</sup>, T. Monteiro<sup>1</sup>, A. Sotelo<sup>2</sup>

<sup>1</sup>IN, Departamento de Física, Universidade de Aveiro, 3810-193 Aveiro, Portugal.

<sup>2</sup>Instituto de Ciencia de Materiales de Aragón (ICMA) (CSIC-Universidad de Zaragoza),  
C/M<sup>a</sup> de Luna, 3 50018 Zaragoza. Spain.

<sup>3</sup>CICECO, Departamento de Eng. de Materiais e Cerâmica, Universidade de Aveiro  
3810-193 Aveiro, Portugal

The global demand for low cost, efficient, sustainable energy production and transport along with energy saving through efficient lighting is rapidly increasing. Therefore, energy related materials design and improvement of their physical properties is of utmost importance. In recent years, a remarkable progress in the development of nanostructured materials for this purpose has been reported. Among all synthesis techniques, laser processing has been a successful approach used in the development of a plethora of materials with superior characteristics.

Advanced laser processing techniques like the laser floating zone technique (LFZ), electrically assisted laser floating zone (EALFZ), laser assisted flow deposition (LAFD) and pulsed laser ablation in liquids (PLAL) were used by our group to produce superconductors, thermoelectrics, ionic conductors and light emitters, among others.

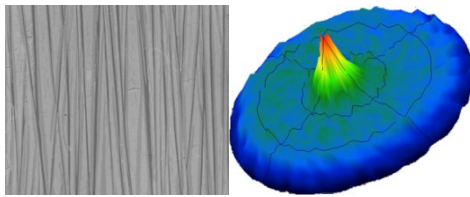
The LFZ technique proved to be suitable for producing mixed ionic conductors for fuel cells applications. Particularly, a novel zirconia-barium zirconate eutectic material was developed in order to combine oxygen ionic conduction through zirconia with protonic conduction from barium zirconate, promoting mixed ionic conduction behavior.

Superconductors and thermoelectric materials were successfully grown by assisting the LFZ process with an electrical current, resulting in enhanced transport properties due to ionic drift intensification in the molten zone towards the crystallization interface. The BiSrCaCuO superconductors, also grown by EALFZ, are able to transport very high electrical currents while thermoelectrics based on cobaltite oxide ceramics exhibit very high thermoelectric figures of merit.

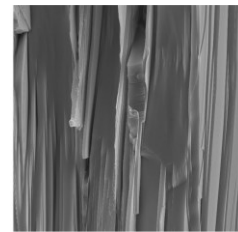
The LAFD is a recent technique based on the vapor-solid mechanism that proved to be very efficient in the synthesis of micro and nanocrystals of ZnO and SnO<sub>2</sub> with very high crystallinity. These oxide semiconductors exhibit well-established properties for optoelectronic and electronic applications and are being subject of an intense research worldwide.

Light emitters based on lanthanides (Ln) doped zirconia were grown by laser floating zone technique. High intensity visible luminescence at room temperature of single crystalline fibres was achieved by optical pumping in the ultraviolet region.

PLAL technique, has found to be a powerful approach to produce nanoparticles of zirconia doped with lanthanides and optically activate  $\text{Ln}^{3+}$  that arise as a new class of luminescent materials of wide interest for photonics applications. Nanoparticles with up-converting properties are being intensely investigated due to their great potentialities for biomedical applications as bio markers and targeting.



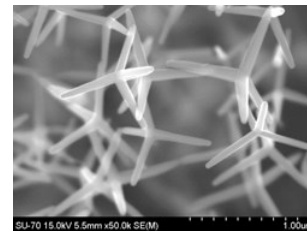
Thermoelectrics,  $\text{Bi}_2\text{Ca}_2\text{Co}_2\text{O}_x$



Superconductors,  $\text{Bi}_2\text{Sr}_2\text{CaCuO}_8$



$\text{ZrO}_2:\text{RE}^{3+}$  light emitters



ZnO tetrapods

# Femtosecond laser Bessel beam drilling of high-aspect-ratio microholes based on electrons dynamics control

Xiaowei Li<sup>1</sup>, Lan Jiang<sup>1</sup>, Qiang Cao<sup>1</sup>, Bo Xia<sup>1</sup>, Xueliang Yan<sup>1</sup>, Yang Liu<sup>1</sup>, YongFeng Lu<sup>2</sup>

1- Laser Micro/Nano Fabrication Laboratory, School of Mechanical Engineering, Beijing Institute of Technology, Beijing 100081, People's Republic of China

2- Department of Electrical Engineering, University of Nebraska-Lincoln, Lincoln, NE 68588-0511, USA

E-mail: jianglan@bit.edu.cn

Drilling of high-quality microholes with small diameters ( $<100\ \mu\text{m}$ ) has recently attracted extensive research due to broad applications in aerospace, optical fiber sensors, microfluidics, biomedical devices, and other areas. However, some challenges remain in achieving deep microholes, particularly for a few micrometer high-aspect-ratio ( $>50:1$ ) holes. A femtosecond (fs) lasers offer unique advantages, such as high-precision materials processing, thereby providing the potential for efficient drilling of deep microholes with reduced recast/microcracks, minimized heat-affected zones, and the absence of plasma-shielding effects. But there remain many challenges in hole drilling by using conventional fs laser with Gaussian beams, such as low aspect ratio (typically  $<16:1$  for micrometer holes) and taper effects.

In this study, we report high-aspect-ratio micro-holes drilling in PMMA (polymethyl methacrylate) using single-shot fs laser Bessel beams and its real-time electrons dynamics measurement as shown in Fig. 1. Bessel beams have a central core surrounded by concentric rings and maintain a long depth of focus far larger than the Rayleigh range generated by Gaussian beams. Axicon is used to transform Gaussian beams into Gaussian-Bessel beams, which was then irradiated on the sample by a telescope consisting of plano-convex lens and microscope objective. The optical setup can generate de-magnified central core diameter down to  $2.0\ \mu\text{m}$  and depth of focus up to  $780\ \mu\text{m}$ . Using the technique, we obtained structures with the diameters of  $1.6\text{-}2.5\ \mu\text{m}$  and the aspect ratio of  $150\text{-}330:1$ . The AFM/SEM images of the sample cross sections and capillary action show the formed structures are high-quality taper-free microholes. Arrays of microholes written by flying punching at a rate of 100 holes per second demonstrate high drilling efficiency and high repeatability. For the fundamental understanding of the drilling process, the formation of such long and uniform microholes are attributed to the stationarity of the Bessel beam, which can effectively adjust photon absorption process and localized transient material properties by controlling electron dynamics such as free electron density spatial distribution. We therefore measured the evolution of electron dynamics in femtosecond bessel beams microholes drilling across multi-time scales, including femtosecond scale (the propagation of fs laser pulse), picosecond-scale (the generation and evolution of plasma), nanosecond-scale (the plasma ejection and expansion process), and microsecond-scale (the high-aspect ratio micro-holes formation).

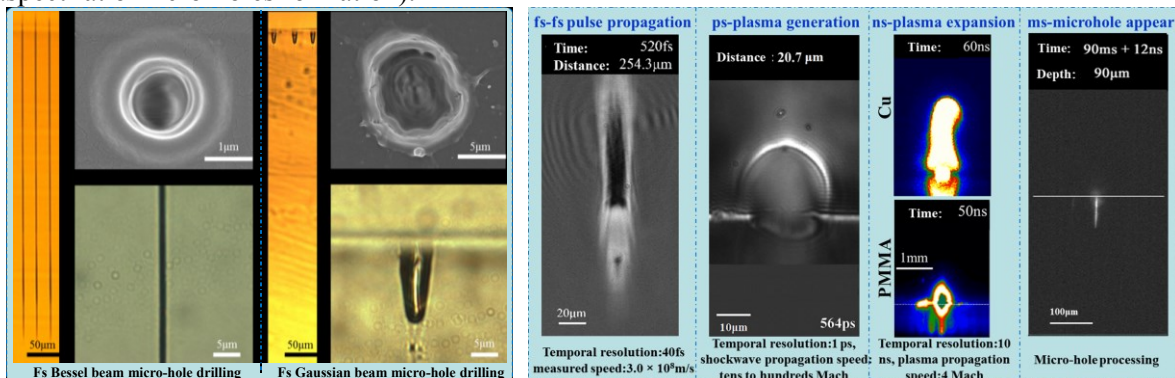


Figure 1. (Left) Microscope images of micro-holes drilled in PMMA substrate by single shot fs laser Bessel beams and Gaussian beams; (Right) Evolution of electron dynamics in femtosecond laser drilling across multiple time scales

[1] L. Jiang, P. Liu, X. Yan, et al., Optics Letters, Vol. 37, pp. 2781-2783 (2012).

[2] X. Yan, L. Jiang, X. Li, et al., Optics Letters, Vol. 39, pp. 5240-5243 (2014).

## **Surface functionalization with femtosecond lasers**

Chunlei Guo

*The Institute of Optics, University of Rochester, Rochester, NY 14627, USA*

In this talk, I will discuss a number of techniques developed in my lab that allow us to dramatically alter the properties of materials through femtosecond laser surface structuring. The techniques led to the creation of the so-called black and colored metals, and more recently significantly altered surface wetting effects. Possible applications of the functionalized surfaces will also be discussed.

**Hybrid femtosecond laser 3D microprocessing  
consisting of subtractive and additive manufacturing**

Koji Sugioka, Jian Xu, Felix Sima, Dong Wu, and Katsumi Midorikawa  
*RIKEN Center for Advanced Photonics, Wako, Saitama 351-0198, Japan*  
*ksugioka@riken.jp*

The rapid development of femtosecond laser has revolutionized materials processing due to its unique characteristics of ultrashort pulse width and extremely high peak intensity [1]. In particular, the high peak intensity allows nonlinear interactions such as multiphoton absorption and tunneling ionization to be induced in transparent materials, which provides versatility in terms of the materials that can be processed. More interestingly, irradiation with tightly focused femtosecond laser pulses inside transparent materials makes three-dimensional (3D) micro- and nanofabrication available due to efficient confinement of the nonlinear interactions within the focal volume.

Using this feature, the femtosecond laser can perform both the subtractive and additive 3D manufacturing [2]. Specifically, the former process involves femtosecond laser internal modification followed by wet chemical etching (Femtosecond Laser Assisted Wet Etching: FLAE) realizing the direct fabrication of 3D microfluidic structures inside glass, while the latter one is two-photon polymerization (TPP) of photocurable resin. In this paper, we propose to conjugate these two processes to further enhance performance of femtosecond laser processing for fabrication of highly functional microdevices [3-5].

The hybrid femtosecond laser microprocessing consists of two main steps. The first step is to fabricate 3D microfluidic structure by FLAE of photosensitive Foturan glass. The second step is to integrate functional microcomponents into the resulting glass 3D microfluidic structure for device functionalization by the TPP procedure.

This technique was applied to fabricate true 3D biochips with high functionalities [3-5]. The fabricated device is referred to as a “ship-in-a-bottle” biochip, since the polymer 3D micro and nano structures are created in the closed 3D glass microfluidic structure after the microfluidics fabrication. The ship-in-a-bottle biochips fabricated showed high capabilities to demonstrate simultaneous filtering and mixing of two kinds of fluids with an 87% mixing efficiency in a short distance, on-chip synthesis of ZnO flower-like microparticles, and coupling-free parallel cell detection and counting with a 100% success rate.

**References:**

- [1] K. Sugioka and Y. Cheng, “Ultrafast lasers - reliable tools for advanced materials processing”, *Light Sci. Appl.* **3**, e149 (2014).
- [2] K. Sugioka and Y. Cheng, “Femtosecond laser three-dimensional micro- and nanofabrication”, *Appl. Phys. Rev.* **1**, 041303 (2014).
- [3] D. Wu, S. Wu, J. Xu, L. Niu, K. Midorikawa, and K. Sugioka, “Hybrid femtosecond laser microfabrication to achieve true 3D glass/polymer composite biochips with multiscale features and high performance: the concept of ship-in-a-bottle biochip”, *Laser Photon. Rev.* **8**, 458-467 (2014).
- [4] D. Wu, J. Xu, L. Niu, S. Wu, K. Midorikawa, and K. Sugioka, “In-channel integration of designable microoptical devices using flat scaffold-supported femtosecond-laser microfabrication for coupling-free optofluidic cell counting”, *Light Sci. Appl.* **4**, e228 (2015).
- [5] D. Wu, L. G. Niu, S. Z. Wu, J. Xu, K. Midorikawa, and K. Sugioka, “Ship-in-a-bottle femtosecond laser integration of optofluidic microlens arrays with center-pass units enabling coupling-free parallel cell counting with 100% success rate,” *Lab Chip* (2015). DOI: 10.1039/c4lc01439a

## High-speed laser-induced forward transfer of inks

**P. Serra, A. Patrascioiu, C. Florian, J.M. Fernández-Pradas, J.L. Morenza**

*Departament de Física Aplicada i Òptica, Universitat de Barcelona  
Martí i Franquès 1, E-08028 Barcelona, Spain*

*pserra@ub.edu*

Laser-induced forward transfer (LIFT) is a printing technique that makes possible the deposition of a wide range of inks allowing the precise printing of micron-sized droplets through a jetting mechanism triggered by a pulsed laser beam. At low and moderate printing speeds each printing event is initiated only after the completion of the previous droplet. However, current industrial demands require working at such high speeds that can result in the coexistence of liquid jets generated sequentially during their expansion. Depending on the separation between adjacent jets, the interaction between them is possible, and this can compromise the printing outcome.

In this work we use time-resolved imaging to investigate such interaction. In a first experiment droplets were simultaneously printed at different inter-beam separations; the analysis of their morphology revealed that a significant departure from the single-beam dynamics was taking place below a specific separation. In a second experiment, time-resolved images of the jetting dynamics revealed the existence of a significant jet-jet interaction that could explain the observed departure, an interaction that proceeds through remarkable jet deflection, for which a possible onset mechanism is proposed.

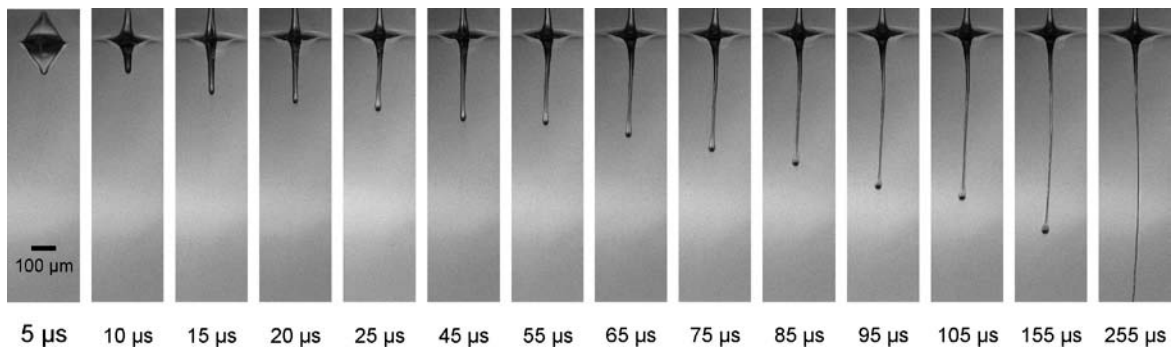


Figure: Jetting dynamics during a laser-induced forward transfer event. The donor substrate is placed in the top of the images, and the laser beam impinges from above. The delay time after the laser pulse is indicated in the bottom.

# High-Efficient Coherent Lyman- $\alpha$ Resonance Radiation Source for Ultra Slow Muon Generation

**Norihito Saito<sup>1</sup>, Yu Oishi<sup>2</sup>, Koji Miyazaki<sup>1</sup>, Kotaro Okamura<sup>1</sup>,  
Oleg A. Louchev<sup>1</sup>, Masahiko Iwasaki<sup>2</sup>, Satoshi Wada<sup>1</sup>**

*1- RIKEN Center for Advanced Photonics, RIKEN, 2-1 Hirosawa, Wako, Saitama 351-0198, Japan*

*2- RIKEN Nishina Center for Accelerator-Based Science, RIKEN*

*Main author email address: norihito@riken.jp*

A high-intensity, low-temperature, high time resolution, and high spin polarized ultra slow muon source is required to realize an ultra slow muon microscope [1] and to ultra-precisely measure the muon anomalous magnetic moment [2]. High-energy coherent Lyman- $\alpha$  resonance radiation source is a critical element to realize the ultra slow muon source. The muonium Lyman- $\alpha$  resonance line, 122.089 nm corresponds to the 1S-2P transition of muonium atom. Ultra slow muons are generated in resonant ionization by the simultaneous irradiation of 122.089 nm and ultraviolet radiation at a wavelength around 355 nm.

In this study, we report on a high-efficient coherent Lyman- $\alpha$  resonance radiation source. We chose two-photon resonance four-wave mixing in krypton, which is a well-known method to generate vacuum ultraviolet (VUV) radiation, to generate coherent radiation at the muonium Lyman- $\alpha$  resonance line [3]. The energy-level spacing between the  $4s^6$  and the  $4p-5p[1/2, 0]$  in krypton is equal to  $h\omega_1 = hc/(212.556 \text{ nm} \times 10^{-9} \text{ m})$ .  $h$  is Planck's constant and  $c$  is the speed of light. Therefore, we need a coherent 212.556 nm light source for two-photon excitation. And a tunable near-infrared light source that can be tuned around 820.649 and 845.015 nm is required to precisely tune VUV radiation emitted by four-wave mixing to 122.089 and 121.568 nm (the hydrogen Lyman- $\alpha$  resonance line). We applied advanced solid-state and fiber laser technology to develop such light sources, and also developed Nd-doped  $\text{Y}_3\text{Ga}_2\text{Al}_3\text{O}_{12}$  ceramic to efficiently amplify 1062.78 nm coherent light. Its fifth-harmonic corresponds with 212.556 nm. Using the pump light sources with a high beam quality, the conversion efficiency in two-photon resonance four-wave mixing reached  $3.6 \times 10^{-3}$  at the hydrogen Lyman- $\alpha$  resonance line. The conversion efficiency is an order of magnitude higher than that of previous studies [3]. The output pulse energy at the Lyman- $\alpha$  resonance line increased up to 8.4  $\mu\text{J}$  at a pulse width of 2 ns and a repetition rate of 25 Hz. The use of power amplifiers with maintenance of beam quality in the Lyman- $\alpha$  resonance radiation source is probably easily scalable towards several 10  $\mu\text{J}$  energies at 122.089 and 121.568 nm.

- [1] Y. Miyake, Y. Ikedo, K. Shimomura *et al.*, Ultra slow muon microscopy by laser resonant ionization at J-PARC, MUSE, *Hyperfine Interact.*, vol. 216, pp. 79-83 (2013), and references therein.
- [2] G. W. Bennett, B. Bousquet, H. N. Brown *et al.*, Final report of the E821 muon anomalous magnetic moment measurement at BNL, *Phys. Rev. D.* vol. 73, pp. 072003-1-072003-41 (2006).
- [3] O. A. Louchev, P. Bakule, N. Saito *et al.*, Mechanism of and computational model for Lyman- $\alpha$ -radiation generation by high-intensity-laser four-wave mixing in Kr-Ar gas, *Physical Review A*, vol. 84, pp. 033842-1-033842-9 (2011), and references therein.

# Models of ultrashort laser modification of bulk transparent materials: Synergy of excitation/relaxation kinetics, thermodynamics and mechanics

**N. M. Bulgakova<sup>1,2</sup>, V. P. Zhukov<sup>3,4</sup>, Y. P. Meshcheryakov<sup>5</sup>**

*1 - HiLASE Centre, Institute of Physics ASCR, Za Radnicí 828, 25241 Dolní Břežany, Czech Republic*

*2 – Kutateladze Institute of Thermophysics SB RAS, 1 Lavrentyev Ave., 630090 Novosibirsk, Russia*

*3 - Institute of Computational Technologies SB RAS, 6 Lavrentyev Ave., 630090 Novosibirsk, Russia*

*4 - Novosibirsk State Technical University, 20 Karl Marx ave., 630073, Novosibirsk, Russia*

*5 - Design and Technology Branch of Lavrentyev Institute of Hydrodynamics SB RAS, Tereshkovo str. 29, 630090 Novosibirsk, Russia*

*e-mail: nbul@itp.nsc.ru*

Ultrafast laser modification of optical glasses and crystals has proven to be an important technique enabling modification of material properties for technological applications based on 3D photonic structures. The physics behind laser-induced modification phenomenon is extremely rich and still far from complete understanding. Laser light excites material during pulse action that is only a starting point of material evolution which can involve a variety of thermodynamic, kinetic and mechanical processes (lattice heating, melting, vaporization, defect formation, material compaction/rarefaction, etc.). Some of these processes extend up to the microsecond timescale when a final modification structure is “frozen” in the glass matrix after a single pulse action. At multi-shot irradiation regimes which are usually utilized for 3D direct writing, the produced structures are strongly dependent on pulse repetition rate that is, at what stage of the evolution triggered by the previous pulse, a new pulse re-excites matter. Each next pulse interacts with already modified matter with new optical properties, redistributed density, accumulated defects, and residual heat from the previous pulses. Hence, the quality of final structures depends on the synergetic action of multiple re-excitations of the confined electron plasma, its relaxation with pushing matter into different thermodynamic states from gentle heating to extreme conditions, generation of GPa-level pressures resulting in shock-induced deformations, and rearranging of covalent bonds upon photo-excitation of the material network. The majority of models developed to date for understanding material evolution in 3D writing regimes are limited to a single pulse consideration at a time scale up to few picoseconds. The aim of this work is to extend modeling to the real timescale of single-shot modification and to make an attempt of simulations of multi-shot irradiation regimes.

The basic idea of the model was proposed in [1] and it assumes a two-stage modeling. At the first stage, the equations describing the laser pulse propagation in transparent matter absorbing light through non-linear processes are solved. The output of such modeling in the form of the spatial distribution of the absorbed energy at the end of the laser pulse action represents input data for applying the thermo-elastoplastic model. The latter is applied to follow the temperature evolution in the irradiated sample and material redistribution with the von-Mises yield criterion of irreversible material deformation. This combined model has allowed to qualitatively explain the possibility to reverse the natural behavior of glass, forcing it to relocate its density in the desired manner. A disadvantage of the model was that, being based on the non-linear Schrödinger equation which implies unidirectional beam propagation, it did not allow to quantitatively describe experimental data. Being redesigned with using Maxwell’s equations [2], the model has demonstrated good agreement with experiments [2-4] and allowed revealing a number of new phenomena such as asymmetry of the absorption region and an umbrella-like defect-mediated shield formation in pump-probe and multi-short irradiation regimes [3]. Further progress in the model development will be reported which reveals the actual timescales of irreversible material deformation induced by individual laser pulses [4] and unusual effects which can be observed upon multipulse irradiation with and without laser beam scanning along the sample such as formation of a transient thermal lens.

[1] A. Mermillod-Blondin, I.M. Burakov, Y.P. Meshcheryakov, N.M. Bulgakova, E. Audouard, A. Rosenfeld, A. Husakou, I.V. Hertel, R. Stoian, Flipping the sign of refractive index changes in ultrafast and temporally shaped laser-irradiated borosilicate crown optical glass at high repetition rate, *Phys. Rev. B*, Vol. 77, 104205, (2008).

[2] N.M. Bulgakova, V.P. Zhukov, Y.P. Meshcheryakov, Theoretical treatments of ultrashort pulse laser processing of transparent materials: Towards understanding the volume nanograting formation and “quill” writing effect, *Appl. Phys. B*, Vol. 113, pp. 437-449 (2013).

[3] N.M. Bulgakova, V.P. Zhukov, Y.P. Meshcheryakov, L. Gemini, J. Brajer, D. Rostohar, T. Mocek, Pulsed laser modification of transparent dielectrics: what can be foreseen and predicted by numerical simulations? *J. Opt. Soc. Am. B*, Vol. 31, pp. C8-C14 (2014).

[4] N.M. Bulgakova, V.P. Zhukov, Y.P. Meshcheryakov, S.V. Sonina, Ultrashort pulse laser processing of transparent materials: What is energetically and mechanically meaningful? To be published (2015).

**Laser-induced semiconductor cluster structures on the solid surface; new physical principles to construct the hybrid elements for photonics**

**S.Arakelian<sup>1</sup>, V. Emel'yanov<sup>2</sup>, S.Kutrovskaya<sup>1</sup>, A.Kucherik<sup>1</sup>, S. Zimin<sup>3</sup>**

<sup>1</sup> *Stoletovs Vladimir State University, Vladimir, Russia;*

<sup>2</sup> *Lomonosov Moscow State University, Moscow, Russia*

<sup>3</sup> *P.G. Demidov Yaroslavl State University, Yaroslavl, Russia.*

*E-mail: [arak@vlsu.ru](mailto:arak@vlsu.ru)*

1. The laser synthesis technique for semiconductor nanoparticles of PbTe is presented by two methods: laser modification of thin films and laser evaporation of substance in liquid to produce the colloidal systems. Under a CW-laser radiation the nanoparticles become quantum dots under some conditions. By drop deposition technique it has been obtained the structures with various morphology which depends on the substrate temperature. The optical and electro-physical properties of the structures can be controlled, and are very important to construct the elements and devices of optoelectronics and photonics on new physical principles.

2. The CW-laser ablation experiments ( $\lambda=1.06 \mu$ , laser intensity – up to  $10^6 \text{ W/cm}^2$ ) with colloidal systems to induce the surface semiconductor nanostructure on substrate have been carry out to study the electrical transport properties under quantum tunneling effect. On the other hand, when the nanoparticles drop on the solid surface they are accumulated in clusters of bigger size  $R_0$ . The electroconductivity vs  $R_0$  has been studied the macroscopic quantum phenomena development in dependence on  $R_0$  are obtained.

3. The main conclusion from our study is that the island conductivity is dominant for the case. An electroresistance can dramatically decrease due to spontaneous selected multichannel/parallel electron transportation trajectories.

Two conditions are the vital items for that: the cluster size  $R_0 < l$ , where  $l$  is the inelastic length, and distance  $a$  between two neighboring clusters less the de Broglie wavelength  $\lambda_{dB}$ . So, the tunneling quantum effect takes place between correlated particles in two domains.

For such laser-induced nanostructures we demonstrated the superconductivity tendency to increase the electrical conductivity (in several times for our case) at room temperature in comparison with homogenous sample. The fact can be explained in analogy with correlated particles/coupling pairs from two sides of the border for double electric layer/two barriers due to quantum hole being under a coherent tunnel effect.

4. Jump conductivity has been detected under some experimental conditions of laser-induced cluster structures. The cluster shell model can be taken into account to explain the results

## ***Advanced Oxide Thin Films Growth by Excimer Laser Assisted Chemical Solution Process for Future Devices***

**T. Tsuchiya, T. Nakajima, T. Nakamura, I. Yamaguchi, H. Matsui**  
*National Institute of Advanced Industrial Science and Technology (AIST)*  
*Japan, 1-1-1 Higashi, Tsukuba, Ibaraki, Japan.*

*tetsuo-tsuchiya@aist.go.jp-*

To construct low carbon society more and more in the world, it is necessary to develop a high performances new green device such as a solar cell, a lithium battery, a power semiconductor, and light emitting diode (LED) lighting, superconducting device and so on. Metal oxides are expected to be key materials which are used for a new device by controlling metal composition, a crystal structure, orientation or multilayer of the film, a carrier, a spin, etc. In order to fabricate the new devices, their parameters controllable process would be effective. Another important problem is the development of the low cost and power saving process for constructing sustainable society in the world. For these purpose, chemical solution process (CSP) would be suitable because it does not require vacuum and high facility investments and any complicated etching process. In addition, precise metal composition control is possible when the materials are made from the more than 3 or 4 metal components. For the thin film processing, we have developed the photo-induced chemical solution process such as excimer laser-assisted metal organic deposition (ELAMOD) and photo reaction of nano-particle method (PRNP) for the preparation of the patterned metal oxide thin film on organic, glass and single crystalline substrates.

### 1. Flexible applications

By using the PRNP process, ITO and phosphor thin films were prepared on glass and PET substrates at room temperature as shown in Fig 1. The luminescent thin film show higher luminescence compared with commercially available one.



Fig. 1 ITO film on PET by PRNP

### 2. Epitaxial applications

On the other hand, to prepare the epitaxial film, the use of the metal organic compound and single crystal substrate with large optical absorbance was found to be effective. By using the ELAMOD, epitaxial ITO, SnO<sub>2</sub>, LSMO, PZT films with patterning were successfully obtained at low temperature in air as shown in Fig. 2. TCR of a VO<sub>2</sub> films obtained by ELAMOD exhibit much higher than present uncooled IR sensor.

In this presentation, we demonstrate a preparations of ITO and phosphor thin films on PET substrate. Also, we show the preparation of various epitaxial thin films by photo-induced chemical solution process at low temperature in air, and their prominent unusual properties of the obtained film.

### References

- [1] T. Tsuchiya et al., *Appl. Surf. Sci.*, **186** (2002) 173.
- [2] T. Tsuchiya et al., *Appl. Phys. A* **99** (2010) 745.
- [3] T. Tsuchiya et al., *Mater. Res. Soc. Symp. Proc.* **1454** (2012) 189.
- [4] T. Nakajima et al., *Chem. Soc. Rev.* **43** (2014) 2027

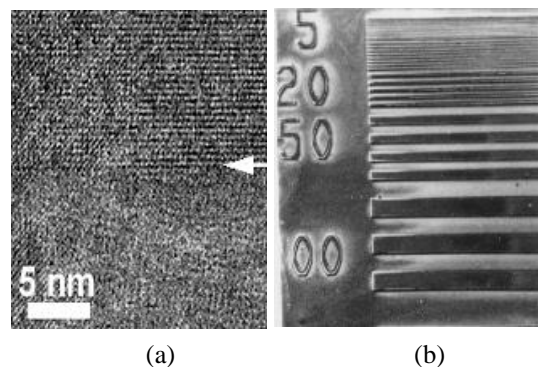


Fig.2 (a)TEM of the epi film, and (b) patterned film by ELAMOD

# High throughput surface structuring with high power sub ps laser in synchronized mode

**B. Neuenschwander<sup>1</sup>, B. Jaeggi<sup>1</sup>, M. Zimmermann<sup>1</sup>, V. Markovic<sup>2</sup>, B. Resan<sup>2</sup>,  
K. Weingarten<sup>2</sup>, R. de Loor<sup>3</sup>, L. Penning<sup>3</sup>**

*1- Bern University of Applied Sciences, Pestalozzistrasse 20, CH-3400 Burgdorf, Switzerland*

*2- JDSU Ultrafast Lasers AG, Ruetistrasse 12, CH-8952 Schlieren, Switzerland*

*3- Next Scan Technology, Ulftseweg 14, 7064 BD Silvolde, The Netherlands*

Main author email address: [beat.neuenschwander@bfh.ch](mailto:beat.neuenschwander@bfh.ch)

For laser surface texturing with ultra-short pulses the material removal rate per average power, the specific removal rate, shows a maximum value at an optimum fluence [1,2]. Based on the logarithmic ablation law this optimum fluence directly scales with the threshold fluence leading to peak fluence of  $\phi_{opt} = e^2 \cdot \phi_{th}$  for a Gaussian beam. For metals this finally leads to applied fluences in the range from 0.3 to 1.5 J/cm<sup>2</sup> corresponding to pulse energies ranging from several to several 10s of  $\mu$ J for spot radii below 50  $\mu$ m. For high average power exceeding several 10s of W, which is essential for high throughput, the corresponding repetition rates should be in the range of some MHz, requiring scanning speeds in the range of 100 m/s which are offered today by polygon line scanners [3]. However, it has to be verified to what average power the ablation process will be scalable when the applied fluence per pulse and the pulse overlap are kept constant or if heat accumulation effects may influence the removal rate and the machining quality.

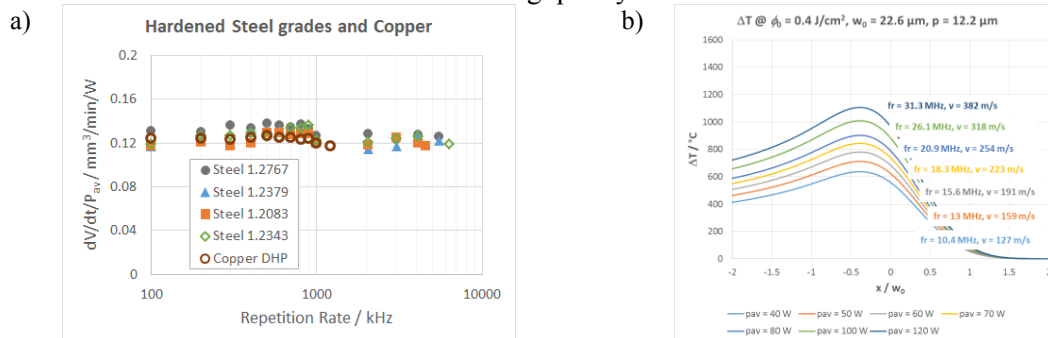


Figure 1: a) Specific removal rates for different steel grades and copper. (b) Estimated surface temperatures as a function of the average power for a spot radius of 22.6  $\mu$ m and an overlap of about 75%.

For different steel grades and average powers up to more than 40 W no significant influence on the specific removal rate, Fig. 1a), and the machining quality was observed [4]. But in [5] it was reported that at surface temperatures exceeding a threshold value of about 610  $^{\circ}\text{C}$ , bumpy surfaces can appear and destroy the good machining quality for steel 1.4301. A short estimation for a spot radius of  $w_0 = 22.6 \mu\text{m}$  and an overlap of about 75% shows that this critical temperature will already be achieved for an average power exceeding 40 W, Fig. 1b). Therefore, it is subject of running investigations to clarify if the power scaling up to 100W without a reduction of the machining quality will be possible at all and if other metals as e.g. copper or brass also show this reduction of the surface quality due to heat accumulation.

[1] G. Raciukaitis et al., "Use of High Repetition Rate and High Power Lasers in Microfabrication: How to keep Efficiency High?", JLMN Journal of Laser Micro/Nanoengineering; 4, 186-191 (2009)

[2] B. Neuenschwander et al., "Processing of metals and dielectric materials with ps-laserpulses: results, strategies, limitations and needs", Proc. of SPIE, 7584, paper 26 (2010)

[3] B. Jaeggi et al., "High Throughput and High Precision Laser Micromachining with ps-Pulses in Synchronized Mode with a fast Polygon Line Scanner", Proceedings of SPIE 8967-25 (2014)

[4] B. Neuenschwander et al., "Influence of Particle Shielding and Heat Accumulation Effects onto the Removal Rate for Laser Micromachining with Ultra-Short Pulses at High Repetition Rates", Proc. of ICALEO, M1104 (2014)

[5] F. Bauer et al., "Heat accumulation in ultra-short pulsed laser processing of metals", Opt. Expr., 23, 1035 – 1043 (2015)

# High-order harmonic source based femtosecond core-level photoelectron spectroscopy for carrier transport dynamics on semiconductor surface

**Katsuya Oguri, Takanobu Tsunoi, Keiko Kato, Hidetoshi Nakano, Tadashi Nishikawa, Kouta Tateno, Tetsuomi Sogawa, and Hideki Gotoh**

*NTT Basic Research Laboratories, Nippon Telegraph and Telephone Corporation,  
3-1 Morinosato Wakamiya, Atsugi, Kanagawa 243-0198, Japan*

*e-mail: [oguri.katsuya@lab.ntt.co.jp](mailto:oguri.katsuya@lab.ntt.co.jp)*

Recent progress in high-order harmonic generation (HHG) has opened the door to new diagnostic techniques for exploring ultrafast electronic processes during and after ultrashort laser-solid interactions. One of the most attractive processes is likely to be the dynamical behavior of non-equilibrium carrier transport in semiconductor surface region, because it is closely related to not only the performance in a wide variety of semiconductor applications, but also the fundamental physical process in laser-processing applications [1]. Although time-resolved ultrafast laser spectroscopy techniques are conventionally used for measuring the dynamics, a time-resolved core-level photoelectron spectroscopy (TR-PES) in the EUV region has been used as a more direct approach than such optical measurements [2]. The core-level TR-PES with femtosecond temporal resolution based on HHG in the extreme ultraviolet (EUV) region are expected to provide complementary information in the photo-generated carrier dynamics, while experimental realization of such techniques is still challenging.

Here, we present the study of ultrafast dynamics of the photo-generated carriers on semi-insulating GaAs surface using a femtosecond core-level PES system based on a HHG source [3]. The system, which is based on the 59th harmonic-probe (92 eV) and a near-infrared laser-pump scheme, consists of a 1-TW Ti:sapphire laser system, an HHG vacuum chamber, a photoelectron energy analyzer, and a sample preparation plus load-lock chamber. We used a semi-insulating GaAs (001) substrate as the sample. Figure 2 shows typical transient changes in the photoelectron spectrum of the Ga-3d core-level peak and its time evolution when a 100-fs laser pulse with an intensity of  $1 \times 10^9$  W/cm<sup>2</sup> was irradiated. We observed a transient change in surface potential where the Ga-3d peak instantaneously shifted towards a higher binding energy within 2 ps. By comparing the experimental result to the numerical simulations, we clarified that the Ga-3d peak change is mainly due to the dynamical photo-Dember effect, where an induced electric field as a result of the large difference in diffusion of between electrons and holes modifies the surface potential. Thus, the core-level TR-PES technique enables us to access the dynamical information of the photo-generated carriers in femtosecond regime.

This work was supported by JSPS KAKENHI Grant Number 23310086.

- [1] Kang et al., *Nat. Photonics* **3**, 59 (2009); S. K. Sundaram and E. Mazur, *Nat. Materials* **1**, 217 (2002).  
[2] Tanaka et al, *Phys. Rev. B* **64**, 155308 (2001); Siffalovic et al., *Europhys. Lett.* **60**, 924 (2002).  
[3] Oguri et al., *Appl. Phys. Express* **8**, 022401 (2015); Oguri et al., *Jpn. J. Appl. Phys.* **51** 072401 (2012).

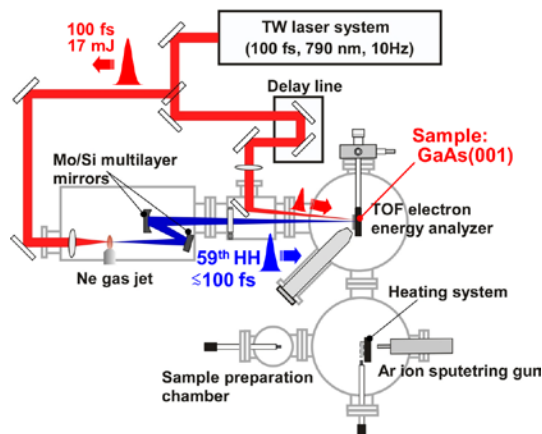


**Fig. 1.** Schematic illustration of the core-level TR-PES system.

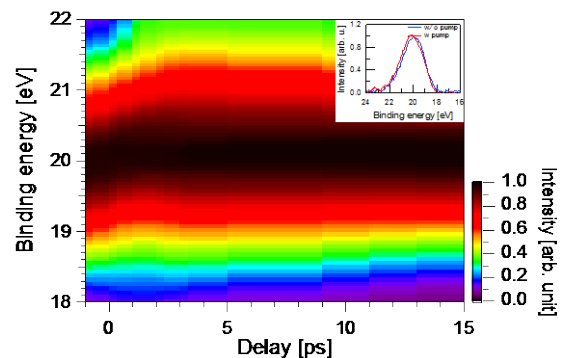


**Fig. 2.** Temporal evolution of the Ga-3d photoelectron peak in the photo-excited GaAs(001). Typical profile obtained with (red) and without (blue) laser irradiation is also shown (inset).

**Laser surface texturing of Ti alloys for orthopaedic applications**

**R. Vilar, A. Cunha, V. Oliveira, A. Almeida**

Department of Chemical Engineering and CeFEMA – Centre for the Physics and Engineering of Advanced Materials, Instituto Superior Técnico, Lisbon University.

The presentation will review recent results on the assessment of femtosecond laser surface texturing methods for enhancing the osseointegration capability of Ti alloys for dental and orthopaedic implant applications. The laser treatments aim at enhancing the wettability of implants by biological fluids and favour matrix mineralisation and bone formation, while reducing bacteria adhesion and biofilm formation.

Different femtosecond laser surface treatment direct writing methods were applied to create a range of surface structures, thus allowing to evaluate the influence of surface topography, surface individual features size and roughness on cells behaviour. The biological behaviour was assessed by wetting measurements and by studying the behaviour of human mesenchymal stem cells (hMSCs) and Staphylococcus aureus bacteria brought into contact with the treated surfaces in appropriate controlled conditions. The surface texture was combined with biofunctionalisation by covalent grafting of a RGD peptide sequence as well.

The surface textures studied can be classified in the following categories: (a) Low-frequency Laser-Induced Periodic Surface Structures (LIPSS); (b) nanopillars arrays (NP); (c) arrays of microcolumns covered with LIPSS, forming a bimodal roughness distribution (MC-LIPSS). All these textures enhance surface wettability by water and Hank's balanced salt solution (HBSS). Moreover, LIPSS and MC-LIPSS textures induce an anisotropic wetting behaviour, which superwetting appearing in the LIPSS direction. Matrix mineralisation is observed for all surfaces of both Ti alloys when human mesenchymal stem cells (hMSCs) are cultured in osteogenic medium. Matrix mineralisation and formation of bone-like nodules are significantly enhanced on LIPSS and NP textured surfaces. On the contrary, Staphylococcus aureus adhesion and biofilm formation are significantly reduced for LIPSS and NP textured surfaces. The biofunctionalisation of the laser textured surfaces of cp Ti is successfully achieved. In general, these results suggest that surface texturing of Ti alloys using femtosecond laser direct writing is a promising method for enhancing surface wettability of dental and orthopaedic implants by biological fluids and their osseointegration (osteoblastic differentiation and matrix mineralisation), while reducing Staphylococcus aureus adhesion and biofilm formation. Finally, the combination of laser texturing and covalent grafting of a RGD peptide sequence may be potentially useful for increasing cell adhesion and facilitating bone formation.

**Keywords:** Femtosecond lasers; Surface texturing; Titanium alloys; Dental and orthopaedic implants; Wettability; Mesenchymal Stem Cells differentiation into Osteoblasts; Osseointegration; Bacteria; Staphylococcus aureus; Biofilm; Biofunctionalisation.

# Ultrapure laser-synthesized nanomaterials for biomedical applications

**Andrei V. Kabashin**

*Aix-Marseille University (AMU), LP3 UMR 7341 CNRS, Campus de Luminy,  
Case 917, 13288 Marseille Cedex 09, France*

*Email address: [kabashin@lp3.univ-mrs.fr](mailto:kabashin@lp3.univ-mrs.fr)*

Inorganic nanomaterials demonstrate extremely promising characteristics for tasks of cancer diagnostics and therapy (theranostics), but biomedical prospects of such nanomaterials are complicated by toxicity issues arising as a result of relatively dirty pathways for their fabrication. As an example, Si nanoparticles are biocompatible and even biodegradable in pure state, but conventional chemical and electrochemical routes for their synthesis inevitably lead to a surface contamination by toxic products. As a solution of the toxicity problem, we recently introduced a series of physical methods based on ultrashort laser ablation and fragmentation in aqueous biocompatible solutions in order to synthesize novel classes of ultrapure nanomaterials for biomedical tasks [1-8].

This presentation will overview our results on the laser synthesis of some important inorganic nanomaterials (Si, Au etc), including direct fs laser ablation from a solid target in aqueous solutions [2,3,5] and fs laser fragmentation from preliminarily formed nano- and microcolloids [4,6,7]. Then, it will overview first successful tests of laser-synthesized nanomaterials in biological systems [8,9]. In particular, our tests in vitro using cancer and normal cell lines demonstrate the innocuousness and safety nanoparticles (zero toxicity), while protein covering after the incubation of nanoparticles in real biological environment suggests potential successful transport of nanoparticles in vivo and minimal immune response effects [9]. In vivo tests in small animal model using systemic administration of nanoparticles also do not reveal any sign of toxicity effects. We then examine optical, photochemical and photo-thermal characteristics of laser-synthesised nanomaterials in the view of their potential cancer theranostic applications [5-7,9,10]. Finally, we describe a novel method for mild cancer therapy, in which Si nanoparticles are used as sensitizers of radio-frequency induced hyperthermia [10]. The efficiency of this method is confirmed by successful tests in vitro and in vivo.

[1] A. V. Kabashin, Ph. Delaporte, A. Perreira, D. Grojo, R. Torres, Th. Sarnet, M. Sentis, Nanofabrication with pulsed lasers, *Nanoscale Res. Lett.*, vol. 5, pp. 454–463 (2010).

[2] A.V. Kabashin, M. Meunier, Synthesis of colloidal nanoparticles during femtosecond laser ablation of gold in water, *J. Appl. Phys.*, vol. 94, pp. 7941-7943 (2003)

[3] A.V. Kabashin, M. Meunier, Femtosecond laser ablation in aqueous solutions: a novel method to synthesize non-toxic metal colloids with controllable size, *J. Phys.: Conf. Series*, vol. 59, pp. 354-357 (2007)

[4] S. Besner, A.V. Kabashin, M. Meunier, Fragmentation of colloidal nanoparticles by femtosecond laser-induced super continuum generation, *Appl. Phys. Lett.*, vol. 89, pp. 233121 (2006)

[5] D. Rioux, M. Laferriere, A. Douplik, D. Shah, L. Lilge, A.V. Kabashin, M. Meunier, Silicon Nanoparticles Produced by Femtosecond Laser Ablation in Water as Novel Contamination-Free Photosensitizers, *J. Biomed. Optics*, vol. 14, pp. 021010 (2009).

[6] P. Blandin, K. A. Maximova, M. Gongalsky, J. F. Sanchez-Royo, V. S. Chirvony, M. Sentis, V. Yu. Timoshenko, A. V. Kabashin, Femtosecond laser fragmentation from water-dispersed microcolloids: toward fast controllable growth of ultrapure Si-based nanomaterials for biological applications, *J. Mater. Chem. B*, vol. 1, pp. 2489-2495 (2013).

[7] K. Maximova, A. I. Aristov, M. Sentis, A. V. Kabashin, Size-controllable synthesis of bare gold nanoparticles by femtosecond laser fragmentation in water, *Nanotechnology*, vol. 26, pp. 065601 (2015)

[8] L. Lysyakova, N. Lomadze, D. Neher, K. Maximova, A. Kabashin, S. Santer, Light-Tunable Plasmonic Nanoarchitectures using Au NPs–Azobenzene Cationic Surfactant Complexes, *J. Phys. Chem. C.*, vol. 119, pp. 3762 (2015)

[9] F. Correard, K. Maximova, M.-A. Estève, C. Villard, A. Al-Kattan, M. Sentis, M. Roy, M. Gingras, A. V. Kabashin, D. Braguer, Gold nanoparticles prepared by laser ablation in aqueous biocompatible solutions: assessment of safety and biological identity for nanomedicine applications, *Int. J. Nanomedicine*, vol. 9, pp. 5415–5430 (2014).

[10] K. P. Tamarov, L.A. Osminkina, S.V. Zinoviyev, K.A. Maximova, J.V. Kargina, A.P. Sviridov, M. Sentis, A.V. Ivanov, V.N. Nikiforov, A. Kabashin, V. Yu. Timoshenko, RF radiation-induced hyperthermia using biodegradable Si-based nanosensitizers for biomedical applications, *Scientific Reports*, vol. 4, 7034, DOI: 10.1038/srep07034 (2014).

# New results with pulsed laser technologies for transfer of organic and biological substances: applications in biomedicine

**Ion N. Mihailescu and Carmen Ristoscu**

National Institute for Lasers, Plasma and Radiation Physics, POB MG-36, Magurele, Ilfov,  
Romania

e-mail: [ion.mihailescu@inflpr.ro](mailto:ion.mihailescu@inflpr.ro)

Recent results in organic/inorganic composite nanostructured layers synthesized by PLD, MAPLE and LDW are reviewed. The optimum deposition regime was reached based upon the results of investigations by SEM, TEM, SAED, XTEM, AFM, XRD, XPS or FTIR methods. Biocompatibility, bioactivity and biodegradation were assessed by dedicated *in-vitro* tests [1-3].

The coating of metallic implants with composite alendronate-HA or Sr-HA layers by MAPLE and PLD, respectively, was demonstrated to enhance human osteoblasts proliferation and differentiation, while inhibiting osteoclasts growth, with benefic effects for the treatment of bone diseases.

Magnesium or strontium substituted OCP deposited by MAPLE on Ti substrates efficiently boost osteoblast activity and differentiation [4].

Urease immobilized by MAPLE in form of thin films was shown to preserve its activity in breaking down and diagnose of urea content in blood.

The application of MAPLE was extended to the transfer and immobilization of IgG molecules. We studied the effect of the lipid addition in the initial solution upon the protein thin films adhesion to substrate.

We showed that the composite PMMA-bioglass films deposited by MAPLE efficiently protects metal implants against the action of human fluids.

The antifungal efficiency of the nano-sized HA and Ag:HA layers obtained by PLD was tested against the *Candida albicans* and *Aspergillus niger* strains. The Ti substrates modified with TiO<sub>2</sub> nanotubes covered with Ag:HA thin films demonstrated the highest antifungal activity [5].

The MAPLE obtained nanocomposites Ag:HA-organosolv lignin proved noncytotoxic, supporting the normal development and promoting the proliferation of the adhered human mesenchymal cells. The lignin addition potentiated the anti-microbial activity of HA doped with silver ions against either bacterial or fungal biofilms [6].

Mesotetraphenylporphyrin clean and liquid-free micropatterns on Si substrates were fabricated by LDW. The propulsor metal film thickness was found to be a key parameter, which determines the laser fluence range allowing the clean transfer, predominant mechanism of the blister formation and laser-induced heating of the transferred material.

We conclude that the thin films prepared by PLD, MAPLE and LDW techniques were identical in chemical composition, structure, morphology, and most likely functionality resembling the base material, as proved by physical-chemical characterization and *in-vitro* assays.

[1] V. Nelea, M. Jelinek, I.N. Mihailescu, Biomaterials: new issues and breakthroughs for biomedical applications, in: Pulsed Laser Deposition of Thin Films: Applications-Lead Growth of Functional Materials, Wiley, Hoboken, New Jersey, 2007, pp. 421–456 (Chapter 18)

[2] Carmen Ristoscu and Ion N. Mihailescu "Laser Technology in Biomimetics", Volker Schmidt, Maria Regina Belegratis (Eds.), Basics and Applications, Series: Biological and Medical Physics, Biomedical Engineering, Springer-Verlag Heidelberg, New York, Dordrecht, London, chapter "Biomimetic Coatings by Pulsed Laser Deposition", Pages 163-191, 2013

[3] Felix Sima and Ion N. Mihailescu, "Laser Technology in Biomimetics", Volker Schmidt, Maria Regina Belegratis (Eds.), Basics and Applications, Series: Biological and Medical Physics, Biomedical Engineering, Springer-Verlag Heidelberg, New York, Dordrecht, London chapter "Biomimetic Assemblies by Matrix-Assisted Pulsed Laser Evaporation", Pages 111-141, 2013

[4] E. Boanini, P. Torricelli, M. Fini, F. Sima, N. Serban, I. N. Mihailescu, A. Bigi, "Magnesium and strontium doped octacalcium phosphate thin films by matrix assisted pulsed laser evaporation", Journal of Inorganic Biochemistry 107, 65–72 (2012)

[5] S. Eraković, A. Janković, C. Ristoscu, L. Duta, N. Serban, A. Visan, I.N. Mihailescu, G.E. Stan, M. Socol, O. Iordache, I. Dumitrescu, C.R. Luculescu, Dj. Janačković, V. Mišković-Stanković, "Antifungal activity of Ag:hydroxyapatite thin films synthesized by pulsed laser deposition on Ti and Ti modified by TiO<sub>2</sub> nanotubes substrates", Applied Surface Science 293, 37-45 (2014)

[6] A. Janković, S. Eraković, C. Ristoscu, N. Mihailescu (Serban), L. Duta, A. Visan, G.E. Stan, A.C. Popa, M.A. Husanu, C.R. Luculescu, V.V. Srdić, Dj. Janačković, V. Mišković-Stanković, C. Bleotu, M.C. Chifiriuc, I.N. Mihailescu, "Structural and biological evaluation of lignin addition to simple and silver doped hydroxyapatite thin films synthesized by matrix-assisted pulsed laser evaporation", Journal of Materials Science: Materials in Medicine 26, 5333 (2015)

**ADDITIVE MANUFACTURING WITH LASER GENERATED NANOPARTICLES**

Boris N. Chichkov

*Laser Zentrum Hannover e.V., Nanotechnology Department, Hollerithallee 8,  
30419 Hannover, Germany*

Laser generation of colloidal nanoparticles by high-power laser ablation and laser printing of nanoparticles are two rapidly progressing technologies. I will briefly report on our advances in these fields and will show how these nanoparticles can be used for additive manufacturing applications.



# Laser synthesis of nanometric 2D heterostructures of transitional metal oxides for photo sensors with high sensitivity

S. A. Mulenko

*G.V. Kurdyumov Institute for Metal Physics NAS of Ukraine,  
36, Academician Vernadsky Blvd., UA-03142, Kiev- 142, Ukraine*

*e-mail: [mulenko@ukr.net](mailto:mulenko@ukr.net)*

The reactive pulsed laser deposition (RPLD) based on a KrF-laser ( $\lambda = 248$  nm) was used before for photon synthesis of nanometric single layer iron oxide and chromium oxide films and their application for thermo-photo-chemical sensors [1-4].

Here, ultraviolet photons of a KrF-laser were used for the synthesis by RPLD of  $\text{Cr}_{3-x}\text{O}_{3-y}/\text{Fe}_2\text{O}_{3-x}$  multilayer heterostructures with the stoichiometry of each oxide  $\text{Fe}_2\text{O}_{3-x}$  ( $0 \leq x \leq 1$ ) and  $\text{Cr}_{3-x}\text{O}_{3-y}$  ( $0 \leq x \leq 2$ ;  $0 \leq y \leq 2$ ). Each nanometric multilayer heterostructure with definite number of layers of iron oxide and chromium oxide was deposited in 2 dimensional forms (2D) on  $\langle 100 \rangle$  Si substrate at its temperature 293-800 K. The number of  $\text{Fe}_2\text{O}_{3-x}$  and  $\text{Cr}_{3-x}\text{O}_{3-y}$  layers was being changed from 4 up to 8 resulted in changing of multilayer 2D heterostructure thickness in the range 25-85 nm. XRD analysis confirmed that these heterostructures deposited on Si substrate had polycrystalline structure.

All synthesized 2D heterostructures demonstrated semiconductor temperature trend with variable  $E_g$  less than 1.0 eV, depending on oxygen pressure in the reactor, the number of laser pulses and substrate temperature. The band gap of these multilayer 2D heterostructures was being changed in the range 0.36-0.72 eV. The more substrate temperature was the more  $E_g$  value, and the more multilayer 2D heterostructure photosensitivity. Optimum parameters (i.e. oxygen pressure in the reactor of 0.5 Pa, substrate temperature 800 K and film thickness 30 nm) were found out for the highest photosensitivity of multilayer 2D heterostructures, which was about  $420 \text{ V}_c/\text{W}$  at white light power density  $\sim 6 \times 10^{-3} \text{ W}/\text{cm}^2$ . While this heterostructure deposition on Si substrate at 293 K at the same conditions, photosensitivity was about  $4.3 \text{ V}_c/\text{W}$ .  $V_c$  is “chemical” photo electromotive force induced in the deposited films by white light,  $W$  is white light power. To this end, the highest photosensitivity of nanometric single layer chromium oxide film was about  $7.7 \text{ V}_c/\text{W}$  and of nanometric single layer iron oxide film was about  $44 \text{ V}_c/\text{W}$  for the same white light power density [1].

High photosensitivity nature of multilayer 2D heterostructure synthesized on heated substrate is explained by sufficiently increasing of heterogeneity of charge carriers' concentration in these heterostructures. Therefore,  $\text{Cr}_{3-x}\text{O}_{3-y}/\text{Fe}_2\text{O}_{3-x}$  multilayer 2D heterostructures exhibiting high photosensitivity are exceptionally strong candidate for effective photo sensors and photo converters of white light. RPLD is up-to-date method for the synthesis of photosensitive materials based on non-toxic atoms as a background for green “technologies”.

[1]. S.A.Mulenko, N.T. Gorbachuk, Synthesis of nanometric iron oxide films by RPLD and LCVD for thermo-photo sensors, Appl. Phys., B : Laser and Optics, vol. 105, pp. 517-523, (2011).

[2] S.A. Mulenko, Yu.N. Petrov, N.T. Gorbachuk, Photon synthesis of iron oxide thin films for thermo-photo-chemical sensors, Appl. Surf. Science, vol. 258, pp. 9186-9191, (2012).

[3] S.A.Mulenko., N.T.Gorbachuk and N..Stefan, Laser Synthesis of Nanometric Iron Oxide Films with High Seebeck Coefficient and High Thermoelectric Figure of Merit, Lasers Manufact. Materials Process., vol. 1, pp.21-35, (2014 ).

[4] S.A..Mulenko, N.T. Gorbachuk, and N. Stefan, Laser synthesis of nanometric chromium oxide films with high Seebeck coefficient and high thermoelectric figure of merit, Intern. Res. Journ. Nanoscience and Nanotechn., vol. 1 (2), pp. 008-016, (2014).

# Laser assisted patterning of thin film solar cells

Zs. Geretovszky<sup>1</sup> and A. Búzás<sup>2</sup>

<sup>1</sup>University of Szeged, Department of Optics and Quantum Electronics, Dóm tér 9., H-6720 Szeged, Hungary

<sup>2</sup>Hungarian Academy of Sciences, Biological Research Centre, Institute of Biophysics, Temesvári krt. 62., H-6726 Szeged, Hungary

Main author email address: gero@physx.u-szeged.hu

Solar energy is the cleanest and most plentiful green power available on Earth. The bottleneck of its utilisation is the efficient conversion of solar power to electrical power. This manufacturing challenge is hindered by the lack of cost efficient solutions. Advances in solar cell manufacturing technology are boosting production efficiencies and laser-based processes are in the forefront of this manufacturing revolution.

Lateral patterning of the individual layers of thin film solar cell multilayer structures is one area in which laser assisted processes has unique potentials to offer. The ultimate goal of laser scribing is therefore to remove the material of the layer in a narrow straight line as selectively, as possible, i.e. completely without damaging the underlying layer and the material in the vicinity of the irradiation zone. Since the three patterning steps inevitably decrease the useful area of the solar cell, it is a must to minimize the so called dead zone, a region affected by the patterning process. Via decreasing the laser processed area and the inter-scribe separation distances the difference between the conversion efficiency of a solar cell structure and the integrated module can be decreased. For the  $\text{CuIn}_x\text{Ga}_{(1-x)}\text{Se}_2$  (CIGS) cell studied the current, validated world record cell and module efficiencies are  $20.5\% \pm 0.6\%$  and  $15.7\% \pm 0.5\%$ , respectively [1].

Entire and partial multilayer structures of CIGS-based solar cell modules were processed by laser pulses of an industrial DPSS Nd:YVO<sub>4</sub> laser ( $\lambda=1064$  nm, PRR=5 kHz,  $\tau=25$  ns,  $E=2-60$   $\mu\text{J}$ ). The traverse rate of the sample with respect to the laser beam was 50 cm/s, while the sample was slightly inclined with respect to the direction of movement to achieve a gradual variation in the laser irradiated area along the scanned path (hence the beam diameter was varied between 10-70  $\mu\text{m}$ ). The morphology and chemical composition of the slightly elliptical laser irradiated regions were studied by optical, atomic force and scanning electron microscopies, while the surface topology was measured by contact profilometry.

We found that the morphology of the laser patterned area can be put into one of the following three categories. At one extreme, *evaporation* is the dominant mechanism that determines crater morphology and leaves considerable amount of molten residue both inside and at the edge of the laser-processed area. At the other extreme, thermally driven *mechanical stress* is the dominant material removal mechanism which produces craters of rather different morphology with negligible amount of molten residue both in and around these craters.

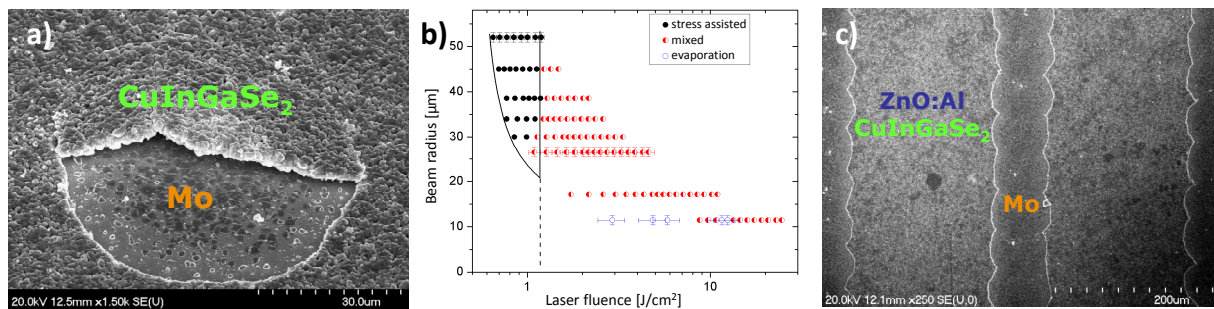


**Figure 1.** a) SEM micrograph of a mechanically removed CIGS layer from an undamaged Mo layer achieved by a single laser pulse. b) Spread of crater morphology type on the beam radius vs fluence plane. c) Laser driven mechanical removal of the top ZnO:Al and CIGS layers from the underlying Mo film (25 cm/s, beam radius 45  $\mu\text{m}$ , fluence 1  $\text{J}/\text{cm}^2$ ).

In-between these two ultimate types, a third, transitional category exists (referred to as *mixed*), the craters of which exhibit the morphological characteristics of both the evaporative and the stress assisted removal to some extent, and typically materializing in sharp crater edges but with considerable amount of molten residue inside it. For the selective removal of the 2  $\mu\text{m}$  thick absorber layer the stress dominated mechanism is the most appealing (cf. Fig. 1a)) which can be distinctively achieved by the proper combination of the size and the fluence of the laser pulses (cf. Fig. 1b)). The thermomechanical modelling of the underlying processes was used to facilitate how this laser initiated stress assisted process can be made dominant under even nanosecond long laser pulse durations [2] and hence to realize clean and selective material removal of the solar cell layers, as exemplified in Fig. 1c). Further details of this model will be given in my talk.

[1] M. A. Green, K. Emery, Y. Hishikawa, W. Warta and E.D. Dunlop, Prog. Photovolt: Res. Appl., **22**, pp. 701-710, (2014)

[2] A. Búzás and Zs. Geretovszky, Phys. Rev. B, **85**, 245304 (2012)

# **Laser Precision Drilling Technologies with Nanosecond and Picosecond Laser Pulses**

ZHOU Ming, ZHANG Hongyu , DI Jianke

State Key Laboratory of Tribology, Tsinghua University, Beijing 100084, China

Abstract:

Precision drilling with picosecond laser has been advocated to significantly improve the quality of micro-holes with reduced recast layer thickness and almost no heat affected zone. However, a detailed comparison between nanosecond and picosecond laser drilling techniques has rarely been reported in previous research. In the present study, a series of micro-holes are manufactured on stainless steel 304 using a nanosecond and a picosecond laser drilling system, respectively. The quality of the micro-holes, e.g., recast layer, micro-crack, circularity, and conicity, etc, is evaluated by employing an optical microscope, an optical interferometer, and a scanning electron microscope. Additionally, the micro-structure of the samples between the edges of the micro-holes and the parent material is compared following etching treatment. The researching results show that a great amount of spattering material accumulated at the entrance ends of the nanosecond laser drilled micro-holes. The formation of a recast layer with a thickness of  $\sim 25 \mu\text{m}$  is detected on the side walls, associated with initiation of micro-cracks. Tapering phenomenon is also observed and the circularity of the micro-holes is rather poor. With regard to the micro-holes drilled by picosecond laser, the entrance ends, the exit ends, and the side walls are quite smooth without accumulation of spattering material, formation of recast layer and micro-cracks. The circularity of the micro-holes is fairly good without observation of tapering phenomenon. Furthermore, there is no obvious difference as for the micro-structure between the edges of the micro-holes and the parent material. This study proposes a picosecond laser helical drilling technique which can be used for effective manufacturing of high quality micro-holes: Precision drilling with picosecond laser has been advocated to significantly improve the quality of micro-holes with reduced recast layer thickness and almost no heat affected zone. However, a detailed comparison between nanosecond and picosecond laser drilling techniques has rarely been reported in previous research. In the present study, a series of micro-holes are manufactured on stainless steel 304 using a nanosecond and a picosecond laser drilling system, respectively. The quality of the micro-holes, e.g., recast layer, micro-crack, circularity, and conicity, etc, is evaluated by employing an optical microscope, an optical interferometer, and a scanning electron microscope. Additionally, the micro-structure of the samples between the edges of the micro-holes and the parent material is compared following etching treatment. The researching results show that a great amount of spattering material accumulated at the entrance ends of the nanosecond laser drilled micro-holes. The formation of a recast layer with a thickness of  $\sim 25 \mu\text{m}$  is detected on the side walls, associated with initiation of micro-cracks. Tapering phenomenon is also observed and the circularity of the micro-holes is rather poor. With regard to the micro-holes drilled by picosecond laser, the entrance ends, the exit ends, and the side walls are quite smooth without accumulation of spattering material, formation of recast layer and micro-cracks. The circularity of the micro-holes is fairly good without observation of tapering phenomenon. Furthermore, there is no obvious difference as for the micro-structure between the edges of the micro-holes and the parent material. This study proposes a picosecond laser helical drilling technique which can be used for effective manufacturing of high quality micro-holes

## **Giant resonances and other peculiarities of light scattering by particles with high refractive index**

**Michael I. Tribelsky**<sup>1,2</sup>

*1-Faculty of Physics, Lomonosov Moscow State University, Moscow, 119991, Russia*

*2-Moscow State University of Information Technologies, Radioengineering and Electronics MIREA,  
Moscow 119454, Russia*

*E-mail: tribelsky\_at\_mirea.ru; replace \_at\_ by @*

A detailed inspection of light scattering by a particle with high refractive index  $m+i\kappa$  and small dissipative constant  $\kappa$  is presented. It is shown that there is a dramatic difference in the behavior of the electromagnetic field within the particle (*inner problem*) and the scattered field outside it (*outer problem*). With an increase in  $m$  at fix values of the other problem parameters the field within the particle asymptotically converges to a periodic function of  $m$ . The electric and magnetic type Mie resonances of different orders overlap substantially. It may lead to a giant concentration of the electromagnetic energy within the particle. At the same time, it is demonstrated that identical transformations of the solution to the outer problem allow to present each partial scattered wave as a sum of two partitions. One of them corresponds to the  $m$ -independent wave, scattered by the perfectly reflecting particle, while the other is associated with the excitation of a sharply- $m$ -dependent resonant Mie mode. The interference of the partitions brings about a typical asymmetric Fano profile. At an increase in  $m$ , in contrast to the inner problem, the resonant modes of the outer problem die out, and the scattered field converges to the universal,  $m$ -independent profile. The behavior of the resonances at a fixed  $m$  and varying particle size parameter ( $x$ ) is also examined in detail. The similarities and differences of the two cases (fixed  $x$  – varying  $m$  and fixed  $m$  – varying  $x$ ) are disclosed. The relevant experiments are discussed.

**Biomimetic technologies of new materials syntheses  
for photonics applications**

Yu.N.Kulchin

Institute of Automatic and Control Processes, FEB RAS, Russia;  
National Research Nuclear University MPhI, Russia  
e-mail: kulchin@iacp.dvo.ru

Lately in the industry, medicine, ecology, etc., there is an increased interest in the photon gas, bio - and chemosensors [1]. To solve this problem seems promising use of small and highly sensitive photonic sensors based on fiber and integrated optics. Silica is widely used in industry and medicine, e.g. for the fabrication of glasses, ceramics, paints, adhesives, catalysts and photonic materials. The technological production of silica mostly requires high temperature conditions and extremes of pH. At lower temperatures, silica can also be produced by sol-gel technology. Noteworthy, certain single- and multicellular organisms, including diatoms, sponges and higher plants are able to form their silica skeletons under ambient, low temperature and pressure, and near-neutral pH conditions. In addition, the skeletal elements of these organisms are produced with high fidelity and in large copy number, making these organisms and the mechanism (s) underlying the formation of their skeletons of interest for the fabrication of novel bio-silica's materials with unique optical properties. In this regard, the development of biosiliphycations process in nature are of considerable interest for the development of biomimetic nanotechnology in photonics. Wonderful process model of the biosiliphycations can serve sol-gel technology.

The purpose of this report is to present the results of the study of complex material skeleton of glass deep-sea sponges, allowed the development of sol-gel technology to create new biomineral nanocomposite materials with high optical and nonlinear optical properties, promising to create devices photonics and photonic sensors biomatrix [2]

**References**

1. Fun X., White I.M., et.al. Sensitive optical biosensors for unlabeled targets: A review// *Analytica Chemical Ata.* - 2008- V.620.-p.8-26.
2. 2. Kulchin Yu.N., Avramenko V.A., Bulgakov V.P. Photonics of self-organizing nanostructured biomineral oceanic objects and their analogs// *Herald of The Russian Academy of Sciences.* - 2013.- V.83. -No. 1.- P.19-30.

# Laser Nanolithography by Thermoplasmonics

Theobald Lohmüller\*

*Photonics and Optoelectronics Group, Department of Physics and Center of Nanoscience (CeNS), Ludwig-Maximilians-Universität München, Amalienstr. 54, 80799, Munich, Germany*

Noble metal particles feature intriguing optical properties, which can be utilized to manipulate them by means of light.<sup>1</sup> Light absorbed by gold nanoparticles, for example, is very efficiently converted into heat and single particles can thus be used as a fine tool to apply heat to only a nanoscopic area. At the same time, gold nanoparticles are subject to optical forces when they are irradiated with a focused laser beam which renders it possible to print, manipulate, and optically trap them in two- and three dimensions.

Based on these properties, I will present how gold nanoparticles can be used to control chemical reactions at the nanoscale and how this can be applied to perform laser lithography with sub-diffraction limited resolution.<sup>2</sup>

This approach is an all-optical analogue to conventional scanning probe lithography in a sense that only light is used to optothermally manipulate a single nanoparticle which is the equivalent to a probe tip. No further mechanical connection between the particle and the microscope is required which offers a new way for direct-writing of polymer fibers and fiber networks in two and three dimensions.

[1] A. S. Urban, S. Carretero-Palacios, A. A. Lutich, T. Lohmüller, J. Feldmann, F. Jäckel, "Optical trapping and manipulation of plasmonic nanoparticles: fundamentals, applications, and perspectives," *Nanoscale*, **6**, 4458-4474 (2014)

[2] M. Fedoruk, M. Meixner, S. Carretero-Palacios, T. Lohmüller, J. Feldmann, "Nanolithography by Plasmonic Heating and Optical Manipulation of Gold Nanoparticles," *ACS Nano*, **7**, 7648-7653 (2013)

\*t.lohmueller@lmu.de

## Nanogratings generated in transparent glasses by femtosecond laser radiation

**V. Oliveira<sup>1,2</sup>, S.P. Sharma<sup>1,3</sup> and R. Vilar<sup>1,3</sup>**

<sup>1</sup> *Centre of Physics and Engineering of Advanced Materials (CeFEMA), Instituto Superior Técnico, Av. Rovisco Pais, 1049-001, Lisboa, Portugal*

<sup>2</sup> *Instituto Superior de Engenharia de Lisboa, Avenida Conselheiro Emídio Navarro No. 1, 1959-007, Lisboa, Portugal*

<sup>3</sup> *Instituto Superior Técnico, Universidade de Lisboa, Av. Rovisco Pais, 1049-001, Lisboa, Portugal*

*voliveira@adf.isel.pt*

In recent years, femtosecond lasers have found application in the direct writing of surface and internal structures in a wide variety of transparent materials. This technique involves focusing an intense ultrafast laser pulse in a very small focal point. Due to their extremely high peak intensity and short pulse duration, femtosecond lasers induce nonlinear electron excitation processes such as multiphoton and tunnel ionization processes, which promote electrons to the conduction band and eventually lead to the formation of a plasma. Since the interaction is highly nonlinear, the excitation is localized to a very small volume. This localization is further enhanced because heat transport to the material during the duration of the laser pulse is negligible. As the plasma recombines and its energy is dissipated, permanent structural changes can be induced in the material. Depending on the numerical aperture of the focusing lens and laser parameters, such as pulse duration, wavelength, energy, and repetition rate, several types of modifications can be achieved. Among these, the formation of self-ordered structures oriented perpendicularly to the polarization of the incident laser beam radiation has attracted most attention due to its potential application in photonic devices. These so-called nanogratings, nanoplanes or nanocracks have a period smaller than the incident laser radiation wavelength and proportional to the incident laser radiation wavelength.

In the present work we report on nanogratings generated in transparent glasses by a direct femtosecond laser writing method using 1030 nm radiation wavelength. Nanogratings were inscribed in fused silica, soda-lime glass and lithium niobate wafers. Nanogratings with an average spatial periodicity of about 350 nm were created at low radiation energies for all three materials. The results achieved for fused silica show that the laser-affected regions are elongated ellipsoids with a typical major diameter of about 30  $\mu\text{m}$  and a minor diameter of about 6  $\mu\text{m}$ . The nanogratings within these regions are composed of alternating nanoplanes of damaged and undamaged material. The damaged nanoplanes contain nanopores randomly dispersed in a material containing a large density of defects.

## Laser – nanostructuring of dielectric surfaces assisted by laser-shaped chrome templates

P. Lorenz<sup>1</sup>, C. Grüner<sup>1</sup>, M. Klöppel<sup>2</sup>, M. Ehrhardt<sup>1</sup>, L. Bayer<sup>1</sup>, K. Zimmer<sup>1</sup>

<sup>1</sup>-Leibniz-Institut für Oberflächenmodifizierung e. V., Permoserstraße 15, 04318 Leipzig, Germany

<sup>2</sup>-Institute of Scientific Computing, Department of Mathematics, TU Dresden, 01062 Dresden, Germany

*pierre.lorenz@iom-leipzig.de*

The fast and large area nanostructuring of dielectrics is a big challenge for laser patterning methods. In this study a novel laser structuring method for the fabrication of periodic surface nanostructures in dielectrics, using a modified IPSM-LIFE method (laser-induced front side etching using in situ pre-structured metal layers) [1], is shown. Therefore, fused silica substrate was covered by periodically ordered polystyrene (PS) spheres with a diameter of 1.59  $\mu\text{m}$  (see Fig. 1, step 1). Subsequently, this system was covered by 30 nm chromium by electron beam evaporation (step 2). Afterwards the PS spheres were removed (step 3) and the bare and resultant periodic Cr triangles were irradiated with a KrF excimer laser (pulse duration  $\Delta t_p = 25$  ns, wavelength  $\lambda = 248$  nm, repetition rate  $f = 1 - 100$  Hz) with low laser fluences. The low laser fluence irradiation resulted in a melting, shape transformation of the triangles due to the surface tension and resolidification of the Cr where the resultant structures are dependent on the laser parameter (laser fluence  $\Phi$  and number of laser pulses  $N$ ) (see Fig. 1 step 4). The high laser fluence irradiation of the resultant metal structures causes the formation of patterns at the surface of the dielectric due to localized ablation and melting processes of the dielectric surface induced by the absorption of the laser energy by the metal structures and the local energy transfer into the dielectric surface (step 5). The resultant structures in the dielectric depend on the metal structure as well as the laser parameters. The surface topography after the different steps was studied by scanning electron microscopy (SEM) and atomic force microscopy (AFM). Furthermore, the triangle shaping process (step 4) as well as the dielectric surface structuring process (step 5) were simulated and compared with the experimental results.

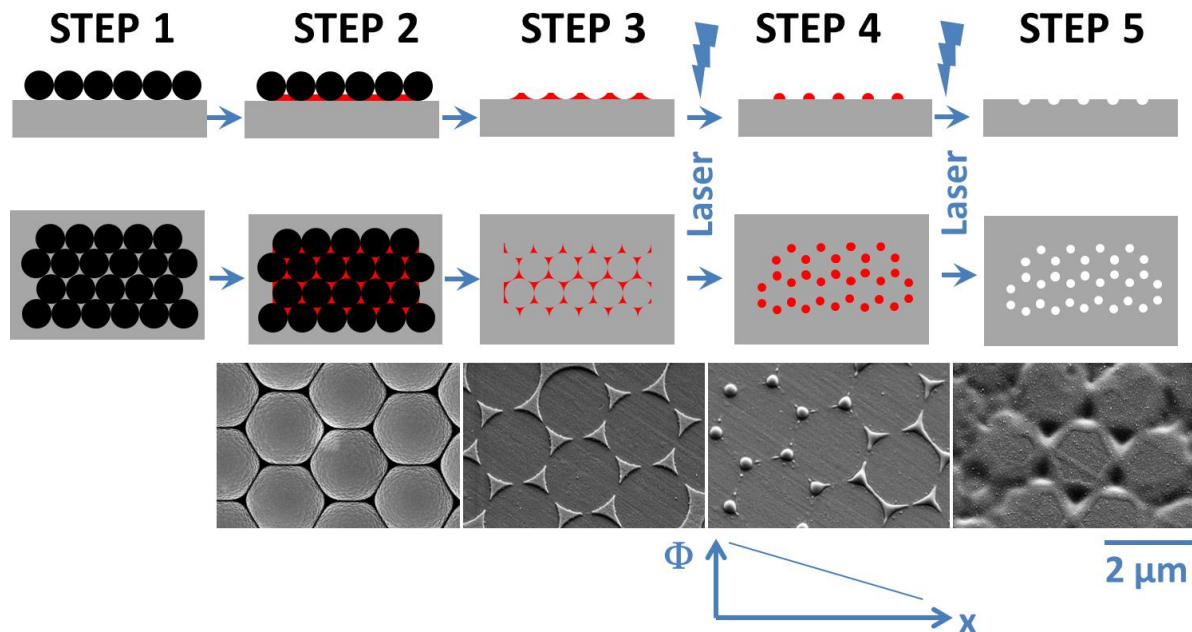


Fig. 1 Schematic illustration of the structuring process as well as exemplary SEM measurements

[1] P. Lorenz, F. Frost, M. Ehrhardt, K. Zimmer, Laser-induced fabrication of randomly distributed nanostructures in fused silica surfaces, Applied Physics A 111, pp. 1025 – 1030 (2013)

# Optimization of a sub-picosecond $K_{\alpha}$ x-ray source generated by Ultra high intensity laser-solid target interaction at 100Hz

**Y. Azamoum, V. Tcheremiskine, R. Clady, L. Charmasson, N. Sanner, O. Uteza  
and M. Sentis**

*Aix-Marseille University, CNRS, LP3 laboratory, Luminy Campus, 13288 Marseille cedex 9, France  
azamoum@lp3.univ-mrs.fr*

Our work focuses on an optimization of an x-ray source ( $K_{\alpha}$ ) characteristics, generated by interaction of an Ultra High Intensity femtosecond laser with a metallic solid target.

Intense femtosecond x-ray sources are already obtained in accelerator community such as free electron laser facilities (LCLS, FLASH ...) [1]. Since these installations are huge and costly, alternative and complementary sources based on laser produced plasma are still under development to produce intense table-top radiations [2] such as secondary sources of  $K_{\alpha}$  x-ray which present interesting characteristics suitable for applications. In fact, by focusing the laser beam into few microns, the x-ray source is characterized by a micrometric size, a key parameter to reach high spatial resolution in medical imaging when phase contrast technique is applied [3]. Also because the laser pulse is a femtosecond duration, the x-ray pulse emission has a sub-picosecond duration, which is required in experiments such as time resolved x ray diffraction, in which probing atomic motion during a phase change occurring on material (ps time scale) is possible.

The laser source consists on a Ti:Sa laser system that delivers very energetic pulses either up to 500mJ at 10Hz or 250mJ@ 100Hz, with 30fs pulse duration. Also the temporal pulse shape exhibits an excellent quality of contrast ratio better than  $10^{-9}$  at ns scale. In addition to this, thanks to our adaptive optics component, it is possible to focus the laser beam into 3.5 $\mu$ m diameter @FWHM with 75% laser energy within  $1/e^2$  maximum intensity. Thus, we can reach intensities  $> 10^{19}$  W cm $^{-2}$ .

Laser-plasma x-ray source has been studied by many groups in the past. But no study was done on enhancement of the source characteristics with such pumping source which is a unique one that exhibits this high contrast ratio at 800nm and such energetic pulses (250mJ) at 100Hz.

In the present work, our goal is to reach high  $K_{\alpha}$  photon fluxes (up to  $10^{12}$  photons/s), and few microns source size with an energy conversion efficiency into  $K_{\alpha}$  photons ( $\eta_{\alpha}$ ) close to  $10^{-4}$ . Our last experiments using Molybdenum target and 5mJ laser energy show a 10 $\mu$ m (FWHM) source size characterized by knife edge technique and a photon flux of  $10^9$  ph/s measured with photomultipliers tubes and x ray CCD.

The laser source consists on a Ti:Sa laser system that delivers very energetic pulses either up to 500mJ at 10Hz or 250mJ@ 100Hz, with 30fs pulse duration. Also the temporal pulse shape exhibits an excellent quality of contrast ratio better than  $10^{-9}$  at ns scale. In addition to this, thanks to our adaptive optics component, it is possible to focus the laser beam into 3.5 $\mu$ m diameter @FWHM with 75% laser energy within  $1/e^2$  maximum intensity. Thus, we can reach intensities  $> 10^{19}$  W cm $^{-2}$ .

In this contribution, we will discuss our results on enhancement of source characteristics (size, photon flux and  $\eta_{\alpha}$ ). A detailed study on effect of laser intensity, incidence angle and the temporal contrast ratio will be presented. With a particular attention to this parameter since it is related to the plasma gradient density created on the target, hence it has a direct effect on x-ray source size. Also recent studies show an enhancement of  $\eta_{\alpha}$  at intensities  $> 10^{18}$  W cm $^{-2}$  using high contrast ratio [4].

[1] T. Elsaesser and M. Woerner, "Perspective: Structural dynamics in condensed matter mapped by femtosecond x-ray diffraction", *J. Chem. Phys.* **140**, 020901 (2014).

[2] Jannick Weisshaupt, Vincent Juvé, Marcel Holtz *et al.*, "High-brightness table-top hard X-ray source driven by sub-100-femtosecond mid-infrared pulses", *Nature Photonics*, vol **8**, (2014).

[3] R. Toth, J. C. Kieffer, S. Fourmaux, T. Ozaki and A. Krol, "In-line phase-contrast imaging with a laser-based hard x-ray source", *Rev. Sci. Instrum.* **76**, 083701 (2005).

[4] Z. Zhang, H. Nishimura, M. Nishikino *et al.*, "Efficient multi-keV X-ray generation from high-contrast laser plasma interaction" *EPJ Web of Conferences* **59**, 18003 (2013).

**Laser-induced local profile transformation of multilayered graphene on a substrate**

V.I. Konov<sup>1,2</sup>, V.D. Frolov<sup>1,2</sup>, P.A. Pivovarov<sup>1,2</sup>, E.V. Zavedeev<sup>1,2</sup>, A.A. Khomich<sup>1</sup>,  
A.N. Grigorenko<sup>3</sup>

<sup>1</sup> *A.M. Prokhorov General Physics Institute of RAS, Vavilov str. 38, 119991 Moscow, Russia*

<sup>2</sup> *National Research Nuclear University MEPhI, Kashirskoyesh. 31, Moscow 115409, Russia*

<sup>3</sup> *Manchester Centre for Mesoscience and Nanotechnology, University of Manchester, Oxford Road, Manchester M13 9PL, UK*

The new regime of graphene nanostructuring with laser is presented. 3-6 layered graphene sheets were deposited onto silicon wafer surface and irradiated in air by sequences ( $\approx 10^5$ ) of nanosecond laser pulses. The number of graphene layers was controlled by Raman spectroscopy. Nd:YAG laser with wavelength 532 nm, pulse duration 7 ns and 2000 Hz repetition rate was used. The laser beam was focused normally to the sample surface into a spot of  $\approx 0.5 \mu\text{m}$  diameter at  $1/e$  intensity level. The samples were positioned inside a scanning probe microscope that was operated in a tapping mode and allowed to study graphene sheet morphology before and after irradiation.

It is found that at laser fluence  $\sim 0.04 \text{ J/cm}^2$  well below graphene ablation threshold ( $\approx 0.25 \text{ J/cm}^2$ ) local profile transformations can be induced if sufficiently long sequences of laser pulses are applied. Depending on laser pulse parameters ultra-shallow craters (cavities) with depth up to  $\approx 2 \text{ nm}$  or microholes (at slightly higher fluence) in graphene sheet were obtained. The diameter of these structures was close to that of the laser spot.

The observed effects result from laser pulse heating (boiling) and expulsion of adsorbed water layer between the silicon substrate and graphene.

The work was supported by the Russian Science Foundation, project # 14-22-00243.

# Bessel beam array formation using micro-structures fabricated via four-beam interference lithography

**E. Stankevičius, M. Garliauskas, G. Račiukaitis**

*Center for Physical Sciences and Technology (CPST), Savanoriu av. 231, LT-02300 Vilnius, Lithuania*

*e-mail: [estankevicius@ar.fi.lt](mailto:estankevicius@ar.fi.lt)*

An ideal Bessel beam [1] is non-diffracting beam characterized by a field distribution that is proportional to the zero-order Bessel function  $J_0$ , contains equal energy in all fringes and infinite total energy, and propagates with a stable radial intensity pattern [2]. Bessel beams due to their unusual properties (propagation invariance and self-reconstruction [3, 4]) are widely used in many fields: optical manipulation [5, 6], laser drilling [7, 8], trapping [9, 10], etc.

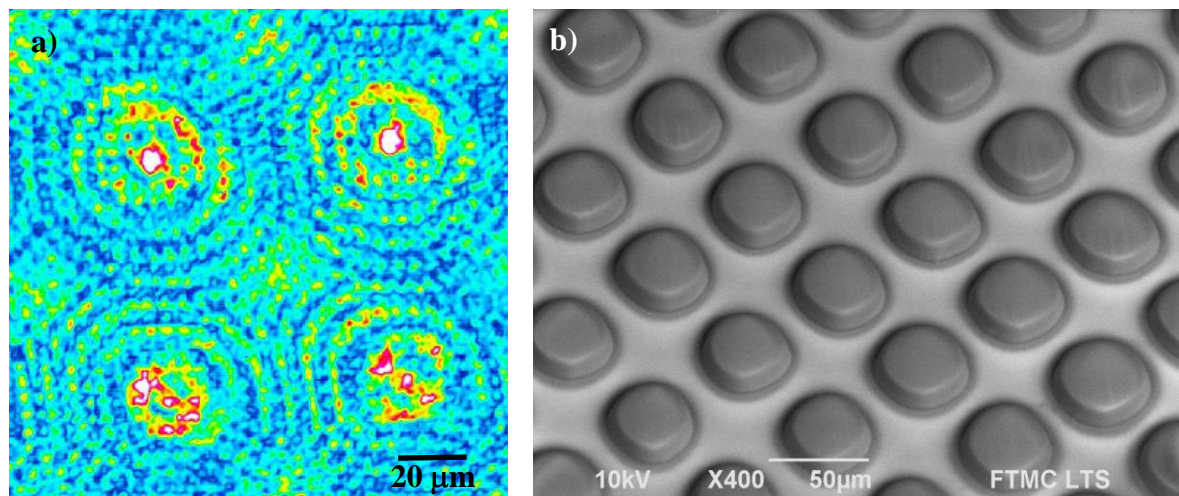


**Fig. 1.** a) Bessel beams intensity distribution formed by structures shown in b); b) Micro-structures fabricated by interference lithography by using the laser average power  $\sim 930$  mW and exposure time 30 s. Laser processing parameters: wavelength - 515 nm, repetition rate - 100 kHz. The distance between micro-structures is  $\sim 60$   $\mu\text{m}$ . SEM images of the structures are tilted by 34 deg.

Here, we will introduce an easy method to form Bessel beam array (Fig. 1a) by using microstructures fabricated via four-beam interference lithography (Fig. 1b). Also, we will present the ability to manipulate the beam characteristics using different shape of microaxiconlike structures and analyze the factors determining the shape of these structures during the four-beam interference lithography process.

## References

- [1] J. Durnin, et al., "Diffraction-free beams", *Physical Review Letters* **58**, 1499-1501, 1987.
- [2] R. Grunwald, et al., "Generation of femtosecond Bessel beams with microaxicon arrays", *Optics Letters* **25**, 981-983, 2000.
- [3] Z. Bouchal, et al., "Self-reconstruction of a distorted nondiffracting beam", *Opt. Commun.* **151**, 207-211, 1998.
- [4] V. Garcés-Chavez, et al., "Simultaneous micromanipulation in multiple planes using a self-reconstructing light beam", *Nature* **419**, 145-147, 2002.
- [5] J. Arlt, et al., "Optical micromanipulation using a Bessel light beam", *Opt. Commun.* **197**, 239-245, 2001.
- [6] K. Dholakia, et al., "Shaping the future of manipulation", *Nat Photon* **5**, 335-342, 2011.
- [7] Y. Matsuoka, et al., "The characteristics of laser micro drilling using a Bessel beam", *Applied Physics A* **84**, 423-430, 2006.
- [8] F. Courvoisier, et al., "Applications of femtosecond Bessel beams to laser ablation", *Applied Physics A* **112**, 29-34, 2013.
- [9] J. A. Kim, et al., "Atom trap in an axicon mirror", *Optics Letters* **22**, 117-119, 1997.
- [10] J. Arlt, et al., "Generation of high-order Bessel beams by use of an axicon", *Opt. Commun.* **177**, 297-301, 2000.

# Picosecond laser micromachining of silicon for integrated circuit defect analysis

**A. Sikora, T. Sarnet, M. Sentis**

*Laboratoire LP3, UMR 6182 CNRS-Aix-Marseille Université  
C. 917, 163 Avenue de Luminy, 13288 Marseille Cedex 9, France*

*sikora@lp3.univ-mrs.fr*

In the microelectronic industry, there is an increasing need to access quickly the deep layers of an integrated circuit for defect detection and analysis. In order to reveal precisely the structure of the materials, the samples are usually characterized by TEM. This requires the opening of cavities and the Focused Ion Beam (FIB) elaboration of thin lamella. Currently, the FIB removal rate of matter reaches hardly  $10^4 \mu\text{m}^3/\text{s}$ , which corresponds typically to several hours of processing to reach the targeted zone. Thus, other techniques such as pulsed-laser ablation are investigated in order to accelerate tremendously the process [1]. To minimize the FIB polishing time and not damage the area of interest, the laser ablation has to be optimized to limit the heat affected and induced dislocation zones, achieve vertical side walls for quite big deepness ( $> 200 \mu\text{m}$ ) and obtain surfaces with roughness as low as possible. In the present work, we tested the use of a picosecond laser ( $\sim 50 \text{ ps}$ ) at two wavelengths (343 and 515 nm) to engrave cavities in silicon wafers using different fluences and various numbers of scans on the surface where main studies have been performed with nanosecond and femtosecond lasers. The morphology of the cavities has been characterized by SEM. As the number of scans increases we observed an evolution of both cross sectional shapes and surface topology of the laser micro-machined cavities. In optimized laser ablation conditions, the side wall inclination may reach almost  $90^\circ$ . In each condition, the removal rates, tuned by the fluence, have been estimated. Typically, at 200 kHz, a high removal rate of  $10^6 \mu\text{m}^3/\text{s}$  has been achieved. We found better ablation efficiency with the 343 nm laser. Furthermore, in complement to previous studies performed with different wavelengths and pulse durations [2-4], ablation thresholds in silicon have been measured.

**Acknowledgement :** This work has been carried out thanks to the support of the A\*MIDEX project (n° ANR-11-IDEX-0001-02) funded by the « Investissements d'Avenir » French Government program, managed by the French National Research Agency (ANR).

- [1] M. Halbwx, T. Sarnet, J. Hermann, P. Delaporte, M. Sentis, L. Fares, G. Haller, Micromachining of semiconductor by femtosecond laser for integrated circuits defect analysis, *Applied Surface Science*, 254, 911-915, (2007).
- [2] P. P. Pronko, P. A. VanRompay, C. Horvath, F. Loesel, T. Juhasz, X. Liu, G. Mourou, Avalanche ionisation and dielectric breakdown in silicon with ultrashort laser pulses, *Physical Review B*, 58, 2387-2390 (1998).
- [3] X. Wang, Z. H. Shen, J. Lu, X. W. Ni, Laser induced damage threshold of silicon in millisecond, nanosecond and picosecond regimes, *Journal of Applied Physics*, 108, 033103 (2010).
- [4] J. Bonse, S. Baudach, J. Krüger, W. Kautek, M. Lenzner, Femtosecond laser ablation of silicon-modification thresholds and morphology, *Applied Physics A*, 74, 19-25 (2002).

## **Printing of aluminium microstructure using LIFT**

**O. Fogel<sup>1</sup>, M. Zenou<sup>1</sup>, Z. Kotler<sup>1</sup>**

*1- Additive manufacturing lab, Orbotech Ltd., PO Box 215, Yavne 81101, Israel*

*E-mail: ofer.fogel@orbotech.com*

Laser Induced Forward Transfer (LIFT) [1] is a printing method which allows solid bulk metals to be printed directly. The backside of the supplier material, which is a transparent substrate coated with a thin layer of metal, is heated with a pulsed laser. The metal undergoes a phase change and a small volume of the metal is propelled towards an acceptor substrate. By using nanosecond laser pulses and by tuning the laser spot size, energy and the metal layer thickness, LIFT can be performed in the droplet regime where each laser pulse causes the ejection of a single metal droplet. The high resolutions which are attainable by LIFT when working in the droplet regime, as well as the ability to print almost any material, gives LIFT a strong potential to be used in printed electronics applications.

In this work we study the electrical properties of aluminum structures printed by LIFT. Controlling the printing conditions allow us to tune the volume and jitter time of a single drop. In the case of Al there is a connection between the drop parameters and the resistivity. During the jetting the Al drop oxidizes and the resulting printed droplet is enveloped by an aluminum-oxide shell. The resistivity of the aluminum/aluminum-oxide printed structure is a function of the shell thickness, which can be controlled by the time of flight of the droplets and the droplet volume.

[1] D.A.Willis and V.Grosu, "Microdroplet deposition by laser-induced forward transfer", Appl. Phys. Lett. , 86 (2005).

## Time-resolved investigations of laser-dielectric interaction mechanisms

**S. Guizard<sup>1</sup>, A. Mouskeftaras<sup>2</sup>, S. Klimentov<sup>3</sup>, P. Palianov<sup>4</sup>,  
L. Haahr-Lillevang<sup>5</sup>, P. Balling<sup>5</sup>, M. Garcia-Lechuga<sup>6</sup>, J. Siegel<sup>6</sup> and J. Solis<sup>6</sup>**

*1- Laboratoire des Solides Irradiés, CEA/CNRS, Ecole Polytechnique 91128 Palaiseau, France*

*2- Galatea lab, STI/IMT, Ecole Polytechnique Fédérale de Lausanne (EPFL), Neuchâtel, Switzerland*

*3- General Physics Institute of the Russian Academy of Sciences, Vavilova St 38, 11991 Moscow, Russia*

*4- Institute of High Current Electronics of the Russian Academy of Sciences, Tomsk, Russia*

*5- Department of Physics and Astronomy, Aarhus University, DK-8000 Aarhus C, Denmark*

*6- Instituto de Óptica, C.S.I.C., Serrano 121, 28006 Madrid, Spain*

*stephane.guizard@cea.fr*

**Abstract:** Laser processing and machining of dielectrics is a growing field, involving increasingly complex laser temporal and spatial pulse shaping. Predicting and modeling the optimum pulse characteristic for a given application requires a detailed knowledge of all the elementary events involved during the interaction. To understand and observe these physical mechanisms in detail, we carry out time resolved experiments, using spectral interferometry and reflectivity change as a probe. Thus, we can measure in real time the excitation density achieved in the solid and the following relaxation of excited carriers. Since many processes (non-linear excitation, impact ionization, modification of pulse shape and propagation) arise during the pump laser pulse itself, usual pump-probe experiments are not capable to distinguish and directly observe them. To encompass this difficulty, we used a flexible double pump scheme [1], allowing modulating the excitation density and controlling the carrier heating steps.

We have been able to derive the following conclusions:

- The appropriate criterion to determine the ablation or damage threshold is the amount of deposited energy in the solid, not the density of carriers. The latter, measured at breakdown threshold, decreases with increasing pulse duration.

- We report a direct observation of laser induced impact ionization/avalanche. This phenomenon is a hypothesis in a huge number of publications, but has never been directly demonstrated. More important, we show that it is not connected to the optical breakdown, occurring far above the threshold for damage/ablation. Finally, the most interesting result is that it does not take place in all materials. The possible reason for this selective occurrence of impact ionization will be discussed.

- Time-resolved reflectivity exhibits different behavior compared to time resolved interferometry [2]. Since the latter measurement concern the bulk, the difference indicates that carrier excited at the surface relax following specific channels and with different dynamics.

- We have measured the lifetime of self-trapped excitons in SiO<sub>2</sub>, and found quite different values from the ones previously reported in the literature. This has important consequences for instance in the description or modelization of damage mechanism in the case of nanosecond pulses.

### Reference :

[1] S. Guizard, S. Klimentov, A. Mouskeftaras, N. Fedorov, G. Geoffroy, G. Vilmart, *Ultrafast Breakdown of dielectrics: Energy absorption mechanisms investigated by double pulse experiments*, Applied Surface Science 336 (2015) 206–211.

[2] K. J. Wædegaard, D. B. Sandkamm, A. Mouskeftaras, S. Guizard and P. Balling, *Probing ultrashort-pulse laser excitation of sapphire: From the initial carrier creation to material ablation*, Euro Phys. Lett., 105 (2014) 47001.

## Laser-induced synthesis of nanostructured carbon/metal-carbon clusters and complexes

S. Arakelian<sup>1</sup>, S. Kutrovskaia<sup>1</sup>, A. Kucherik<sup>1</sup>, A. Osipov<sup>1</sup>, A. Povolotckaia<sup>2</sup>,  
A. Povolotskiy<sup>2</sup>, A. Manshina<sup>2</sup>

*Stoletovs' Vladimir State University, Vladimir, Russia*  
*Saint-Petersburg State University, St.Petersburg, Russia*

E-mail: [kucherik@vlsu.ru](mailto:kucherik@vlsu.ru)

Synthesis of new carbon materials by laser irradiation of carbon target is an actual branch of laser physics. Laser sources with different pulse duration allow to change the heating rate of carbon with realization of different transition scenarios such as solids-liquid-vapor.

The obtaining of different allotropic forms of carbon depends on the conditions (pulse duration, energy, repetition rate etc.) of laser action. Last years, methods of laser irradiation on the carbon target in a liquid medium are actively developed. In this case the formation of a cavitations bubble, which can provide additional pressure on the target surface, the value of which can reach values of 10 GPa depends on laser irradiation conditions. Also, using laser setups with femtosecond pulse duration near the target surface, leads to a transition of the liquids into the "liquid plasma", which ensures both high temperature and high pressure in the area of influence.

Experiments of laser action on carbon target in the air and in water are presented in this paper. For the realization of different regimes of laser surface modification of the target and the formation of micro-nanoparticles in a liquid the YAG: Nd laser with a pulse duration from 0.5 ms up to 20 ms (pulse energy up to 50J) and the Ti: Sa femtosecond laser with 50 fs pulse duration (pulse energy up to 0.01 J) were applied.

During the process of laser irradiation of the target in the water, the surface layer explosion of the target due to local boiling supercritical fluid, "cold" ablation, solid-phase modification of the sample surface were observed. The formation of the carbon amorphous and crystalline nanoparticles in colloidal system was observed.

In this work we have investigated additionally the mechanism of the metal-carbon cluster formation during the process of irradiation of colloidal system which were consisted of separate carbon, silver and gold nanoparticles. This system was irradiated by nanosecond laser (100 ns) with average energy 10 J.

The studying method of laser metal-carbon nanostructuring resulted in the possibility of the bulk-materials producing which have a domination of metallic phase or a partial carbon inheritance properties. Such shape effect is made by adding of 10% of nanodiamonds of the total mass fraction. The investigations of the structure of the target by Raman spectroscopy have showed that there is an order in the array of carbon structure in all cases after laser treatment.

This work was supported by RFBR grant # 13-02-97513, from VISU 2014/13 government program and for young scientist grant MK-4321.2014.2.

# Silicon Nitride layer modification with UV femtosecond laser for PV applications

**Darius Andrijauskas<sup>1</sup>, Valius Cyras<sup>1</sup>, Dainius Horbaciauskas<sup>3</sup>, Karolis Sulinskas<sup>2</sup>, Tomas Lukstaraupis<sup>2</sup>**

1- PhD student at CENTER FOR PHYSICAL SCIENCES AND TECHNOLOGY

2- Non-profit "The Applied Research Institute for Prospective Technologies"

3- JSC "Precizika-MET SC"

Darius.Andrijauskas@gmail.com

Recently with silver becoming ever more expensive an interest in chemical and electrochemical contact deposition technologies, such as Ni/Cu plating, has risen within PV industry and with that a problem of how to selectively remove/open front passivation layer of silicon nitride[1, 2]. The classical solution of lithography is too expensive therefore cannot be used in solar cell application, so a search for alternative methods is under way. One of them is proposed in this work. Silicon nitride layer deposited on top of a crystalline silicon wafer is opened/removed by first modifying silicon nitride with a shot of femtosecond UV laser pulse and then removed by a chemical solution (see Figure 1). The important thing in this

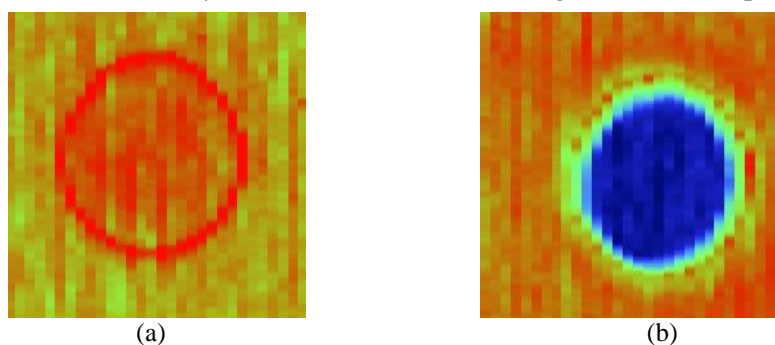


Figure 1: Surface maps of SiN on c-Si wafer: (a) ablated with 343nm 300fs laser; (b) same area after chemical etching.

scheme is that required laser energy is much lower than in the case of a more direct approach - silicon nitride ablation. Therefore the silicon surface is not damaged and preserved instead. Also homogeneity of opened surface is much greater. In case of standard ablation approach nonablatable rims of SiN are produced by first laser impulse, but not by suggested lower energy density silicon nitride modifying impulses. In the Figure 1 (a) we see a surface map of a silicon nitride layer deposited with PECVD on crystalline silicon wafer that was modified by a 300fs 343nm UV laser pulse. It can be seen most of the material is left intact. This indicates that no ablation or liftoff processes have occurred [3]. On the Figure 1 (b) we see the same sample area but after 10 minutes of chemical etching in an HF based solution. In Figure 2 we can see how the thickness of remaining silicon nitride decreases with increasing etching time. Further details analysis and conclusions will be presented in the main body of this work.

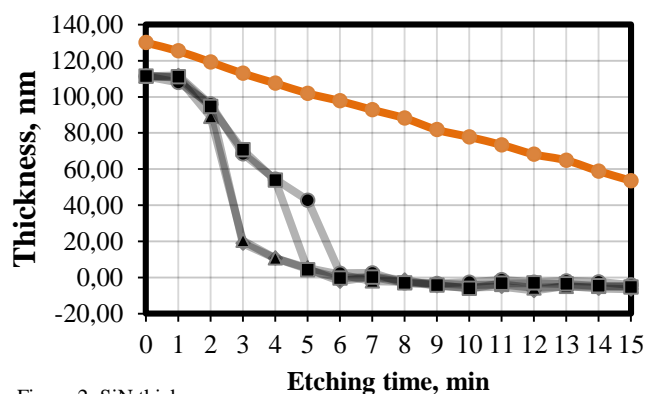


Figure 2: SiN thickness:  
orange line – unaffected/control area; gray lines – modified area;

- [1] A. Galdikas, V. Juzumas, K. Sulinskas, D. Andrijauskas, V. Janušonienė, V. Cyras, L. Jaraminė, J. Paulauskas, A. Selskis, Characterisation of selective femtosecond UV laser ablation of Si<sub>3</sub>N<sub>4</sub> layers, Proc. of the 27th European Photovoltaic Solar Energy Conference, 1641-1644 (2012)
- [2] V. Juzumas, J. Janusonis, V. Janusoniene, K. Sulinskas, D. Andrijauskas, L. Jaramine, T. Lukstaraupis, D. Janusonis, Selective Removal of SiN<sub>x</sub> by Ultrashort Laser Pulses and Nickel Silicide Formation, 26th European Photovoltaic Solar Energy Conference proceedings, 1757 – 1761 (2011)
- [3] Gerrit Heinricha, Alexander Lawerenz, Non-linear absorption of femtosecond laser pulses in a SiN<sub>x</sub> layer—influence of silicon doping type, Solar Energy Materials and Solar Cells, Volume 120, Part A, Pages 317–322, 2014

# Explosive crystallization of ferroelectric nanostructures by femtosecond laser

A. Elshin<sup>1</sup>, N.Firsova, E. Mishina<sup>1</sup>, O.Zhigalina<sup>2</sup>, V.Emelyanov<sup>3</sup>

1- Moscow State University of Information Technologies, Radioengineering and Electronics (MIREA), Vernadsky ave. 78, Moscow, Russia

2- The Shubnikov Institute of Crystallography of the Russian Academy of Sciences, Leninsky ave. 59, Moscow, Russia

3- Physics Department, Lomonosov Moscow State University, Vorobiev Gory, Moscow, Russia

mishina\_elenas7@mail.ru

Quasi-amorphous precursors require annealing for crystallized into functional ferroelectric and piezoelectric perovskite phase  $\text{PbZrTiO}_2$  (PZT). Contrary to conventional oven annealing, laser annealing can provide sufficient thermal energy to ferroelectric precursor thin film and transform it into the perovskite phase without keeping low temperature of the bulk of the material as well as of a substrate. In this paper we present the results of femtosecond laser annealing of PZT film on a platinized substrate, using wavelength which falls down into the transparency range of the film. It was found that regime exists for which crystallization starts at the surface of the film although the heat source is located at the platinum/film interface. The model is suggested describing propagation of a heat wave within the film.

$\text{Pb}(\text{Zr}_{0.54}\text{Ti}_{0.46})\text{O}_3$  films of 300 nm thickness were deposited by RF magnetron sputtering of the ceramic target onto platinized silicon substrate forming the structure PZT (300 nm)/Pt(20 nm)/ $\text{SiO}_2$ (10 nm)/Si (200  $\mu\text{m}$ ). For annealing, radiation of titanium-sapphire laser was used with pulse duration of 100 fs, wavelength in a range of 800 nm, repetition rate of 100 MHz. It was focused onto the sample using confocal microscope (NA=0.65), which gives a focal spot of 1  $\mu\text{m}$  in diameter. The obtained nanostructures were studied by transmission electron (TEM) and optical (linear and second harmonic generation (SHGM)) microscopies.

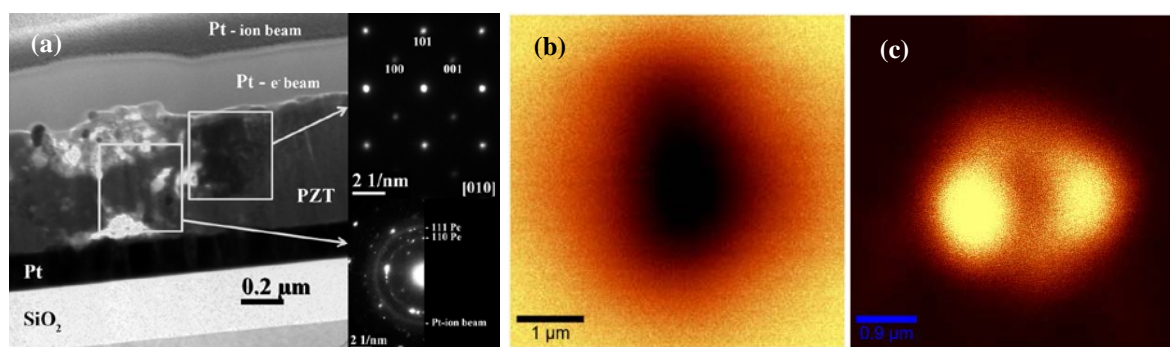


Fig. 1. (a) TEM image of the annealed area and appropriate diffraction pattern of different grains; (b) and (c) – linear and SHGM images of the annealed area, respectively. Annealing time is 11 s.

TEM image (Fig. 1 (a)) shows that the annealed area is a hemisphere with the center at the film surface. Annealing time is very short (from 0.5 to 15 s), the heat propagates as a spherical wave. Such process can be described within the model of explosive crystallization [1,2].

Within the annealed area both perovskite (piezoelectric and ferroelectric) and pyroclore (isotropic) nanocrystals can be found. The annealing process can be easily monitored optically: annealing results in changing of refractive index, giving rise to linear-optical microscopic image (Fig. 1 (b)) and appearance of non-zero second-order optical susceptibility, giving rise to SHGM (Fig. 1 (c)).

[1] V.I. Emel'yanov, I.M. Panin, Heat "Superemission" and Nucleation-Front Propagation Laser-Induced Crystallization of Thin Amorphous Films, *Appl. Phys.* A57, 561-566 (1993).

[2] A.S.Elshin, N.Yu. Firsova, V.I. Emelyanov, I.P. Pronin, S.V. Senkevich, E.D. Mishina, A.S. Sigov. Nonlinear-optical diagnostics of the local annealing of PZT films by femtosecond laser radiation. *J. Tech. Phys. Lett.* 41,16-23 (2015)

# Laser-induced metal deposition in different temperature zones of the laser beam

I. I. Tumkin, A. A. Smikhovskaia, D. I. Gordeychuk, L. S. Logunov, V. A. Kochemirovsky

*Saint-Petersburg State University, Institute of chemistry, 198504 Russian Federation,  
Saint-Petersburg, Petrodvorets, Universitetsky pr. 26.*

*lasergroupspb@gmail.com*

Laser-induced chemical liquid-phase deposition of metals (LCLD) is one of the promising techniques for patterning of the microelectronic devices. In this method metal reduction reaction proceeds in local volume of solution in the vicinity of the laser beam focal point and results in deposition of metal microstructures with high electrical conductivity on the surface of dielectric substrate [1-3]. It was found out that the composition of the structures deposited upon laser irradiation depends on the distance between the deposition region and the focal point of the laser beam (energy density maximum). For example, the copper and molybdenum deposition undergoes thermally induced mechanism and reveals significant dependence on the temperature zones of the moving laser beam. As a result, we propose three temperature zones distinguished by the mechanism of laser-induced copper deposition on the surface of dielectric substrate:

1. Focal (high-temperature) zone, 7-10  $\mu\text{m}$ , that is, the region near the laser beam focal spot (5-7  $\mu\text{m}$  in diameter) and in its direct vicinity. Focal spot zone is characterized by high temperatures, 500-1000  $^{\circ}\text{C}$  and greater, according to the different estimates.
2. Average temperatures zone, within this region temperature drops from the focal spot temperatures to 100-500  $^{\circ}\text{C}$ . This region corresponds to the temperature range in which thermal destruction of organic salts and copper complexes may takes place.
3. Low temperatures zone – it is the region of autocatalytic processes and classical chemical and electrochemical coppering processes.

In addition, the experimental results showed that the composition of obtained microstructures is substrate-dependent. Therefore, we calculated the temperature profile in the vicinity of the focal point of the laser beam focused on the surface of different substrates. Temperatures calculated at the distance of 0.001  $\mu\text{m}$  away from the focal point of the laser beam focused on glass-ceramics, silica and clouded glasses were found to be approximately 977, 397 and 557  $^{\circ}\text{C}$ , respectively. We observed that metallic molybdenum and molybdenum dioxide deposit at temperatures greater than or equal to 977 and 397  $^{\circ}\text{C}$ , respectively, whereas mixture of both deposits at approximately 557  $^{\circ}\text{C}$ . Thus, the results of experimental observations supported by the aforementioned theoretical considerations demonstrate the correlation between temperatures calculated in the vicinity of the laser beam focused on the surface of substrates and composition of deposited structures which was used to propose the mechanism of metal thermo-induced deposition upon laser irradiation.

We acknowledge the Russian Fund for Basic Research (grants 15-03-05139) and Saint-Petersburg State University for a research grants (2015–2017, 12.38.219.2015) and postdoctoral fellowship (No. 12.50.1189.2014). The authors also highly appreciate the Interdisciplinary Resource Center for Nanotechnology St. Petersburg State University.

[1] V. A. Kochemirovsky, L. G. Menchikov, S. V. Safonov, M. D. Bal'makov, I. I. Tumkin, Yu. S. Tver'yanovich, Laser-induced chemical liquid phase deposition of metals: chemical reactions in solution and activation of dielectric surfaces, *Russian Chemical Reviews* (Russ. Chem. Rev.), 80, 869-882, (2011).

[2] V. A. Kochemirovsky, E. M. Khairullina, S. V. Safonov, L. S. Logunov, I. I. Tumkin, L. G. Menchikov, The influence of non-ionic surfactants on laser-induced copper deposition, *Appl. Surf. Sci.*, 280, 494–499, (2013).

[3] K. Kordas, J. Remes, S. Leppavuori, L. Nanai, Laser-assisted selective deposition of nickel patterns on porous silicon substrates, *Appl. Surf. Sci.*, 178, 93-97, (2001).

## Evaluation of melt flow velocity in the process of laser cutting of metals

**A.V. Dubrov, Yu. N. Zavalov, V. D. Dubrov**

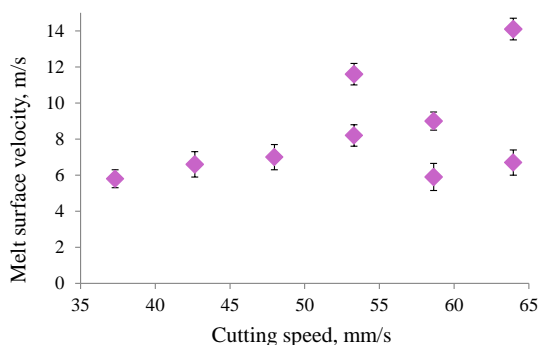
*Institute on Laser and Information Technologies of Russian Academy of Sciences (ILIT RAS),  
1 Svyatoozerskaya St., 140700 Shatura, Moscow Region, Russia*

*dubrov.av@gmail.com*

Among the thermal laser technologies, gas-assisted laser cutting of the metals is the most mastered in practice and widely used technology. However, there is a gap between its practical application and understanding of the physical processes that accompany laser radiation action on the material and determine the dynamics of the melt flow. This is largely due to the lack of the experimental data on the structure of the melt flow, which could allow selection and refining of the developed theoretical models. The difficulty of obtaining information from the cutting zone usually leads to carrying the experimental study of the dynamics of the melt in model experiments, the conditions of which differ from the actual process. This limits the applicability of the obtained results.

We have developed and tested the optical correlation method that allows measuring the surface velocity of the melt flow in a real process of gas-assisted laser cutting of metal. With the two-color pyrometer the brightness temperature fluctuations in four areas of the cutting front were simultaneously measured during the cutting process with the CO<sub>2</sub>-laser. The samples of mild steel of different thicknesses were cut with the use of an auxiliary gas - oxygen. The temperature measurements were made in the local areas with a diameter of 100 μm each, arranged under each other along the cutting front at a distance of approximately 0.6 mm. Sampling rate: 16 kHz, exposure time: 2.5 μs [1].

Under the effect of intensive tangential gas flow the hydrodynamic waves are likely to form on the melt surface, they move with a certain velocity relative to the melt. Surface relief inhomogeneities modulate the absorption of laser radiation, leading to non-uniform heating. Thus, the propagation of waves is accompanied by the corresponding propagation of temperature inhomogeneities and does not allow an accurate determination of the melt flow velocity using the cross-correlation function of the original temperature signal.



Stable values of the melt flow surface velocity depending on the cutting speed. Mild steel 3 mm, CO<sub>2</sub>-laser 1.5 kW, assist gas (O<sub>2</sub>) pressure 0.1 MPa,

We present the algorithm for processing the optical correlation method data, comprising preliminary frequency filtering, calculation of cross-correlation functions for a plurality of frequency bands, and the subsequent analysis of the obtained frequency dependence of the inhomogeneities velocity. The use of this algorithm allows us to distinguish the velocity of the temperature inhomogeneities formed by different mechanisms. Thus it is possible to determine the surface velocity of the melt flow in case of hydrodynamic waves propagation with certain velocities.

The dependences of the melt flow surface velocity on the laser cutting process parameters have been obtained. It has been found that under certain process parameters the melt velocity periodically varies alternately taking one of several stable values (see the figure), whereby the duration of velocity change is much shorter than the duration of movement with a steady velocity.

[1] A. V. Dubrov, Yu. N. Zavalov and V. D. Dubrov, Evaluation of Speed of Melt Evacuation in the Technology of Laser Cutting of Metals by the Optical Correlation Method, Technical Physics Letters, vol. 40, No. 6, pp. 491–494, (2014).

**Numerical simulation of solute evolution during laser cladding with nickel  
superalloy powder injection**

**Khomenko M.D., Niziev V.G., Mirzade F.Kh.**

Institute on laser and information technology, Russian academy of sciences (ILIT RAS)  
1, Svyatoozerskaya st., Shatura, Moscow Region, Russia, 140700

**Abstract**

A transient 3-D numerical model including heat transfer, solute transport and phase change kinetics is developed for laser cladding with coaxial injection of nickel superalloy powder. The evolution of temperature and composition distribution of build-up layer is investigated. Modified Kolmogorov-Johnson-Mehl-Avrami (KJMA) equation is used for phase change modeling considering non-homogeneous temperature distribution of melt pool. Influence of self-consistent heat conduction and phase change kinetics as well as substrate boundary and soluble impurity atoms on phase change process is analyzed. Results show the influence of main processing parameters (powder feed rate, laser power, scanning velocity) on the rapid crystallization at laser cladding and can be used for functionally graded components build-up.

# Continual-Atomistic Simulation of Metal Targets under the Action of Double Femtosecond Laser Pulses

**V.B. Fokin<sup>1</sup>, P.R. Levashov<sup>1,2</sup>, M.E. Povarnitsyn<sup>1</sup>**

*1- Joint Institute for High Temperatures RAS, Izhorskaya 13 Bldg 2, Moscow 125412, Russia*

*2- Moscow Institute of Physics and Technology, Institutsky 9, Dolgoprudny 141707, Russia*

*Vladimir.Fokin@phystech.edu*

In this work, we study the mechanisms responsible for the dynamics of femtosecond double-pulse laser ablation of metals. In several experiments [1] it was previously shown that the crater depth in double pulse irradiation monotonically drops when the delay between pulses increases. This decrease of the crater depth starts from the delay of several picoseconds and for delays longer than the time of electron–ion relaxation the crater depth can be even smaller than that produced by only a single pulse. To describe this complex dynamics we use an advanced specially developed hybrid method based on combination of atomistic and continual approaches [2]. The atomistic system describes the evolution of a target irradiated by the laser pulses, takes into account melting, evaporation, nucleation and recoil effects while electronic subsystem is responsible for correct description of the laser energy absorption, thermal conductivity process and electron-phonon coupling. Our version of this model takes into account laser absorption according to Helmholtz equation as well as dependencies of electron thermal conductivity and electron–ion coupling on density and temperature [3]. The Thomas–Fermi model is used for describing the electronic heat capacity, the inter-ions interaction is defined using inter-particle EAM-potential.

The results of simulation of the double-pulse ablation obtained for different delays from 1 to 100 ps correlate with the experimental findings.

[1] A. Semerok, C. Dutouquet, *Thin Solid Films*, 501, 453–454, (2004).

[2] D.S. Ivanov, L.V. Zhigilei, Combined atomistic-continuum modeling of short-pulse laser melting and disintegration of metal films, *Phys. Rev. B*. V. 68. P. 064114 (2003).

[3] M. E. Povarnitsyn, N. E. Andreev, E. M. Apfelbaum, T. E. Itina, K. V. Khishchenko, O. F. Kostenko, P. R. Levashov, M. E. Veysman, A wide-range model for simulation of pump-probe experiments with metals, *Applied Surface Science*. V. 258 P. 9480–9483 (2012).

# Laser formation of relativistic subfemtosecond electron bunches from gas jets

**Victor V. Kulagin<sup>1,2</sup>, Vladimir A. Cherepenin<sup>2</sup>, Vladimir N. Kornienko<sup>2</sup>**

*1- Sternberg Astronomical Institute of Lomonosov Moscow State University,  
Universitetsky prosp. 13, Moscow, 119992, Russia*

*2- Kotel'nikov Institute of Radioengineering and Electronics of RAS, Mohovaya 11, Moscow, 125009, Russia*

*victorvkulagin@yandex.ru*

Generation of short relativistic electron bunches is very important for many applications. One important application is a generation of an ultrashort x-ray pulse through Thomson backscattering of a counter-streaming probe laser pulse off such a relativistic electron bunch [1].

In the presentation, interaction of strong laser pulses with thin plasma layers is investigated in details. A formation of relativistic electron mirrors (electron bunches with diameter of the order from several microns to tens of microns and thickness from a few tens to hundreds of nanometers) from the tape gas jets of subcritical concentration with a powerful laser pulse is considered. In the case of perpendicular incidence of the laser pulse with relativistic intensity at the gas jet, a longitudinal component of the Lorentz force causes a shift of the plasma electrons in the direction of propagation of the laser pulse and can accelerate them to relativistic velocities. If the pulse amplitude is sufficiently large, and the electron density of the gas jet is reasonable, then full evacuation of the electrons from the plasma layer takes place. As a result, a relativistic electron mirror can be formed, which diameter is determined by the diameter of the laser pulse. This can occur only if the initial thickness of the plasma layer is less than some threshold value determined by the amplitude and duration of the laser pulse and the initial density of electrons in the layer.

An idea for using a nanofilm for synchronous acceleration of electrons with a superintense nonadiabatic laser pulse and formation of a relativistic electron mirror was considered in [2,3]. However, the front of the accelerating laser pulse should be sharp enough in this case. Requirements to the front of the laser pulse for the gas targets are significantly decreased in comparison with the nanofilm targets, and the lifetime of relativistic electron mirrors can be much larger, besides, use of gas targets facilitates creation of installations with high pulse repetition rate. All these significantly expand the scope of applicability for such relativistic electron mirrors.

For studying the process of formation of relativistic electronic mirrors from tape gas jets, two-dimensional numerical simulations were used. Potential characteristics of the mirrors were found, such as the maximum energy of the electrons and the spread of the electrons' energy in the mirror, maximum achievable electron density in the mirror, minimum achievable thickness, lifetime, etc. It is shown that for a moderate electron density of the layer and sufficiently large diameter of the laser beam, dynamic characteristics of the plasma layer electrons can be analytically estimated based on equations of motion for a single electron in the field of a laser pulse. Besides, the formation of the mirrors from a variable density plasma layer, as well as the formation with laser pulses of different duration was also investigated. It is shown that in all considered cases, it is possible to choose the system parameters (pulse amplitude, density and thickness of the plasma layer) in such a way that a single relativistic electron mirror can be formed, which parameters correspond to those required for generation of coherent x-ray pulse using the counter reflection of the probe laser pulse [4].

[1] V.V. Kulagin et al., "Generation of relativistic electron mirrors and frequency upconversion in laser-plasma interactions", *Appl. Phys. Lett.*, vol. 85, pp. 3322-3324 (2004).

[2] V.V. Kulagin et. al., "Theoretical investigation of controlled generation of a dense attosecond relativistic electron bunch from the interaction of an ultrashort laser pulse with a nanofilm", *Phys. Rev. Lett.*, vol. 99, pp. 124801 (2007).

[3] V.V. Kulagin et. al., " Characteristics of relativistic electron mirrors generated by an ultrashort nonadiabatic laser pulse from a nanofilm", *Phys. Rev. E*, vol. 80, 016404 (2009).

[4] V.V. Kulagin et. al., "Generation of intense coherent attosecond X-ray pulses using relativistic electron mirrors", *Quant. Electron.*, vol. 43, pp. 443 – 448 (2013).

## Ablation of thin gold film by ultrashort laser pulse

**N. Inogamov<sup>1</sup>, V. Zhakhovsky<sup>2</sup>, Yu. Petrov<sup>1,3</sup>, V. Khokhlov<sup>1</sup>, S. Anisimov<sup>1</sup>**

1- Landau Institute for Theoretical Physics of Russian Academy of Sciences,  
Russian Federation, 142432 Chernogolovka, prospekt Akademika Semenova, 1A

2- Joint Institute for High Temperatures of Russian Academy of Sciences,  
Russian Federation, 125412 Moscow, Izhorskaya street, 13 Bd.2

3- Moscow Institute of Physics and Technology,  
Russian Federation, 141700 Dolgoprudny, Moscow region, Institutskii pereulok, 9

*nailinogamov@gmail.com*

Laser action onto a gold film mounted above a glass substrate is considered. Solution of this problem is important for many applications. There are few different regimes depending on absorbed fluence, thickness of a film, diameter of an irradiated spot, and cohesion strength between metal and substrate. We consider the films 50-100 nm thick. A substrate has thickness of the order of submillimetres and may be regarded as infinitely thick. Presence of the substrate is dynamically significant; behaviour in the case of a freestanding film is different [1-3]. Thermal evolution of the films 50-100 nm thick differs from evolution of bulk gold because thickness of a heated surface layer in the case of bulk gold target is larger than 50-100 nm. Two-temperature hydrodynamic code and molecular dynamics simulations are used to describe ablation. Hydrodynamic code includes modern descriptions of an equation of two-temperature and one-temperature states [4], an electron-ion coupling and a two-temperature electron heat conductivity [5,6]. Even in the case with a small irradiated spot its diameter of the order of micron (for the small spot) is much larger than thickness of a film. Thus an initial stage of ablation motion is close to one-dimensional motion. One-dimensional approximation may be used till the stage when displacement of a film becomes of the order of a spot diameter. At the larger displacements the ablation flow gradually transforms from one-dimensional to three-dimensional geometry [2,3,7]. In the case of a small spots the nanobumps and nanojets are formed after recrystallization of a flying film separated from a substrate [2,3,7]. Below an ablation threshold the film exhibits oscillation on a substrate. The oscillations decay in time. The oscillating film irradiates a chain of acoustic waves into a substrate [7]. There is splitting of an ablation threshold if cohesion between a substrate and a film is weak [7]. In this case there is a delamination threshold above which a film as whole delaminates from the substrate. The delamination creates a cavity between a substrate and a film flying out from the substrate. There is a breaking threshold above the delamination threshold if cohesion is weak. Above the breaking threshold the breaking of a film takes place *inside the film*. Above the breaking threshold the upper part of a film flies out (the substrate is below the film) while the bottom part remains in contact with a substrate. The value of the delamination threshold increases as cohesion increases, while the film breaking threshold is insensitive to cohesion. Therefore above some definite value of cohesion the delamination threshold increases up to the breaking threshold and the delamination threshold and delamination itself disappear. Cohesion is significantly increased if a chromium layer is used as an intermediate layer between gold and glass substrate. Both cases with weak and strong cohesion are described in the proposed report. Addition of a chromium layer influences dynamics of a film. E.g., slightly above the breaking threshold the stretched gold nucleates at a larger depth. Acknowledgement. Authors acknowledge financial support from Russian Science Foundation (RSCF), grant # 14-19-01599.

[1] B. Demaske et al., Ablation and spallation of gold films irradiated by ultrashort laser pulses, Phys. Rev. B, vol. 82, 064113 (2010).

[2] N. Inogamov and V. Zhakhovskii, Formation of Nanojets and Nanodroplets by an Ultrashort Laser Pulse at Focusing in the Diffraction Limit, JETP Lett., vol. 100, No. 1, pp. 4-10 (2014).

[3] N. Inogamov, V. Zhakhovskii, and V. Khokhlov, Jet Formation in Spallation of Metal Film from Substrate under Action of Femtosecond Laser Pulse, Journal of Experimental and Theoretical Physics (JETP), vol. 120, No.1, pp. 15-48 (2015).

[4] Yu. Petrov, K. Migdal, N. Inogamov, V. Zhakhovsky, Two-temperature equation of state for aluminum and gold with electrons excited by an ultrashort laser pulse, Appl. Phys., B, DOI 10.1007/s00340-015-6048-6B.

[5] Yu. Petrov, N. Inogamov, and K. Migdal, Thermal Conductivity and the Electron-Ion Heat Transfer Coefficient in Condensed Media with a Strongly Excited Electron Subsystem, JETP Lett., vol. 97, No. 1, pp. 20-27 (2013).

[6] Yu. Petrov et al., Therm. cond. of condensed gold in states with the strongly excited electron subsystem, J. Phys. Conf. Ser. (accepted).

[7] N. Inogamov et al., [www.chemphys.edu.ru/pdf/2014-11-29-005.pdf](http://www.chemphys.edu.ru/pdf/2014-11-29-005.pdf)

## Double wave-length lasers-induced reversible microchannels fabrication inside Foturan glass

M. S. Sergeev, M. P. Veiko, E. M. Matutin, E. I. Iugntseva

ITMO University, 197101, Kronverkskiy Pr., 49, St. Petersburg, Russia

maks-sv-32@yandex.ru

Structure change and phase transformation of local areas inside photostructurable glass (PhG) are taking of great interest [1]. An initiation of crystalline areas inside PhG and subsequent chemical etching of these structures is a technique of microchannels or other cavities in the bulk of glass fabrication [1, 2]. Direct laser writing, resulting in changes of structure and phase transformation inside PhG without the stage of annealing in a furnace has several advantages unlike to other techniques.

The purpose of this work is a realization of microchannels formation inside PhG plates by direct laser writing and stage of chemical etching. Laser irradiation at two wavelengths—the second harmonic of Nd:YAG laser (532 nm, 30 ps, 10 mJ) and CO<sub>2</sub> laser (10.6 μm, 190 ns, 5 kJ) were used for formation of crystallization areas [3]. At the first step the area of nucleation in the form of local structural defects was created under the action of picosecond laser pulses. At the next step the crystalline phase was fully formed by CO<sub>2</sub> laser-induced fast annealing (LIFA). At the same time the overgrowing of microcracks around of defect by the annealing was allowed, which eliminated a rough distortion of topology (fig.). On the last step of microchannels formation the crystalline areas inside PhG plate were exposed to chemical etching in 10% water solution of hydrofluoric acid (HF). Duration of this stage (from several minutes (15 – 20 min) to several hours (1 – 2 h) were correlated with the size (diameter and length) and the shape (line or curve) of crystalline area.

From experimental results the chemical etch rate ratio of the amorphous and crystalline phases was in the range from 45% to 53%. So, the line with length of 685 μm and diameter of 10 μm was transformed to a channel by the chemical etching for 15 min with average rate of 45 μm/min. The average rate of chemical etching of amorphous phase was about 0.6–0.8 μm/min that is consistent to experimental results in the other works [1, 2]. At this, the chemical etch rate ratio constants of alternative techniques less than 40% and 58% [1, 4].

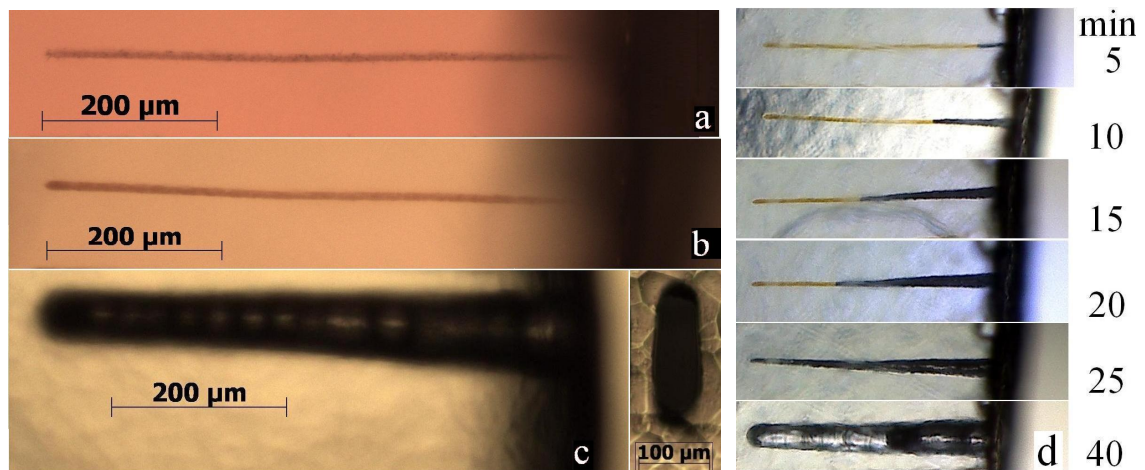


Fig. Image of line inside PhG—before (a) and after (b) the laser-induced fast annealing—after (c) and during (d) of chemical etching.

**Acknowledgements**—The presented work was completed under financial support due to Russian Federation Government grant 074-U01, RSF agreement № 14-12-00351 and by the Leading State Universities of Russian Federation subsidy NS 1364.2014.2.

[1] Sugioka K., Cheng Q. Femtosecond laser 3D micromachining for microfluidic and optofluidic applications, Springer Science & Business Media, 129 p 2014.

[2] Livingston F.E., Jelvajian J. Photophysical processes that activate selective changes in photostructurable glass ceramic material properties, Photon-based Nanoscience and Nanobiotechnology. Weinheim. Springer, pp. 225–265 (2006).

[3] Vadim P. Veiko, Maksim M. Sergeev, Eduard I. Ageev, Andrew A. Petrov 3D express crystallization of Foturan glass at CO<sub>2</sub> laser annealing on the defects produced by picosecond laser, SPIE., Vol. 9065 (33), pp. 90650M–90650M-7 (2013).

[4] F. Ye, Q. Liao, J. Lin, J. Song, L. Qiao, Q. Cheng, K. Sugioka, Femtosecond Laser Fabrication of Monolithically Integrated Microfluidic Sensors in Glass, Sensors, 14, pp. 19402–19440 (2014).

## Increase of wear-resistance of coverings introduction of nanocarbides of refractory metals at laser cladding

V.P. Birukov<sup>1</sup>, V.N. Petrovskiy<sup>2</sup>, M.F. Murzakov<sup>2</sup>, O.N. Churlyayeva<sup>1</sup>, N.M. Prokopova<sup>2</sup>

1- Institute of Machines Science of the Russian Academy of Sciences

4 Maly Kharitonyevsky Pereulok, Moscow 101990, Russia

2-National Research Nuclear University MEPhI (Moscow Engineering Physics Institute),

31 Kashirskoe sh., Moscow, 115409, Russia

[vnpetrovskij@mephi.ru](mailto:vnpetrovskij@mephi.ru)

Use of additives of nanoparticles of refractory connections such as carbide of tantalum (TaC) and carbide of tungsten (WC), leads to that superficial properties of a coating improve (wear-resistance, microhardness). Wear-resistance of coatings with a nickel matrix can increase considerably with addition of refractory particles such as WC, TaC, NiC. The main matrix contains rather soft phase with the maintenance of firm phases of carbides which provide increase of abrasive wear of coating. When using additives of the powder WC it was noticed that with increase in density of power of laser radiation, the quantity of particles of WC decreases. It is explained to that secondary carbide phases start being formed and by that sensitivity to formation of cracks in a coating increases.

Experiments were made with use of the powders two types on a nickel basis of production of HOGANAS firm – 1360 and 1559. The sizes of granules of powders were 50-140 microns, as additives of nanopowders are chosen – TaC and WC, with sizes up to 100 nanometers. Cladding of standard powder and powder with additives of nanopowder was carried out on flat surfaces of substrates from steel 34XH1MA with sizes of 15x70x10 mm. As binding substance water solution of an oksietiltellyuloza. Power of radiation varied in the range from 500 to 3000 W. Speed of movement of a laser beam of 5-25 mm/s.

In the first part of experiments the layer of mixture of powders 1559 and the nanopowder WC with various volume concentration was applied on a substrate (5%, 10%, 15% and 20% respectively), mixture was prepared with binding substance of an oksietiltellyuloza on a water basis, thickness of previously put layer made about 1 mm.

In figure 1 comparison of measurements of microhardness of the built-up samples powder 1559 without nanocarbide additives ( $\approx 6000$  MPa), and with additives of 15% nano-WC ( $\approx 9000$  MPa) is carried out. Apparently from comparison, there is a significant increase in microhardness in the claddings with additives of nanoparticles of carbide of tungsten.

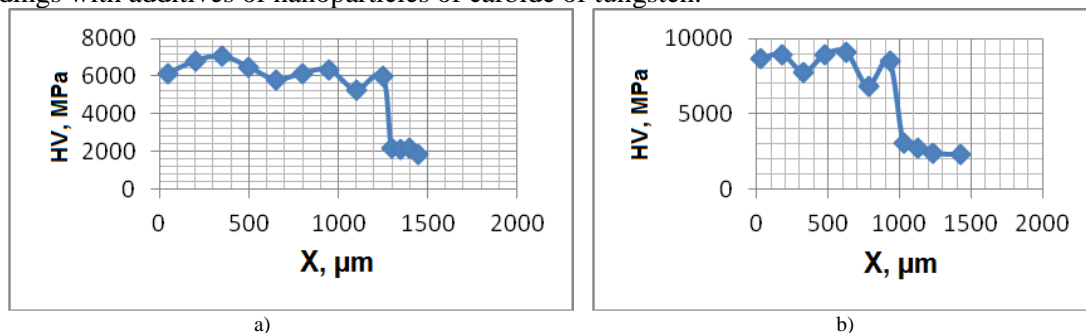


Fig. 2. Dependence of microhardness on thickness of the built-up layer:  
a) - powder 1559 cladding, b) - powder 1559 cladding with additives of 15% nano-WC

In the second series of experiments applied powders on a nickel basis 1360 with a size of particles of 40 - 150 microns. For increase of resistance to abrasive wear entered 10 - 40% of the volume mixture, tantalum carbide nanopowder, through each 10%.

With increase of the amount of nanocarbide of tantalum with 10 to 40% average microhardness increases with 7400 (10% of TaC) to 8600 (40% of TaC) MPa.

Tantalum carbide nanopowder introduction within 10% of the volume mixture allows to increase wear-resistance of the built-up layers by 4 times. The further increase in the content of nanopowder up to 40% of the volume of furnace charge leads to increase of wear-resistance to 6 times.

## Multilayer cladding using high-power fiber laser radiation

V.N. Petrovskiy, D.P. Bykovskiy, P.S. Dzhumaev, V.I. Polskiy, N.M. Prokopova

*National Research Nuclear University MEPhI (Moscow Engineering Physics Institute),  
31 Kashirskoe sh., Moscow, 115409, Russia  
[vnpetrovskij@mephi.ru](mailto:vnpetrovskij@mephi.ru)*

Nowadays, there is a growing interest of using additive technologies in the industry which also include laser cladding coatings - a complicated process, whose goal is to restore the damaged parts of surfaces, as well as giving them the required properties. Using a fiber laser allows to achieve the most concentrated source of energy (beam size is a few tenths of a millimeter) and its high optical quality of the radiation, high power and the ability to transport laser radiation through the fiber lines significantly simplifies problem of creating a high-quality coating and improve the economic performance of the technology.

Study is carried out on the installation consisting of five main parts: the cell coordinate system Huffman HC-205, the computer system control, feeder for powders Sulzer Metco Twin 10-C, fiber laser LS-3.5 power up to 3.5 kW, chiller for cooling the laser and the optical head. We used a powder of the brand PR-10R6M5, the grain size of which is in the range up to 140 microns. Sieving through a flat sieve was performed for improving the properties of the cladding. The cell size varied from 63 to 100 microns. The powder became more homogeneous, without large teardrop-shaped beads after screening. Additionally, the substrate surface grinding of used steel 34HMA (iron content of ~ 98.54%) was carried out for removal of oxides before the experiment.

Experiments showed that the most powerful influence on the width and depth of the cladding track has laser power variation, and height of the track - the powder feed rate. Following optimal mode of deposition track was selected with all of the above requirements: laser power is 400 W, linear speed of substrate is 37.5 cm/min, powder feed rate 1 g/min and a height above the surface of the nozzle 5 mm, in this case the spot diameter at the surface was 0.9 mm.

Initial gradual cladding in the above-mentioned regime and different overlap of  $1/3W$ ,  $1/2W$ ,  $2/3W$  was carried out, where  $W$  is a width of one track. After a visual inspection and cross-sectional analysis, taking into account the uniformity of penetration of the track proved to be the most optimal layer applied with overlapping  $2/3W$ .

The distribution of the substrate temperature during laser cladding was measured by a thermal imager FLIR T650SC. Further the following strategy of the layer fabrication was chosen. After application of the track 1 substrate material was displaced at the distance  $D$  where thermal field of one track falls significantly. On the basis of the analysis devoted to the measured distribution of substrate material temperature within welding the value of  $D = 5$  mm was chosen. Then track 2 was applied, and once again shift at the distance  $D$  happened, track 3 was applied. Further substrate material was turned back to the roller 1 and was moved in direction of the roller 1 at the pace  $L = 1/3W$ , and after that the layers 4, 5 and 6 were applied. The procedure was repeating, until the whole layer was completed.

Bilayer cladding was conducted in different conditions. First of all the first layer was created by means of gradual application of tracks with overlapping of  $2/3$ . Then the second layer was fabricated under the same regime, but with the tracks direction different than in the first case: at an angle  $0^\circ$ ,  $45^\circ$  and  $90^\circ$ . Penetration of the substrate was similar in all cases. Also the samples have the same iron content in the coating and equal microhardness but if the direction of the second cladding layer at an angle of  $0^\circ$ , this dependence is more homogeneous.

The results of the research demonstrated, that alteration of the laser radiation power influences most of all the width and the depth of the cladding track, but rate of the powder feed – on the depth of melt-through for substrate material. In the process of fabrication one layer coating overlapping rate of  $2/3$  showed the least grade of intermixture and more even melt-through of substrate material compared with coefficients  $1/3$  and  $1/2$ . According to the results of the thermal fields research at the distance of 5 mm from the driven roller substrate temperature falls significantly. In the layer, which was applied in respect with thermal fields, intermixture of substrate material and coating appeared to be minimal, due to less heating. Bilayer coating was created with different directions of the second layer ( $0^\circ$ ,  $45^\circ$  and  $90^\circ$ ) and overlapping rate of  $2/3$ . Distribution of microhardness at cross-cutting is more uniform in the case of parallel application of layers.

## Structural, electrical, and optical properties of the SnO<sub>2</sub>:Sb films prepared on inorganic and flexible organic substrate by the pulsed laser deposition method

L.S. Parshina<sup>1</sup>, O.A. Novodvorsky<sup>1</sup>, O.D. Khramova<sup>1</sup>, I.A. Petukhov<sup>2</sup>, F.N. Putilin<sup>2</sup>,  
V.A. Mikhalevskiy<sup>1</sup>, A.V. Shorokhova<sup>1</sup>

1- Institute on Laser and Information Technologies of RAS, 140700, Shatura, Russia

2 - M.V. Lomonosov Moscow State University, Faculty of chemistry, 119991 Moscow, Russia

ParshinaLiubov@mail.ru

Thin films of transparent conducting oxide (TCO) have been studied for many years because of their importance in various fields, such as solar cells, gas sensors, optoelectronic devices, heat mirrors and flat panel displays [1]. The films of SnO<sub>2</sub>:Sb (ATO), which have the greatest thermal and chemical stability among TCO films, attract special attention of researchers. They possess the good mechanical durability, high conductivity and are transparent in the visible range. Besides, they are cheap. In general, glass is the most used material as substrates for synthesis of the ATO films. However, for future development in flexible devices, e.g. liquid-crystal displays with a touch sensitive overlay, glass is limited by its intrinsic inflexibility, thickness, and weight characteristics [2]. Flexible organic substrates are necessary for plastic electronics and flexible displays. High temperature technological processes are unsuitable for such substrates. Therefore synthesis of high-quality ATO films at low temperatures of a substrate is quite an actual task [3].

In this work at low temperatures of a substrate, up to room temperature, the high-conductivity transparent in the visible range SnO<sub>2</sub>:Sb thin films (Sb - 2 at. %) have been produced by the droplet-free pulsed laser deposition (PLD) method on quartz substrates and flexible organic substrates from polyethyleneterephthalate (PET), with varying deposition parameters such as energy density on a target and oxygen partial pressure during deposition. Structural, optical and electric researches of the received films were conducted. XRD analysis indicated that the films grown at low temperatures (25-200 °C) were amorphous. Films were exposed to post-growth annealing by laser radiation with the wavelength of 248 nm for the purpose of their fullest crystallization. The optimum power density and a radiation dose providing the maximum increase in crystallization of the films without damage of the substrate was determined. The optical transmittance spectra of the SnO<sub>2</sub>:Sb films were showed that the films possessed a high transparent in the visible range from 400 nm to 700 nm. The SnO<sub>2</sub>:Sb films minimum resistivity of  $1,2 \cdot 10^{-3}$  Ohm·cm was reached on inorganic substrates. On PET organic substrates it made  $6,5 \cdot 10^{-3}$  Ohm·cm without the post-growth laser annealing.

This work has been supported by grants RFBR № 14-07-00408, 14-07-00688, 14-47-03605, 15-38-20369, 15-29-01171, 15-07-04142, 15-07-03331, 15-07-03580.

[1] B. Yoo, K. Kim, S. H. Lee, W. M. Kim, and N. G. Park: Sol. Energy Mater. Sol. Cells, ITO/ATO/TiO<sub>2</sub> triple-layered transparent conducting substrates for dye-sensitized solar cells vol. 92, pp. 873-877, (2008).

[2] W. M. Cranton, S. L. Wilson, R. Ranson, et. al., Excimer laser processing of inkjet-printed and sputter-deposited transparent conducting SnO<sub>2</sub>:Sb for flexible electronics, Thin Solid Films, vol. 515, pp. 8534-8538, (2007).

[3] S. U. Lee, J.-H. Boo, and B. Hong, Structural, electrical, and optical properties of SnO<sub>2</sub>:Sb films prepared on flexible substrate at room temperature, Japanese Journal of Applied Physics, vol. 50, pp. 01AB10 -1-01AB10 -5, (2011).

# **Diffusion-strain coupling and dispersion of surface waves in anisotropic laser-excited solids**

**F.Kh. Mirzade**

Institute on Laser and Information Technologies, Russian Academy of Sciences, 140700,  
Moscow, Russia

**E-mail: fmirzade@rambler.ru**

## **Abstract**

The boundary value problem in elasticity theory concerning the propagation behavior of harmonic waves and vibrations on the surface of the anisotropic laser-excited crystalline solids with atomic defect generation is considered theoretically. Coupled dynamical diffusion-deformation interaction model is employed to study this problem. The complex frequency equations of surface waves for transversely isotropic solids are derived and discussed. The three motions, namely, longitudinal, transverse, and diffusion of the medium are found to be dispersive and coupled with each other due to the defect concentration changes and anisotropic effects. The phase velocity and attenuation (amplification) of the surface waves get modified due-to the defect-strain coupling and anisotropic effects, and are also influenced by the defect relaxation time. In general, the frequency equation has solutions describing qualitatively different types of surface instability: a) if the viscosity is taken into account the dispersion equation describes laser excitation of acoustical waves (instability of the amplitude of acoustic waves); b) a softening of frequencies of surface acoustic waves (instability of frequencies); c) generation of ordered static micro-sized structures. Numerical calculations and graphs are presented in the case of Rayleigh waves. Relevant results of previous investigations are deduced as special and limiting cases.

## Structural and optical properties of silicon nanostructures obtained via laser ablation in gases

**F.V. Kashaev<sup>1</sup>, T.P. Kaminskaya<sup>1</sup>, P.A. Perminov<sup>2</sup>, L.A. Golovan<sup>1</sup>, S.V. Zaboltnov<sup>1</sup>**

<sup>1</sup>*Department of Physics, M.V. Lomonosov Moscow State University, 119991, Moscow, Russia*

<sup>2</sup>*NRC 'Kurchatov Institute', 123182, Moscow, Russia*

*E-mail: [kashaev.fedor@gmail.com](mailto:kashaev.fedor@gmail.com)*

One of the most promising methods for producing nanostructures is a laser ablation of the solid surface. Among advantages of the laser ablation technique one could mention low content of undesired impurities and possibility of nanoparticle formation of various materials [1]. The great interest of researchers around the world to the formation of silicon nanoparticles is due to their variety of possible applications in optoelectronics, photonics and biomedicine. In particular, the electronic properties of silicon nanoparticles of small size (less than 5 nm) allows us to use them as photoluminescent labels for photodynamic therapy and diagnosis [2, 3].

This paper presents the results of experiments on the nanoparticle formation as a result of laser ablation of crystalline silicon in various gases and study of influence of the gas pressure on structural, electronic, and optical properties of the nanoparticles. During the experiment, the surface of crystalline silicon was irradiated with Cr:forsterite femtosecond laser (1250 nm, 180 fs, 1 mJ, 10 Hz) pulses in helium, nitrogen and argon at room temperature.

The nanostructure sizes are shown to depend on the surrounding gas pressure and composition. In all gases in the pressure range 50 to 700 mbar average nanoparticle size and their dispersion decreases with increasing pressure. The concentration of particles with diameter up to 6 nm is maximum at irradiation in helium at pressures of 500-700 mbar (Fig. 1).

Raman scattering measurements evidence that the formed silicon nanoparticles are crystalline, whereas amorphous phase was detected in the samples obtained at low gas pressures.

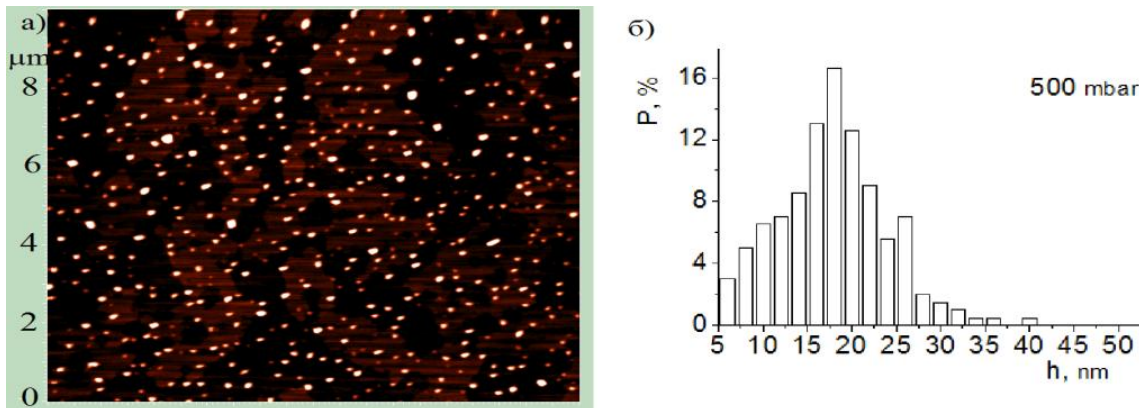


**Figure 1** AFM image of the silicon nanoparticles formed by means of the laser ablation in helium at 500 mbar (a) and particle size distribution (b)

This work was supported by RFBR grants nos. 14-22-0186 and 15-32-20227.

### References:

- [1]. J. Bonse, S. Baudach, J. Krüger, W. Kautek, M. Lenzner., Femtosecond laser ablation of silicon-modification thresholds and morphology, *Appl. Phys.*, vol. 74, pp. 19-25, (2002).
- [2]. D. Riabinina, C. Durand, F. Rosei, M. Chaker, Luminescent silicon nanostructures synthesized by laser ablation, *Physica status solid*, vol. 204, pp. 1623 – 1638, (2007).
- [3] Jusenas P., Chen W., Sun Ya-Ping, et al. Quantum dots and nanoparticles for photodynamic and radiation therapies of cancer., *Adv. Drug Delivery Rev.*, vol. 60, pp. 1600. - 1614, (2008).

# Laser Cutting and Drilling of Sandwich Structures “Pyrolytic Graphite - Pyrolytic Boron Nitride - Pyrolytic Graphite”

**T. Sokolova<sup>1</sup>, E. Surmenko<sup>1</sup>, V. Shesterkin<sup>2</sup>, D. Bessonov<sup>1</sup>**

1- Saratov State Technical University named after Yu.A. Gagarin, 77 Polytechnicheskaya st., 410054, Saratov, Russia

2- JSC “SPE “Almaz”, 1 Panfilova st., 410033, Saratov, Russia  
sokolova@pribor-t.ru

X-ray analysis and optical microscopy in polarized light show that laser cutting of sandwich structures “pyrolytic graphite - pyrolytic boron nitride - pyrolytic graphite” leads to internal stresses in treated material. Internal stresses look like concentric periodic rings from the center of the laser beam focus [1] (Figure 1). Rings appear on the front surface and on the bottom side of the structure. These areas can damage the workpiece. The value of internal residual stresses must be reduced by optimizing mode laser treatment.

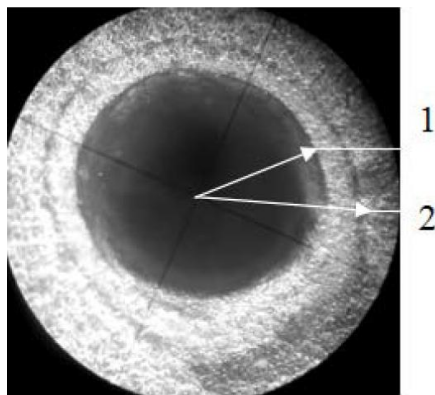


Figure 1 Frontal surface of the workpiece after laser drilling,  $\tau=4$  ms: 1 – first ring , 2 – second ring

The set-ups based on CW and Q-switched YAG-lasers with a pulse duration 7 ns - 4 ms were used in experiment. The dependence of the number of rings and their width on the pulse duration has a threshold nature: with decreasing pulse duration below 70 ns, the width of the rings is sharply reduced, the amount is reduced to zero (in power density range  $10^6 - 10^7$  W / cm<sup>2</sup>).

Processing mode can be optimized using the criterion characterizing the connection between the parameters of the laser (pulse repetition rate  $f$  and pulse duration  $\tau$ , spot diameter  $d$ ) and the thickness of the workpiece  $h$ :

$$K = \frac{f \cdot \tau \cdot d}{h}.$$

The value of the criterion is chosen from the ratio of  $7 \cdot 10^{-5} \leq K \leq 12 \cdot 10^{-5}$ .

**Acknowledgements:** The work was implemented on the equipment of VCCU “Laser & Optical Technologies”.

[1] T. N. Sokolova, O. A. Trofimova, Pyrographite grids of EHF electrovacuum devices and formation of their structures by laser precise treatment, Vacuum Science and Technics, N3, 227-230 (2006).

## Control of phase composition in the cadmium sulphide thin films for solar cells applications

**D.A. Zuev<sup>1</sup>, I.A. Petukhov<sup>2</sup>, O.A. Novodvorsky<sup>1</sup>, A.V. Shorokhova<sup>1</sup>,  
O.D. Khramova<sup>1</sup>, F.N. Putilin<sup>2</sup>, V.F. Kozlovskii<sup>2</sup>,  
M.N. Rumyantseva<sup>2</sup>, A.M. Gaskov<sup>2</sup>**

*1- ILIT RAS, 1 Syvatoozerskaya St., 140700 Shatura, Moscow Region, Russia  
2- MSU, Faculty of Chemistry, Russia, 119991, Moscow 1, GSP-1, 1-3 Leninskiye Gory*

*zuewda@yandex.ru*

The cadmium sulfide (CdS) is used as a wide-band "window" layer in the thin-film solar cells based on the CdTe and Cu (In, Ga) Se<sub>2</sub> materials. The intensive studies on the synthesis and characterization of CdS properties are conducted to improve the efficiency of the solar cells. This work is devoted to the study of the crystalline phase formation in the CdS thin films produced by the pulsed laser deposition (PLD) method.

The possibility of the hexagonal and cubic phases content control in the composition of the CdS thin films was studied. The analysis of dependences of the phase composition, microstructure and optical properties of the CdS thin films on the PLD process parameters was conducted. It was found that all investigated CdS films are composed of the mixture of the two phases – cubic and hexagonal. This effect was theoretically substantiated in [1] and experimentally observed in a number of papers [2-3]. We have shown that the phase composition of the CdS films affected by the substrate type, substrate temperature and laser energy density on the target [4]. It was established that the relative content of the hexagonal and cubic phases in the composition of the CdS thin films can be controlled by the PLD process parameters. We have also demonstrated that the photosensitivity of the samples depends on the phase composition of CdS the thin films.

The obtained results lay the groundwork for the research of the phase composition influence of the CdS thin films on the photovoltaic properties of the thin-film solar cells based on the CdTe and Cu (In, Ga)Se<sub>2</sub> materials.

### Acknowledgements.

The work was supported by the RFBR research grants:

15-07-03331\_a, 15-07-03580\_a, 15-07-04142\_a, 14-07-00408\_a, 14-07-00688\_a, 14-47-03605, 15-38-20369\_mol\_a\_ved, 15-29-01171\_ofi\_m

### References.

- [1] A.S. Vorokh, A.A. Rempel, Atomic structure of cadmium sulfide nanoparticles, *Physics of the Solid State*, vol. 49, iss. 1, pp. 148-153, (2007)
- [2] M. Kostoglou, N. Andritsos, A.J. Karabelas, Incipient CdS thin film formation, *Journal of Colloid and Interface Science*. vol. 263, pp. 177-189, (2003)
- [3] A.A. Ziabari, F.E.Ghods, Growth, characterization and studying of sol-gel derived CdS nanocrystalline thin films incorporated in polyethyleneglycol: Effects of post-heat treatment, *Solar Energy Materials & Solar Cells*, vol. 105, pp. 249-262, (2012)
- [4] D.A. Zuev, I.A. Petuhov, A.V. Shorokhova, O.A. Novodvorsky, A.A. Lotin, L.S. Parshina, O.D. Khramova, E.A. Cherebilo, V.A. Mikhalevsky, Ph.N. Putilin, V.F. Kozlovski, V.K. Ivanov, M.N. Rumyantseva, A.M. Gaskov, Control of the CdS films phase composition for thin film solar cells, *Bulletin of the Russian Academy of Sciences: Physics*, In Press.

## Developing of $p$ -(InSb+MnSb)/ $n$ -InSb magnetic semiconductor heterojunction using PLD

**V. A. Mikhalevsky<sup>1</sup>, L. S. Parshina<sup>1</sup>, O. D. Khramova<sup>1</sup>, A. N. Aronov<sup>2</sup>, S. F. Marenkin<sup>2</sup>, B. A. Aronzon<sup>3</sup>, O. A. Novodvorski<sup>1</sup>**

1- The Institute on Laser and Information Technologies of the Russian Academy of Sciences, 1 Svyatoozerskaya St., Moscow Region, Russia, 140700

2- Kurnakov Institute of general and inorganic chemistry of the Russian Academy of Sciences, 31 Leninsky prospect, Moscow, Russia, 119991

3- The P.N. Lebedev Physical Institute of the Russian Academy of Sciences, 53 Leninsky Prospekt, Moscow, Russia, 119991

Email address: uhr@inbox.ru

It is of great interest for spintronic applications such as spin valves, high sensitive magnetic sensors and etc. to produce diode structures providing spin injection. Curie temperature is the main characteristic of the materials used. InSb+MnSb ferromagnetic semiconductors have Curie temperature about 600 K [1-3].

The films from targets of InSb+MnSb alloy composite with the content of 3,5%, 5%, 10% MnSb have been received by the pulsed laser deposition (PLD) on  $c$  - sapphire substrates and have been investigated.

The composition, microstructure and thickness of the films were studied by XRD, SEM and AFM. Conductivity, concentration and carrier mobility was measured by the Hall. The films have  $p$ -type conductivity. The best samples have the carrier concentration  $2,9 \cdot 10^{18} \text{ cm}^{-3}$ , the mobility of  $10,7 \text{ cm}^2/(\text{V}\cdot\text{s})$  and resistivity  $2 \cdot 10^{-1} \text{ Ohm}\cdot\text{cm}$ . It was observed that the concentration, mobility of the charge carriers and resistance depend on the film deposition temperature and the energy density on the target. The SEM analysis showed the presence of a uniform distribution of the elements In, Sb and Mn on the surface of the film. According to XRD, the content of these elements corresponded to the composition of the original target. It was found that the films include MnSb ferromagnetic clusters of 4 nm size.

Heterojunction  $p$ -(InSb+MnSb)/ $n$ -InSb was formed by PLD on the single-crystalline  $n$ -type InSb substrate. The InSb+MnSb layer contains MnSb of 3,5%. The I-V characteristics of the diode measured at room temperature under magnetic field  $B=0 \text{ T}$  and different directions of the field  $B=0,15 \text{ T}$  (Fig. 1) show very high field sensitivity. The current at zero field is 0,35 A. The current at magnetic field of 0,15 T perpendicular to the surface of the junction is 0,04 A. The current was measured at constant voltage of 1 V.

This work has been supported by grants RFBR № 15-29-01171, 14-47-03605, 15-07-04142, 15-07-03580, 14-03-90004, 14-08-00688.

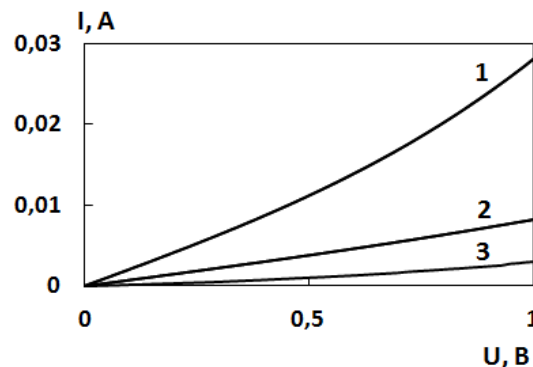


Fig. 1. I-V characteristics of the diode, measured at temperature of 300 K: 1 -  $B = 0 \text{ T}$ ; 2 -  $B = 0,15 \text{ T}$ , the field is parallel to the surface of heterojunction; 3 -  $B = 0,15 \text{ T}$ , the field is perpendicular to the surface of heterojunction.

[1] A.V. Kochura, B.A. Aronzon, K.G. Lisunov, et al., J. Appl. Phys. **113**, 083905 (2013).

[2] N. D. Parashar, N. Rangaraju, V. K. Lazarov, et al., Phys. Rev. B **81**, 115321 (2010).

[3] J. A. Peters, N. Rangaraju, C. Feeser et al, Appl. Phys. Lett. **98**, 193506 (2011).

## Transport and magnetic properties of $\text{Si}_{1-x}\text{Mn}_x$ layers produced by the pulsed laser deposition method

**A.V. Shorokhova<sup>1</sup>, O.A. Novodvorskii<sup>1</sup>, V.V. Rylkov<sup>2</sup>, D.A. Zuev<sup>1</sup>,  
S.N. Nikolaev<sup>2</sup>, K.Yu. Chernoglazov<sup>2</sup>**

*1-Institute on Laser and Information Technologies RAS, 140700 Shatura, Moscow Region, Russia,*

*2-National Research Centre "Kurchatov Institute", 123182 Moscow, Russia*

*e-mail: [av.shor@yandex.ru](mailto:av.shor@yandex.ru)*

In recent times, considerable attention is paid to the creation and research of properties of magnetic semiconductor systems based on Si, because such materials are attractive for creating elements of spintronics, which could be easily integrated into existing microelectronic technology. The aim of this work was to create and study the magnetic and transport properties of  $\text{Si}_{1-x}\text{Mn}_x$  with  $x \approx 0.5$  films. Thin films of SiMn were produced by the pulsed laser deposition (PLD) method [1] onto the single crystalline  $\text{Al}_2\text{O}_3$  substrates at 340 °C. The method allows to completely prevent the drops deposition onto the growing film, the presence of which is a major factor in reducing their quality when using PLD

The composition of the samples was investigated by X-ray photoelectron spectroscopy (XPS). Structural features of the films were studied by X-ray diffraction, which revealed the presence of a polycrystalline phase SiMn. Transport and magnetic properties of  $\text{Si}_{1-x}\text{Mn}_x$  layers were studied in the temperature range 5-400K in magnetic fields up to 2 Tesla. It has been found that the defects with local magnetic moments (LMM) are formed with a slight excess content Mn ( $x \leq 0.55$ ) [2]. Moreover, the depletion of Mn films on the value  $\Delta x \approx -0.05$  leads to almost complete suppression of FM order. In the sample with a slight excess of Mn ( $x \approx 0.52$ ), the concentration of charge carriers (holes) in the films decreases more than an order of magnitude, and the mobility of charge carriers increases in comparison with the single-crystal SiMn.

The work was partly supported by the RFBR (grant Nos. 15-07-01170, 15-07-01171, 15-07-04142, 14-07-91332, 14-07-00688, 14-47-03605),

[1]. O.A. Novodvorskii, V. Ya. Panchenko. Modern technology of pulsed laser deposition for the synthesis of new materials and structures for micro - and nanophotonics. «Modern laser-information technologies». Collective monograph under the editorship of acad. V. Ya. Panchenko and prof F.V. Lebedev. OOO «Intercontact Nauka», Moscow, accepted for publication in 2014

[2] V.V. Rylkov, A.S. Bugaev, O.A. Novodvorskii, V.V. Tugushev, E.T. Kulatov, A.V. Zenkevich, A.S. Semisalova, S.N. Nikolaev, A.S. Vedenev, A.V. Shorokhova, D.V. Aver'yanov, K.Yu. Chernoglazov, E.A. Gan'shina, A.B. Granovsky, Y. Wang, V.Ya. Panchenko, S. Zhou, High-temperature ferromagnetism of  $\text{Si}_{1-x}\text{Mn}_x$  ( $x \approx 0.52-0.55$ ) alloys. Journal of Magnetism and Magnetic Materials, article is accepted in the press.

# Non-thermal laser patterning of functional thin-films

M. Ehrhardt, P. Lorenz, L. Bayer, K. Zimmer

1- Leibniz-Institut für Oberflächenmodifizierung e. V., Permoserstraße 15, 04318 Leipzig, Germany

klaus.zimmer@iom-leipzig.de

Laser scribing of thin-film especially for flexible electronic application is of great interest. However the damage-free micro structuring of thermal sensitive thin films like e.g. copper-indium-gallium-diselenide (CIGS) thin film solar cells is still challenging. A commonly used approach to reduce the thermal load from the laser radiation onto the sensitive thin film is the usage of ultrashort laser pulse. However, also by the usage of ultrashort laser pulses undesired material modifications could not be prevent completely which can influence the functionality of the thin film. A pronounced example for these undesired thermal material modifications by using ultrashort laser pulses can be found by patterning of CIGS thin film solar cells [1, 2]. In figure 1 (left) a scanning electron microscope (SEM) image of typical laser scribed CIGS sample performed with a picosecond laser pulses ( $t_{\text{pulse}}=10$  ps,  $\lambda = 1064$  nm) is shown. In this image the thermal effects like molten edges can be seen clearly. These thermal modifications of the CIGS material can be reduced by optimising the laser parameter for the scribing process but cannot exclude totally. To overcome these limitations new laser patterning approaches are required.

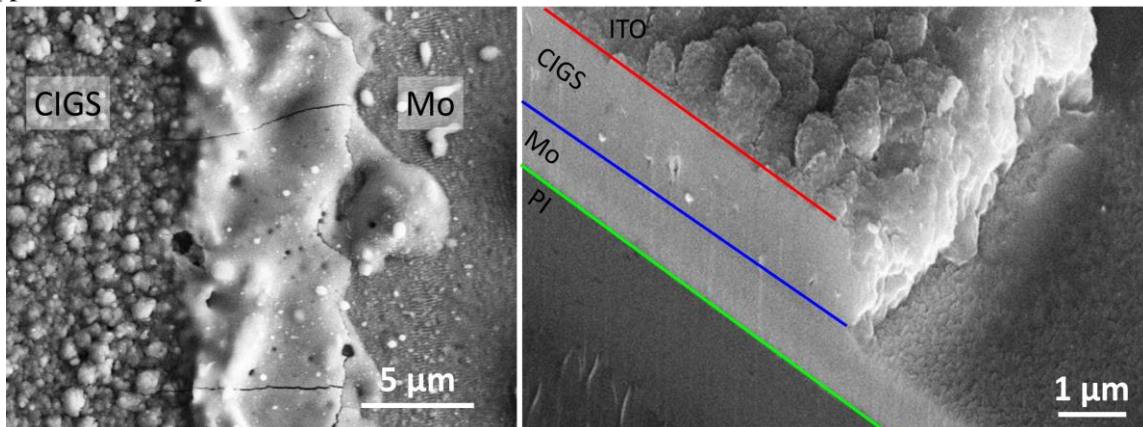


Figure 1: SEM images of edges of the scribed CIGS thin film solar cell. (Left) front side scribing with picosecond laser pulses (Right) patterning with back side approach using nanosecond laser pulses.

In the present study a non-thermal laser micro structuring process of functional thin films is shown. In contrast to the usually used direct irradiation of the thin film to ablate the material here the material removal is achieved by laser irradiation of carrier foils which mechanical support the reverse side of the functional thin film. Exemplary the patterning of CIGS thin film solar cells deposited on a polyimide carrier foil will be shown. The experiments were performed with a KrF Excimer laser. The resultant pattern dependent on the laser parameters (laser fluence, number of laser pulses, laser beam diameter) were studied by SEM and optical microscope (see figure 1 right). The obtain results were analysed with regard to the accuracy of the resultant structures as well as to the electrical properties. For the improving of the physical understanding the laser-induced delamination effect was measured by shadowgraph experiments [3]. This measurement allows the identification of the time-dependent delamination of the CIGS layer dependent on the laser parameters, respectively.

[1] A. Wehrmann, Analysis of laser scribes at CIGS thin-film solar cells by localized electrical and optical measurements, *Optics and Laser Technology*, 44(6), pp. 1753-1757, (2012).

[2] X. Wang, In-process measuring of the electrical shunt resistance of laser-scribed thin-film stacks by nested circular scribes, *Review of Scientific Instruments*, 84(10), pp. 1753-1757, (2013).

[3] P. Lorenz, Shadowgraph studies of laser-assisted non-thermal structuring of thin layers on flexible substrates by shock-wave-induced delamination processes, *Applied Surface Science*, 336, pp. 43-47, 2015.

## PLD of perspective inorganic thin-film materials for the creation of memristors and spin valves

O.A. Novodvorsky, V.A. Mikhalevskiy, A.A.Lotin, A.V.Shorokhova,  
L.S.Parshina, D.A. Zuev

*Institute on Laser and Information Technologies of RAS, 140700 Shatura, Moscow Region, Russia*

*e-mail: onov@mail.ru*

At the present time the spin and memristive technologies are actively developed for creation of the devices modeling chains on neurons and synapses [1,2]. Recently there were prototypes of the devices realizing possibility of memristors application as the switch, an memory element and components of logical elements. [3]. Computer modeling of logical operations in such structures showed that on the basis of krossbar with memristors it is possible to construct the full-fledged processor [4].

Thin films of metals, semiconductors and dielectrics are necessary for creation of spin valves and memristors. In work results of researches on receiving by the PLD method of the  $\text{TiO}_2$ ,  $\text{VO}_2$ ,  $\text{Si}_{1-x}\text{Mn}_x$  ( $x \sim 0.5$ ) thin films from 1 nm to 200 nm thick on single-crystal and metal substrates are presented. Influence of energy density on targets on films characteristics was established. The analysis of the received films confirmed with methods of a x-ray scatterometry of high resolution high structural perfection and showed that the roughness of films doesn't exceed 1 nm that is very important at creation of memristors on their basis. Influence of the  $\text{TiO}_2$ ,  $\text{VO}_2$  films thickness on possibility of creation of the alloyed areas of the structures which are grown poor by oxygen for creation the memristive structure was established. For creation of spin valves magnetotransport properties of the  $\text{Si}_{1-x}\text{Mn}_x$  ( $x \sim 0.5$ ) films in the wide range of temperatures were investigated [5]. It was established that thin films of  $\text{Si}_{1-x}\text{Mn}_x$  with small excess of Mn possess the specific resistance typical for strongly degenerate semiconductors, and are perspective for creation of magnetic tunnel transitions on their basis. The received results are original and open prospects of use of these materials for creation of new backs - injection and the memristive structures.

The work was supported by the RFBR research grants: 15-07-03331, 15-07-03580, 15-07-04142, 14-07-00408, 14-07-00688, 14-47-03605, 15-38-20369, 15-29-01171, 15-32-50690, 14-03-9004.

[1] H. Choi et al., An electrically modifiable synapse array of resistive switching memory, *Nanotechnology*, vol. 34, № 20, p. 345201, (2009).

[2] X. Marti et. al., Room-temperature antiferromagnetic memory resistor, *Nature Materials*, vol. 13, p. 367, (2014).

[3] P.J. Kuekes, G.S. Snider, R.S. Williams, Crossbar nanocomputers, *Scientific American*, vol. 293, p. 72, (2005).

[4] J. Borghetti et al., Memristive switches enable stateful logic operations via material implication, *Nature letters*, vol. 464, p. 873, (2010).

[5] V.V. Rylkov, E.A. Gan'shina, O.A. Novodvorskiy et. al., Defect-induced high-temperature ferromagnetism in  $\text{Si}_{1-x}\text{Mn}_x$  ( $x = 0.52-0.55$ ) alloys, *Europhys. Lett.*, vol. 103, № 5, p. 57014, (2013).

## **Influence of annealing on the magnetization, structural and electrical properties of alloy films GaSb-MnSb, obtained by PLD**

**O.D. Khramova<sup>1</sup>, O.A. Novodvorsky<sup>1</sup>, A.V. Shorokhova<sup>1</sup>, L.S. Parshina<sup>1</sup>,  
V.A. Mikhalevskiy<sup>1</sup>, S.F. Marenkin<sup>2</sup>, I.V. Fedorchenko<sup>2</sup>, B.A. Aronzon<sup>3,4</sup>, A.B. Davydov<sup>3</sup>,  
Ju.M. Chesnokov<sup>3</sup>, A.L. Vasiliev<sup>3</sup>**

*1 Institute on Laser and Information Technologies of RAS, 140700 Shatura, Moscow Region, Russia*

*2 Institute of the general and inorganic chemistry of a name of N. S. Kurnakov of the Russian Academy of Sciences, 119991, Moscow, Leninsky Avenue, 31.*

*3 National Research Centre, Kurchatov Institute, 123182 Moscow, Russia*

*4 Prokhorov General Physics Institute, Russian Academy of Sciences, ul. Vavilova 38, Moscow, 119991 Russia*

*e-mail: onov@mail.ru*

The thin films of GaSb – MnSb were received by the method of pulse laser deposition (PLD) from the eutectic alloy of GaSb – MnSb (41 % of MnSb and 59% of GaSb). The single-crystal sapphire (0001) was used as substrates. The ablation of the target was carried out by the radiation of the second harmonica ( $\lambda = 532$  nanometers) Q-switched laser Nd<sup>3+</sup>YAG. The films of the thickness  $d = 80 - 130$  nanometers were received in vacuum ( $10^{-6}$  Torr) at the temperature of substrate from 50 to 350 °C. At deposition of films of GaSb-MnSb the separator of the deposited particles on speed was applied to avoid the hit of drops on the growing film. The roughness of samples doesn't exceed 6 nanometers by the results of AFM measurements, films are smooth and uniform. The received films show ferrimagnetism at the room temperature. The ferromagnetic state is shown as in magnetometric measurements, and in occurrence of anisotropic magnetoresistance and the abnormal Hall effect. The dependence of the electric properties of thin films of GaSb– MnSb on receiving temperature was investigated. The dependence of size of the magnetoresistance and the abnormal Hall effect on the charge carriers concentration was established.

The influence of annealing on electric, structural and magnetic properties of samples was analysed. Structural research of samples was accomplished in the translucent raster electronic microscope (PEM/PREM) of TITAN 80 - 300 (FEI, the USA) with the proofreader of a spherical aberration of a probe in the modes of a light and dark field. The analysis of structure of films was carried out according to images of high resolution with the subsequent transformation of Fourier of separate grains of a film. It is possible to conclude that annealing causes phase transition of the hexagonal phase GaSb:Mn to the cubic. After annealing in films the ferromagnetism at the room temperature remains, it was shown in a magnetic hysteresis, an anisotropic magnetoresistance and the abnormal Hall effect. The deposition temperature was lower, the magnetization of a film changes when annealing more strongly. At the small deposition temperatures (50-100 °C) annealing increases magnetization of saturation almost twice while at high deposition temperatures annealing practically doesn't change magnetic properties of a sample.

The work was supported by the RFBR research grants: 15-07-03331, 15-07-03580, 15-07-04142, 14-07-00408, 14-07-00688, 14-47-03605, 15-38-20369, 15-29-01171, 15-32-50690, 14-03-9004.

# Multiwavelength Laser Excitation Study of Silicon-Vacancy Color Center Emission Lineshape in Nanocrystalline Diamond Films

**L. Himics<sup>1</sup>, S. Tóth<sup>1</sup>, M. Veres<sup>1</sup>, P. Csikvári<sup>2</sup>, M. Koós<sup>1</sup>**

*1- Institute for Solid State Physics and Optics, Wigner Research Center for Physics, Hungarian Academy of Sciences, H-1525 Budapest, P.O. Box 49, Hungary*

*2- Department of Atomic Physics, Budapest University of Technology and Economics, H-1521 Budapest, Hungary*

*himics.laszlo@wigner.mta.hu*

The diversity of promising properties (low electron-phonon coupling, intensive and stable emission at room temperature, one photon emission) of nanodiamonds containing color centers is one of the major reasons inducing continuously increasing interest of many research groups and companies to this material [1]. Some exciting applications like solid state one photon source, biomarker for imaging and labeling or solid state qubit source were already demonstrated and realized with nanodiamond [2].

Among optically active defects studied in diamond the silicon-vacancy (SiV) center occupies a noble place due to its relatively narrow and intensive zero-phonon line (ZPL) and negligible electron-phonon coupling even at room temperature (RT) compared to other centers. The defect consists of a silicon atom and a vacancy in split configuration. The ZPL position of the center in bulk diamond is located at 738 nm (1.681 eV), while in nanocrystalline diamond films the position was observed in a quiet a wide range [3]. For most of the applications the peak position and emission line width are critical and need to be well-controlled, preferably during the formation process.

In this paper we report on multiwavelength laser excitation study of spectral lineshape of SiV center emission in nanocrystalline diamond films grown at different precursor gas ratio using CVD technique.

Nanocrystalline diamond films were deposited on silicon substrate from  $H_2/CH_4/Ar$  gas mixture using 1200 W microwave power and 650 °C substrate temperature. While the  $CH_4$  concentration in source gas mixture was constantly kept at 1 %, the Ar content was varied between 10-95 % to the detriment of  $H_2$  content. The pressure in the chamber was kept at 40 mbar.

The spectral lineshape characteristics of SiV center in the samples were investigated by photoluminescence (PL) spectroscopy, while the bonding structure and morphology of the films were examined with Raman spectroscopy and SEM, respectively. Raman and PL measurements were performed on the Renisaw 1000 spectrometer attached to a Leica microscope. The 488 nm line of an argon-ion laser and additional diode lasers were used as an excitation sources for PL and Raman measurements.

Our results show that the emission lineshape characteristics and intensities of SiV centers depend on the deposition parameters of the films. The residual internal stress, determined by Raman spectroscopy, increases with decreasing  $H_2$  content and this has an influence on the emission line position and width of SiV color center. Addition of Ar gas to the precursor gas mixture could be an effective tool to control the grain size of SiV center containing nanocrystals. Lowering of the average grain size of diamond films was observed with increasing Ar content.

[1] I. Aharonovich, A. D. Greentree, S. Prawer, *Diamond Photonics*, *Nature Photonics*, 5, 397–405, (2011)

[2] I. Aharonovich, S. Castelletto, D. Simpson, C. Su, A. Greentree, and S. Prawer, *Diamond-based single-photon emitters*, *Rep. Prog. Phys.* 74, 076501 (2011)

[3] E. Neu, D. Steinmetz, J. Riedrich-Möller, S. Gsell, M. Fischer, M. Schreck, C. Becher, *Single photon emission from silicon-vacancy colour centres in chemical vapour deposition nano-diamonds on iridium*, *New J. Phys.* 13, 025012, (2011)

## **Role of recombination processes during multipulse femtosecond irradiation of silicon**

**I.V. Guk, G.D. Shandybina, E.B. Yakovlev**

*ITMO University, 197101, Kronverkskiy Pr., 49, St. Petersburg, Russia*

*corchand@gmail.com*

The technology of microstructuring of semiconductor surfaces under femtosecond and picosecond laser pulses action developing rapidly. Depending on the characteristics of laser irradiation and material properties, ripples, ordered grained structures, microcones, oxide layers can be formed on the surface. In these regimes traditionally the technology of multipulse processing is used with different pulse repetition rates. Recombination processes can play important role in the final result of the process of femtosecond multipulse microstructuring.

Indeed, the heat of the surface may occur not only due to the heat exchange between electron gas and the lattice, but due to recombination processes. Wherein, for silicon two types of recombination are typical: Auger recombination and non-radiative recombination. Auger recombination decreases concentration of nonequilibrium carriers, without participating directly in the heating of the lattice, and due to non-radiative recombination additional heating of the lattice occurs, shifted in time relative to the heating by electron gas.

In the report the results of quantitative evaluations of the contribution of recombination processes in heat accumulation effect during multipulse femtosecond laser microstructuring of silicon surface are presented to discussion. In the calculations the quantitative-analytical method is used, in which the dynamics of electron processes and the heat of the lattice are modeled by quantitative method, and the cooling stage are described on the basis of analytical solution, which conducts thermophysical properties of the material and pulse repetition rate.

It is shown, that the role of Auger recombination during laser pulse action is insignificant, but its high rate can noticeably reduce concentration of nonequilibrium carriers after the end of laser pulse action. This reduces the contribution of nonradiative recombination in the heating of silicon before the next laser pulse.

The contribution of nonradiative recombination in the dynamics of maximum surface temperature of silicon surface is compared with the contribution in the heating, caused by the change of surface absorptivity from pulse to pulse, due to the evolution of surface structures. The increase of the role of nonradiative recombination with the increase of pulse repetition rate is shown.

## Invisible inks containing upconversion nanoparticles for anti-counterfeit applications

**V. Rocheva<sup>1</sup>, K. Mironova<sup>1,2</sup>, A. Generalova<sup>1,2</sup>, A. Nechaev<sup>1,3</sup>,  
V. Semchishen<sup>1</sup>, E. Khaydukov<sup>1</sup>**

1- Institute on Laser and Information Technologies Russian Academy of Sciences,  
1 Svyatoozerskaya St., 140700 Shatura Moscow, Russia

2- Shemyakin-Ovchinnikov Institute of Bioorganic Chemistry Russian Academy of Sciences,  
16/10 Miklukho-Maklaya, 117997 Moscow, Russia

3- Lomonosov Moscow University of Fine Chemical Technology,  
86 Prospect Vernadskogo, 119571 Moscow, Russia

*vrocheva@mail.ru*

Invisible biocompatible inks visualized under infrared irradiation for security printing applications were developed. For inks formation lanthanide-doped nanoparticles and water were used. Several ink compositions were created for color printing generating infrared, green and blue luminescence under 970-980 nm excitation. We synthesized monodisperse core@shell nanoparticles NaYF<sub>4</sub>:YbEr/YbTm@NaYF<sub>4</sub> with high upconversion efficiency (4-5%) by thermal decomposition route in the presence of oleic acid and octadecene. To produce stable water inks the surface of nanoparticles was modified by amphiphilic polymer PMAO. The hydrophilic nanoparticles were shown to be non-toxic by MTT assay on human fibroblast cells. The inks properties were characterized and optimized for a digital write on paper and plastics utilizing standard inkjet printer. Upconversion of the printed patterns under near infrared laser irradiation was observed and imaged. Stability and adhesion tests were performed to evaluate the mechanical stability of the upconverting inks on paper. Higher levels of security were achieved by printing upconverting inks based on optical multiplexing capability combinations of Ln<sup>3+</sup> nanoparticles. The developed technology is promising for fast, easy and low cost inkjet printing for anti-counterfeit and security application.

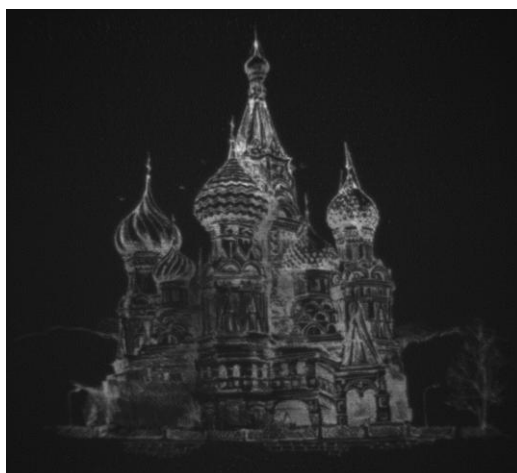


Fig. 1. Upconversion luminescence of the printed image under near infrared laser irradiation obtained by CCD.

The work was supported by RFBR grants 14-02-00875 and 14-29-07241.

# The study of phonon excitations in the crystal of ferroelectric semiconductors $\text{Sn}_2\text{P}_2\text{S}_6$ by time-resolved spectroscopy

K. Brekhov<sup>1</sup>, K. Grishunin<sup>1</sup>, D. Afanasev<sup>2</sup>, S. Semin<sup>1,2</sup>, N. Sherstyuk<sup>1</sup>, E. Mishina<sup>1</sup>, A. Kimel<sup>1,2</sup>

1- Moscow State University of Information Technologies, Radioengineering and Electronics (MIREA),  
Vernadsky ave. 78, Moscow, Russia

2- Radboud University, Comeniuslaan 4, 6525 HP Nijmegen, Netherlands

brekhov\_ka@mail.ru

During the last decade ultrafast magnetism was transformed from the exciting scientific area to industrial applications [1-2]. Ultrafast manipulation of spins can be obtained by femtosecond lasers via opto-magnetic phenomenon, in which polarized light affects magnetism via the inverse Faraday or Cotton-Mouton effects. The control of spins by light is one of the promising approaches to the problem of ultrafast data manipulation, since a laser pulse is one of the shortest ever man-made events.

Can light manipulate dielectric polarization? Positive answer provides wide class of materials and effect for new era for all-optical informational technologies.

The problem arises from the fact that light easily control electrons (spins), while ferroelectricity is associated with ions. For switching of magnetism, re(orientation) of spin by magnetic field is required, while for switching of polarization, displacement of ions by electric field is required. The former can be achieved in two ways: firstly by direct transfer of momentum from circular polarized light to electron, and secondly by exciting coherent magnons due to inverse Cotton-Moutone effect. For the latter no direct mechanism exists, but analogously to the second mechanism zero coherent phonon (soft mode) excited by inverse Cotton-Moutone effect may result in coherent displacement of sublattice in a crystal, which is equivalent to displacement of ions under electric field application. In ferroelectrics–semiconductors additional channel for electron control appears during light excitation: material goes to electret state which influences ferroelectric polarization [3].

In this paper we present the results of ultrafast optical characterization and coherent phonon excitation in ferroelectric-semiconductor  $\text{Sn}_2\text{P}_2\text{S}_6$  (SPS). Conditions are found and parameters are measured for acoustic and optical phonons.

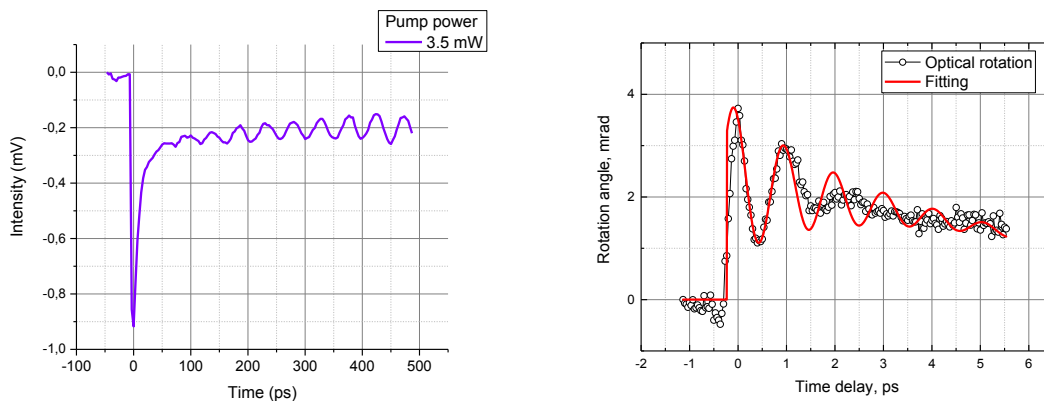


Fig. 1. Acoustic (a) and optical (b) phonons; frequency of optical phonon via temperature in SPS crystal.

Acoustic phonon (Fig. 1 a) frequency equals to 23 GHz and does not depend on temperature. Optical phonon (Fig. 1 c) frequency changes from 0.89 to 0.75 THz when passing through a phase transition (Fig. 1 b). It shows clear polarization dependence and can be attributed to the zero (soft) mode. Interplay between excitation power and external temperature gives and instrument for polarization change.

[1] J. Stöhr, H. C. Siegmann, Magnetism: from fundamentals to nanoscale dynamics (Springer, Berlin, 2006).

[2] AnQuan Jiang, ZhiHui Chen, Wen Yuan Hui, Dongping Wu and James F. Scott, Adv. Func. Materials 22, 2148 (2012)

[3] V. M. Fridkin Ferroelectrics semiconductors. (Consultant Bureau, New-York and London, 1980).

# First order phase transitions during laser ablation in the framework of continual and molecular dynamic descriptions

**V.I.Mazhukin<sup>1,3</sup>, A.A.Samokhin<sup>2</sup>, A.V.Shapranov<sup>1,3</sup>, P.A.Pivovarov<sup>2</sup>**

1- Keldysh Institute of Applied Mathematics, RAS, Myuskaia sq. 4, Moscow 125047, Russia

2- A.M. Prokhorov General Physics Institute, RAS, Vavilov str.38, Moscow 119990, Russia

3- National Research Nuclear University MPhI (Moscow Engineering Physics Institute), Moscow, Russia

[vim@modhef.ru](mailto:vim@modhef.ru)

Fast heating of condensed matters results in various phase transitions which can be dealt with different methods including continual and molecular dynamic (MD) approaches. The continual description using multiphase equation of state is not complete because some additional information is needed about non-equilibrium features of the first order phase transitions. This information concerns, in particular, boundary conditions at the moving phase fronts in the Stefan-like continual model of melting and vaporization processes as well as superheating limits of the considered metastable states [1]. Such questions do not arise in MD simulations which give more complete picture of the non-equilibrium phase transitions.

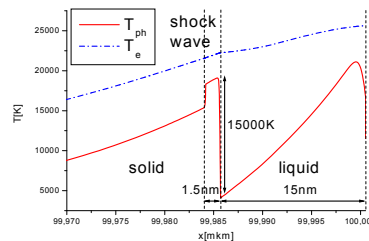


Fig 1. The spatial distribution of the temperatures  $T_e$  and  $T_{ph}$ , obtained from the continuum model.  $G = G_0 \exp(-(t/\tau)^2)$ ,  $G_0 = 3.95 \times 10^{12} \text{ W/cm}^2$ ,  $\tau_L = 100 \text{ fs}$ ,  $\lambda = 0.8 \mu\text{m}$ ,  $t = +2 \text{ ps}$ .

In the case of liquid-vapor phase transition the question arises about appearance of explosive boiling in metals irradiated with intense laser pulses is not evident beforehand because of high values of thermal conductivity and small radiation penetration length. For this reason in some theoretical descriptions of the explosive boiling process in irradiated metals (see [2] and cited there earlier papers) it is declared that in such a case subsurface superheating is impossible. However, our recent results [3,4] obtained with the help of molecular-dynamic modeling show that it is the subsurface superheating which gives rise to metal explosive boiling during nanosecond laser pulse irradiation as it was supposed in the earlier paper [5].

According to Van der Waals equation of state constant pressure heat capacity diverges and changes its sign at spinodal line. In real physical systems no such well defined line exists because of growing unstable thermodynamical fluctuations. Our estimations based on the results MD calculations [6] shows that heat conduction coefficient grows near superheating temperature limit. Spinodal and critical point manifestations in strongly non-equilibrium conditions of laser ablation need more experimental and theoretical investigations.

This work was partially supported by Russian Fund of Basic Research grants № 13-02-01129, № 13-07-00597, № 15-07 – 05025

[1] A.V.Mazhukin, V.I.Mazhukin, M.M.Demin. Modeling of femtosecond laser ablation of Al film by laser pulses. *Applied Surface Science*. 2011, № 257, pp. 5443–5446.

[2] M. Q. Jiang, Y. P. Wei, G. Wilde, L. H. Dai. “Explosive boiling of a metallic glass superheated by nanosecond pulse laser ablation”. *Appl. Phys. Lett.* 106, 021904 (1-6), (2015).

[3] V.I.Mazhukin, A.A. Samokhin, M.M. Demin, A.V.Shapranov. *Quantum Electronics*. 44, No. 4, 283–285, (2014).

[4] V.I.Mazhukin, A.A. Samokhin, M.M.Demin, A.V.Shapranov. *Mathem. Montisnigri*. 29, 68 - 90, (2014).

[5] A.A.Samokhin, Some aspects of the intense evaporation of condensed media by laser radiation, *Soviet Journal of Quantum Electronics*, vol.4, №9, pp.1144–1145 (1975)

[6] V.I. Mazhukin, A.V. Shapranov, A.A. Samokhin, A.Yu. Ivochkin, *Mathematical modeling of non-equilibrium phase transition in rapidly heated thin liquid film*, *Mathematica Montisnigri*, vol. 27, pp.65-90 (2013).

# Investigation of main mechanisms of disintegration of thin Al film by a nanosecond Gaussian laser pulse

**A.V.Mazhukin<sup>1,3</sup>, V.I.Mazhukin<sup>1,3</sup>, A.A.Samokhin<sup>2</sup>, M.M.Demin<sup>1</sup>, A.V.Shapranov<sup>1,3</sup>**

1- Keldysh Institute of Applied Mathematics, RAS, Myuskaia sq. 4, Moscow 125047, Russia

2- A.M. Prokhorov General Physics Institute, RAS, Vavilov str.38, Moscow 119990, Russia

3- National Research Nuclear University MPhI (Moscow Engineering Physics Institute), Moscow, Russia

[vim@modhef.ru](mailto:vim@modhef.ru)

Molecular dynamics simulations performed on the basis of a hybrid continuum - atomistic model [1] was used to study the mechanisms of ablation of metal (Al) film at an unsteady nanosecond laser action. For the molecular dynamics simulation was used aluminum foil with dimensions of the coordinates  $X \times Y \times Z$ , respectively  $200 \times 5 \times 5$  nm with total number of 284,000 atoms and the initial temperature of  $300^\circ \text{K}$ . Along the axes  $y, z$  were used periodic boundary conditions. Temporal form of laser pulse was chosen as a Gaussian curve. Among the studied mechanisms: surface evaporation, mechanical spallation, explosive boiling, spinodal decomposition and supercritical disintegration. The boundaries of different mechanisms of ablation in the variables of length-fluence ( $\tau \times F$ ) and duration-intensity ( $\tau \times G$ ) have been determined. Such ablation modes of aluminum film under the influence of continuous laser radiation were considered in [2,3]. Taking into account of the effects of nonstationarity showed the presence of several mechanisms of ablation transforming into each other during a single pulse, Fig.1.

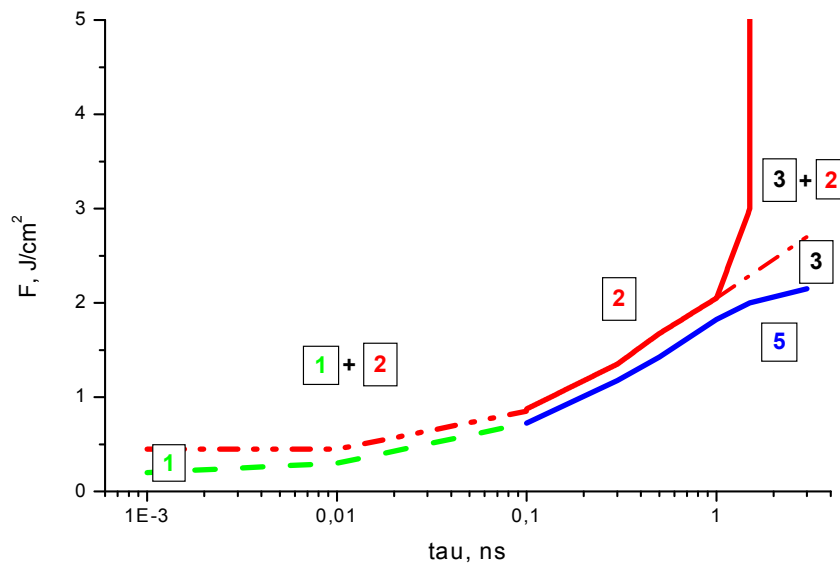


Fig.1. The boundaries of regions of different modes of ablation: 1 -only mechanical spallation; 2 - supercritical expansion; 1 + 2 - mechanical spallation and supercritical expansion; 3 - only explosive boiling; 3 + 2 - explosive boiling and supercritical expansion; 5 - only surface evaporation.

This work was partially supported by RSCF grant №15-11-00032.

[1] C. Wu, L.V. Zhigilei Microscopic mechanisms of laser spallation and ablation of metal targets from large-scale molecular dynamics simulations Applied Physics A 114 (1), 11-32 (2014)

[2] V.I.Mazhukin, A.A. Samokhin, M.M.Demin, A.V.Shapranov. Modeling of nanosecond laser vaporization and explosive boiling of metals. Mathem. Montisnigri. 29, 68 - 90, (2014)

[3] V.I.Mazhukin, A.A. Samokhin, M.M.Demin, A.V.Shapranov "Explosive boiling of metals during nanosecond laser pulse action" Quantum electronics 44, p. 283 (2014)

## **Numerical modeling of 3D heat and mass transfer processes during laser cladding of metal powders**

**Dubrov A.V., Mirzade F.Kh., Niziev V.G.**

*Institute on Laser and Information Technologies of Russian Academy of Sciences (ILIT RAS),  
1 Svyatoozerskaya St., 140700 Shatura, Moscow Region, Russia*

*dubrov.av@gmail.com*

Numerical simulation of 3D fluid flow and heat transfer in the molten pool and deposition layer during the process of laser cladding of metal powders was performed, using a finite volume method. Steep surface temperature gradients specific for laser cladding of metal powders lead to considering the Marangoni effect (due to temperature-dependent surface tension) to be the major driving force for the melt flow. It has a strong influence on the shape of melt pool and the profile of cladded layer. To explicitly track the evolution of the free surface under the effects of convective liquid movements and mass addition we implement the dynamically moving mesh approach.

The influence of process parameters (laser power, scanning velocity, powder feed rate and the powder material) on the molten pool and cladded track geometry, the temperature distribution, as well as on the melt flow vortex structure has been studied. The results obtained are useful for selection of process parameters in experiments, and could be taken into account in modelling the microstructure formation and residual stresses in clad layers.

## Laser-induced graphitic nanostructures generated inside diamond bulk

**K.Ashikkalieva<sup>1,2</sup>, T.Kononenko<sup>1,2</sup>, E.Obratsova<sup>2</sup>, E.Zavedeev<sup>1,2</sup>, A.Khomich<sup>1</sup>, V.Konov<sup>1,2</sup>**

*1- Natural Science Center, General Physics Institute, Vavilov Street 38, 119991 Moscow, Russia*

*2- National Research Nuclear University "MEPhI", Kashirskoe Shosse 31, 115409 Moscow, Russia*

*kuralay.physics@mail.ru*

Laser processing is successfully used for fabrication of buried conductive structures in diamond bulk based on phase transition of diamond to graphite upon laser irradiation [1, 2]. By translating the laser focal plane through the diamond crystal it is possible to fabricate extended graphitic structures in diamond. Buried conductive structures have wide applications ranging from radiation detectors to field emitters. Technological aspects of diamond laser processing are extensively studied, whereas data concerning the internal structure of laser-modified area and distribution of graphitic phase within it are lacking. In this paper, we report on the peculiarities of internal structure of the graphitized plate fabricated in diamond by fs-laser irradiation.

In our study, the graphitized rectangular plate of  $100 \times 115 \times 8 \text{ mkm}^3$  was fabricated in the diamond bulk by Ti:sapphire-laser irradiation ( $\tau=140\text{fs}$ ,  $\lambda=800\text{nm}$ ,  $f=1\text{KHz}$ ) falling normally to the  $\langle 100 \rangle$  face of a CVD single crystal diamond. The diamond face  $\langle 110 \rangle$  was mechanically polished to remove overlying diamond and expose the graphitized plate. The obtained cross-section of the graphitized plate was carefully examined by means of Raman spectroscopy, optical microscopy and scanning electron microscopy techniques. To study the graphite phase distribution we examined surface electrical properties of the polished plate section by a Scanning probe microscope ("INTEGRA Spectra", NT-MDT) using the Scanning Spreading Resistance Microscopy (SSRM) technique.

According to the microscopic observations, the graphitized plate cross-section is an opaque laser-modified region with a quite irregular structure. Although, the Raman analysis revealed an intensive diamond signal in the spectra recorded from the laser-modified region thus evidencing the presence of diamond phase within it. The obtained Raman spectra demonstrated the signal of graphite, but its intensity was unexpectedly low in comparison with the intensity of diamond signal. Raman mapping showed the presence of compressive stresses within the laser-processed region.

A detailed study of the polished plate surface with a scanning electron microscope (SEM) revealed a large fracture extending along the central part of the plate section and a set of numerous quasi-parallel cracks crossing the fracture practically perpendicularly. The areas between cracks are filled with unmodified diamond. The quasi-parallel cracks up to  $2,5\mu\text{m}$  in length and about  $100\text{nm}$  in width are spaced apart from each other at an average distance of  $300 \text{ nm}$ . By means of SSRM technique, it has been found out that the spatial location of conductive features in the SSRM maps is fully coincided with "skeleton" of cracks in the SEM images of the laser-graphitized plate section. In other words, the set of cracks appeared to be conductive, whereas the areas between conductive cracks exhibited the same resistivity as original diamond.

On the base results obtained, we can conclude that just small part of diamond has transformed to graphite in the zone of laser treatment. The laser-modified diamond is a network of extended graphitic nanostructures surrounded with unmodified diamond. Space arrangement of the graphitized nanostructures is connected with preferential cracking of diamond along the weakest  $(111)$  planes as a result of the tensile stress relaxation. The graphitized structures are high absorbing, that is why the laser-processed plate looks like an opaque structure. The obtained experimental findings have confirmed the model of crack-assisted diamond graphitization proposed in [3].

[1] T.V. Kononenko, V.I. Konov, S.M. Pimenov, N.M. Rossukanyi, A.I. Rukovichnikov, V. Romano, Three-dimensional laser writing in diamond bulk, *Diamond & Related Materials*, 20, pp.264–268, (2011).

[2] Sun Bangshan, S. Salter Patrick and J. Martin, Booth High conductivity micro-wires in diamond following arbitrary paths, *Applied Physics Letters*, 105, pp. 231105-1 - 231105-4, (2014).

[3] T.V. Kononenko, E.V. Zavedeev, V.V. Kononenko, K. K. Ashikkalieva, V.I. Konov, Graphitization wave in diamond bulk under ultrashort laser pulses, *Applied Physics A*, 119, pp. 405-414, (2015).

# Pulsed laser ablation of titanium in liquid media: Influence of radiation parameters on nanoparticles synthesis

A. Aryshev, V. Veiko, A. Loginov, A. Samokhvalov

*National Research University of Informational Technologies, Mechanics and Optics, Saint-Petersburg, Russia*

*veiko@lastech.ifmo.ru*

Laser ablation of a solid target material in a liquid is a quick, easy and green method for nanoparticles synthesis. Most importantly, it provides with the opportunity to synthesize NPs in a surfactant free environment and thus obtain NPs with impurity free surfaces. NPs of the oxides of the titanium are important nanomaterials for a large number of applications in environmental engineering usually for the photocatalytic degradation of water pollutants, paints industry, as electrically conductive fillers, biomedicine and fabrication of organic solar cells.

In this work we report the synthesis of titanium dioxide nanoparticles by pulsed laser ablation of a bulk titanium metal target in deionized water. Fiber Yb-laser radiation source with a wavelength 1,06  $\mu\text{m}$  and tunable parameters of pulse duration, repetition rate, laser power and scanning speed was used for the ablation. The as-prepared products were characterized by scanning electron microscopy (SEM). The results indicate that the nanoparticles shape depends on pulse repetition rate. SEM images of the samples shown, that the variation of laser ablation's pulse rate promote synthesis of nanoparticles in different morphologies, such as nanostructured foam, which is an agglomeration of small nanoclusters, right-shaped spherical nanoparticles, separate nanorods and single nanocrystals. A possible formation mechanism was discussed.

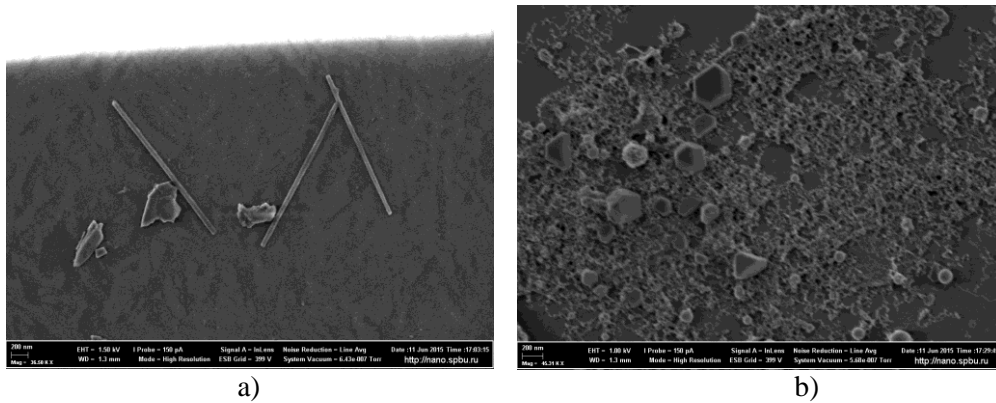


Figure 1. SEM images of  $\text{TiO}_2$  nanoparticles, synthesised by pules laser ablation of bulk titanium in water with different repetition rate: a) 5 kHz b) 10 kHz

## Surface-Enhanced Raman Scattering (SERS) of Gold-plated Silicon Nanostructures

**I. Rigo<sup>1</sup>, L. Himics<sup>1</sup>, M. Koós<sup>1</sup>, S. Tóth<sup>1</sup>, M. Veres<sup>1</sup>, P. Fürjes<sup>2</sup>**

<sup>1</sup>*Wigner Research Centre for Physics, Hungarian Academy of Sciences, PO Box 49., Budapest, Hungary, H1525*

<sup>2</sup>*Institute of Technical Physics and Materials Science (MFA), Centre for Energy Research, Hungarian Academy of Sciences, PO Box 49., Budapest, Hungary, H1525*

*rigo.istvan@wigner.mta.hu*

Nanotechnology requires the development of highly efficient characterization techniques. The study of very low amounts of molecules is essential for analysis in biology, molecular electronics and materials science. Surface-Enhanced Raman Scattering (SERS) is a phenomenon in which the Raman scattering intensity of molecules close to the surface of certain finely divided metals (usually Au or Ag) is dramatically enhanced. This is achieved by the local amplification of the electromagnetic field of the exciting and/or scattered light via surface plasmons excited on the surface of metal nanoparticles or nanostructures. The enhancement can reach even a level of  $10^8$ – $10^{10}$ . SERS is characterized by surface selectivity and it is a highly sensitive and reliable technique for surface studies that allows the detection of ultra-low amounts of analytes [1-2].

Many techniques have been developed for the preparation of metallic nanostructured substrates for SERS measurements [3]. In this study the SERS-performance of different gold-coated silicon substrates was evaluated. Structures with different sizes and shapes were obtained by lithography and subsequent etching of the silicon surface. The created structures were coated with a few nanometer thick layer of gold. The SERS-amplification of different nanostructures was determined and compared by Raman measurements on benzophenol and o-aminophenol solutions of the same concentration. The samples were excited with 488 nm and 785 nm lasers. In addition, optical reflectance spectroscopy was used to record the plasmon spectra of the silicon-gold nanostructures.

Our results showed that both the shape and the size strongly affect the plasmonic characteristics and SERS enhancement of silicon-gold nanostructures. The correlation between SERS amplification and the angle of incidence of the excitation light was also studied. Optimal configurations were determined for 488 nm and 785 nm excited SERS measurements.

M. Veres is grateful for the support of the Bolyai János Research Scholarship of the Hungarian Academy of Sciences.

[1] A. J. McQuillan, The discovery of surface-enhanced Raman scattering, *Notes Rec. R Soc.* 63, pp. 105-109, (2009).

[2] G. S. Petreska, J. Blazevska-Gilev, R. Fajgar, R. Tomovska, Surface-Enhanced Raman Scattering activity of Ag/graphene/polymer nanocomposite films synthesized by laser ablation, *Thin Solid Films* 564, pp. 115-120, (2014).

[3] A. Merlen, V. Chevallier, J. C. Valmalette, L. Patrone, P. Torchio, S. Vedraïne, F. Flory, G. Moula, *Surface Science* 605, pp. 1214-1218 (2014).

## **Laser cancellation of Euler instability of buckling column**

**A.Omelchenko**

*Institute on Laser and Information Technologies of Russian Academy of Sciences,  
Troitsk, Moscow reg., Russia  
omelch@laser.ru*

It is well known, that stability is the necessary condition for engineering. It provides the normal operating regime for the machines. This condition is required for a number of the modern technologies.

Laser technologies of material surface heat treatment including laser hardening, laser strain annealing, surface coating with laser spraying and others require stable laser radiation. Strong requirements to laser operating regime are needed in laser medical applications, such as laser reshaping of cartilage, laser stimulation of cells for biotissue regeneration etc.

Laser heating of elastic materials is often carried out in non-isothermal conditions. These conditions depend on the geometry of laser irradiation of material and high gradient of the temperature caused by absorption of intensive laser radiation in small space.

A number of instabilities show itself in heterogeneous reactions of metal oxidation stimulated by laser heating. They influence on the formation of oxide films on the metals heated by laser radiation. Sometimes it leads to the growth of the gigantic crystals of oxide at the metal surface [1]. Kinetics of the laser-stimulated metal oxidation have been studied [2], but the reason caused the gigantic crystals formation is still unknown.

This paper considers thermomechanical effect of laser radiation on cancellation of instabilities of metal oxidation and strain annealing at the reshaping of the hydrated biotissues stimulated by laser heating. Both effects, as it appears to be caused by instability of buckling column firstly studied by Leonard Euler.

Analysis of experimental data [1] on heat and mass transfer shows on the storage of high value of thermal stress in oxide film at the crystal growth. This stress is caused by the difference between the coefficients of thermal expansion of oxide and metal. Also, it is dependent on the difference of Young's modules of oxide and metal. Stress is generated in the film by thermal expansion of oxide under the absence of its adhesion contact with metal in some spot at the laser irradiated surface. Melting of metal under the film's noncontact spot induces internal stress upper threshold of instability of oxide film buckling. It leads to reshaping of oxide film on the metal surface laser irradiated and stimulates instabilities of heat mass transfer of metal through oxide. As presented in this paper, heat and mass transfer modelling of the crystal growth, confirmed our early experiments.

General consideration of the conditions for Euler's instability cancellation in the different laser application, including medical treatments, is presented.

**Acknowledgements:** Thanks to Russian Foundation for Basic Research for financial assistance Grant No.15-42-00106a.

[1] D.Alimov, A.Omelchenko, P.Khabibullaev and others Thermochemical instabilities in heterogeneous processes stimulated by laser radiation" *Poverkhnost. Fizika.Khimiya. Mekhanika*.1982.No.8, pp.12-21(in Russian).

[2] D.Alimov, A.Omelchenko, P.Khabibullaev. Thermophysical processes of diffusion electro-mass transfer in the thermal oxidation of laser-heated metals. *High Temperature*.1989. V.27, no.2, pp.220-224.

# Laser-assisted forming of the bimetal thin films with changing optical and electrical properties

A. Antipov<sup>1</sup>, S. Arakelian<sup>1</sup>, T. Vartanyan<sup>2</sup>, A. Istratov<sup>1</sup>, S. Kutrovskaia<sup>1</sup>,  
A. Kucherik<sup>1</sup>, T. Itina<sup>3</sup>

<sup>1</sup>Stoletovs' Vladimir State University, Vladimir Russia

<sup>2</sup>St. Petersburg National Research University of Information Technologies, Mechanics and Optics,  
St. Petersburg, Russia

<sup>3</sup>Hubert Curien Laboratory, Saint-Etienne, France

E-mail: [11stella@mail.ru](mailto:11stella@mail.ru)

Laser ablation of solid targets in the liquid medium widely used method for fabrication nanostructures with various compositions such as metals, alloys, oxides, carbides, hydroxides, etc. At the same time a great advantage of the method is the possibility to re-irradiate the suspended nanomaterials that can be applied to further modify their size, shape, and composition. In the past two decades, with the rise of nanoscience, laser ablation has been broadly applied and developed for the synthesis of metal nanostructures such as gold (Au), silver (Ag), nickel (Ni) and copper (Cu) or their alloys. Bimetallic structures of these metals have improved physical and chemical stability and selectivity compared with isometric structures. The bimetallic complex is related to change the optical and electrical properties, in particular transmission and absorption, depending on the nanoparticles (NPs) size and composition. Separate direction of controlling the physical properties of such nanostructures formation of clusters with variable morphology.

Promising method of obtaining bimetallic clusters is the laser formation of colloidal alloys. In this work we used method of action of CW-laser radiation with moderate intensity in liquid (water, ethanol, etc.). Colloidal systems formation were obtained by CW-laser ( $\lambda = 1.06 \mu\text{m}$ ,  $I \sim 10^6 \text{ W/cm}^2$ ,  $t = 10 \text{ min}$ ). Particle size in the colloidal solution is approximately 8 nm. After that, two colloidal systems were mixed and NPs were deposited on the  $\text{SiO}_2$  substrate by two different methods: laser-induced thermal deposition of metal particles from colloidal solution and deposition of particles from small drop of colloid.

The morphological properties of deposited clusters were investigated using atomic force microscopy (AFM), scanning electron microscopy (SEM) and transparent electron microscopy (TEM). It was found that the transmission spectra of the resulting structures depend on the concentration of gold and silver nanoparticles in the colloidal solution and from morphology properties of deposited layer.

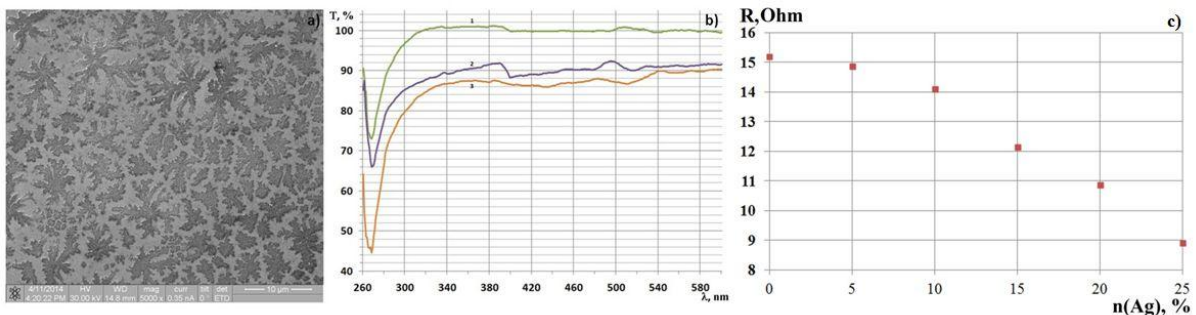


Figure 1 REM-images of deposited bimetal cluster (a) and transmission spectra (b) of deposited cluster for various mass ration of Au and Ag particles in colloidal solution: 1- 1(Au):1(Ag); 2 -1:3;; 3 - 3:1. Dependence of electrical resistance of Ag-Ni clusters at concentration of Ag nanoparticles (c).

This study was performed within the design part of a government contract for research work with VISU #16.440.2014/K and RFBR grant #№ 13-02-91057.

---

---

**SECTION LS**

**Laser Systems and Materials**

---

---

## Q-switched microchip lasers at 2 $\mu\text{m}$

**X. Mateos<sup>1</sup>, J.M. Serres<sup>1</sup>, P. Loiko<sup>2</sup>, K. Yumashev<sup>2</sup>, V. Petrov<sup>3</sup>, U. Griebner<sup>3</sup>, M. Aguiló<sup>1</sup>, F. Díaz<sup>1</sup>**

*1-Física i Cristal·lografia de Materials i Nanomaterials (FiCMA-FiCNA), Universitat Rovira i Virgili (URV),*

*Campus Sescelades, c/ Marcel·lí Domingo, s/n., Tarragona, Spain E-43007*

*2-Center for Optical Materials and Technologies, Belarusian National Technical University,*

*65/17 Nezavisimosti Ave., 220013 Minsk, Belarus*

*3-Max Born Institute for Nonlinear Optics and Short Pulse Spectroscopy,*

*Max-Born-Str. 2a, Berlin, Germany D-12489*

*Main author email address: xavier.mateos@urv.cat*

The Q-switching technique enables the generation of high energy short laser pulses. Compared to active Q-switching, passive Q-switching (PQS) in more compact laser cavities with reduced round trip time provides shorter pulses, down to picosecond pulse duration [1]. Such short laser pulses are of special interest at wavelengths around 2  $\mu\text{m}$  for applications in medicine (due to the high water absorption), remote sensing (water and  $\text{CO}_2$ ) and for pumping of mid-IR OPOs.

The microchip concept consists of sandwiching the laser active medium between two plane mirrors or depositing dielectric coatings with proper transmission/reflection for laser oscillation at the desired wavelength directly on the active medium. Such a configuration, only under the condition of positive thermal lens in the active medium, ensures laser mode stabilization and very low intracavity losses. The extremely short cavity length provided by the microchip results in further shortening of the round trip time, and with this, of the pulse duration.

Several PQS microchip lasers at 2  $\mu\text{m}$  have been studied in the past, based on YLF,  $\text{GdVO}_4$ ,  $\text{YVO}_4$  and YAP crystals doped with Tm or co-doped with Tm and Ho [2,3]. The monoclinic potassium lutetium double tungstate,  $\text{KLu}(\text{WO}_4)_2$  or  $\text{KLuW}$ , was demonstrated to be very suitable for Yb (1  $\mu\text{m}$ ), Tm (1.9  $\mu\text{m}$ ) and Ho (2.1  $\mu\text{m}$ ) doping for laser operation in continuous-wave (CW), Q-switched and mode-locked regimes due to its excellent spectroscopic features due essentially to its high degree of optical anisotropy [4]. In addition, light propagation along one of its principal optical axes,  $N_g$ , provides positive thermal lens for the two meridional planes and low astigmatism [5]. We recently reported on the CW microchip laser operation at 1 and 2  $\mu\text{m}$  in Yb, Tm or Ho-doped  $\text{KLuW}$  crystals [6].

The PQS technique uses a passive optical modulator, the so-called saturable absorber (SA), whose desirable characteristics include low saturation intensity, low non-saturable losses, high modulation depth, broadband saturable absorption and high damage threshold. For this reason, new SAs that satisfy these requirements are being intensively studied.

In the present talk, we review the recent achievements in PQS of Tm or Ho microchip lasers based on  $\text{KLuW}$  using novel SAs, such as PbS quantum dots (QD), graphene and carbon nanotubes (CNTs).

The shortest pulse duration achieved from a Ho: $\text{KLuW}$  microchip laser, in-band pumped with a Tm: $\text{KLuW}$  microchip laser with PbS QD-SA is 55 ns with an average output power of 84 mW at 2061 nm. In the case of the co-doped crystal, the diode-pumped Ho,Tm: $\text{KLuW}$  microchip laser delivered 201 ns pulses with an average output power of 74 mW at 2061 nm using graphene as a SA. The shortest pulse duration achieved from a Tm: $\text{KLuW}$  microchip laser with CNT-SA is 97 ns with an average output power of 260 mW.

Further optimization, such as shortening of the cavity length, reduction of heating of the SA or proper modulation depth of the SAs could additionally shorten the pulse duration.

[1] E. Mehner, B. Bernard, H. Giessen, D. Kopf, and B. Braun, Sub-20-ps pulses from a passively Q-switched microchip laser at 1 MHz repetition rate, *Opt. Lett.*, Vol. 39, pp. 2940-2943 (2014).

[2] J. J. Zayhowski, J. Harrison, C. Dill III, and J. Ochoa, Tm: $\text{YVO}_4$  microchip laser, *Appl. Opt.*, Vol. 34, pp. 435-437, (1995).

[3] J. Sulc, H. Jelínková, K. Nejezchleb, and V. Skoda, High-efficient room-temperature CW operating Tm:YAP laser with microchip resonator, *Proc. of SPIE*, Vol. 7193, pp. 71932H-1-9 (2009).

[4] V. Petrov, M. C. Pujol, X. Mateos, O. Silvestre, S. Rivier, M. Aguiló, R. M. Sole, J. Liu, U. Griebner, and F. Díaz, Growth and properties of  $\text{KLu}(\text{WO}_4)_2$ , and novel ytterbium and thulium lasers based on this monoclinic crystalline host, *Laser & Photon. Rev.*, Vol. 1, pp. 179-2012 (2007).

[5] P. A. Loiko, J. M. Serres, X. Mateos, K. V. Yumashev, N. V. Kuleshov, V. Petrov, U. Griebner, M. Aguiló, and F. Díaz, Characterization of thermal lens in Tm: $\text{KLu}(\text{WO}_4)_2$  and microchip laser operation, *Laser Phys. Lett.*, Vol. 11, pp. 075001-1-7 (2014).

[6] M. Serres, X. Mateos, P. Loiko, K. Yumashev, N. Kuleshov, V. Petrov, U. Griebner, M. Aguiló, and F. Díaz, Diode-pumped microchip Tm: $\text{KLu}(\text{WO}_4)_2$  laser with more than 3 W of output power, *Opt. Lett.*, Vol. 39, pp. 4247-4250 (2014).

# SPECTROSCOPIC AND LASER PROPERTIES OF $\text{Cr}^{2+}$ AND $\text{Fe}^{2+}$ IONS IN $\text{ZnMnSe}$ SOLID SOLUTION

M.E. Doroshenko<sup>1</sup>, H. Jelinkova<sup>2</sup>, M. Jelinek<sup>2</sup>, M. Nemeč<sup>2</sup>, N.O. Kovalenko<sup>3</sup>,  
A.S. Gerasimenko<sup>3</sup>

1- General Physics Institute RAS, Moscow, Russia

2- Czech Technical University, Prague, Czech Republic

3- Institute for Single Crystals NAN, Kharkov, Ukraine

email:dorosh@lst.gpi.ru

A set of  $\text{Zn}_{1-x}\text{Mn}_x\text{Se}$  crystals with different Mn concentrations  $x$  doped with divalent chromium and iron was synthesized using the Bridgman technique, and their spectroscopic and laser properties in a broad temperature range were investigated.

The room-temperature absorption and fluorescence spectra of  $\text{Cr}^{2+}$  ions measured in  $\text{Zn}_{1-x}\text{Mn}_x\text{Se}$  solid solutions of different compositions were approximated by a set of Gaussian curves as shown in Fig.1, and the maxima of these curves were plotted versus the Mn content ( $x$ ) (see Fig.2). An increase in the Mn content ( $x$ ) results in a close-to-linear shift of both absorption and fluorescence maximums of chromium ions to longer wavelengths compared to ZnSe crystal as  $\lambda_{\text{max}} = \lambda_{\text{max}}(\text{ZnSe}) + 150x$ , which is approximately three times smaller than that observed previously for  $\text{Zn}_{1-x}\text{Mg}_x\text{Se}$  solid solution (shown in Fig.2 by squares).

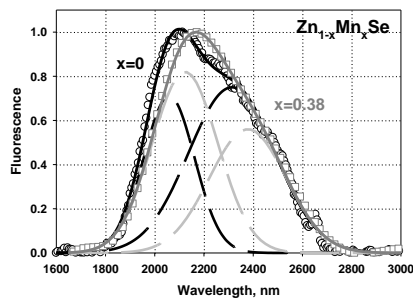


Fig.1 Fluorescence spectra of  $\text{Cr}^{2+}$  ions in  $\text{Zn}_{1-x}\text{Mn}_x\text{Se}$  crystal for different Mn content ( $x$ ) with decomposition into two Gaussians.

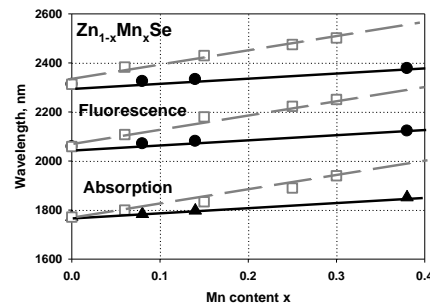


Fig.2 Positions of Gaussian peaks in the fluorescence (circles) and absorption (triangles) spectra of  $\text{Cr}^{2+}$  ions in  $\text{Zn}_{1-x}\text{Mn}_x\text{Se}$  crystals with different Mn content ( $x$ ) compared to  $\text{Zn}_{1-x}\text{Mg}_x\text{Se}$  crystal (squares).

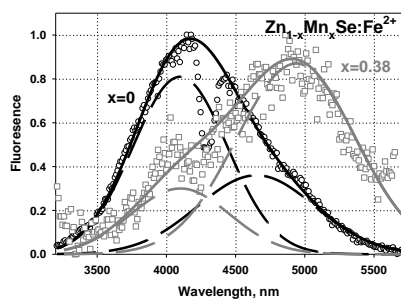


Fig.3 Fluorescence spectra of  $\text{Cr}^{2+}$  ions in  $\text{Zn}_{1-x}\text{Mn}_x\text{Se}:\text{Fe}^{2+}$  crystal for different Mn content ( $x$ ) with decomposition into two Gaussians.

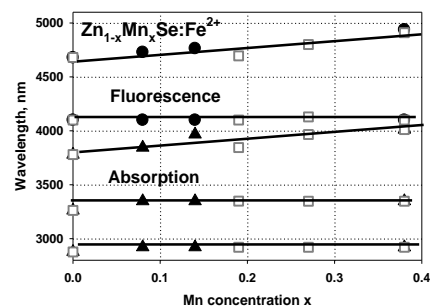


Fig.4 Positions of Gaussian peaks in the fluorescence (circles) and absorption (triangles) spectra of  $\text{Fe}^{2+}$  ions in  $\text{Zn}_{1-x}\text{Mn}_x\text{Se}$  crystals with different Mn content ( $x$ ) compared to  $\text{Zn}_{1-x}\text{Mg}_x\text{Se}$  crystal (squares).

The room-temperature absorption spectrum of  $\text{Fe}^{2+}$  ions was found to be more complex compared to  $\text{Cr}^{2+}$  and was approximated by a set of three Gaussian curves, while the fluorescence spectrum was still approximated by a pair of Gaussians (see Fig.3). As was found from this approximation, an increase in the Mn concentration in the case of  $\text{Fe}^{2+}$  ions almost does not change the positions of the short wavelength components of both the absorption and fluorescence spectra but leads to a long-wavelength shift of their long-wavelength components (see Fig.4). This shift was found to be nearly the same for  $\text{ZnMnSe}$  and  $\text{ZnMgSe}$  solid solutions.

# Broadband applicability of nanocarbon-based saturable absorbers for ultrafast laser technology

F. Rotermund

*Department of Physics and Department of Energy Systems Research, Ajou University, Suwon 443-749, Korea*

*e-mail address: [rotermun@ajou.ac.kr](mailto:rotermun@ajou.ac.kr)*

Passive mode-locking of lasers by utilizing suitable mode-locking devices is a well-known technique for ultrashort pulse generation. Widespread saturable absorbers based on semiconductor heterostructures such as semiconductor saturable absorber mirrors (SESAMs) have revolutionized ultrafast laser technology [1]. They provide an efficient nonlinear optical switching mechanism with ultrafast responses enabling applications for developing different ultrafast lasers.

In recent years, saturable absorbers (SAs) based on low-dimensional nanocarbons such as single-walled carbon nanotubes (SWCNTs) and graphene have been developed and successfully employed for ultrashort pulse generation in various bulk solid-state and fiber lasers operating at different wavelengths [2-4]. Such novel SAs exhibit broadband absorption with quite large third-order nonlinearities and ultrafast recovery and require relatively simple manufacturing processes, whereas SESAMs provide spectrally narrowband nonlinearity and applicability. In addition, they require sophisticated manufacturing processes with additional treatments to reduce response times of devices. To overcome those limiting characteristics of SESAMs, SWCNT-SAs and graphene SAs are newly suggested as real-world alternatives. The absorption band of SWCNT-SAs can be controlled by varying the nanotube diameter and chirality, and hence, SWCNT-SAs are readily applicable within a broad spectral range throughout the near-infrared from 800 nm up to 2.1  $\mu\text{m}$ . Compared to SWCNT-SAs, which operation wavelength depends on the diameter and chirality of nanotubes defining the bandgap, graphene exhibits an additional superior advantage of ultrafast saturable absorption over an ultrabroad spectral region far beyond 2  $\mu\text{m}$  without any bandgap engineering processes due to its unique point-bandgap structure and linear dispersion of Dirac electrons [5-6]. In this talk, recent progress in nanocarbon-based saturable absorbers and their characteristics and applications in various passively mode-locked ultrafast and Q-switched lasers will be presented.

- [1] U. Keller, K. J. Weingarten, F. X. Kärtner, D. Kopf, B. Braun, I. D. Jung, R. Fluck, C. Hönninger, N. Matuschek, and J. Aus der Au, Semiconductor saturable absorber mirrors (SESAMs) for femtosecond to nanosecond pulse generation in solid-state lasers, *IEEE J. Sel. Top. Quantum Electron.* 2, 435 (1996).
- [2] S. Y. Set, H. Yaguchi, Y. Tanaka, and M. Jablonski, Laser mode locking using a saturable absorber incorporating carbon nanotubes, *J. Lightwave Technol.* 22, 51 (2004).
- [3] J. H. Yim, W. B. Cho, S. Lee, Y. H. Ahn, K. Kim, H. Lim, G. Steinmeyer, V. Petrov, U. Griebner, and F. Rotermund, Fabrication and characterization of ultrafast carbon nanotube saturable absorbers for solid-state laser mode locking near 1  $\mu\text{m}$ , *Appl. Phys. Lett.* 93, 161106 (2008)
- [4] W. B. Cho, J. H. Yim, S. Y. Choi, S. Lee, A. Schmidt, G. Steinmeyer, U. Griebner, V. Petrov, D.-I. Yeom, K. Kim, and F. Rotermund, Boosting the nonlinear optical response of carbon nanotube saturable absorbers for broadband mode-locking of bulk lasers, *Adv. Funct. Mater.* 20, 1937 (2010).
- [5] W. B. Cho, J. W. Kim, H. W. Lee, S. Bae, B. H. Hong, S. Y. Choi, I. H. Baek, K. Kim, D.-I. Yeom, and F. Rotermund, High-quality, large-area monolayer graphene for bulk laser mode-locking near 1.25  $\mu\text{m}$ , *Opt. Lett.* 36, 4089 (2011).
- [6] M. N. Cizmeciyan, J. W. Kim, S. Bae, B. H. Hong, F. Rotermund, and A. Sennaroglu, Graphene mode-locked femtosecond Cr:ZnSe laser at 2500 nm, *Opt. Lett.* 38, 341 (2013).

# Physics and Engineering of Cryogenically Cooled Slab RF Discharge First-Overtone CO Laser

Andrey Ionin, Andrey Kozlov, Dmitry Sinitsyn

*Lebedev Physical Institute of Russian Academy of Sciences, 53 Leninsky pr., 119991 Moscow, Russia*

*aion@sci.lebedev.ru*

Repetitively pulsed first-overtone CO lasers excited by a slab RF-discharge with electrode cryogenic cooling have been researched and developed. One of them (Figure 1) has slab volume of  $3 \times 15 \times 400 \text{ mm}^3$  pumped by 60 MHz RF power supply.

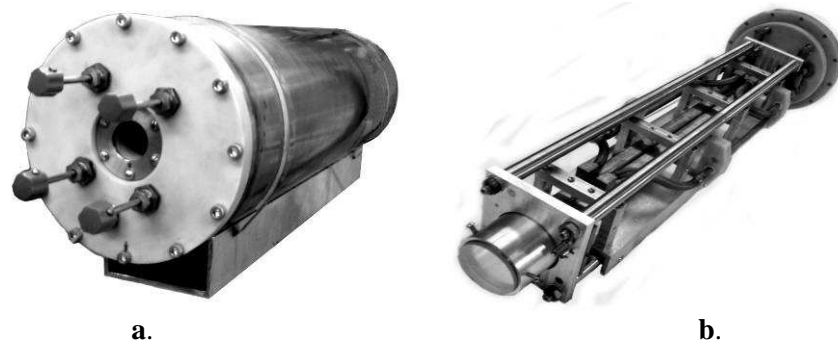


Figure 1. Slab RF-discharge first-overtone CO laser design. External view of the laser head (a) and internal design with cryogenic electrode system and laser resonator module (b).

Maximal average output power of  $\sim 2.0 \text{ W}$  was obtained with efficiency of  $\sim 1.6\%$  at the pulse repetition rate of 400 Hz. Output spectra of the first-overtone CO laser consisted typically of a few tens of lines and covered the spectral range of 2.5 - 4.0 micron depending on the laser resonator mirrors set used in the experiments. Typical first-overtone CO laser spectra are presented in Figure 2.

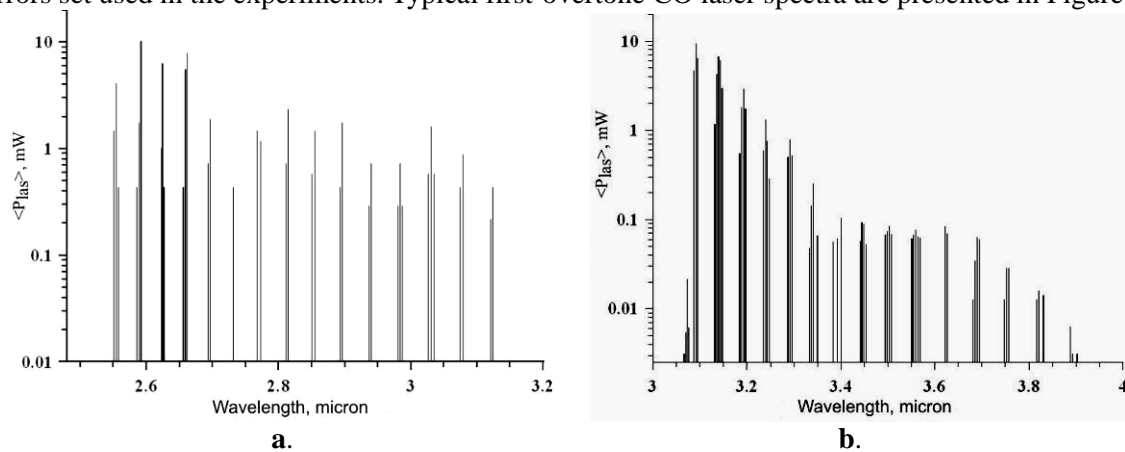


Figure 2. Typical first-overtone CO laser spectra obtained with short- (a) and long-wavelength (b) laser resonator mirrors sets.

The laser parametric optimization demonstrated that using active gas mixtures with anomalous high content of oxygen (up to 50% with respect to CO concentration) resulted in a stable quasi sealed-off CO laser operation during the long time interval corresponding to  $\sim 10^6$  laser pulses. Different modes of the laser operation were studied depending on pulse repetition rate from 100 Hz up to 5 kHz. A long time behavior of the RF discharge plasma luminescence spectrum and output laser radiation spectrum redistribution were experimentally studied in correlation with long time output power behavior to identify the main cryogenic plasma-chemical processes responsible for the laser gas mixture degradation. The research was supported by the Russian Fund for Basic Research (Grant # 15-02-01378).

# Full characterization of the nonlinear optical properties of crystals for the infrared parametric generation

**P. Segonds<sup>\*</sup>, B. Boulanger, E. Boursier, J. Debray, B. Ménaert,  
C. Félix, D. Jegouso, A. Pena, J. Zaccaro, V. Boutou**

<sup>1</sup>*Institut Néel Centre National de la Recherche Scientifique - Université Joseph Fourier BP 166, F38402  
Grenoble Cedex 9, France,*

*\*[patricia.segonds@neel.cnrs.fr](mailto:patricia.segonds@neel.cnrs.fr)*

Quadratic frequency down conversion in nonlinear crystals pumped in the visible and at  $1\ \mu\text{m}$  is a preferred route for the design of widely tunable solid state sources emitting in the infrared. However, the choice for nonlinear crystals enabling frequency down-conversion associated with a large quadratic nonlinear coefficient and a wide transparency range in the infrared is rather limited [1].  $\text{KTiOPO}_4$  (KTP) and periodically poled  $\text{LiNbO}_3$  (PPLN) are the two main nonlinear crystals, but their emission is between  $2\ \mu\text{m}$  and  $4.5\ \mu\text{m}$ , covering Band II of transparency of the atmosphere [1]. A current potential alternative to cover Band III ( $5\ \mu\text{m}$  -  $8\ \mu\text{m}$ ) is the newly developed  $\text{BaGa}_4\text{Se}_7$  (BGSe) that is transparent from  $0.78\ \mu\text{m}$  up to  $14.72\ \mu\text{m}$  [2].

The selection of new nonlinear crystals has relied on the full characterization of properties for the generation of parametric light. The main ones are phase-matching conditions that will be discussed in detail in birefringent crystals (BPM) and crystals with periodical ferroelectric domains (QPM). We will focus in the direct measurement of phase-matching directions, walk-off, associated frequency conversion efficiencies, spectral and angular acceptances. Quadratic difference frequency generation (DFG) will be considered, but also for second harmonic generation (SHG) and sum frequency generation (SFG), one important point being to involve the three main refractive indices at wavelengths well spread out in the transparency range of the crystal [3].

Our experimental method uses one crystal cut as a sphere with a some millimeter diameter that is compatible with the early stage of crystal growth. The sphere is polished to optical quality and stuck on a goniometric head under orientation, using X-Rays in a backscattered Laue geometry. Then it is placed at the center of 3 axis goniometer giving access to all directions of propagation with an angular accuracy of  $\pm 0.5^\circ$ . SHG phase-matching conditions are determined with one incoming beam only. It is a 15-ps-width pulse (FWHM) Excel Technology Nd:YAG laser at  $1.064\ \mu\text{m}$  pumping an OPG from Light Conversion tunable between  $0.6\ \mu\text{m}$  and  $2.4\ \mu\text{m}$ . With the OPG beam combined with the  $1.064\ \mu\text{m}$  beam in a DFG stage based on a  $\text{AgGaS}_2$  crystal, a tunable beam between  $2.5\ \mu\text{m}$  and  $12\ \mu\text{m}$  is generated. For SFG and DFG, the OPG and  $1.064\ \mu\text{m}$  beams are combined collinearly in the sphere. We also use a homemade dual OPO based on two 5%MgO:PPLN crystals cut as partial cylinders and simultaneously pumped by a 5-ns-width (FWHM) pulse Nd:YAG laser at  $1.064\ \mu\text{m}$ : it provides two independently tunable beams ranging from  $1.4\ \mu\text{m}$  and  $4.4\ \mu\text{m}$  [4]. The beams are properly focused in the sphere in order to keep the propagation parallel to its diameter for any orientation of the sample. Achromatic half-wave-plates give access to all possible polarization schemes.

All our experimental data can be used *per se* but phase-matching directions also allow us to refine the Sellmeier equations, the associated conversion efficiencies leading to the determination of the value and sign of involved non-zero second-order coefficients. Then OPG tuning curves associated with maximal conversion efficiency can be calculated for emission of idler wavelengths from the infrared or a super continuum. Using this *modus operandi*, we will show in detail the recently performed full characterization of nonlinear crystals for infrared generation of light as BGSe, LGT, CdSe, CdSiP<sub>2</sub>.

[1] A. Godard, "Optical parametric sources for the infrared (2–12  $\mu\text{m}$ ) solid-state laser sources: a review" *C.R. Phys.* 8, 1100–1128 (2007).

[2] V. Badikov *et al.*, "Phase-matching properties of  $\text{BaGa}_4\text{S}_7$  &  $\text{BaGa}_4\text{Se}_7$ : Wide-bandgap nonlinear crystals for mid-IR" *Phys. Stat. Sol. RRL* 5, 31-33 (2011).

[3] E. Boursier, P. Segonds, B. Boulanger, C. Felix, J. Debray, D. Jegouso, B. Ménaert, D. Roshchupkin, I. Shoji, "Phase-matching direction, refined Sellmeier and second-order nonlinear coefficient of the infrared langatate Crystal LGT", *Optics Letters* 39, 4033-4036 (2014).

[4] V. Kemlin, D. Jegouso, J. Debray, P. Segonds, B. Boulanger, B. Menaert, H. Ishizuki, and T. Taira, "Widely tunable optical parametric oscillator in a 5 mm thick 5% MgO:PPLN partial cylinder," *Opt. Lett.* 38, 860-862 (2013).

# Influence of Cr<sup>3+</sup> and Ni<sup>3+</sup> Doping on Composition (x), Structure and Structure-Dependent Properties of Sr<sub>x</sub>Ba<sub>1-x</sub>Nb<sub>2</sub>O<sub>6</sub>

**L.I. Ivleva<sup>1</sup>, G.M. Kuz'micheva<sup>2</sup>, P.A. Lykov<sup>1</sup>, P.G. Zverev<sup>1</sup>, V.V. Osiko<sup>1</sup>**

*1-Prokhorov General Physics Institute RAS, 119991, Vavilov str., Moscow, Russia*

*2-Lomonosov State University of Fine Chemical Technology, 119571, Moscow, Russia*

*e-mail: [ivleva@lst.gpi.ru](mailto:ivleva@lst.gpi.ru)*

Strontium Barium Niobate, Sr<sub>x</sub>Ba<sub>1-x</sub>Nb<sub>2</sub>O<sub>6</sub> (SBN) belongs to relaxor ferroelectrics family. Due to very high values of  $\epsilon'$ , large piezoelectric constants and electro-optic coefficients, the relaxors have been a focus of intense experimental and theoretical studies [1, 2]. It is commonly accepted that the unique properties of relaxors are related to inherent chemical disorder. Here we report the XRD studies of chemical composition and structure peculiarities of TM-doped SBN crystals. Ferroelectric and non-linear properties of the materials were investigated taking into account the distribution of doping ions over regular and interstitial positions in the tetragonal tungsten bronze structure.

The nominally pure Sr<sub>0.61</sub>Ba<sub>0.39</sub>Nb<sub>2</sub>O<sub>6</sub> (SBN:61) and SBN:61 doped with Cr<sup>3+</sup> (0.005 at.%) and Ni<sup>3+</sup> (0.03; 0.50 at.%) were grown by modified Stepanov technique. It was shown that TM-doping of SBN leads to a change in the content of Ba<sup>2+</sup> and Sr<sup>2+</sup> ions in SBN crystal compositions and to their redistribution over the crystallographic sites: Sr content in Sr(1) sites as well as Ba and Sr content in Sr(2) sites and presence vacancies in niobium Nb and oxygen sites. The presence of Cr<sup>3+</sup> ions in the vicinity of the Nb(2) atoms and in the triangular channels with octahedral coordination was shown.

The Ni<sup>2+</sup> (0.7 Å) and Ni<sup>3+</sup> (0.56 Å) ions can occupy octahedral coordinated Nb<sup>5+</sup> (0.7 Å) in Nb(2) sites; however Ni<sup>2+</sup> (0.7 Å) ions can also occupy Sr<sup>2+</sup> (1.12 Å) sites. It results in some distortions in the SBN:61 lattice. The increase in the Ni content in the SBN structure leads to a change in its formal charge (Ni<sup>3+</sup> → Ni<sup>2+</sup>). The linear dichroism was defined as the difference ( $\alpha_e - \alpha_o$ ) at 476.5, 488 and 514.5 nm. Virtually isotropic absorption spectra were obtained for Cr<sup>3+</sup> doped SBN:61. The crystals doped with Ni are characterized by the strong linear dichroism. The low substituting Ni level does not affect the temperature T<sub>c</sub> characterizing dielectric anomalies, but decreasing (twice) the electric conductivity. At a higher concentration of Ni the doped sample exhibits a very broad and frequency-dependent dielectric anomaly with low dielectric constant values. The configuration of the ferroelectrics microdomains is strongly defined by Ni ions concentration. At low Ni concentration introduced into SBN:61 the switching process promotes by reducing the value of threshold nucleation field, and thus coercive field E<sub>c</sub> decreased by about twice in comparison with the undoped SBN:61, full switching times – ms. The switching process in the highly doped sample requires the field exposure times up to several tenths of seconds, even for E > E<sub>c</sub>. The investigation of second harmonic generation (SHG) of 1.064 μm laser radiation was performed on the ground SBN samples with average particle size of 2-4 μm, which corresponds to the maximum coherence length of the SHG process in SBN crystals at 1.064 μm. Nonlinear second-order susceptibilities,  $\chi^{(2)}$ , were obtained based on the temperature dependences of the SHG intensity. Sample investigation was carried out in the temperature range of 5-90°C. As a result, it was found that an increase of TM-dopant content in the SBN composition leads to an increase in the “a” and decrease “c” unit cell parameters, reduces the  $\chi^{(2)}$  value. On the basis of established relationship between the unit cell parameters and Sr content in Sr(1) sites in SBN structures it can be revealed that the  $\chi^{(2)}$  value should decrease with increasing Sr content in Sr(1) sites. SBN crystals with low and high transition ion (Cr, Ni) doping level demonstrate strongly different physical properties. The difference in the properties for SBN crystals with low and high concentration of transition ions indicates, apparently, on the existence of some boundary concentrations above which the degree of disorder of a material increases and causes reduced physical parameters. The Ni substitution at a small amount is effective in compensating the chemical and electronic defects of the complex oxide system.

[1] H. Takenaka, I. Grinberg, A. M. Rappe, Anisotropic Local Correlations and Dynamics in a Relaxor Ferroelectric, Phys. Rev. Lett. **110**, 147602 (2013)

[2] G. G. Guzmán-Verri, P. B. Littlewood, C. M. Varma, Paraelectric and ferroelectric states in a model for relaxor ferroelectrics, Phys. Rev. B **88**, 134106 (2013)

## **Comparison of thermal effects in slab lasers with different configuration of diode pumping**

**V.B.Tsvetkov, I.A.Shcherbakov**

*General Physics Institute, 119991, Vavilov str., 38, Moscow, Russia.*

*e-mail: [tsvetkov@lsk.gpi.ru](mailto:tsvetkov@lsk.gpi.ru)*

Average output power of the solid-state laser is limited, mainly, by thermal effects. For achievement of lasing with high average power together with high beam quality in 80th years of 20 century it was offered to use planar active elements, in particular, slab shaped active elements with a zigzag beam propagation. Use of semi-conductor lasers with possibility of a pumping beam collimation has allowed creating different designs in which the pumping is made not only from planes of full internal reflection, but also through an end face or a lateral surface of an active element.

However the use of diode lasers leads to high absorption coefficients of a pumping power. Thereof, temperature distribution in the active medium at use of diode pumping can be essentially non-uniform in various directions and additional research of influence of thermo-optical effects on a laser beam is required at use of various optical schemes of a pumping.

In the report the results of experimental studies and computer modelling of distribution of phase distortions and temperatures in slab are resulted at use of three configurations of an optical pumping - through lateral faces of an active element, through planes of full internal reflection and through end faces of a slab. Experiments were done with the same slabs that allow minimizing the effects introduced by optical quality of active medium.

The obtained data allows qualitatively and quantitatively to define merits and demerits of each of optical pumping schemes and to define optimum for a specific task.

# High-efficiency backward stimulated polariton scattering in periodically poled ferroelectrics

H. Jang, A. Zukauskas, C. Canalias, and V. Pasiskevicius

*Department of Applied Physics, Royal Institute of Technology, KTH, Roslagstullsbacken 21, 10691 Stockholm, Sweden  
vp@laserphysics.kth.se*

Periodically poled  $\text{KTiOPO}_4$  (PPKTP) is a well-established nonlinear material employed in frequency conversion schemes from visible to mid-infrared. Its beneficial crystal-symmetry properties allow fabrication of ferroelectric domain structures with very large aspect ratios, defined as a ratio of the domain height to the domain width. This allows, among other things, fabricating PPKTP with large apertures for applications in high pulse-energy parametric devices [1] and structures with submicron periodicity for applications in counter-propagating nonlinear devices [2]. Single-domain KTP has also been demonstrated to be an efficient material for forward stimulated polariton scattering (FSPS) [3], the process responsible for parametric THz generation by exploiting phase-matching afforded by the dispersion in the phonon-polariton spectral region.

In this work we demonstrate that the backward polariton scattering (BSPS) emerges as a major nonlinear interaction in PPKTP as the periodicity of the structure becomes smaller. BSPS requires participation of slow polaritons with high index of refraction in order to satisfy momentum conservation condition. In PPKTP two strongest  $A_1$ -symmetry infrared-active TO modes attributed to  $\text{TiO}_6$  group vibrations at 8 THz and 21 THz contribute mostly to the BSPS process. The observed stark asymmetry of SPS in PPKTP - where forward scattering is totally suppressed while the backward scattering becomes highly efficient, with efficiencies easily exceeding 50%, indicates that the  $\chi^{(2)}$ -related three-wave mixing is the main mechanism responsible for the BSPS as well as FSPS in PPKTP. The BSPS is then a highly efficient optical parametric generation process with counter-propagating signal, phase-matched by exploiting polariton dispersion and occurring under the conditions of strong idler (polariton) absorption. The high absorption is unavoidable feature of the backwards phonon-polariton scattering where large-momentum polaritons are involved.

The high absorption regime for the polariton wave drastically changes spatial distributions of the waves participating in the three-wave mixing process in the counter-propagating geometry. For instance, the spatial intensity distribution of the forward propagating slow polariton wave reaches maximum at some point inside the nonlinear crystal and then decays towards the crystal end face. On the other hand, the high second order nonlinearity enhanced by the proximity to the lattice resonances, ensures strong coupling with the counter-propagating signal (Stokes) wave which, at high pump intensities acquires exponential spatial intensity distribution. This distribution is similar to what one expects in the third-order backwards stimulated Raman scattering. As could be expected, the experiments show that the backwards propagating signal is compressed in time with a compression factor of 10 as compared to the forward propagating pump.

BSPS is a competing process to quasi-phase matched mirrorless oscillators [2] in submicron-periodicity PPKTP and sets the upper limit for the fabrication errors of the quasi-phase matched structure.

[1] A. Zukauskas, N. Thilmann, V. Pasiskevicius, F. Laurell, and C. Canalias "5 mm thick periodically poled Rb-doped KTP for high energy optical parametric frequency conversion" *Optical Mat. Express*, **1**, 201-206 (2011).

[2] C. Canalias, V. Pasiskevicius, "Mirrorless optical parametric oscillator" *Nature Photonics*, **1**, 459-462 (2007).

[3] H. Jang, G. Strömqvist, V. Pasiskevicius, C. Canalias, "Control of Forward Stimulated Polariton Scattering in Periodically Poled KTP Crystals," *Optics Express*, **21**, 27277-27283 (2013).

# Magnetic optical activity in Bi-doped Mg-Al-Si glass

O. Laguta<sup>1</sup>, B. Denker<sup>2</sup>, B. Galagan, S. Sverchkov, I. Razdobreev<sup>1</sup>

1- CERLA/PHLAM, UMR CNRS 8523, University Lille-1, 59655 Villeneuve d'Ascq, France

2- A. M. Prokhorov General Physics Institute of RAS, Vavilov str. 38, Moscow 119991, Russia

Oleksii.Laguta@univ-lille1.fr

Bi-doped silica glasses have attracted much attention due to promising applications in the field of fiber lasers and amplifiers [1]. Since the first demonstration of the near infrared photoluminescence (NIR PL) in Al/Bi co-doped silica glass [2], its nature remains unclear and is under intense discussion [3]. Mainly this poor understanding of the mechanisms of NIR PL obstructs the development of high efficient devices.

In present talk, we report the results of the experiments on the magnetic optical activity in Bi-doped Mg-Al-Si oxide glass [4] in the temperature range 1.48-200 K and high magnetic fields – up to 6.5 T. The photoluminescence from the first excited state (Fig. 1a) exhibits magnetic circular polarization that indicates the spin multiplicity of this state. The band of the magnetic circular polarization of luminescence (MCPL) is red shifted compared with the luminescence band. The degree of MCPL, shown in Fig. 1b, completely saturates below 10 K at any magnetic field in the range 1-6 T and the saturation values are different for each magnetic field value. The experimental data can be explained in the assumption that the first excited state is an isolated non-Kramers doublet and, as a consequence, the luminescence center is an even-electron system with the axial and rhombic zero-field splitting [5].

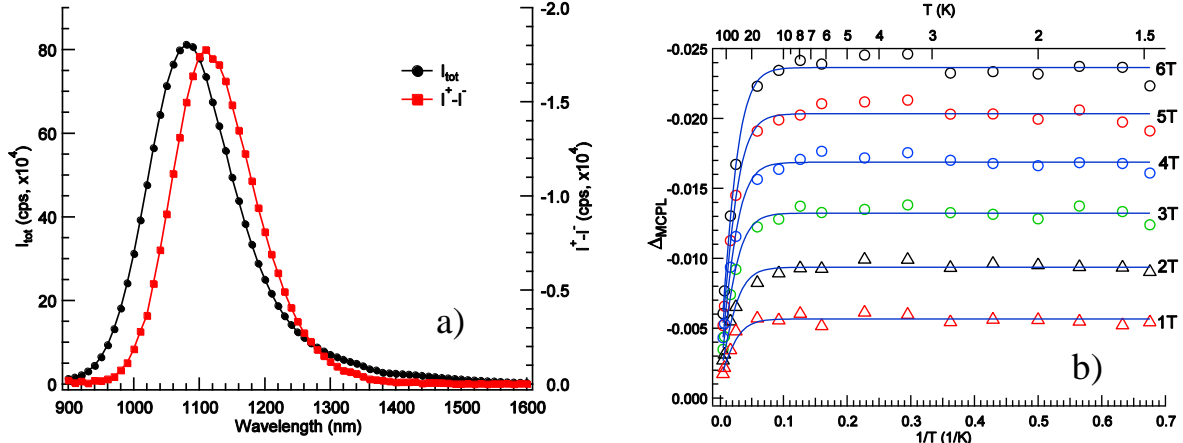


Fig. 1 a) Spectra of the NIR PL and MCPL intensities under excitation at 532 nm,  $T = 1.48$  K,  $B = 6.5$  T,  $P_{\text{exc}} = 10$  W; b) temperature dependence of the MCPL signal in different magnetic fields;  $\lambda_{\text{exc}} = 532$  nm;  $P_{\text{exc}} = 10$  W;  $\lambda_{\text{det}} = 1110$  nm.

- [1] I. Bufetov and E. Dianov, "Bi-doped fiber lasers", *Laser Phys. Lett.*, 6, 487-504 (2009).  
 [2] Y. Fujimoto and M. Nakatsuka, "Infrared luminescence from Bismuth-doped silica glass", *Jpn. J. Appl. Phys.*, 40, L279-L281 (2001).  
 [3] M. Peng, G. Dong, L. Wondraczek, L. Zhang, N. Zhang and J. Qui, "Discussion on the origin of NIR emission from Bi-doped materials", *J. Non-Cryst. Solids*, 357, 2241-2245 (2011).  
 [4] B. Denker, B. Galagan, V. Osiko, I. Shulman, S. Sverchkov, E. Dianov, "Absorption and emission properties of Bi-doped Mg-Al-Si oxide glass system", *Appl. Phys. B*, 95, 801-805 (2009).  
 [5] A. Abragam and B. Bleaney, *Electron Paramagnetic Resonance of Transition Ions* (Oxford University Press), Chapter 3 (1970).

## An Effect of Post-Pulse Generation in a Q-switched Nd:YLF laser

Andrey Shaykin, Konstantin Burdonov, Efim Khazanov

*Institute of Applied Physics of the Russian Academy of Science, 46 Ulyanov Str., N.Novgorod, 603950 Russia  
efimkhazanov@gmail.com*

Q-switched, solid-state lasers are widely used in different fields of science and engineering. After generation of a giant pulse, inversion in the active medium is usually much lower than the threshold level and the next pulse either cannot be generated or will be generated only after a long time during which the pump will again increase inversion up to the threshold level. We have revealed the effect of post-pulse generation in an Nd:YLF Q-switched laser.

At a different cavity length, the laser generated single-mode (Fig.1a), or two-mode (Fig.1b) giant pulse as usual. The round-trip cavity lengths in these two cases differ by approximately 500nm. We discovered that at intermediate cavity length, a second giant pulse was generated (Fig.2a-d). We called it post-pulse. Its duration was about 100ns, and its amplitude was always significantly lower than amplitude of the main pulse. Its delay, amplitude, and duration depend on the cavity length. If cavity length is close to single mode generation we observed weak, long post-pulse, with maximum delay 400 ns (Fig.2a). When the cavity length towards to two modes generation the post pulse becomes shorter, more intense, and closer to the main pulse (Fig.2b,c). Finally, the post-pulse leading front overlapped in time with the tail of the main pulse (Fig.2d). We observed modulation in the overlapping interval with period equals the cavity round trip - 4 ns. We conjectured that the post-pulse is always generated at a neighbouring longitudinal mode.

This hypothesis was verified in experiment. We transmitted to the photodiode the output laser radiation and replica with a delay of about 40 m. The results are shown in Fig. 3. It is clear from the figures that when the replica of the main pulse and the post-pulse overlap in time, resulting in intensity modulation with a period of the cavity round trip. Depth of this modulation varied from very small when intensities of overlapping pulses were rather different (Fig.3b) to 100% when the intensities were comparable (Fig.2c,d). This proves the fact of post-pulse generation at the neighbouring cavity longitudinal mode. We believe that the effect of post-pulse generation is possible due to holes burning in Nd:YLF.

In the majority of applications, a weak post-pulse makes no problem, as the main pulse is not modulated because of delay. With a further amplification in the saturation mode it becomes negligibly small. At the same time, the revealed effect enables controlling the cavity length, thus excluding intensity modulation in a giant pulse even though cavity length is changed in time due to thermal effects. Generation of a weak post-pulse indicates that the cavity length should be corrected so as to fully remove the post-pulse.

We revealed the effect of generation of the second giant pulse in a Q-switched Nd:YLF laser and proved that this pulse (if generated) is always at neighbouring longitudinal cavity mode. Based on this effect we have proposed and successfully approved the method of longitudinal mode selection that excludes lasing of a two-mode giant pulse with intensity modulation.

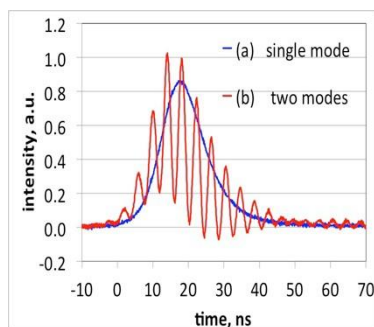


Fig.1. Single (a) and two (b) mode giant pulses (no post-pulse)

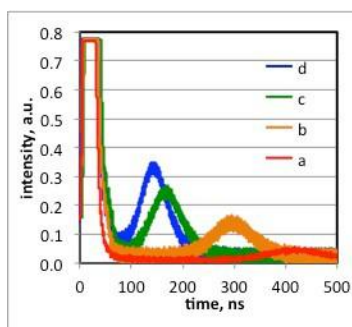


Fig.2. Post-pulse generation for different cavity length. Amplitude of the main pulse is about 3 a.u.

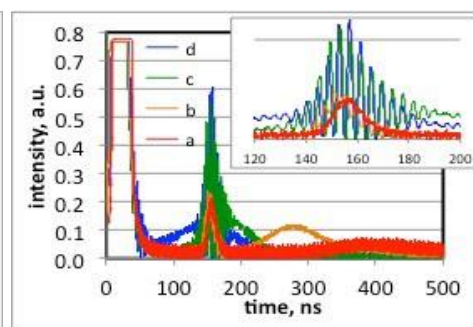


Fig.3. Output + 130ns-delayed replica pulse for different cavity length. Amplitude of the main pulse is about 3 a.u.

## Superfocusing of high- $M^2$ laser diode beams and application to optical trapping of microscopic objects

**G. S. Sokolovskii<sup>1</sup>, V. V. Dudelev<sup>1</sup>, V. Melissinaki<sup>2</sup>, S. N. Losev<sup>1</sup>,  
K. K. Soboleva<sup>3</sup>, A. G. Deryagin<sup>1</sup>, V. I. Kuchinskii<sup>1,4</sup>,  
M. Farsari<sup>2</sup>, W. Sibbett<sup>5</sup>, E. U. Rafailov<sup>6</sup>**

*1- Ioffe Institute, St. Petersburg, Russia*

*2- IESL-FORTH, Heraclion, Greece*

*3- St. Petersburg State Polytechnical University, St. Petersburg, Russia*

*4- St. Petersburg State Electrotechnical University "LETI", Saint Petersburg, Russia*

*5- University of St. Andrews, St. Andrews, UK*

*6- Aston Institute of Photonic Technologies, Aston University, Birmingham, UK*

*gs@mail.ioffe.ru*

We report on recent progress of the ‘interference’ superfocusing of high- $M^2$  laser diodes with a technique developed for generation of the Bessel beams. Focusing of the multimode laser diode beams is probably the most significant problem that hinders their expansion in many applications demanding both the high power and the spatial-quality of the laser radiation.

Generally, the ‘quality’ of laser beams is characterized by the beam propagation parameter  $M^2$  [1,2], which is a ratio of the divergence of the laser beam to that of a diffraction-limited counterpart.  $M^2$  defines the ratio of the beam focal-spot size to that of the ‘ideal’ Gaussian beam focused by the same optical system. High-power broad-stripe laser diodes have the  $M^2$  value of 20-50. This makes the focal-spot 1-2 orders of magnitude larger than the diffraction limit. The idea of the ‘interference’ superfocusing of high- $M^2$  beams relies on a technique developed for the generation of Bessel beams from laser diodes using a cone-shaped lens (axicon) [3]. With traditional focusing of the multimode radiation, different curvatures of the wave-fronts of the various constituent modes lead to a shift of their focal points along the optical axis. This in turn implies larger focal-spot sizes with correspondingly increased values of  $M^2$ . In contrast, the generation of a Bessel-type beam with an axicon relies on ‘self-interference’ of each mode thus eliminating the underlying reason for an increase in the focal-spot size [4].

In our experiments, we used a fiber-coupled laser diodes with  $M^2$  values of  $\sim 20$  and an emission wavelength in  $\sim 1\mu\text{m}$  range. Utilization of the axicons with apex angle of  $140^\circ$ , made by direct laser writing on a fiber tip [5], enables the demonstration 2-4  $\mu\text{m}$  diameter focused laser ‘needle’ beams with tens-micrometer propagation lengths. This is an order of magnitude decrease of the focal-spot size compared to that achievable using an ‘ideal’ lens of a unity numerical aperture. Utilization of the same technique using a  $160^\circ$  axicon allowed us to demonstrate few- $\mu\text{m}$ -wide laser ‘needle’ beams with about 100  $\mu\text{m}$  propagation lengths. These were utilized for optical trapping of 5-6  $\mu\text{m}$  rat blood red cells in a water-heparin solution. Our results indicate the good potential of superfocused diode laser beams for applications relating to optical trapping and manipulation of microscopic objects including with aspirations towards novel lab-on-chip configurations.

- [1] A.E. Siegman, How to (maybe) measure laser beam quality, OSA Trends in Optics and Photonics Series 17<sup>th</sup> OSA Annual Meeting (1998).
- [2] ISO Standard 11146, Lasers and laser-related equipment – Test methods for laser beam widths, divergence angles and beam propagation ratios (2005).
- [3] G.S.Sokolovskii, V.V.Dyudelev, S.N.Losev, S.A.Zolotovskaya, A.G.Deryagin, V.I.Kuchinskii, E.U.Rafailov, W.Sibbett, “Generation of propagation-invariant light beams from semiconductor light sources,” Tech. Phys. Lett. vol.34, pp.1075-1077 (2008).
- [4] G.S.Sokolovskii, V.V.Dudelev, S.N.Losev, K.K.Soboleva, A.G.Deryagin, K.A.Fedorova, V.I.Kuchinskii, W.Sibbett, E.U.Rafailov, “Bessel beams from semiconductor light sources”, Progress in Quantum Electronics, vol.38(4), pp. 157–188 (2014).
- [5] G.S.Sokolovskii, V.Melissinaki, V.V.Dudelev, S.N.Losev, K.K.Soboleva, E.D.Kolykhalova, A.G.Deryagin, V.I.Kuchinskii, E.A.Viktorov, M.Farsari, W.Sibbett, E.U.Rafailov, “Superfocusing of high- $M^2$  semiconductor laser beams: experimental demonstration”, Proc. SPIE, vol. 9134, 9134-57 (2014).

**Controlled Raman amplification and generation of intense lasers with orbital angular momentum in plasmas**

**J. Vieira<sup>1</sup>, R. Trines<sup>2</sup>, E.P. Alves<sup>1</sup>, J.T. Mendonça<sup>1</sup>, R. Bingham<sup>2</sup>, L.O. Silva<sup>1</sup>**

<sup>1</sup> *GoLP/Instituto Superior Tecnico, Universidade de Lisboa, Portugal*

<sup>2</sup> *CLF/STFC Rutherford Appleton Laboratory and Lancaster University*

Since the seminal work by L. Allen et al [1], an abundance of new applications has been identified for laser beams with Orbital Angular Momentum (OAM), including super-resolution microscopy, quantum computation or ultra-fast optical communications. The potential of OAM light for laser-plasma interactions, however, is yet to be fully realized. One of the topics where OAM lasers could have a major impact is laser-wakefield acceleration [2]. Laser-wakefield acceleration requires a high intensity (above  $10^{18}$  W/cm<sup>2</sup>) laser beam to excite relativistic plasma waves with electric fields in excess of 1 GV/cm. The use of intense OAM light has thus been recently proposed as a driver for large amplitude plasma waves capable to accelerate electrons and positrons to high energies [3].

Typical configurations for OAM light generation, however, have not yet been able to produce laser beams with OAM at the high intensities required for laser plasma interactions. To this end, we explore stimulated Raman backscattering of OAM lasers in plasmas [4]. We show analytically and through three-dimensional particle-in-cell simulations using the code Osiris [5], that Raman amplification can be used to amplify OAM modes to the required intensities for relativistic laser plasma interactions. In addition, we demonstrate that Raman backscattering can be used to generate lasers with new, well-defined OAM modes, which are not present initially in the laser beams that drive the instability [6]. We also demonstrate generation and amplification of light with arbitrarily large OAM states through cascading processes. This work opens new perspectives for the use of OAM light in relativistic laser plasma interactions.

[1] L. Allen et al, Phys. Rev. A 8185 (1992).

[2] T. Tajima and J. Dawson, Phys. Rev. Lett. 43, 267 (1979).

[3] J. Vieira and J.T. Mendonça, Phys. Rev. Lett. 112 215001 (2014).

[4] J. T. Mendonça et al, Phys. Rev. Lett. 102 185005 (2009).

[5] R.A. Fonseca et al, Lecture Notes in Computer Science, Vol. 2331, p. 342 (2002).

[6] J. Vieira et al, in preparation (2014).

## Extended performance of the L2I high intensity laser facility

Gonçalo Figueira<sup>1\*</sup>, Joana Alves<sup>1,2</sup>, Luís Cardoso<sup>1</sup>, João M. Dias<sup>1</sup>, Marta Fajardo<sup>1</sup>, Nuno Gomes, Victor Hariton<sup>1</sup>, Tayyab Imran<sup>3</sup>, Jiasheng Jiang<sup>1</sup>, Celso P. João<sup>1</sup>, Swen Kunzel<sup>1</sup>, Nelson C. Lopes<sup>1</sup>, Hugo Pires<sup>1</sup>, Filipe Ruão<sup>1</sup>, and Gareth Williams<sup>1</sup>

<sup>1</sup> GoLP/Instituto de Plasmas e Fusão Nuclear – Laboratório Associado, Instituto Superior Técnico, Universidade de Lisboa, Portugal

<sup>2</sup> Faculdade de Ciências e Tecnologia, Universidade Nova de Lisboa, Portugal

<sup>3</sup> Department of Physics, College of Science, King Saud University, Riyadh, Saudi Arabia

\*E-mail: [goncalo.figueira@ist.utl.pt](mailto:goncalo.figueira@ist.utl.pt)

The Laboratory for Intense Lasers (L2I) is one of the leading research centers in optics and lasers in Portugal, having been recently selected to a top group of a research infrastructures of strategic relevance. It is dedicated to experimental research in high intensity laser science and technology, ultrashort diagnostics and laser plasma interaction, with emphasis in plasma particle accelerators, high harmonic generation and advanced radiation sources.

The main laser of L2I is a 15 terawatt Ti:sapphire-Nd:glass system, based on the chirped pulse amplification technique, and operating at 1053 nm. Over the past years we have been developing a diode-pumped laser program, with the objectives of improving the experimental capability of the laboratory. This was mainly motivated by the need to increase the shot repetition rate at the 100 mJ level. The work has also led to the development of compact pre-amplifiers based on a single chirped volume Bragg grating for pulse chirping [1].

On the other hand, the compactness and efficiency of ytterbium-doped, diode-pumped lasers makes this technology very attractive for pumping optical parametric amplifiers. We have carried out in parallel an optical parametric chirped pulse amplification (OPCPA) program based on ultrabroadband, noncollinear amplification in the nonlinear crystal YCOB [2], with the objective of providing mJ-level, sub-20 fs pulses for experiments.

In this work we describe the implementation of the three beam capability at L2I, in particular evaluating the potential of the ultrabroadband OPCPA system [5]. With the successful conclusion of a dual-stage, diode-pumped amplifier based on Yb:CaF<sub>2</sub> and Yb:YAG operating at 1030 nm / 100 mJ / 1 Hz, making this beam available for experiment, we have recently started the development of a high-energy, frequency-doubled pump pulse for OPCPA.

### Acknowledgments

This work is partially supported by Fundação para a Ciência e a Tecnologia, Laserlab-Europe (EC's FP7, grant agreement no. 284464), and Association EURATOM/IST.

### References

- [1] C. P. João, H. Pires, L. Cardoso, T. Imran and G. Figueira, "Dispersion compensation by two-stage stretching in a sub-400 fs, 1.2 mJ Yb:CaF<sub>2</sub> amplifier", Opt. Express 22, 10097 (2014).
- [2] H. Pires, M. Galimberti and G. Figueira, "Numerical evaluation of ultrabroadband parametric amplification in YCOB", J. Opt. Soc. Am. B 31, 2608 (2014).

## **Potassium-Helium Diode Pumped Alkali Vapor laser**

**B.V. Zhdanov, M.D. Rotondaro and R.J. Knize**

*US Air Force Academy, Laser and Optics Research Center, 2354 Fairchild Dr.,  
Ste. 2A31, USAF Academy, CO 80840, USA*

*boris.zhdanov.ctr@usafa.edu*

This talk presents the results of our experiments on development of a hydrocarbon free Potassium Diode Pumped Alkali Laser (DPAL). For our experiments we have chosen a so called “low pressure DPAL approach”, which uses buffer gas pressure of about 1 atm for spin-orbit mixing of the excited states of alkali atoms to provide population inversion in the gain medium. This approach has several advantages compared to the “high pressure (more than 10 atm) DPAL approach”, but requires significant narrowbanding of the emission line of the pumping laser diodes (to the value less than 20 GHz), which was done using a technique developed in our lab. The experiments were performed using both static and flowing gain medium. For the second case we designed and built a closed cycle flowing system to circulate the gain medium through the laser cell, which also allowed varying the buffer gas pressure, gain medium temperature and flow rate. In our experiments, we studied the performance of this laser both in CW and pulsed modes with different pulse duration and observed output power degradation in time from the initial value to the level corresponding to the CW mode of operation. To study possible contribution of thermal effects we used low power probe beam from HeNe laser propagating through the lasing gain medium. Also we recorded a fluorescence spectrum from the lasing gain medium which allowed us to analyze contribution of such effects as energy pooling collisions and ionization + recombination. As a result of these experiments, we demonstrated a first Potassium DPAL operating in CW mode with efficiency higher than 30%.

# Efficient TEM<sub>00</sub> laser action in a short-length heavily Yb-doped composite fiber with phosphate core and silica cladding

O. N. Egorova<sup>1</sup>, S. L. Semjonov<sup>1</sup>, O. I. Medvedkov<sup>1</sup>, M. S. Astapovich<sup>1</sup>,  
A. G. Okhrimchuk<sup>1</sup>, E. M. Dianov<sup>1</sup>, B. I. Denker<sup>2</sup>, B. I. Galagan<sup>2</sup>, S. E. Sverchkov<sup>2</sup>

1- Fiber Optics Research Center, Russian Academy of Sciences, 38 Vavilov Street, 119333 Moscow, Russia

2- General Physics Institute, Russian Academy of Sciences, 38 Vavilov Street, 119991 Moscow, Russia

egorova@fo.gpi.ru

Heavily rare-earth-doped phosphate glass fibers, with both core and cladding manufactured from phosphate glass, are promising media for laser applications where a short cavity is required. But phosphate glass fibers suffer from serious drawbacks. First, fusion splicing of phosphate glass fibers with silica fibers is difficult, owing to highly different physical properties of these two glasses. Second, phosphate glass is prone to water absorption, which could result in degradation of the fiber even with polymer coating. In [1,2], the possibility of manufacturing a composite fiber with phosphate glass core and silica cladding has been demonstrated. Silica cladding facilitates the splicing process, provides more mechanically reliable joints as compared to phosphate glass fiber joints, and protects the phosphate core from degradation. But the large difference in the refractive indices of silica and phosphate glass resulted in a considerable difference in the refractive indices between the core and cladding. Thus the composite fiber was multimode even with a relatively small core diameter. This could be a significant drawback because many applications require high beam quality. In this paper, we demonstrate the possibility of achieving high-beam quality laser action in an Yb-doped ( $5 \times 10^{20} \text{ cm}^{-3}$ ) phosphate core/silica cladding fiber. The laser cavity was constructed using a fiber Bragg grating, with a reflectivity of more than 99 % at 1018 nm, and a fiber end-face (see Fig.1). The slope efficiency (73-74%) was observed at active fiber lengths in the 48 to 90 mm range (Fig.2). Despite the fact that the active fiber was not single-mode at the lasing wavelength, the measured  $M^2$  factors were as low as 1.05-1.22 at a pump power of 200 mW. The reason for this was that one of the ends of the cavity was formed by a Bragg grating written in a single-mode fiber that was spliced with the active fiber. This provided suppression of higher order modes in the cavity. To achieve lasing at shorter fiber length, we used a fiber Bragg grating with 30% reflectivity at the output. Lasing at an active fiber length of 25 mm was achieved with 50% slope efficiency with respect to launched pump power. Thus, because of its very high beam quality and high efficiency phosphate glass core – silica cladding composite fiber has potential application where a short cavity and high lasing efficiency are required.

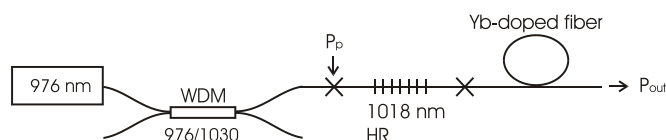


Fig.1. Scheme of Yb<sup>3+</sup>-doped laser.

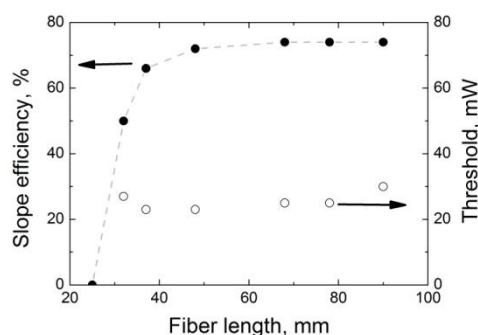


Fig.2. Slope efficiency with respect to the launched pump power (filled circles) and threshold (open circles) versus active fiber length.

This work was supported by RFBR grants #13-02-00571 and # 14-29-08168.

[1] R.A. Martin and J.C. Knight, "Silica-clad neodymium-doped lanthanum phosphate fibers and fiber lasers," IEEE Photonics Technology Letters, **18**, pp. 574–576 (2006).

[2] O.N. Egorova, S.L. Semjonov, V.V. Velmiskin, Y.P. Yatsenko, S.E. Sverchkov, B.I. Galagan, B.I. Denker, and E.M. Dianov, "Phosphate-core silica-clad Er/Yb-doped optical fiber and cladding pumped laser," Optics Express, **22**, 7, pp.7632–7637 (2014).

## Temporal Localized Structures in VCSELs with delays

Invited talk - International Conference on Advanced Laser Technologies (ALT)

Dr Julien Javaloyes

E-mail: [julien.javaloyes@uib.es](mailto:julien.javaloyes@uib.es)

Web: <http://www.uib.eu/personal/ABTixNDUx/> ("Ramon y Cajal" Researcher)

**Affiliation:** Departament de Física, Edifici Mateu Orfila, Universitat de les Illes Balears.

Cra. de Valldemossa, km 7.5. E-07122 Palma, SPAIN. Tel: +34 971 61 17 33, Fax: +34 971 61 17 61

**Abstract:** Localized structures are nonlinear inhomogeneous states of dissipative extended systems characterized by a correlation range much shorter than the size of the system, thus allowing for individual addressing. In this presentation we will review the results recently obtained on Temporal Localized Structures (TLS) in VCSELs coupled to an external cavity. We show that, when the cavity round-trip is much larger than the medium timescales, this system exhibits a temporal aspect-ratio large enough to host TLS. Three configurations will be considered. In the first one the system is submitted to cross-polarization re-injection which leads to the formation of vectorial TLS [1, 2]. Here the TLS are interpreted as topological kinks in the polarization that is circling around the equator of the Stokes Sphere. In the second one the external cavity is closed by a Resonant Saturable Absorber Mirror, a scheme conventionally used to obtain mode-locked pulses [3, 4]. Here we will show how TLS can be obtained from the well known regime of mode-locking. The third setup combines optical feedback and optical injection with leads to the regeneration of optical phase slips that we interpret as overdamped Sine-Gordon Solitons [5].

### Recent relevant papers:

- [1] M. Marconi, J. Javaloyes, S. Barland, S. Balle, and M. Giudici. Vectorial dissipative solitons in vertical-cavity surface-emitting lasers with delays. <http://arxiv.org/abs/1406.0730>, under revision, 2014.
- [2] J. Javaloyes, M. Marconi, and M. Giudici. Phase dynamics in vertical-cavity surface-emitting lasers with delayed optical feedback and cross-polarized reinjection. *Phys. Rev. A*, 90:023838, Aug 2014.
- [3] M. Marconi, J. Javaloyes, S. Balle, and M. Giudici. How lasing localized structures evolve out of passive mode locking. *Phys. Rev. Lett.*, 112:223901, Jun 2014.
- [4] M. Marconi, J. Javaloyes, S. Balle, and M. Giudici. Passive mode-locking and tilted waves in broad-area vertical cavity surface emitting lasers. *Selected Topics in Quantum Electronics, IEEE Journal of*, PP(99):1\_1, 2014.
- [5] B. Garbin, J. Javaloyes, G. Tissoni, and S. Barland. Topological solitons as addressable phasebits in a driven laser. *Nat. Com.*, 6, 2015.

## Performance analysis of thermally bonded Er,Yb:glass/Co:MALO microchip lasers

J. Mlynczak<sup>1</sup>, N. Belghachem<sup>1</sup>, K. Kopczynski<sup>1</sup>

*1-Institute of Optoelectronics, Military University of Technology, Kaliskiego 2 Str., 00-908 Warsaw, Poland*

*Main author email address: jaroslaw.mlynczak@wat.edu.pl*

Eye safe microchip lasers have found many applications in such fields as telecommunication or remote sensing and ranging. Thus there are many articles concerning investigation of such lasers operating at 1.5  $\mu\text{m}$  [1-8]. Researchers put a lot of effort into enhancing such output parameters as pulse peak power and pulse width [7-9]. Erbium and ytterbium doped glass was proven to be very efficient active media for 1.5  $\mu\text{m}$  generation while  $\text{MgAl}_2\text{O}_4$  (MALO) crystal doped with cobalt ions turned out to be the most adequate saturable absorber for pulse generation [5, 9].

In our work, we developed enhanced microchip laser based on a new type of erbium ytterbium doped glass PAL 77 thermally bonded with Co MALO saturable absorber. The obtained pulses had the peak power of almost 8 kW and a pulse width between 2.9 and 4 ns. More details concerning these results will be presented at the conference. The generation parameters such as peak power, pulse width, generated spectrum and beam quality of thermally bonded microchip laser will be compared with the parameters of unbonded microchip laser.

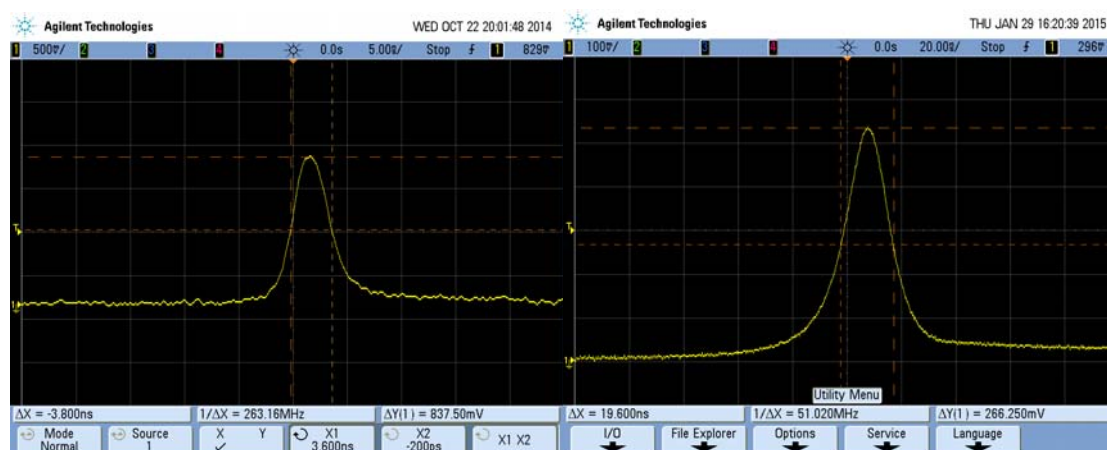


Fig. 1. Pulse width of bonded sample (left) and unbonded sample (right)

- [1] P. Laporta, S. De Silvestri, V. Magni, O. Svelto, Diode-pumped cw bulk Er:Yb:glass laser, *Opt. Lett.*, vol 16, pp. 1952-1956 (1991).
- [2] J. Mlynczak, K. Kopczynski, Z. Mierczyk, M. Malinowska, P. Osiwianski, Comparison of cw laser generation in  $\text{Er}^{3+}$ ,  $\text{Yb}^{3+}$ : glass microchip lasers with different types of glasses, *Opto-electron. Rev.* vol. 19, pp. 491-495 (2011).
- [3] T. Schweizer, T. Jensen, E. Heumann, G. Huber, Spectroscopic properties and diode pumped 1.6  $\mu\text{m}$  laser performance in Yb-codoped Er:  $\text{Y}_3\text{Al}_5\text{O}_{12}$  and Er:  $\text{Y}_2\text{SiO}_5$ , *Opt. Commun.* vol. 118, pp. 557-561 (1995).
- [4] B. Denker, B. Galagan, V. Osiko, S. Sverchkov, Materials and components for miniature diode-pumped 1.5  $\mu\text{m}$  erbium glass lasers, *Laser Phys.* vol. 12, pp. 697-701 (2002).
- [5] J. Mlynczak, K. Kopczynski, Z. Mierczyk, M. Malinowska, P. Osiwianski, Pulse generation at 1.5  $\mu\text{m}$  wavelength in new EAT14 glasses doped with  $\text{Er}^{3+}$  and  $\text{Yb}^{3+}$  ions, *Opto-electro. Rev.* vol. 20, pp. 87-90 (2012).
- [6] J. Sulc, H. Jelinkova, W. Ryba-Romanowski, T. Lukasiewicz, 1.6  $\mu\text{m}$  microchip laser, *Laser Phys. Lett.* vol. 6, pp. 207-211 (2009).
- [7] Y. Chen, J. Huang, Y. Zou, Y. Lin, X. Gong, Z. Luo, Y. Huang, Diode-pumped passively Q-switched  $\text{Er}^{3+}$ : $\text{Yb}^{3+}$ : $\text{Sr}_3\text{Lu}_2(\text{BO}_3)_4$  laser at 1534 nm, *Opt. Exp.* vol. 22, pp. 8333-8338 (2014).
- [8] G. Karlsson, F. Laurell, J. Tellefsen, B. Denker, B. Galagan, V. Osiko, S. Sverchkov, Development and characterization of Yb-Er laser glass for high average power laser diode pumping, *Appl. Phys. B*, vol. 75, pp. 41-46 (2002).
- [9] G. Karlsson, V. Pasiskevicius, F. Laurell, J. Tellefsen, B. Denker, B. Galagan, V. Osiko, S. Sverchkov, Diode-pumped Er-Yb:glass laser passively Q switched by use of  $\text{Co}^{2+}$ : $\text{MgAl}_2\text{O}_4$  as a saturable absorber, *Appl. Opt.* vol. 39, pp. 6188-6192 (2000).

# Spectral gain function in Nd, Y-codoped CaF<sub>2</sub> single crystals

V.A. Kamynin, A.Ya. Karasik, V.A. Konyushkin, V.F. Seregin, A.I. Trikshev,  
V.B. Tsvetkov

General Physics Institute, Vavilov str., 38, 119991, Moscow, Russia  
e-mail: tsvetkov@lsg.gpi.ru

Laser materials based on fluorides have a number of essential advantages in comparison with oxide materials, especially for creation of wide spectral range amplifiers or ultra-short pulses generation. Mixed fluoride crystals can be doped by rare-earth ions with high concentration (up to  $10^{21}$  cm<sup>-3</sup>) without essential luminescence quenching.

Despite the old history of research of Nd-doped yttrifluorite crystals (CaF<sub>2</sub>-YF<sub>3</sub>-NdF<sub>3</sub>), direct researches of gain coefficient were not done. However the real spectral function of the gain coefficient is very important for a number of applications. In our research the spectral gain characteristics have been investigated for two compositions of the mixed fluoride crystals — (AE1) CaF<sub>2</sub>-YF<sub>3</sub>(12wt.%) -NdF<sub>3</sub>(2wt. %) and (AE2) CaF<sub>2</sub>-YF<sub>3</sub>(5wt.%) -NdF<sub>3</sub>(2wt.%). The luminescence spectra of crystals with the yttrium fluoride content 5 and 12 wt.% are similar (Figure 1) unlike a case of smaller concentration of YF<sub>3</sub> [1].

The experimental spectral function of the small-signal gain coefficient is resulted in Figure 2.

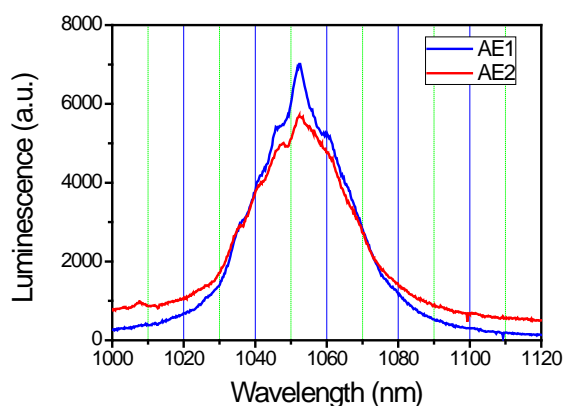


**Fig.1.** Room temperature emission spectra of the <sup>4</sup>F<sub>3/2</sub> — <sup>4</sup>I<sub>11/2</sub> transition in Nd:CaF<sub>2</sub>-YF<sub>3</sub> crystals.

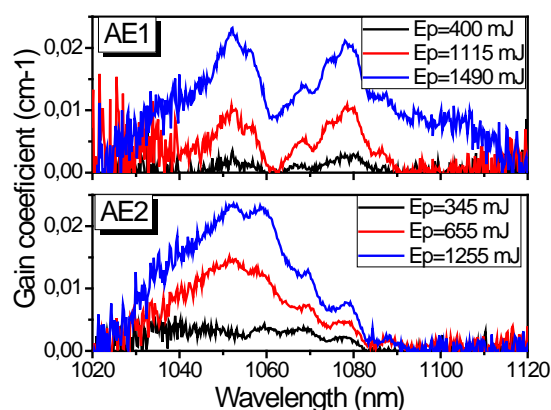


**Fig.2.** Gain coefficient for Nd:CaF<sub>2</sub>-YF<sub>3</sub> crystals.

It is visible, that the spectral gain coefficient differs for the crystals with different YF<sub>3</sub> content. Besides, it is known, that in a lasing spectrum of yttrifluorite crystals two characteristic lines B and C, corresponding to the different optical centers of Nd<sup>3+</sup> ion in a crystal are observed. The lasing wavelength for the centers B and C makes about 1054 nm and 1063 nm accordingly [2,3]. From Figure 2 one could see that the gain value at 1075 nm wavelength is comparable with the one at 1054 nm and considerably surpasses the gain at 1063 nm. However the 1075 nm line is not observed in experiment. It can testify that for a luminescence (gain) at 1075 nm the centers B are mainly responsible, therefore the lasing occurs at a wavelength corresponding to bigger gain value (1054 nm).

In summary it is possible to notice, that both compositions provide high gain at the wavelength around 1054 nm and can be used as a part of laser systems based on Nd-glass active medium. The crystals composition CaF<sub>2</sub>-YF<sub>3</sub>(12wt.%) -NdF<sub>3</sub> will have advantage for ultrashort pulses generation over CaF<sub>2</sub>-YF<sub>3</sub>(5wt.%) -NdF<sub>3</sub> crystals.

## References

- [1] L. B. Su, Q. G. Wang, H. J. Li, G. Brasse, P. Camy, J. L. Doualan, A. Braud, R. Moncorgé, Y. Y. Zhan, L. H. Zheng, X. B. Qian and J. Xu, Spectroscopic properties and CW laser operation of Nd, Y-codoped CaF<sub>2</sub> single crystals, *Laser Phys. Lett.* **10**, 035804 (2013)
- [2] A. A. Kaminskii, Procedure for the investigation of auto-resonant energy transfer in laser active media, *Soviet physics JETP*, **27**, No.6, 889 (1968)
- [3] I. Iparraguirre, J. Azkargorta, J. Fernández, R. Balda, A. Oleaga, A. A. Kaminskii, Laser spectral dynamics of Nd<sup>3+</sup> in CaF<sub>2</sub>-YF<sub>3</sub> crystals, *J. Opt. Soc. Am. B*, **16**, No. 9, 1439 (1999)

## **Automatic system for gauge block calibration using optical interferometry**

**Z. Buchta, M. Čížek, M. Šarbort, V. Hucl, J. Lazar, O. Číp**

*Institute of Scientific Instruments of the Czech Academy of Sciences, v. v. i., Královopolská 147, 612 64 Brno, Czech Republic*

*buchta@isibrno.cz*

This paper presents a fully automatic system for gauge blocks calibration based on a novel principle combining low-coherence interferometry and laser interferometry. The designed optical system combines a Dowell interferometer and a Michelson interferometer to ensure the gauge block length measurement with direct traceability to the primary length standard [1]. The key advantage of the presented optical setup is its contactless measurement of the absolute gauge block length done as a single-step measurement giving complete information of the gauge block length, without any additional gauge block manipulation or any length comparison with a reference dimension.

Since gauge blocks are typically delivered in large sets to overlap entire measurement range of instruments intended to be calibrated, it make sense to combine the optical setup with an automatic gauge block changer to reach high-effectivity of the calibration process. In our system, we employ the automatic handling system designed for a set of 126 gauge blocks (up to 100 mm in length). By series of movements, each of those gauge blocks is placed on the carrier which transports the gauge block into the optical setup. The carrier positioning is controlled by optical sensor monitoring the transported gauge block position to place the block correctly onto the gauge block holder. Then, the gauge block is aligned to the measuring beam to minimize a cosine measurement error [2]. Working in this way, the measurement is fully automatic and allows the automatic contactless calibration without a human operator presence. Pilot experimental results compared with the reference numbers are presented in this article too.

**Acknowledgements:** The research was supported by Technology Agency of CR, project no. TA03010663. The research infrastructure was funded by the Ministry of Education, Youth and Sports CR, projects LO1212, CZ.1.05/2.1.00/01.0017, and by Academy of Sciences CR, project RVO: 68081731.

[1] Z. Buchta, Š. Řeřucha, B. Mikel, M Čížek, J. Lazar and O Číp, Novel Principle of Contactless Gauge Block Calibration, *Sensors*, vol. 12, pp. 3350-3358, (2012).

[2] Z. Buchta, Š. Řeřucha, V. Hucl, M Čížek, M. Šarbort, J. Lazar and O Číp, Active angular Alignment of Gauge Blocks in Doble-Ended Interferometers, *Sensors*, vol. 13, pp. 13090-13098, (2013).

## Optical properties of Nd,Cr-codoped crystals for solar-pumped lasers

T. Ogawa<sup>1</sup>, S. Wada<sup>1</sup>, M. Higuchi<sup>1,2</sup>

1- RIKEN Center for Advanced Photonics, 2-1 Hirosawa, Wako, Saitama 351-0198 Japan

2- Graduate School of Engineering, Hokkaido University, N13, W8, Kita-Ku, Sapporo, Hokkaido 060-8628, Japan

pogawa@riken.jp

Sunlight is well known as an important source of clean energy. One way to use solar energy is to convert it to laser energy. Since electrical power is not required for such a laser, this next-generation technology offers great promise for the future. However, since the conversion efficiency from solar energy to laser energy is only a few percent, such lasers are not yet in practical use [1-3]. To improve the efficiency of solar-pumped lasers, the selection of a suitable crystal is the most important factor. Large and broad absorption from the ultraviolet to visible region and high thermal conductivity to allow high-energy pumping are required for the crystal of solar-pumped lasers.

In this work, Nd<sup>3+</sup>,Cr<sup>3+</sup>-codoped YVO<sub>4</sub> and CaYAlO<sub>4</sub> crystals were grown for the first time to the best of our knowledge. Nd:YVO<sub>4</sub> is a laser crystal with a large emission cross section. Figure 1 shows absorption spectra of Nd,Cr:YVO<sub>4</sub> crystals. We found a strong and wide absorption band in the ultraviolet region upon the addition of Cr ions.

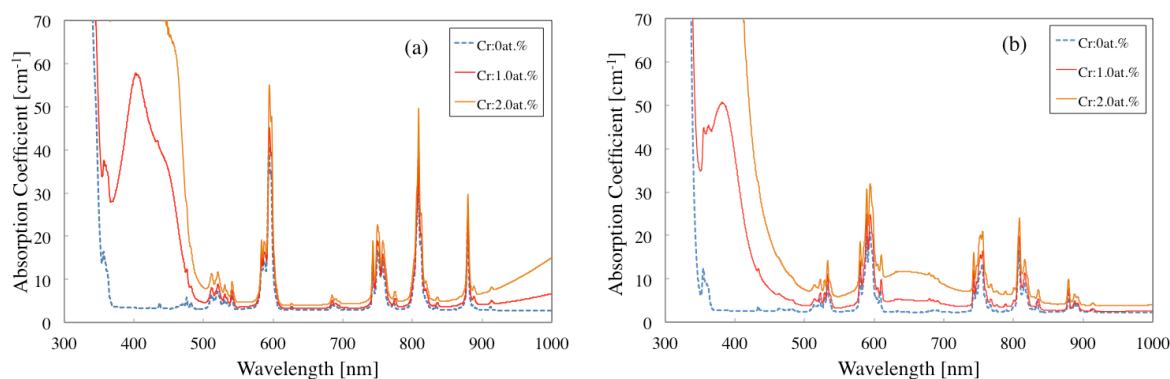


Fig. 1 Absorption spectra of Nd,Cr:YVO<sub>4</sub> crystals showing (a)  $\pi$ - and (b)  $\sigma$ -polarization.

Furthermore, the absorption cross section of Nd,Cr:CaYAlO<sub>4</sub> around 400 nm was more than 70 times that of Nd,Cr:YAG crystals. We also measured the fluorescence spectra of these crystals. Fluorescence at 1  $\mu$ m was observed by pumping at 400 nm. This indicates that energy transfer from Cr to Nd occurred effectively. The above results suggest that these crystals have potential for use in efficient solar-pumped lasers. We are currently developing a solar-pumped laser system using these crystals. We believe that solar-pumped lasers will become an important tool for renewable energy generation.

Acknowledgement :

This work was supported by JSPS KAKENHI Grant Number 24686108.

[1] T. Ohkubo, T. Yabe, K. Yoshida, S. Uchida, T. Funatsu, B. Bagheri, T. Oishi, K. Daito, M. Ishioka, Y. Nakayama, N. Yasunaga, K. Kido, Y. Sato, C. Baasandash, K. Kato, T. Yanagitani, and Y. Okamoto: Opt. Lett. 34, 175 (2009).

[2] S. Mizuno, H. Ito, K. Hasegawa, T. Suzuki, and Y. Ohishi: Opt. Express 20, 5891 (2012).

[3] T. Saiki, M. Nakatsuka, K. Fujioka, S. Motokoshi, K. Imasaki, and Y. Iida: Opt. Photonics Lett. 6, 1350003 (2013).

# Spatiotemporal transformation of 3D optical pulses using phase-shifted Bragg grating

**L. Doskolovich, D. Bykov, N. Golovastikov**

*Image Processing Systems Institute of the Russian Academy of Sciences,  
151 Molodogvardeiskaya st., Samara 443001, Russia  
Technical Cybernetics Department, Samara State Aerospace University,  
151 Molodogvardeiskaya st., Samara 443001, Russia*

leonid@smr.ru

Optical devices that perform temporal and spatiotemporal transformations of optical signals are of great interest for a wide range of applications including ultrafast all-optical information processing and analog optical computations. Among the most important operations of the analog processing of optical signals are the operations of temporal and spatial differentiation and integration. Temporal differentiation and integration of optical pulses can be performed with a phase-shifted Bragg grating (PSBG) [1, 2]. The use of PSBG for spatial differentiation and integration of 2D optical beams was proposed in the authors' recent works [3, 4]. In particular, it was shown that PSBG can be used for the optical computation of the first and the second derivatives of 2D incident beam profile in reflection regime [3]. The operation of 2D spatial integration is performed in the transmission regime [4]. At the same time, the use of PSBG for spatial transformations of 3D optical beams and for spatiotemporal transformations of 3D optical pulses has not been considered yet.

In the present work, we propose a new theoretical model describing spatiotemporal transformations of 3D optical pulses by a PSBG. The diffraction of a 3D optical pulse on a PSBG is described in terms of linear systems. Simple analytical approximations for the transfer function and the impulse response of the system are derived. The presented numerical simulation results demonstrate that the PSBG can perform complex pulse transformations, such as simultaneous spatial and temporal differentiation of the optical pulse envelope. As a special case, we consider spatial transformations of 3D monochromatic optical beams by PSBG. In this case, the possibility of the optical computation of the Laplace operator in spatial coordinates using a PSBG is demonstrated (see Fig. 1).

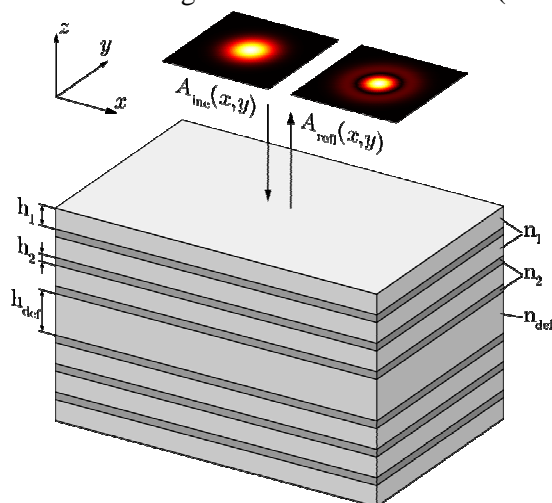


Figure 1. A phase-shifted Bragg grating. Transverse field distributions of the reflected beam (right) corresponding to the Laplacian of the incident field (left) are shown.

This work was supported by RSF grant 14-19-00796, and RFBR grants 13-07-00464, 15-07-00548.

[1] N.K. Berger, B. Levit, B. Fischer, M. Kulishov, D.V. Plant, José Azaña // Temporal differentiation of optical signals using a phase-shifted fiber Bragg grating // *Opt. Exp.*, 15, 371-381 (2007).

[2] N.Q. Ngo, Design of an optical temporal integrator based on a phase-shifted fiber Bragg grating in transmission, *Opt. Lett.*, 32, 3020-3022 (2007).

[3] L.L. Doskolovich, D.A. Bykov, E.A. Bezus, and V.A. Soifer, Spatial differentiation of optical beams using phase-shifted Bragg grating, *Opt. Lett.*, 39, 1278-1281 (2014)

[4] N.V. Golovastikov, D.A. Bykov, L.L. Doskolovich, E.A. Bezus, Spatial optical integrator based on phase-shifted Bragg gratings, *Opt. Comm.*, 338, 457-460 (2015).

# Laser Beam Profile Shaping by Means of Acousto-Optics

**S.I. Chizhikov, V.Ya. Molchanov, K.B. Yushkov**

*Acousto-Optical Research Center, National University of Science and Technology "MISIS",  
4 Leninsky prospect, 119049 Moscow, RUSSIA*

*Main author email address: aocenter@isis.ru*

Spatial profiling of laser beams is an urgent problem in design of high-power laser systems. One of the common methods of solving this problem is using soft-edge diaphragms [1, 2]. Traditional soft-edge diaphragms are fabricated as stationary amplitude masks that suppress diffraction of laser beams by the edges of the aperture. This design principle sufficiently limits adaptivity of the soft-edge diaphragms.

In the report, we propose a novel adaptive method of flat-top diffraction-free spatial shaping of laser beams based on acousto-optic (AO) Bragg interaction. For implementation of this method, transformation of laser beam plane wave spectrum due to angular selectivity of isotropic Bragg diffraction is used.

Diffraction of divergent laser beams by divergent ultrasound in the strong-field limit was studied in Ref. [3]. According to that results, distribution of diffracted laser field  $E^d(x, z)$  can be expressed as

$$E^d(x, z) = \frac{\pi}{\lambda} E_2^0(z) \int_{-\infty}^{\infty} E_1^0(x - x') J_0 \left( 2\pi \frac{W}{\lambda} \sqrt{\left(\frac{L\lambda}{2\Lambda}\right)^2 - x'^2} \right) \text{rect}\left(\frac{\Lambda}{L\lambda} x'\right) dx', \quad (1)$$

where  $E^0(x, z) = E_1^0(x)E_2^0(z)$  is the spatial distribution of input laser beam along orthogonal coordinates  $x$  and  $z$ ;  $W$  is the ultrasonic power parameter;  $\lambda$  and  $\Lambda$  are the wavelength of light and ultrasound;  $L$  is the length of AO interaction.

For the incoming Gaussian laser beam with the waist radius  $w_0$ , Eq. (1) in the weak-field limit can be integrated analytically. The result is expressed as

$$E^d(x, z) \sim \exp\left(-\frac{z^2}{w_0^2}\right) \left[ \text{erf}\left(\frac{x}{w_0} + a\frac{\pi}{4}\right) - \text{erf}\left(\frac{x}{w_0} - a\frac{\pi}{4}\right) \right], \quad (2)$$

where  $a = 2\lambda L / (\pi w_0 \Lambda)$ . According to Eq. (2), the diffracted field has a flat-top shape along the diffraction plane and remains Gaussian in orthogonal plane. Thus, an AO Bragg cell can be considered as adaptive one-dimensional soft-edge diaphragm. The edge width in the field distribution is determined by the parameter  $a$ . To perform rectangular beam shaping, a two-coordinate Bragg cell can be used.

During AO interaction in weak-field limit, the angular spectrum of the diffracted field is a product of the angular spectrum of incoming light and the angular spectrum of ultrasound. As a result, the angular spectrum of the diffracted field is always narrower, than the angular spectrum of the incoming light. That makes the principal difference with diffraction of light by the aperture, when the angular spectrum always widens. Thus, controlling of the spectral components of the ultrasonic field one can affect the spatial distribution of the diffracted light.

Experimental Bragg cell was designed and fabricated from dense flint glass. The experiments were performed with single-frequency emission of frequency-doubled Nd:YAG laser at the wavelength 532 nm. Adaptive amplitude apodization of the laser beam distribution corresponded to the theoretical predictions.

[1] I.K. Krasnyuk, S.G. Lukishova, P.P. Pashinin, et al., Forming transversal distribution of laser beam intensity by means of "soft" diaphragms, *Sov. J. Quantum Electron.*, vol. 3, pp. 1337-1339 (1976).

[2] L.M. Vinogradsky, V.A. Kargin ; S.K. Sobolev, et al., Soft diaphragms for apodization of powerful laser beams, *Proc. SPIE*, vol. 3889, p. 849-860 (2000).

[3] L.N. Magdich and V.Ya. Molchanov, Diffraction of divergent beams by intense acoustic waves, *Opt. Spectrosc.*, vol. 42, p. 533 (1977).

# High Repetition Rate Picosecond and Nanosecond 1342 nm Laser for Micromachining and High Order Harmonics Conversion

**A.M. Rodin<sup>1,2</sup>, M. Grishin<sup>1,2</sup>, A. Michailovas<sup>1,2</sup>**

1- Solid State Laser Laboratory, Dept. of Laser Technologies, Center for Physical Sciences and Technology, Savanoriu 231, LT-02300 Vilnius, Lithuania

2- UAB Ekspla, Savanoriu 237, LT-2053 Vilnius, Lithuania

aleksej.rodin@ftmc.lt

Laser emission near 1342 nm wavelength has applications in selective scribing and stealth dicing, high order 224 nm and 192 nm harmonics generation, surgical treatment and deep tissue imaging in biology and medicine. Efficient wavelength conversion into the red 671 nm by 2nd harmonic generation or into the blue 447 nm by the sum frequency mixing is attractive for RGB displays, spectroscopy, medical diagnostics and treatment. The known approaches to manage thermo-optical problems in Nd:YVO<sub>4</sub> lasers include grazing incident angle slabs, longer rods with lower Nd doping level, double-end pumped or twin rods, pumping at 880 nm absorption band and the composite rods with undoped ends or variable Nd doping. Astigmatic thermal lens deteriorates the beam in slab configurations whereas the end-pumping is limited in power scalability by thermally induced distortions and fracture. Reducing the thermal load by direct pumping to 880 nm band is vital when the pump level approach to hundred watts. Thermal effects in the end-pumped amplifiers are substantially aggravated by strong longitudinal inhomogeneity of the pump distribution. A large variation of the absorption factor within the pump linewidth and absorption anisotropy lead to strong excessive pumping of the laser rod entrance resulting in severe rise of temperature and stress. The composite rod with variable Nd doping concentration wasn't reported at 1342 nm wavelength operation. It is of particular interest in combination with pumping to 880 nm band.

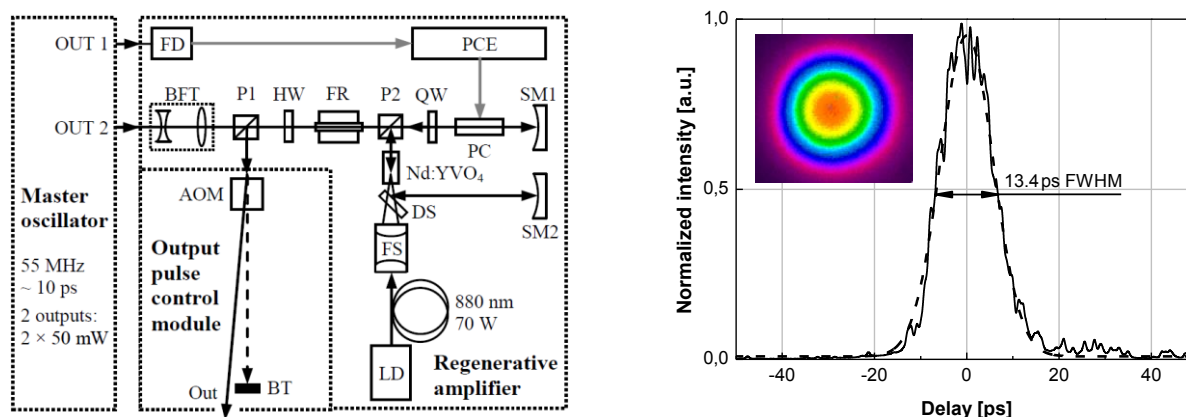


Fig. 1. Left: experimental setup for high average output power ps and ns 1342 nm laser. Right: the temporal profile of amplified output pulse (solid line) with Gaussian fit (dashed line) and spatial beam profile recorded at maximum output power (inset).

We studied the performance of high repetition rate Nd:YVO<sub>4</sub> laser operating at 1342 nm wavelength. Picked from the train of master oscillator ~ 12.5 ps seed pulses were injected into the cavity of regenerative amplifier (Figure 1, left) based on composite Nd:YVO<sub>4</sub> crystal with diffusion-bonded segments of multiple Nd concentration end-pumped at 880 nm wavelength. Hereby, we demonstrate the generation of ~ 13 ps pulses (Figure 1, right) with the average output power of 11 W at 300 kHz repetition rate and beam propagation factor of  $M^2 < 1.1$ . This is, to the best of our knowledge, the highest average output power in ps mode of operation and highest peak power ~ 2.8 MW achieved with DPSS laser operating at 1342 nm wavelength. Fraction of output power is converted to the 2nd, 3rd and 6th harmonics at 671 nm, 447 nm and 224 nm wavelengths with up to 80 %, 50 % and 15 % efficiency. Without the seed regenerative amplifier produces 10 ns pulses at high repetition rates with average power of up to ~ 11 W and nearly diffraction limited beam quality  $M^2 < 1.1$ .

## Determination of the Planetary Boundary Layer Height by a Scanning Lidar

**M. F. Huseyinoglu<sup>1</sup> and K. R. Allakhverdiev<sup>1,2</sup>**

<sup>1</sup>TUBITAK Marmara Research Center, Gebze, Kocaeli, Turkey

<sup>2</sup>Azerbaijan National Academy of Aviation, Bina 25th km., Baku 1045, Azerbaijan

*fatih.huseyinoglu@tubitak.gov.tr*

Information about the Planetary Boundary Layer (PBL) height has uttermost importance since it is the region of the lower troposphere where Earth's surface strongly influences temperature, moisture, and wind through the turbulent transfer of air mass. At the Gebze station in Turkey, extensive lidar measurements of tropospheric aerosols have been realized since 2009 [1-3]. The system is based on an Nd:YAG laser with its second and third harmonics to measure three backscatter and two extinction coefficients from which particle microphysical parameters such as number, area and volume densities, effective radius, complex refractive index and polarization can be retrieved. The addition of the scanning module to the existing lidar, allowed us to determine the PBL height in larger areas by making scanning measurements with 20 degrees to the horizontal. This presentation aims to describe the experimental set up of the scanning KA 09 lidar system at TUBITAK Marmara Research Center (MRC) and to demonstrate the results from the PBL height measurements.

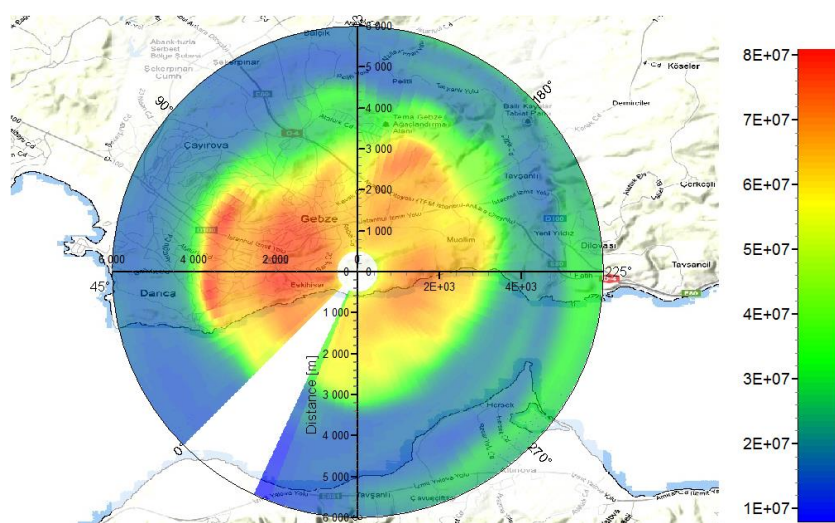


Figure 1: Conic lidar measurement determining the PBL height.

- [1] K. R. Allakhverdiev, T. K. Baykara, M. Bekbolet, M. F. Huseyinoglu, S. Ozbek, Z. Salaeva, A. Secgin, S. Vartapetov, I. Veselovskii, M. Korenskiy, Preliminary Results from the New Multiwavelength Aerosol LIDAR in Turkey, *Fizika*, 16, 22-25, 2009.
- [2] I. Veselovskii, O. Dubovik, A. Kalgotin, M. Korenskiy, D. N. Whiteman, K. R. Allakhverdiev, M. F. Huseyinoglu, Linear estimation of particle bulk parameters from multi-wavelength lidar measurements, *Atmospheric Measurement Techniques*, 5, 1135-1145, 2012.
- [3] M. F. Huseyinoglu, Z. Salaeva, A. Secgin, K. R. Allakhverdiev, Preliminary Results from the New Multiwavelength Aerosol Lidar Scanning System, *Proc. of SPIE Vol. 8677*, doi: 10.1117/12.2014958, 2013.

# ELECTROHYDRODYNAMIC FLOW FOR GAS LASER CIRCULATION SYSTEM

**I.E. Rebrov<sup>1</sup>, V.Yu. Khomich<sup>1</sup>, S.V. Nebogatkin<sup>1</sup>, V.A. Yamshchikov<sup>1</sup>**

*1- Institute for Electrophysics and Electric Power RAS, Dvorzovaya Naberezhnaya 18, 191186, Saint-Petersburg, Russia*

*re\_i@rambler.ru*

We constructed a device with 4 cascades for gas mixtures circulation in electric-discharge lasers. It consist of 4 ion emitters, 4 grid collectors, DC power supply (0-20 kV) and high frequency solid-state pulse generator [1] (with a peak voltage of 0–12 kV, a tunable repetition rate of 10–25 kHz, and a pulse duration of 7  $\mu$ s).

The formation of an electrohydrodynamic (EHD) flow by means of a high-frequency surface dielectric barrier discharge is investigated. Fundamental studies and mathematical modeling of gas-dynamic processes in EHD flow were conducted [2-4].

The influence of variations in pulse generator and DC supply parameters on the current of plasma ion emitter and gas flow velocity is considered. It is shown that the EHD flow velocity is determined by average external electric field, while its maximum value is defined by the breakdown field strength between the emitter and collector. It was finding that the increase in supply voltage and frequency of the plasma emitter leads to extension of ion emission area, ion current and gas flow velocity.

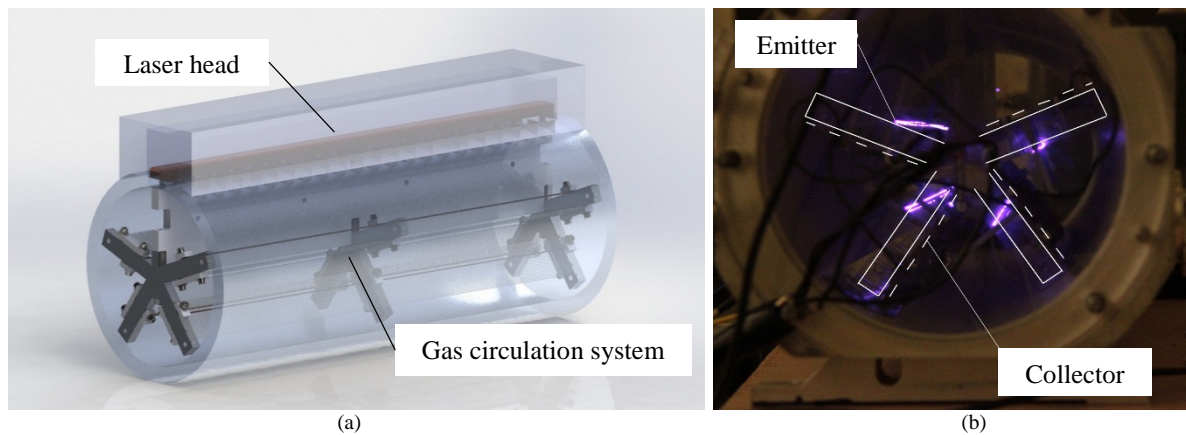


Figure 1. (a) - 3D model of N<sub>2</sub>-laser with EHD circulating system and (b) – EHD system during operation

The electrohydrodynamic gas circulation system with up to 4 cascades (Fig 1) was integrated in high-power N<sub>2</sub>-laser. If one cascade operates the radiation energy of 3 mJ is reached at frequency up to 50 Hz. When two cascades operate the same energy is maintained at frequency up to 100 Hz and up to 150 Hz with 4 cascades.

[1] S.I. Moshkunov et al, High Voltage IGBT Switches for Electro-optical Shutter Control, Advances in Applied Physics, vol. 1. pp. 630–635, (2013).

[2] S.I. Moshkunov et al, Electrohydrodynamic Effect Resulting from High Frequency Barrier Discharge in Gas, Plasma Physics Reports, vol. 38, pp. 1040-1045, (2012).

[3] Rebrov I.E., Yamshchikov V.A., Khomich V.Y. Electrohydrodynamic flow induced by dielectric barrier discharge for gas laser circulation system, 14 th International Symposium on High Pressure Low Temperature Plasma Chemistry (HAKONE XIV), vol. 1, pp. 78. (2014).

[4] V.V. Apollonov, V.A. Yamshchikov, Efficiency of electric-discharge N<sub>2</sub>-laser. Quantum Electronics, vol. 27 (6), pp. 466-472 (1997).

# Optical properties of ZnO-based step quantum wells

A.A. Lotin, O.A. Novodvorsky, E.A. Cherebilo

*Institute on Laser and Information Technologies, Russian Academy of Sciences (ILIT RAS)*

*1 Svyatoozerskaya St., 140700, Shatura, Moscow Region, Russia*

*e-mail: lotin\_82@mail.ru*

The  $\text{Mg}_x\text{Zn}_{1-x}\text{O}/\text{ZnO}$  and  $\text{Mg}_x\text{Zn}_{1-x}\text{O}/\text{Cd}_y\text{Zn}_{1-y}\text{O}$  step quantum well structures have been produced by the pulsed laser deposition method. The low-temperature (10 K) photoluminescence (PL) spectra of step MQW under variation of the width of a single well from 1 nm to 12 nm have been investigated (Fig. 1). It has been established that the total integral intensity of photoluminescence  $I_{\text{tot}}$  in the range of wavelengths 350-750 nm for the  $\text{Mg}_{0.15}\text{Zn}_{0.85}\text{O}/\text{Cd}_{0.05}\text{Zn}_{0.95}\text{O}$  MQW at the room (300 K) and cryogenic (10 K) temperatures nonmonotonously changes at a reduction of the QW width in the range from 12 nm to 1 nm, reaching a maximum at  $L_w=7$  nm (Fig. 2). A contribution to the value of  $I_{\text{tot}}$  intensity is made by the integral intensities of the exciton peak  $I_{\text{exc}}$  in the spectral region of 350-420 nm and of the green band in the range from 420 nm to 750 nm. It has been established that the increase of the barrier height ratio for charge carriers in the conduction and valence bands upon transition from the active ZnO layers in the  $\text{Mg}_x\text{Zn}_{1-x}\text{O}/\text{ZnO}$  system to the active layers of  $\text{Cd}_y\text{Zn}_{1-y}\text{O}$  in a low-dimensional  $\text{Mg}_x\text{Zn}_{1-x}\text{O}/\text{Cd}_y\text{Zn}_{1-y}\text{O}$  system is associated with the fact that the electron concentration in  $\text{Cd}_y\text{Zn}_{1-y}\text{O}$  films rises with an increase in the cadmium content. As the result, the Fermi level is displaced to the bottom of the conduction band. In the range of quantum well widths from 1 nm to 12 nm the nonmonotonous growth of exciton and defect-related intensities in photoluminescence spectra is observed.

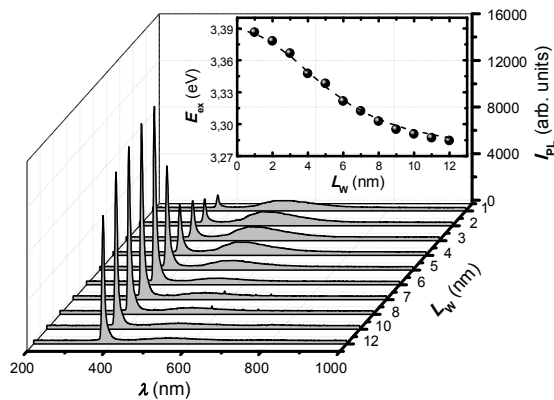


Fig. 1. PL spectra of  $\text{Mg}_{0.15}\text{Zn}_{0.85}\text{O}/\text{Cd}_{0.05}\text{Zn}_{0.95}\text{O}$  MQW as a function of quantum well width  $L_w$  at the temperature of 10 K. An insert represents the dependence of the spectral position of exciton peak on the quantum well width  $L_w$ .

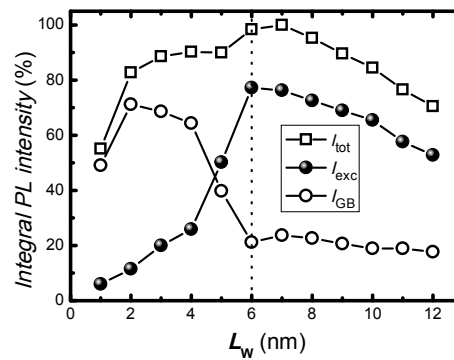


Fig. 2. Dependences of the normalized integral intensities of the exciton peak  $I_{\text{exc}}$  (350-420 nm), the green band of  $I_{\text{GB}}$  (420-750 nm) and the total intensity  $I_{\text{tot}}$  (350-750 nm) in the low-temperature (10 K) photoluminescence spectra of the  $\text{Mg}_{0.15}\text{Zn}_{0.85}\text{O}/\text{Cd}_{0.05}\text{Zn}_{0.95}\text{O}$  MQW on the quantum well width  $L_w$ .

This research was supported by the Russian Foundation for Basic Research projects № 15-07-03331-a, № 15-32-50690-mol-nr, № 15-29-01171-ofi-m, № 15-38-20369-mol-a-ved.

## Optical characterization of electron irradiated lanthanum – gallium tantalate crystals

**N.S. Kozlova<sup>1</sup>, O.A. Buzanov<sup>2</sup>, I.S. Didenko<sup>1</sup>, A.P. Kozlova<sup>1</sup>, E.V. Zabelina<sup>1</sup>, N.A. Siminel<sup>1</sup>**

<sup>1</sup>*National University of Science and Technology "MISIS", Moscow, Russia*

<sup>2</sup>*Company Fomos-Materials, Moscow, Russia*

*kozlova\_nina@mail.ru*

Lanthanum – gallium tantalate crystal  $\text{La}_3\text{Ga}_{5.5}\text{Ta}_{0.5}\text{O}_{14}$  (langatate - LGT) is one of the crystals with calcium-gallium germanate structure. Considerable improvement of optical quality of the crystals with the calcium – gallium germanate structure resulted in the renewed interest on search of the possibility of the application of these crystals as an active laser media. Nowadays langatate attract enhanced attention because of its perspectives in laser and non-linear optics [1]. In this regard, the study of optical and luminescent properties of these crystals is of undoubted interest. However, the presence in the crystals of color centers has hindered their use as active elements in the quantum generators.

The intrinsic emission in langatate crystals at  $T=300\text{K}$  and  $T=95\text{K}$  was observed in 2012 [2]. The luminescence was excited by third harmonic of YAG:Nd<sup>3+</sup> ( $\lambda_{\text{ex}}=355\text{ nm}$ ).

Here we present the results of our studies of the optical and luminescent characteristics of LGT crystals depending on their growth conditions and the electron irradiation dose. All investigated samples were cut from crystals grown in Fomos-Materials using Czochralski method in iridium crucibles, growth atmosphere – argon or argon plus oxygen. Optical transmission spectra were measured using UV-Vis-Nir spectrophotometer «Cary-5000» (Agilent Technologies). The luminescence was excited at  $T=300\text{ K}$  and  $T=95\text{ K}$  by second ( $\lambda_{\text{ex}}=532\text{ nm}$ ) and third harmonic of YAG:Nd<sup>3+</sup> ( $\lambda_{\text{ex}}=355\text{ nm}$ ). The samples were irradiated by electrons with doses  $10^{12}$  -  $3 \cdot 10^{15}\text{ cm}^{-2}$ .

The growth atmosphere significantly influences the coloration and transmission spectra of langatate crystals. Colored langatate crystals are obtained in atmosphere of argon with addition of oxygen, colorless – in argon atmosphere [3]. For the crystals grown in the argon atmosphere the transmission spectra exhibit a weak absorption band with maximum at 290 nm. The optical transmission spectra of the crystals grown in the argon with oxygen atmosphere significantly differ from the spectra of the crystals grown in argon. A spread of the intrinsic absorption edge is observed. Strong absorption bands in the range 290 nm, 360 nm and 480 nm were also observed. After electron irradiation (dose  $1 \cdot 10^{13}\text{ cm}^{-2}$ ) the crystals grown in the argon atmosphere exhibit the strong absorption bands at 290 nm and 350 nm. The doses increase influences on the intensity of those bands for all investigated samples variously. As for crystals grown in the argon with 2% of oxygen the electron irradiation leads to the strong changes of the absorption band at 360 nm and 480 nm.

We revealed significant influence of irradiation on luminescence spectra. For all investigated samples the electron irradiation reduces the intensity of luminescence at 300 K. Five emission peaks are observed at luminescent spectra at 95 K.

### References

- [1] X.H. Fu, Y. Che, Y.L. Li, Diode-pumped Nd:LGS intracavity-doubled green laser at 532 nm, *Solid State and Liquid Lasers*, vol. 21, p.995 – 997, (2011).
- [2] O.A. Buzanov, N.S. Kozlova, N.A. Siminel, Luminescenciya kristallov lantan-gallievogo tantalata, *Izvestiya vysshih uchebnyh zavedeniy. Materialy elektronnoy tekhniki*, №2, p. 21 – 24, (2012) (in russian).
- [3] O.A. Buzanov, E.V. Zabelina, N.S. Kozlova, Optical properties of Lanthanum – Gallium Tantalate at Different Growth and Post-Growth Treatment Conditions, *Crystallography Reports*, Vol. 52, № 4, p. 691-696, (2007).



# **Optimized Laser Sintering of Ag Nano-Particle Inks for RF Components on Flexible Substrates**

F. Zacharatos<sup>1</sup>, N. Iliadis<sup>2</sup>, J. Kanakis<sup>2</sup>, P. Bakopoulos<sup>2</sup>, H. Avramopoulos<sup>2</sup>, I. Zergioti<sup>1\*</sup>

*1. National Technical University of Athens, Physics Department, Heroon Polytehneiou 9, 15780, Zografou, Greece*

*2. National Technical University of Athens, School of Electrical & Computer Engineering, Heroon Polytechniou 9, 15780 Zografou, Greece*

*\*contact: zergioti@central.ntua.gr*

Flexible electronics have emerged as a very promising alternative of CMOS compatible electronics for a plethora of applications. Laser microfabrication techniques, such as Laser ablation and Laser sintering are compatible with flexible substrates and have demonstrated impressive results in the field of flexible electronic devices and sensors. However, laser based manufacturing of RF passive components or devices is still at an early stage. In this work we report on the all-laser fabrication of Silver Co-planar Waveguides (CPWs) on Poly-EthyleneNaphthalate (PEN) substrates. The CPWs have been fabricated to match 50 Ohm ports of an Anritsu Vector Network Analyzer operating from 300MHz - 40GHz, according to the design reported in previous work. The all laser fabrication process consisted of the patterning of a Silver Nano Particle layer spin-coated on a PEN substrate followed by the selective laser sintering of the structures with a ns pulsed Nd:YAG laser source operating at 532nm, according to the optimized parameters extracted from a previous study of the authors. The CPWs have been characterized electrically at the 0.3-40GHz regime and found to be excellent transmission lines with a 40GHz 3dB bandwidth, owing to the high electrical conductivity of Ag and the exquisite dielectric properties of PEN. This novel process is a milestone towards the RF technology transfer to flexible electronics with low cost and specs comparable or even superior to the CMOS compatible equivalents.

# Q-switching of Yb:YGG, Yb:LuGG and Yb:CNGG Lasers by a Graphene Saturable Absorber

**Xavier Mateos,<sup>1,2</sup> Josep Maria Serres,<sup>1</sup> Pavel Loiko,<sup>1,3</sup> Haohai Yu,<sup>4</sup> Huaijin Zhang,<sup>4</sup> Junhai Liu,<sup>5</sup> Konstantin Yumashev,<sup>3</sup> Uwe Griebner,<sup>2</sup> Valentin Petrov,<sup>2</sup> Magdalena Aguiló,<sup>1</sup> and Francesc Díaz<sup>1</sup>**

<sup>1</sup>Física i Cristal·lografia de Materials i Nanomaterials (FiCMA-FiCNA), Universitat Rovira i Virgili (URV), E-43007 Tarragona, Spain

<sup>2</sup>Max Born Institute for Nonlinear Optics and Short Pulse Spectroscopy, Max-Born-Str. 2a, D-12489 Berlin, Germany

<sup>3</sup>Center for Optical Materials and Technologies, Belarusian National Technical University, 65/17 Nezavisimosti Ave., 220013 Minsk, Belarus

<sup>4</sup>State Key Laboratory of Crystal Materials, Shandong University, 250100 Jinan, China

<sup>5</sup>College of Physics, Qingdao University, 308 Ning-Xia Road, 266071 Qingdao, China

Main author email address: xavier.mateos@urv.cat

Graphene, a two-dimensional material composed of a single-layer of carbon atoms arranged in a honeycomb lattice, is nowadays actively studied as a broadband saturable absorber (SA) for near-IR passively Q-switched (PQS) lasers [1]. Ytterbium lasers emitting at  $\sim 1 \mu\text{m}$  are attractive due to the beneficial properties of the  $\text{Yb}^{3+}$  ion such as simple energy-level scheme avoiding up-conversion and excited-state absorption processes, and weak heat transfer to the host and high efficiencies due to a low quantum defect. Graphene PQS and mode-locked Yb waveguide and fiber lasers were realized before [2,3], while no “bulk” Yb-doped laser PQS using graphene has been demonstrated so far.

In the present work, the laser cavity consisted of a flat pump mirror and a concave ( $R = 50 \text{ mm}$ ) output coupler OC ( $T_{\text{OC}} = 10\%$  at the laser wavelength). The SA was a commercial CVD-grown single-layer graphene deposited on 1.05 mm thick fused silica and had an initial transmission at  $\sim 1.04 \mu\text{m}$  of 97.0%.

Stable PQS operation was achieved with all laser crystals. The maximum pulse energy was achieved with Yb:CNGG,  $E_{\text{out}} = 1.9 \mu\text{J}$ . This corresponded to a peak power  $P_{\text{peak}} = 10.0 \text{ W}$ . Thus, the maximum intracavity axial intensity on the SA reached  $1.6 \text{ MW/cm}^2$  that is  $\sim 2$  times higher than its saturation intensity at  $\sim 1 \mu\text{m}$ ,  $I_s \sim 0.9 \text{ MW/cm}^2$ . A summary of the output characteristics of the studied lasers is presented in Table 1. Figure 1 shows the oscilloscope traces of the shortest Q-switched pulses achieved with the Yb:YGG, Yb:LuGG and Yb:CNGG lasers, as well as a typical pulse train for Yb:CNGG measured at  $P_{\text{abs}} = 7 \text{ W}$ . An upper limit for stable Q-switching was observed for all lasers, attributed to the heating of the graphene SA by the residual (non-absorbed) pump.

**Table 1. Output Characteristics of the Graphene Q-switched Yb:YGG, Yb:LuGG and Yb:CNGG Lasers**

Laser	$P_{\text{out}}$ , mW	$\eta$ , %	$\eta_{\text{conv}}$ , %	$t_p$ , ns	PRF, kHz	$E_{\text{out}}$ , $\mu\text{J}$	$P_{\text{peak}}$ , W
Yb:YGG	462	23	55	440	260	1.8	4.0
Yb:LuGG	320	15	45	490	245	1.3	2.7
Yb:CNGG	440	24	30	190	235	1.9	10.0

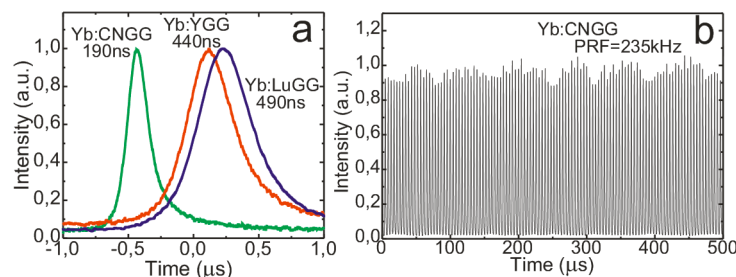


Fig. 1. Oscilloscope traces of the shortest Q-switched pulses achieved with the graphene Q-switched Yb:YGG, Yb:LuGG and Yb:CNGG lasers (a) and the corresponding pulse train for Yb:CNGG,  $P_{\text{abs}} = 7 \text{ W}$  (b).

Further shortening of the Q-switched pulses and increase of the pulse energy should be possible with the use of multi-layered graphene (number of layers,  $n = 2 \dots 4$ ) due to an increased modulation depth. The reduction of cavity losses can be provided by applying AR-coatings on the crystal faces as well as the uncoated substrate of the SA. Our study reveals the potential of graphene-based SAs for passive Q-switching of Yb bulk lasers.

[1] Q. L. Bao, H. Zhang, Y. Wang, Z. Ni, Y. Yan, Z. X. Shen, K. P. Loh, and D. Y. Tang, “Atomic-layer graphene as a saturable absorber for ultrafast pulsed lasers,” *Adv. Funct. Mater.* **19**, 3077–3083 (2009).

[2] A. Choudhary, S. Dhingra, B. D’Urso, P. Kannan, and D. P. Shepherd, “Graphene Q-switched mode-locked and Q-switched ion-exchanged waveguide lasers,” *IEEE Phot. Technol. Lett.* **27**, 646–649 (2015).

[3] J. Liu, S. Wu, Q.-H. Yang, and P. Wang, “Stable nanosecond pulse generation from a graphene-based passively Q-switched Yb-doped fiber laser,” *Opt. Lett.* **36**, 4008–4010 (2011).

---

---

**SECTION NL**

**Nonlinear Optics and Photonics**

---

---

# Sum-frequency generation in the bulk of an isotropic gyrotropic medium by two-colored singular beam

K. S. Grigoriev<sup>1\*</sup>, V. A. Makarov<sup>1,2</sup>, I. A. Perezhogin<sup>2</sup>

*1 - Physics Faculty of M.V. Lomonosov Moscow State University, Russia  
2 - International Laser Center of M.V. Lomonosov Moscow State University, Russia*

\*kir3740@yandex.ru

The space where a heterogeneously polarized monochromatic light beam propagates can possess certain lines, along which the polarization of the beam's electric field is pure circular (*C*-lines). Their intersections with the beam transversal section are the points of circular polarization singularity, or *C*-points. Polarization singularity is characterized by its topological charge, which is equal to total winding number of polarization ellipse during one full counter-clockwise loop around the point of singularity [1]. These singularities are vector analogs of scalar phase singularities (optical vortices) which are of special interest in nonlinear optics of crystals [2, 3].

We considered sum-frequency generation in the bulk of an isotropic gyrotropic medium by two collinear beams with different frequencies. The first beam is elliptically polarized Gaussian mode and the second one is Laguerre-Gaussian mode with right circular polarization and phase singularity on its axis. When propagating in nonlinear media these two modes mix via local quadratic response and the signal beam on sum-frequency is generated. In case of negligible pump depletion the expressions for nonlinear polarization vector field  $\mathbf{P}^{\text{NL}}$  at the sum-frequency are readily obtained analytically. This vector field inherits singular structure of the polarization pattern of the fundamental beams. Depending on the ratios of the frequencies, diffraction lengths of the modes and ellipticity degree of the polarization ellipse of Gaussian mode, the  $\mathbf{P}^{\text{NL}}$  field can contain several polarization singularities with non-zero or zero total topological charge. In the former case corresponding *C*-lines exist in every cross section of the  $\mathbf{P}^{\text{NL}}$  beam and do not meet or intersect each other, while in the latter case *C*-lines form a closed single loop. In both cases the polarization pattern of the signal beam resembles that of the nonlinear polarization of the medium if there is no wave vector mismatch, i.e. no frequency dispersion of the medium. However, in the presence of the dispersion the *C*-lines in the signal beam experiences drastic transformation. If the  $\mathbf{P}^{\text{NL}}$  beam carries non-zero topological charge of its singularities then *C*-lines gain helical structure; the greater is absolute value of the wave vector mismatch the shorter is the mean step of each spiral. In the other configuration of the fundamental modes, when total topological charge of  $\mathbf{P}^{\text{NL}}$  polarization singularities is zero, the loop of *C*-lines undergoes deformation and then splits into new loops.

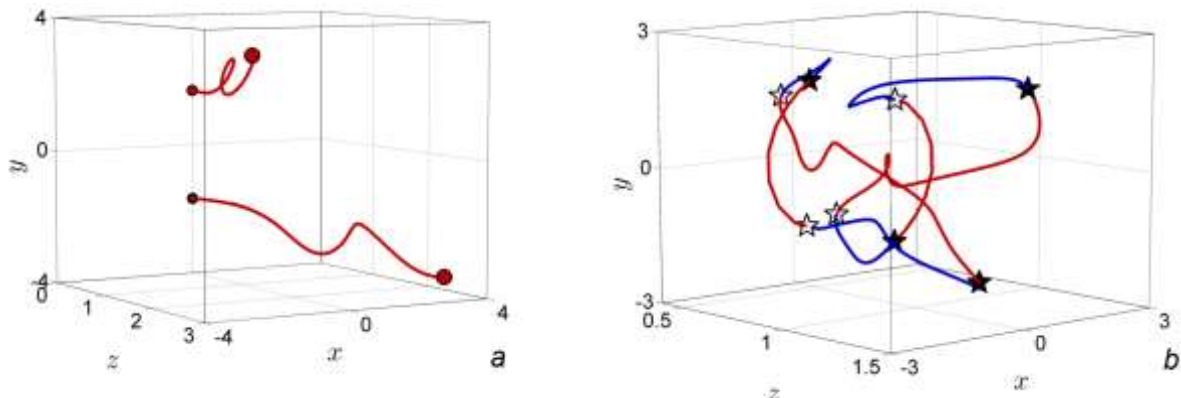


Fig. 1. Spiral (a) and loop (b) structures of the *C*-lines in sum-frequency beam.

- [1] J. F. Nye, Lines of circular polarization in electromagnetic wave fields, Proc. R. Soc. A, 389(1797), 279–290, (1983).  
[2] A.V. Ilyenkov, A.I. Khiznyak, L.V. Kreminskaya, M.S. Soskin, and M.V. Vasnetsov, Birth and evolution of wave-front dislocations in a laser beam passed through a photorefractive LiNbO<sub>3</sub>: Fe crystal. App. Phys. B, 62(5), 465–471, (1996).  
[3] Anatoly P. Sukhorukov, Alexey A. Kalinovich, Gabriel Molina-Terriza, and Lluís Torner, Superposition of noncoaxial vortices in parametric wave mixing, Phys. Rev. E, 66, 036608, (2002).

# **DISSIPATIVE SOLITONS IN OPTICAL TRANSMISSION LINES AND FIBER LASERS**

Mário F. S. Ferreira

I3N – Institute of Nanostructures, Nanomodelling and Nanofabrication.

Department of Physics, University of Aveiro

3810-193 Aveiro, Portugal

## **ABSTRACT**

We introduce the concept of dissipative solitons, which emerge as a result of a double balance: between nonlinearity and dispersion and also between gain and loss. Such dissipative solitons have many unique properties which differ from those of their conservative counterparts and which make them similar to living things. We focus our discussion on dissipative solitons in optical fiber systems, namely transmission lines and fiber lasers, which can be described by the cubic-quintic complex Ginzburg-Landau equation.

# Digital Signal Processing for Coherent Optical Communication Systems

**Armando N. Pinto, Fernando P. Guiomar, Sofia B. Amado, Celestino S. Martins,  
Somayeh Ziaie and Nelson J. Muga**

*Department of Electronics, Telecommunications and Informatics, University of Aveiro and Instituto de Telecomunicações, 3810-193 Aveiro, Portugal*

*anp@ua.pt*

Optical networks form the backbone of the modern Internet. Optical networks comprise nodes and links. The nodes receive and aggregate the traffic and optical fibers are used to interconnect the nodes. The huge amount of traffic that nowadays crosses the Internet is pushing the capacity of carrying information of fiber optic transmission systems toward their limits. We start by discussing the limits to carry information of optical fibers. The linear limit is due to the signal-to-noise ratio degradation because of the accumulation of optical noise originated in the optical amplifiers, this limit follows closely the well-known Shannon limit for a noisy and band-limited communication channel [1]. To maintain a sufficiently large signal-to-noise ratio the signal optical power can be increased, however, this can only be extended up to a certain point. Because, optical fibers present a cubic nonlinear response and the interaction between signals, and between signals and noise mediated by the Kerr effect originates an excess of noise, usually called nonlinear noise, which reduces considerably the fiber capacity [2, 3]. The nonlinear noise are due to two different nonlinear interactions: signal-to-signal and noise-to-signal interactions. Taking advantage of the deterministic nature of signals the signal-to-signal interactions can be effectively mitigated. We present recent advances in digital signal processing technologies for fiber optics transmission systems. Taking advantages of the extraction of both amplitude and phase information, coherent receivers can compensate chromatic dispersion and up to a certain point the nonlinear effects [4, 5]. We review recent breakthroughs in advanced techniques to compensate linear and nonlinear fiber impairments. We also discuss real time implementation issues in very high speed fiber optic transmission links.

**Acknowledgments:** This work was partially supported by the FCT and European Union FEDER through the projects PTDC/EEI-TEL/3283/2012 (DiNEq) and UID/EEA/50008/2013.

- [1] C. E. Shannon, A mathematical theory of communication, The Bell System Technical Journal, vol. 27, pp. 379–423, 623–656, 1948.
- [2] A. N. Pinto, G. P. Agrawal, Nonlinear Interaction Between Signal and Noise in Optical Fibers, IEEE/OSA Journal of Lightwave Technology, July, vol. 26, n. 13, pp. 1847-1853, 2008.
- [3] P. Poggiolini, G. Bosco, A. Carena, V. Curri, Y. Jiang, F. Forghieri, The GN model of fiber non-linear propagation and its applications, IEEE/OSA Journal of Lightwave Technology, vol. 32, no. 4, pp. 694-721, Feb. 2014.
- [4] Fernando P. Guiomar, Armando N. Pinto, Simplified Volterra Series Nonlinear Equalizer for Polarization-Multiplexed Coherent Optical Systems, IEEE/OSA Journal of Lightwave Tech., Vol. 31, No. 23, pp. 3879-3891, December, 2013.
- [5] F. P. Guiomar, S. B. Amado, A. Carena, G. Bosco, A. Nespola, A. L. Teixeira, A. N. Pinto, Fully Blind Linear and Nonlinear Equalization for 100G PM-64QAM Optical Systems, IEEE/OSA Journal of Lightwave Technology, Vol. 33, No. 2, pp. 1265-1274, April 1, 2015.

# Singular polarization patterns of the beam at double frequency generated by singularly polarized fundamental beam

K. S. Grigoriev<sup>1</sup>, V. A. Makarov<sup>1,2</sup>, I. A. Perezhogin<sup>2</sup>

*1 - Physics Faculty of M.V. Lomonosov Moscow State University, Russia*

*2 - International Laser Center of M.V. Lomonosov Moscow State University, Russia*

*kir3740@yandex.ru*

A monochromatic light beam is generally pierced by imaginary lines, along which polarization ellipse is circular (*C*-lines). These lines intersect cross sections of the beam at the points of circular polarization singularity, or *C*-points. Polarization patterns in the vicinity of a *C*-point are divided into three morphological types: “lemon”, “star”, and “monstar”. The main quantity characterizing a polarization singularity is topological charge, which is the number of polarization ellipse rotation counted along one counter-clockwise loop around the *C*-point. “Lemon” and “monstar” patterns have the charge 1/2 (ellipse is rotated by 180 degrees counter-clockwise) and “star” pattern has the charge -1/2 (180 degrees clockwise rotation) [1]. *C*-points are vector analogs of phase singularities (optical vortices); topological charge of the latter shows the phase variation around the singularity.

We have deduced and thoroughly examined analytical expressions for the electric field in the beam at double frequency reflected from the surface of the isotropic gyrotropic medium by normally incident fundamental beam with specially designed polarization pattern, containing a single *C*-point. This beam is a superposition of coaxial Gaussian mode with left circular polarization and two Laguerre-Gaussian vortex modes with opposite signs of topological charges and right circular polarization. Varying the amplitude and phase ratios of the modes one can realize all of three possible morphological types of the singularity. Since the medium does not have local quadratic response we take into account the effects of nonlinear optical activity. Also, the contribution of heterogeneous surface layer is modeled by modified boundary conditions for the fields of the signal beam (see [2]).

In case of purely bulk nonlinearity the signal beam contains two *C*-points with total topological charge equal to doubled charge of the initial singularity (fig. 1a). However, their polarization handedness is not reversed if the *C*-point in the fundamental beam has negative charge. Media with surface response generate far more complicated polarization patterns of the signal beam, which in special cases inherit the symmetry of the fundamental beam (fig. 1b). Total topological charges of left-handed and right-handed *C*-points depend only on the charge of initial *C*-point, but do not reflect the difference between its “lemon” and “monstar” patterns. For the media with both bulk and surface nonlinear response total topological charge may not be equal to doubled charge of the initial *C*-point.

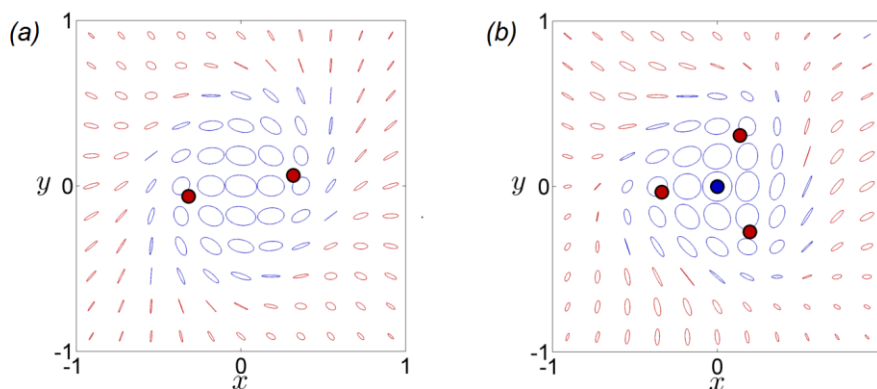


Fig. 1. Examples of polarization patterns and singularities of the signal beam (a) purely bulk response (b) bulk and surface response.

[1] J. F. Nye, Lines of circular polarization in electromagnetic wave fields, Proc. R. Soc. A, 389(1797), 279–290, (1983).

[2] A. A. Golubkov, V. A. Makarov, Boundary conditions for electromagnetic field on the surface of media with weak spatial dispersion, Phys.-Usp., 38, 325-332 (1995)

# Ultrafast nonlinear effects in organic compounds and organic hybrid materials

**H. Gonçalves<sup>1</sup>, Luís Alves<sup>1</sup>, Etelvina de Matos Gomes<sup>1</sup>, Rosa Cristina Moutinho Ferreira<sup>2</sup>, Susana Costa<sup>2</sup>, Manuela Raposo<sup>2</sup>, and Michael Besley<sup>1</sup>**

<sup>1</sup> Center of Physics, University of Minho, Campus de Gualtar, 4710-057 Braga, Portugal

<sup>2</sup> Center of Chemistry, University of Minho, Campus de Gualtar, 4710-057 Braga, Portugal  
goncalves.hmc@ua.pt

Synthesis and solution-processing of specialized chemical compounds can facilitate the fabrication of nano-electronic devices. Many of these emerging applications require organic materials with well-characterized optical properties, specifically, large two-photon absorption (2PA) and nonlinear optical (NLO) responses. The most common strategy to achieve a strong second order nonlinear optical response is to link donor and acceptor moieties on opposite ends of a  $\pi$ -conjugated aromatic spacer. This configuration promotes spatial charge transfer and a strong difference in dipole moments between the ground and excited electronic states. Individual organic molecules, tailor made following this strategy, can often exhibit exceptionally large intrinsic nonlinear optical properties, but the translation to a macroscopic electro-optic activity is often extremely difficult. Roughly more than 80% of all  $\pi$ -conjugated organic molecules crystallize in centrosymmetric space groups producing materials with no second order bulk susceptibility. Our group has demonstrated that is possible overcome this restriction by embedding organic molecules, which normally crystallize in centrosymmetric structures, into nanostructured polymeric matrix[1]. Recently, we observed greatly enhance the nonlinearities of nominally weak nonlinear materials when insert in a polymeric nanofibers, one-dimensional nanostructures (See figure 1). These types of nanostructures are attracting attention because of the unique optical interactions that arise from their sub wavelength size[2].

To explore this phenomena in detail we take advantage of our state of the art custom built Fluorescence Lifetime Imaging Microscope (FLIM) [3]. The temporal resolution of the FLIM is about 25 picoseconds and less than a 1 micron of spatial resolution. This system allows us to monitor the effects of nano-structured environments and their localized optical response. Other systems of current interest in our research group are graphene quantum dots both in solution and dispersed in a thin film of PVA, the interaction of excited dye molecules with a single layer graphene surface and tailor designed molecules for two photon absorption in the near infrared portion of the spectrum.

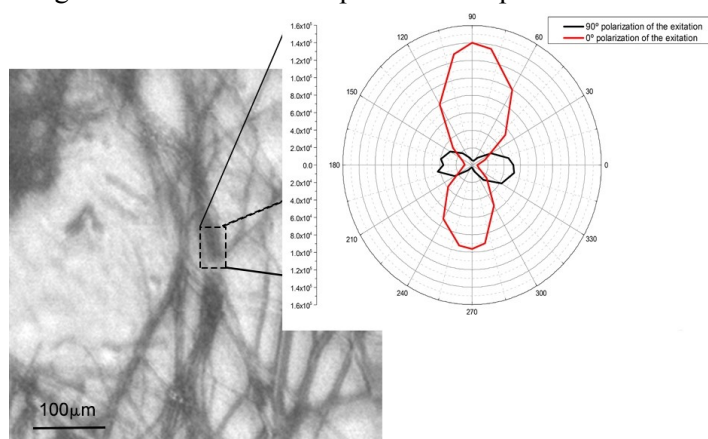


Figure 1 – Polarized light of the second harmonic generation of a nanofiber of poly(L-lactic acid) (PLLA) doped with para-nitroaniline. The red curve correspond to excitation using a polarization parallel to the fibres, the black curve correspond an orthogonally polarization excitation.

- [1] D. V. Isakov, M.S. Belsley, E. de Matos Gomes, H. Gonçalves, P. Schellenberg, B.G. Almeida, Intense optical second harmonic generation from centrosymmetric nanocrystalline para-nitroaniline, *Appl. Phys. Lett.* 104, 181903-181907 (2014).  
 [2] J. Brewer, M. Schiek, I. Wallmann, H.G. Rubahn, First order optical nonlinearities  $\chi^2$  for organic nanofibers from functionalized para-phenylenes *Opt. Commun.* 281, 3892–3896 (2008).  
 [3] C. Bernardo, et al., A versatile fluorescence lifetime imaging system for scanning large areas with high time and spatial resolution, in: M.F.P.C. Martins Costa, R.N. Nogueira (Eds.), *Second Int. Conf. Appl. Opt. Photonics*, International Society for Optics and Photonics, 928637-928641, 2014.

# Pulsating Soliton Solutions of the Complex Ginzburg-Landau Equation

Sofia C. V. Latas<sup>1</sup> and Mário F. S. Ferreira<sup>2</sup>,

*i3N-Institute of Nanostructures, Nanomodelling and Nanofabrication  
Department of Physics, University of Aveiro, 3810-193 Aveiro – Portugal*

<sup>2</sup>[mfernando@ua.pt](mailto:mfernando@ua.pt)

Many non-equilibrium phenomena, such as convection instabilities, binary fluid convection and phase transitions, can be described by the complex Ginzburg-Landau equation (CGLE). In the field of nonlinear optics, the CGLE can describe various systems, namely optical parametric oscillators, free-electron laser oscillators, spatial and temporal soliton lasers, and all-optical transmission lines. In these systems there are dispersive elements, linear and nonlinear gain, as well as losses.

Various techniques have been applied to investigate the soliton solutions of the CGLE. Exact solutions were found, but they can be presented explicitly only for certain relations between the parameters of the equation. Furthermore, so far, only stationary solutions of the CGLE are known in analytical form. The soliton perturbation theory can be used for small values of the parameters. Moreover, approximate expressions for some localized solutions can be derived for arbitrary values of the CGLE parameters by reducing this equation to finite-dimensional dynamical models. The reduced models can be obtained by applying the method of moments, or Lagrangian techniques.

To fully explore the CGLE, massive numerical simulations must be carried out. Different types of soliton solutions were obtained in this way, which can be divided in two classes: localized fixed-shape solutions and localized pulsating solutions. Among the localized pulsating solutions, we may refer the plain pulsating and the creeping solitons, as well as the erupting solitons, which belong to the class of chaotic solutions. The existence of the erupting solitons has been experimentally confirmed in a passively mode-locked solid state laser, where the higher-order effects might have some influence. The impact of some higher-order effects, namely the intrapulse Raman scattering, self-steepening, and third-order dispersion, on localized pulsating solitons have been investigated recently.

In this paper we use the variational approach to finding approximate solutions of the CGLE corresponding both to stationary and to pulsating solitons. Afterwards, the CGLE is solved numerically in order to obtain different types of localized pulsating solutions, namely plain pulsating, erupting, and creeping soliton solutions. Finally, we demonstrate the possibility converting these pulsating solitons into fixed-shape pulses under the simultaneous action of the higher-order effects.

# Nonlinear absorption in hybrid metal/chromophore systems

A.Zasedatelev<sup>1</sup>, T. Dubinina<sup>2</sup>, V. Krasovskii<sup>1,3</sup>, L. Tomilova<sup>2,4</sup> and A. Chistyakov<sup>1</sup>

<sup>1</sup>National Research Nuclear University «MEPhI», Moscow, Russia

<sup>2</sup>Department of Chemistry, M.V. Lomonosov Moscow State University, Moscow, Russia

<sup>3</sup>Prokhorov General Physics Institute, Moscow, Russia

<sup>4</sup>Institute of Physiologically Active Compounds, Chernogolovka, Russia

krasovskii@nsc.gpi.ru

Unique optical properties of hybrid systems based on metal nanostructures and chromophore molecules are very promising in nonlinear optics. Nowadays different hybrid plasmonic nanosystems are used as a basic part of optical modulators and switchers [1,2], nanolasers [3,4], high-sensitive sensors [5,6], harmonic generation materials [7], optical limiters etc. Tight “mixing” of plasmonic properties of metal structures with excitonic properties of chromophore is a key feature of resonant nonlinearity, it leads to dramatic changes in optical nonlinear properties in the whole exciton-plasmon system.

First, the local field factor i.e. enhancement of the near field intensity would result to increase of the nonlinear responses, and second, the enhancement of the decay rate of excited states would lead to acceleration of the rate in a radiative relaxation process. In spite of very different time scales of the processes in the uncoupled regime, when chromophore and plasmon structure don't interact, in the tightly “mixing” exciton-plasmon regime both processes can have similar time scales. Therefore relaxation and excitation rates can turn from independent values into strong correlated ones. In addition to modification of the rates of electronic transitions in plasmon-coupled excitonic systems, the impact of strong near-field on chromophores can lead to appearance of parametric nonlinearities. It is very difficult to predict a character of nonlinear properties in general, without full description of the exciton-plasmon system's dynamics. The subject of our research is an experimental and theoretical study of resonant plasmon-stimulated nonlinear absorption in exciton-plasmon systems, investigation of the involved mechanisms.

The synthesis of hybrid nanostructures based on 3-level chromophores with high resonant interaction was implemented. We experimentally studied their linear optical properties, found out the presence of Fano antiresonance in the differential absorption spectrum conforming to strong exciton-plasmon coupling between chromophore and gold nanoparticle. Relaxation rates of both free chromophores and hybrid nanostructures were measured. The experiment claims to be the first Z-scan study of resonant absorption properties of similar structures in a wide range intensity presented on Fig 1.

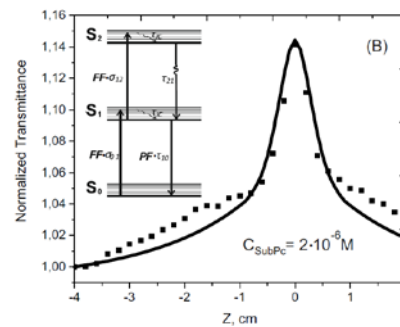


Fig. 1 Open-aperture Z-scans of nano-hybrid systems. Experimental data – dots, simulation curves – solid line.

Based on Maxwell - Bloch formalism, we proposed a model that properly represents the experiment results. By applying the model, we succeeded to define mechanisms of nonlinear resonant response. According to our research Purcell effect and near-field factor equally contribute to the nonlinear response. The enhancement of absorption saturation effect caused by Purcell effect has turned up the surprising result and as far as we are aware observed for the first time.

- [1] M. Sukharev, T. Seideman, Phase and polarization control as a route to plasmonic nanodevices. *Nano Lett.* 6, 715–719 (2006)
- [2] M. Aeschlimann, M. Bauer, D. Bayer et al, Adaptive subwavelength control of nano-optical fields. *Nature* 446, 301–304 (2007)
- [3] M.A. Noginov et al., Demonstration of a spaser-based nanolaser, *Nature* 460: 1110–1112, (2009).
- [4] S.Noda, S. Seeking the ultimate nanolaser. *Science* 314, 260–261 (2006).
- [5] Yu. E. Lozovik, I.A. Nechepurenko et al., Spaser spectroscopy with subwavelength spatial resolution, *Physics Letters*, A378, 723–727 (2014).
- [6] J.N. Anker, W.P. Hall, O. Lyandres, N.C. Shah, J. Zhao, R.P.V. Duyne, Biosensing with plasmonic nanosensors. *Nat. Mater.* 7, 442–453 (2008)
- [7] J. Butet, G Bachelier, I. Russier-Antoine, C. Jonin et al., Interference between selected dipoles and octupoles in the optical second-harmonic generation from spherical gold nanoparticles. *Phys. Rev. Lett.* 105, 077401 (2010).

# Fabrication and optical properties of thin films with sol gel derived di-ureasils doped with Disperse Red 1

**C. Vicente<sup>1,2</sup>, L. Fu<sup>1</sup>, L. D. Carlos<sup>1</sup>, P. S. André<sup>3</sup>, R. A. S. Ferreira<sup>1</sup>**

*1- Physics Department and CICECO, University of Aveiro, 3810-193 Aveiro, Portugal*

*2- Instituto de Telecomunicações, Universidade de Aveiro, Portugal*

*3- Department of Electrical and Computer Engineering and Instituto de Telecomunicações, Inst. Sup. Técnico, Lisboa, Portugal*

*cvicente@av.it.pt*

In the last decades, the introduction of dyes in sol-gel derived organic-inorganic hybrid matrices has received significant attention due to improved mechanical stability, and photostability, the capacity of incorporate higher dye amounts and reduce the undesired neighboring dye interactions when compared with the use of polymer-based hosts. [1]. Depending on the type of dye incorporated in the sol gel matrix these materials can found optical applications such as: solid state lasers, holography, dye-sensitized solar cells, electro optical and photorefractive materials or optical limiting [2]. Within the variety of organic-inorganic hosts that have been developed, the so-called di-ureasils present acceptable transparency, mechanical flexibility and thermal stability to be processed both as thin films and as transparent and shape controlled monoliths. In particular, some of us have reported the use of di-ureasils as cost effective integrated optics (IO) substrates, namely in the production of waveguides, splitters, optical filters and lasers [3] or thermo-optical devices [4] with potential applications in optical telecommunications. Despite the ability of the hybrid host to easily encapsulate large amounts of light emitting centers (organic dyes or trivalent lanthanide ions), the exploitation of active IO components based on organic dyes as restricted until now to the demonstration of a Rhodamine 6G solid state laser [3]. The recent increasing interest in electro-optic (EO) devices with applications in optical telecommunications has motivated developments on the organo-silicon hybrids technology platform. The introduction of these materials in the fabrication process allows to include in the silicon platform the EO functionalities with high modulation speeds and low power consumption. In this work we report the synthesis of thin films of organic-inorganic hybrid di-ureasils doped with Disperse Red 1 (DR1) chromophore. The films reveal an absorption band at 248 nm allowing the use of the UV patterning of the surface. The refractive index is  $1.4797 \pm 0.0006$  at 1550 nm. The global results indicate that DR1 doped di-ureasils are promising candidates as substrates for EO integrated optics and photonic applications. Future work involves the determination of the EO coefficient of DR1 doped di-ureasils and its application in integrated optical devices.

- [1] F. Chaumel, H. Jiang, and A. Kakkar, "Sol-Gel Materials for Second-Order Nonlinear Optics," *Chem. Mater.*, vol. 13, pp. 3389–3395, (2001).
- [2] C. Sanchez, P. Belleville, M. Popall, and L. Nicole, "Applications of advanced hybrid organic-inorganic nanomaterials: from laboratory to market.," *Chem. Soc. Rev.*, vol. 40, pp. 696–753, (2011).
- [3] R. A. S. Ferreira, P. S. André, and L. D. Carlos, "Organic-inorganic hybrid materials towards passive and active architectures for the next generation of optical networks," *Opt. Mater. (Amst)*, vol. 32, pp. 1397–1409, (2010).
- [4] R. A. S. Ferreira, C. D. S. Brites, C. M. S. Vicente, P. P. Lima, A. R. N. Bastos, P. G. Marques, M. Hiltunen, L. D. Carlos, and P. S. André, "Photonic-on-a-chip: a thermal actuated Mach-Zehnder interferometer and a molecular thermometer based on a single di-ureasil organic-inorganic hybrid," *Laser Photon. Rev.*, vol. 7, pp. 1027–1035, (2013).

---

---

**SECTION OC**  
**Optical Communication**

---

---

# Performance Assessment of Fiber-Wireless Systems based on 1.55 $\mu\text{m}$ Directly Modulated VCSELs

**Henrique M. Salgado** (hsalgado@inesctec.pt)

*Faculdade de Engenharia da Universidade do Porto*

*Instituto de Engenharia de Sistemas e Computadores – Tecnologia e Ciência - INESC TEC, Porto, Portugal*

**Abstract:** Radio-over-fiber technology, used in the transport of radio signals over optical fiber by means of an optical carrier between a remote site and a central node of a cellular network, is an attractive solution for backhauling of a large number of remote antennas, enabling the shifting of the hardware complexity from base stations to a central station. Integration of both optical and wireless broadband infrastructures into the same backhaul network permits equipment sharing and dynamic allocation of resources, which in turn leads to simplified system operation and cost reduction of base stations. With respect to the latter the direct modulation of laser diodes is an attractive solution. However, due to the inherent nonlinearity of the laser diode, radio-over-fiber systems are susceptible to non-linear distortion. This is especially relevant when dealing with the most recent wireless standards, based on orthogonal frequency division multiplexing signals employed in the Long-Term Evolution, which exhibit a large peak-to-average power ratio. To model accurately the performance of these systems a realistic model of the semiconductor laser is required. In this work, we compare, experimentally and through simulation, the performance of orthogonal frequency division multiplexing (OFDM) and single carrier frequency division multiple access signals (SC-OFDMA), in radio-over-fiber applications, using directly modulated vertical cavity surface emitting lasers. An accurate theoretical model of a 1.55  $\mu\text{m}$  vertical cavity surface emitting laser is presented, for which device parameters are extracted based on fitting the model to experimental data of frequency response and reflection coefficient measurements. The simulation model fits well the experimental results, and we conclude that since the SC-FDMA modulation presents a lower PAPR than the OFDM modulation, as expected, it is more immune to intermodulation distortion than the OFDM modulation, yet it is more susceptible to noise.

# Reconfigurable memories using temporal localized states of light in time-delayed neuromorphic photonic oscillators

**B. Romeira<sup>1,2</sup>, J. M. L. Figueiredo<sup>1</sup>, J. Javaloyes<sup>3</sup>**

*1- Centro de Electrónica, Optoelectrónica e Telecomunicações, Departamento de Física, Universidade do Algarve, 8005-139 Faro, Portugal*

*2- Present address: COBRA Research Institute, Eindhoven University of Technology, P.O. Box 513, NL-5600 MB Eindhoven, Netherlands*

*3- Departament de Física, Universitat de les Illes Balears, C/Valldemossa km. 7'5, E-07122, Palma, Spain*

*Main author email address: b.m.romeira@tue.nl*

The possibility of writing, storing and control information employing new reconfigurable memory technologies are under intense investigation by both academics and industries in order to realize ultra-high storage density with low power consumption as required in future optical communications systems. Of particular interest are the approaches that work analogously to the brain [1]. These neuromorphic systems can harness the interesting physics being discovered in the development of new devices to emulate the biophysics of real synapses and neurons that could be employed in large-scale artificial neural systems opening new ways of efficiently store and control large amounts of information.

Recent trends in nanoelectronics have been investigating low-power nanoscale devices for extending standard CMOS very large-scale integration (VLSI) electronic technologies [2] beyond the current state of the art – spintronics and memristor devices are the most promising candidates as synapse in neuromorphic systems [3]. On the other hand, integrated photonic platforms offer an alternative approach to electronics taking advantage of the high switching speeds, high communication bandwidth, and low cross talk achievable in photonics [4].

In this work, we shine light in the paradigm of reconfigurable memories proposing a new type of time-delayed neuromorphic photonics-based systems that show a deep relation with the paradigm of neuronal dynamics and regenerative memories. It consists of a nanoscale negative differential conductance memory device, the resonant tunneling diode photo-detector (RTD-PD) [5], integrated with a semiconductor optical laser source in an optical fiber feedback loop. It operates under the physical principle of excitable [5] (i.e. neuron-like) regeneration, whereas a temporal localized state of modulated light re-circulates indefinitely in a time-delayed delayed feedback loop enabling robust regenerative signal buffering and the potential for logical operations. This novel concept system constitute an ideal support for bits in a buffer memory and opens the possibility of writing, storing (i.e. buffer) and control information (i.e. reconfigurable memory) that work analogously to the brain mimicking the biophysics of real synapses and neurons.

[1] C. Mead, "Neuromorphic electronic systems," P. IEEE 78(10), 1629–1636 (1990).

[2] G. Indiveri, E. Chicca, and R. Douglas, "A VLSI array of low-power spiking neurons and bistable synapses with spike-timing dependent plasticity," P. IEEE 17(1), 211–221 (2006).

[3] S. H. Jo, T. Chang, I. Ebong, B. B. Bhadviya, P. Mazumder, and W. Lu, "Nanoscale Memristor Device as Synapse in Neuromorphic Systems," Nano lett. 10(4), 1297–1301 (2010).

[4] L. Schares et al., "Terabus: Terabit/second-class card-level optical interconnect technologies," IEEE J. Sel. Top. Quantum Electron. 12, 1032 (2006).

[5] B. Romeira et al., "Excitability and optical pulse generation in semiconductor lasers driven by resonant tunneling diode photo-detectors," Opt. Express 21, 20931 (2013).

# Photobleaching Phenomenon in Bismuth-Doped Laser-Active Fibers

S. Alyshev, S. Firstov, E. Dianov

Fiber Optics Research Center of the Russian Academy of Sciences, 38 Vavilov Street, 119333 Moscow, Russia

e-mail: [alyshs@fo.gpi.ru](mailto:alyshs@fo.gpi.ru)

It has been shown that bismuth doped optical fibers are promising active medium for lasers and optical amplifiers operating in spectral range of 1100 – 1800 nm [1, 2]. Despite considerable progress demonstrated in this area exact nature of bismuth related active centers is still controversial and opened for debate. From the standpoint of the production of Bi-doped fibers possessing best possible characteristics it is highly desirable to be able to formulate atomic-scale model of bismuth related near IR active center. To that matter, the accumulation of experimental information related to the behaviour of Bi-doped active fibers under wide variety of external condition is essential.

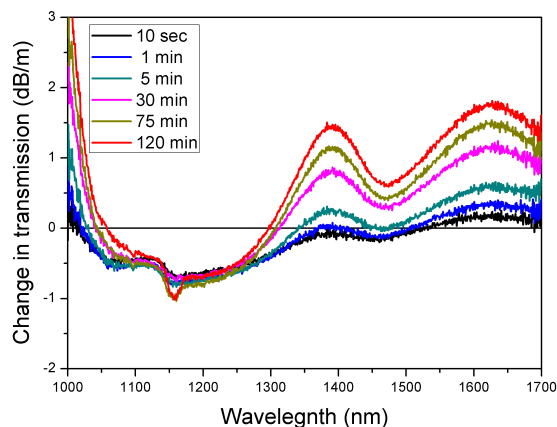


Figure 1. Spectral changes in optical transmission under 532-nm irradiation

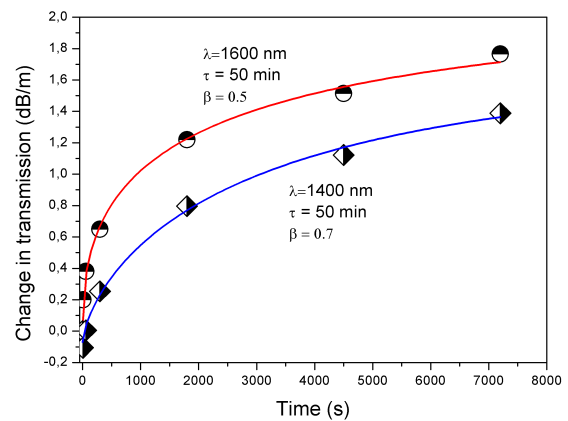


Figure 2. Temporal dependence of photoinduced bleaching effect at 1400 (rhombus) and 1600 nm (circle)

We have established that under 532-nm irradiation the irreversible degradation (photobleaching) of the Bi-related IR-active centers in Bi-doped germanosilicate optical fibers takes place. The figures above are to represent the essence of the phenomenon. Figure 1 shows changes in the optical transmission spectrum of Bi-doped fibers as irradiation at 532 nm progresses in time. The transmission spectra were recorded using wide-band low-power source while green laser was switched off. The temporal dependencies of the bleaching process at wavelength of 1400 and 1600 nm are presented in Figure 2. To estimate the characteristic time of the bleaching process the experimental data were fitted using stretched exponential function.

In this presentation we will report our results on photobleaching phenomenon in Bi-doped optical fibers in more detail. Next, these results will be used as a foundation to provide some clarification in the understanding of the nature of IR active centers in bismuth doped fibers.

## Acknowledgements

The reported study was funded by RFBR according to the research project #15-32-20234.

[1] I.A. Bufetov, M.A. Melkumov, S.V. Firstov, K.E. Riumkin, A.V. Shubin, V.F. Khopin, A.N. Guryanov, and E.M. Dianov, Bi-doped optical fibers and fiber lasers, IEEE J SEL TOP QUANT 20(5), 0903815 (2014).

[2] S. Firstov, S. Alyshev, M. Melkumov, K. Riumkin, A. Shubin, and E. Dianov, Bismuth-doped optical fibers and fiber lasers for a spectral region of 1600–1800 nm, Opt. Lett., Vol. 39, Issue 24, pp. 6927-6930 (2014).

## **Enabling the study of photons OAM applications for optical communications**

**André B. Cunha<sup>1</sup>, G. Figueira<sup>2</sup>, P. S. André<sup>1</sup>**

*1 - Instituto de Telecomunicações, Departament of Electronic and Computer Engineering,  
Instituto Superior Técnico, Universidade de Lisboa, Portugal*

*2 - GoLP – Instituto de Plasma e Fusão Nuclear, Instituto Superior Técnico,  
Universidade de Lisboa, Portugal*

*andre.bastos.da.cunha@tecnico.ulisboa.pt*

The internet data traffic capacity is rapidly reaching the limits imposed by optical fiber nonlinear effects, having almost exhausted the available degrees of freedom needed to orthogonally multiplex data [1]. Therefore, urges to develop new methods in order to avoid the upcoming capacity crunch using classical communications channels. In this regard, the orbital angular momentum (OAM) of photons may be used as an additional degree of freedom, with potentially unlimited number of achievable orthogonal states which is gathering significant attention within the scientific community.[2][3]

Therefore, in this work we report the establishment of a theoretical, operational and experimental basic framework foundation to performing studies in this area, aiming the applications in optical communications.

Furthermore, we demonstrated experimentally the possibility to control the OAM of optical beams using spatial light modulators.

- [1] P. J. Winzer, "Modulation and multiplexing in optical communication systems," *IEEE Leos Newsletter*, 2009.
- [2] N. Bozinovic, N. Bozinovic, Y. Yue, Y. Yue, Y. Ren, Y. Ren, M. Tur, M. Tur, P. Kristensen, P. Kristensen, H. Huang, H. Huang, A. E. Willner, A. E. Willner, S. Ramachandran, and S. Ramachandran, "Terabit-scale orbital angular momentum mode division multiplexing in fibers.," *Science*, vol. 340, no. 6140, pp. 1545–1548, Jun. 2013.
- [3] J. Wang, J.-Y. Yang, I. M. Fazal, N. Ahmed, Y. Yan, H. Huang, Y. Ren, Y. Yue, S. Dolinar, M. Tur, and A. E. Willner, "Terabit free-space data transmission employing orbital angular momentum multiplexing," *Nature Photon*, vol. 6, no. 7, pp. 488–496, Jun. 2012.

# Energy aware performance for next-generation Flex-Grid vs Fixed-Grid Optical Network

**N. Gouveia<sup>1</sup>, M. Henriques<sup>2</sup>, P. Pinho<sup>1,3</sup>**

*1- Electronics, Telecommunications and Computer Dept., ISEL, Lisbon, Portugal*

*2- Coriant, Lisbon, Portugal*

*3- Instituto de Telecomunicações, Aveiro, Portugal*

*A32089@alunos.isel.pt*

The evaluation and reduction of energy consumption of core network has been a popular subject of academic research in the last years. The network services use high bandwidth and put the onus on the network operators to efficiently use the network resources. The Standardization Groups are doing a significant progress moving from available optical channels (10, 40, 100 Gbps) up to the future expected 400 Gbps or even 1 Tbps in core networks [1].

In the next generation of WDM (Wavelength Division Multiplexing) the spectrum-efficient optical transmission with bitrates of 400 Gbps and beyond can be achieved using flex-grid networks. Flex-grid provide flexibility to the operators when assigning spectrum compared to traditional fixed-grid WDM networks using the 50GHz ITU grid [2]. Flex-grid breaks the spectrum into small slots (typically 12.5 GHz) as recently defined by ITU-T [2].

This additional flexibility will allow faster transport by using a mixed bit rate or mixed modulation format transmission system to allocate frequency slots with different widths. From the use of these new spectrum efficient modulation formats and finer control over spectrum allocations, a key benefit that flex-grid offers network operators is that their WDM networks can carry more traffic with optimized spectral efficiency and reduction of OPEX.

In this paper, we propose a reference optimization model for IP (Internet Protocol) over WDM networks [3] with focus on energy aware routing techniques. Also a realistic approach of traffic pattern [4] and forecast (from 2006 to 2019) [5-7], was considered based at statistical information. Comparisons between different models allow us to conclude the advantage by using flex-grid, by additional energy consumption savings over those that are using a traditional fixed-grid network.

**Keywords:** Flex-grid, Fixed-grid, IP, WDM, efficiency, energy, spectrum.

[1] Ethernet Alliance, “2015 Ethernet Roadmap”, 2015.

[2] ITU, “Spectral grids for WDM applications: DWDM frequency grid”, Recommendation G694.1, 2012.

[3] G. Shen, & R. S. Tucker, “Energy-Minimized Design for IP Over WDM Networks”, Optical Society of America, 2009.

[4] A. Betker, C. Gerlach, R. Hülsermann, M. Jäger, “Reference Transport Network Scenarios”.

[5] Cisco Systems Inc, “Cisco Visual Networking Index: Forecast and Methodology, 2007–2012”, 2008.

[6] Cisco and/or its affiliates, “Cisco Visual Networking Index: Forecast and Methodology, 2012–2017”, 2013.

[7] Cisco and/or its affiliates, “Cisco Visual Networking Index: Forecast and Methodology, 2014–2019”, 2015.

---

---

## **SECTION S**

### **Sensors**

---

---

# High-speed wavelength-swept lasers and their applications to dynamic optical fiber sensors

**Min Yong Jeon, Myeong Ock Ko, and Yong Seok Kwon**

*Department of Physics, Chungnam National University, Daejeon, Korea*

[myejon@cnu.ac.kr](mailto:myejon@cnu.ac.kr)

High-speed wavelength-swept lasers (WSLs) have potential applications as the optical sources for bio-photonics imaging, fiber-optic sensors, and frequency-swept optical beat source generation [1-3]. WSLs are demonstrated by employing a narrowband wavelength-scanning filter. In particular, a high-speed WSL can be used for dynamic or real-time measurement in optical fiber sensors with a high sensitivity and a wide dynamic range. The main advantage of using the WSL for measurement is the linear relationship that exists between wavelength and time. Therefore a wavelength in the spectral domain exactly corresponds to a pulse signal in the temporal domain. In this presentation, our results related on the dynamic fiber-optic sensors based on the WSL will be reviewed. Two kinds of WSLs are used to demonstrate the dynamic measurement in the fiber-optic sensors. One is the WSL using a polygon-scanner-based wavelength filter[4] and the other is the Fourier domain mode-locked (FDML) WSL using a FFP-TF[5]. The dynamic FBG sensor interrogation up to 2 kHz by using a WSL with a polygon-scanner-based wavelength filter is reported. And by using an FDML WSL with a FFP-TF, we demonstrate a resonance FBG sensor interrogation. As another application of the WSL, we successfully measure a dynamic modulation frequency of the applied electric field using a nematic liquid crystal Fabry-Perot etalon[6].

- [1] S. H. Yun, C. Boudoux, G. J. Tearney, and B. E. Bouma, "High-speed wavelength-swept semiconductor laser with a polygon-scanner-based wavelength swept filter," *Opt. Lett.* **28**, 1981-1983, (2003).
- [2] M. Y. Jeon, J. Zhang, Q. Wang, and Z. Chen, "High-speed and wide bandwidth Fourier domain mode-locked wavelength swept laser with multiple," *Opt. Express* **16**, 2547-2554 (2008).
- [3] M. Y. Jeon, N. Kim, S.-P. Han, H. Ko, H.-C. Ryu, D.-S. Yee, and K. H. Park, "Rapidly frequency-swept optical beat source for continuous wave terahertz generation," *Opt. Express* **19**, 18364-18371 (2011).
- [4] Y. S. Kwon, M. O. Ko, M. S. Jung, I. G. Park, N. Kim, S.-P. Han, H.-C. Ryu, K. H. Park, and M. Y. Jeon, "Dynamic sensor interrogation using wavelength-swept laser with a polygon-scanner-based wavelength filter," *Sensors* **13**, 9669-9678 (2013)
- [5] B. K. Choi and M. Y. Jeon, "Resonance Fiber Bragg Grating Sensor system based on Fourier Domain Mode-locking Laser" *Korea. J. Opt. Photon.*, Vol. 23, p. 211-216 (2012).
- [6] M. O. Ko, S.-J. Kim, J.-H. Kim, B. W. Lee, and M. Y. Jeon, "Dynamic measurement for electric field sensor based on wavelength-swept laser," *Opt. Express* **22**, 16139-16147 (2014).

## Perspective work on optical fibre sensors

**Carlos A. F. Marques<sup>\*</sup>, David. J. Webb**

*Aston Institute of Photonic Technologies, Aston University, B4 7ET, Birmingham, UK*

*\* c.marques@aston.ac.uk*

### Abstract

Optical fibre based sensors are transforming industry by permitting monitoring in hitherto inaccessible environments or measurement approaches that cannot be reproduced using conventional electronic sensors. A multitude of techniques have been developed to render the fibres sensitive to a wide range of parameters including: temperature, strain, pressure (static and dynamic), acceleration, rotation, gas type, and specific biochemical species. Constructed entirely of glass or polymer material, optical fibre devices like fibre gratings offer the properties: low loss, dielectric construction, small size, multiplexing, and so on [1-3]. In this paper, the authors will show the latest developing industrial applications, using polymer optical fibre (POF) devices, and comparing their performance with silica optical fibre devices.

The authors address two pressing commercial requirements. The first concerns the monitoring of fuel level in civil aircraft. There is a strong motivation in the aerospace industry to move away from electrical sensors, especially in the fuel system. This is driven by the need to eliminate potential ignition hazards, the desire to reduce cabling weight and the need to mitigate the effects of lightning strikes in aircraft where the conventional metallic skin is increasingly being replaced by composite materials. In this case, the authors have developed pressure sensors based on a diaphragm in which a polymer fibre Bragg grating (POFBG) has been embedded [3]. These devices provide high pressure sensitivity enabling level measurement in the mm range. Also, it has developed an approach incorporating several such sensors which can compensate for temperature drifts and is insensitive to fluid density. Compared with silica fibre-based sensors, their performance is highly enhanced. Initial results have attracted the interest of Airbus from UK, who is keen to explore the potential of optical technology in commercial aircraft.

The second concerns the monitoring of acoustic signals and vibration in the subsea environment, for applications in geophysical surveying and security (detection of unwanted craft or personnel). There is strong motivation to move away from electrical sensors due to the bulk of the sensor and associated cabling and the impossibility of monitoring over large distances without electrical amplification. Optical approaches like optical hydrophones [5] offer a means of overcoming these difficulties. In collaboration with Kongsberg from Norway, the authors will exploit the sensitivity improvements possible by using POF instead of silica fibre. These improvements will arise as a result of the much more compliant nature of POF compared to silica fibre (3 GPa vs 72 GPa, respectively). Essentially, and despite the strain sensitivity of silica and POFBGs being very similar, this renders the POF much more sensitive to the applied stress resulting from acoustic signals or vibration. An alternative way of viewing this is that the POF is better impedance-matched to the surrounding environment (water for the intended applications), because although its impedance is higher than that of water, it is nearly an order of magnitude smaller than that of silica.

Finally, other future industrial applications will be presented and discussed, showing the vast range of the optical fiber devices in sensing applications.

### References

- [1] D. J. Webb, "Fiber Bragg grating sensors" In: Handbook of Optical Sensors. Boca Raton, USA: CRC Press, Taylor and Francis Group, 50433, 2014.
- [2] K. Peters, "Polymer optical fiber sensors - A review," Smart Mater. Struct. 20(1), 013002 (2011).
- [3] A. Othonos and K. Kalli, Fiber Bragg Gratings – Fundamentals and Applications in Telecommunications and Sensing (Artech House 1999).
- [4] C. A. F. Marques, G.-D. Peng, D. J. Webb, "Highly sensitive liquid level monitoring system utilizing polymer fiber Bragg gratings," Opt. Express 23, 6058 (2015).
- [5] M. Moccia, M. Consales, A. Iadicicco, M. Pisco, A. Cutolo, V. Galdi, A. Cusano, "Resonant Hydrophones Based on Coated Fiber Bragg Gratings," Journal of Lightwave Technology 30, 2472 (2012).

# Optical fiber sensors for central arterial pressure monitoring

**P. Antunes<sup>1</sup>, C. Leitão<sup>1</sup>, João L. Pinto<sup>1</sup>, José M. Bastos<sup>2</sup>, P. André<sup>3</sup>**

1- Instituto de Telecomunicações, I3N and Department of Physics, University of Aveiro, 3810-193 Aveiro, Portugal

2- Centro Hospitalar do Baixo Vouga E.P.E., Avenida Artur Ravara, 3810-501 Aveiro, Portugal

3- Instituto de Telecomunicações and Department of Electrical and Computer Engineering, Instituto Superior Técnico, Technical University of Lisbon, 1049-001 Lisboa, Portugal

pantunes@ua.pt

The central arterial pulse pressure monitoring has been extensively studied in the last years, being considered a new key factor in hypertension assessment and cardiovascular prevention. The pulse waveforms and central pressure values are often related with arterial stiffness and/or other cardiovascular pathologies. Its measurement it is usually performed using radial tonometry and digital processing [1], with piezoelectric pressure sensors, commonly called arterial tonometers [2].

The demand for simpler, user friendly and lower cost solutions, not disregarding reliability, has been motivating the study and implementation of optical sensors for such application. This category of sensors presents significant advantages when compared with conventional transducers, especially for medical applications requirements, such as: high accuracy and sensitivity; robustness; small size and light weight; electrical isolation from the patient, making them intrinsically safer than electronic sensors; immunity to electromagnetic interference; biocompatible and easy to sterilize [3, 4]. Immunity to electromagnetic interference is one of the relevant advantages for medical applications, allowing the real time monitoring of physiological signals simultaneously with the use of electrical cauterization tools, MRI (magnetic resonance imaging), x-ray or other examination procedures. Therefore, optical sensors are being considered as high potential systems for biomedical applications in a near future.

Our work intends to explore user-friendly and/or lower cost sensors for central arterial pulse pressure monitoring, presenting high sensitivity, portability, and electromagnetic immunity. For that we had developed fiber Bragg grating and plastic optical fiber based sensors. Another ongoing approach is based on non-contact sensing, based on speckle measurements, which is an intensity pattern produced by the mutual interference of a set of wavefronts. Figure 1 illustrates some of the developed sensors and acquired pressure wave signals.

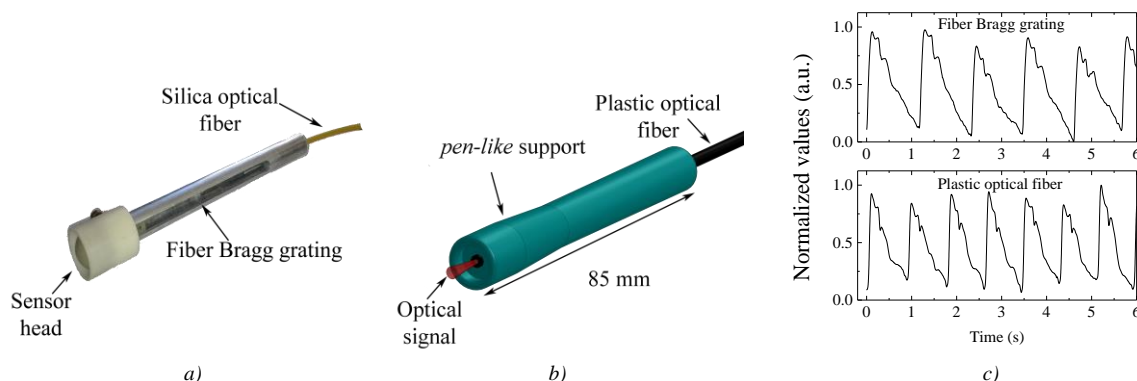


Figure 1. Illustration of a) a fiber Bragg grating based sensor, b) a plastic optical fiber sensor and c) acquired signals.

- [1] C.H. Chen, E. Nevo, B. Fetics, P.H. Pak, F.C. Yin, W.L. Maughan and D.A. Kass., Estimation of central aortic pressure waveform by mathematical transformation of radial tonometry pressure. Validation of generalized transfer function, *Circulation*, vol. 95, pp. 1827–1836, (1997).
- [2] P. Salvi, M.E. Safar and G. Parati, Arterial applanation tonometry: Technical aspects relevant for its daily clinical use, *J. Hypertension*, vol. 31, no. 3, pp. 469–471, (2013).
- [3] S. Silvestri and E. Schena, *Optical-Fiber Measurement Systems for Medical Applications*, Optoelectronics—Devices and Applications, P. Predeep, Ed. Rijeka, Croatia: InTech, (2011).
- [4] N.J. Alberto, L. Bilro, P. Antunes, C. Leitão, H. Lima, P. André, R. Nogueira and J.L. Pinto, Optical fiber technology for eHealthcare, in *Handbook of Research on ICTs and Management Systems for Improving Efficiency in Healthcare and Social Care*, M. Cruz-Cunha, I. Miranda, P. Gonçalves, Eds. Hershey, PA, USA: IGI Global, pp. 180–200, (2013).

## Recent Progress in the Fiber Sensing for Petroleum Industry

**Maria José Pontes<sup>1</sup>, Rogerio S. Marques<sup>1,2</sup>, Adilson R. Prado<sup>1,3</sup>, V. M. Sperandio<sup>1</sup>, Carlos E. S. Castellani<sup>1</sup>, A. Frizera Neto<sup>1</sup>, Moises R. N. Ribeiro<sup>1</sup>, Paulo Antunes<sup>4</sup>, Paulo André<sup>5</sup>**

*1- Federal University of Espírito Santo, Dept. of Electrical Engineering, Goiabeiras, Vitória, Brazil*

*2- Federal Institute of Espírito Santo, Bairro Aviso, Linhares, Brazil*

*3- Federal Institute of Espírito Santo, Rodovia ES 010, km 6.5, Manguinhos, Serra, Brazil*

*4- Instituto de Telecomunicações, I3N and Physics Department, University of Aveiro, Campus Universitário de Santiago, Aveiro 3810-193, Portugal*

*5- Instituto de Telecomunicações and Department of Electrical and Computer Engineering, Instituto Superior Técnico, Universidade de Lisboa, Av. Rovisco Pais, Lisboa 1049-001, Portugal*

*mjpontes@ele.ufes.br*

Optical fiber sensors have experienced growing interest in the determination of several physical and chemical parameters for the environment. Similar outcome was also observed in the petroleum industry. The oil & gas industry is a very important and active economic sector in the world economy, and the state of Espírito Santo in Brazil has experienced increased oil exploration onshore and offshore in recent years. This paper focuses particularly on the recent progress and developments of optical sensors applied in this field; the working principles and basic fiber sensor under development at UFES (Laboratory of Telecommunications – LabTel) motivated by the oil industry.

One application is the temperature monitoring, which is a fundamental problem in this industry, especially for crude oil, since the volumetric efficiency, viscosity, and density directly depends on the fluid temperature. Therefore, accurate and reliable temperature measurements are critical all along the production chain. It means checking the temperature during oil extraction, transportation, storage, and refining [1, 2]. There are also important operational and economical procedures that heavily depended on accurate temperature measurements. Besides the temperature issues, another important sensing parameter in the oil plants is the liquid level existent in oil tanks. It requires constant monitoring and registration for fiscal or production record purposes [3]. Pressure monitoring in classified areas is another theme that can be sensed by applying optical technology. Electrical equipment installed in hazardous location to control process in rigs and platforms vessels is especially designed and tested to avoid risk of explosion, due to arcing contacts or high surface temperature of equipment in case of failure. A new optical pressure control concept in petroleum industry based on laser speckle analysis, with inherent safety light, was proposed and it is under evaluation [4]. Several conventional technologies are available for sensing the oil plants, however the fiber sensing technology is becoming attractive and even competitive with some of already well known existing conventional sensors.

In terms of new technologies to be explored for applications in such industry that impose severe operational restrictions, owing to its explosive, toxic, and corrosive nature, chemical sensors are been studied [5]. The addition of sulfide in a sample of citrate-stabilized gold nanoparticles is under development and considered as sensors for detecting sulfide compounds. Those challenges bring along opportunities, since small innovations in the oil industry can generate large economic returns.

[1] K. Kashfi, A. Chapoy, K. Bell, B. Tohidi, Viscosity of binary and multicomponent hydrocarbon fluids at high pressure and high temperature conditions: measurements and predictions. *Journal of Petroleum Science and Engineering*, 112, 153-160, 2013.

[2] A. Werner, J. C. Hemptinne, F. Behar, E. Behar, C. Boned, A new viscosity model for petroleum fluids with high asphaltene content. *Fluid Phase Equilibria*, 147, 319-341, 1998.

[3] ISO 4266-1/02. Petroleum and Liquid Petroleum Products - Measurement of Level and Temperature in Storage Tanks by Automatic Methods - Part 1: Measurement of Level in Atmospheric Tanks. Geneva, 18 p., 2002.

[4] V. M. Sperandio, L. G. Webster, A. Frizera Neto, M. J. Pontes, A new optical pressure sensor interrogated by speckles pattern for oil industry, accepted for presentation at International Conference on Optical Fibre Sensors (24<sup>th</sup> OFS), Sept 28 to Oct 2<sup>nd</sup> Curitiba/PR, Brazil, 2015.

[5] A. R. Prado, J. P. Oliveira, R. H. A. Pereira, M. C. C. Guimarães, B. V. Nogueira, E. V. R. Castro, L. C. P. Almeida, M. R. N. Ribeiro, M. J. Pontes, Surface-Enhanced Raman Plasmon in Self-Assembled Sulfide-Coated Gold Nanoparticle Arrays, *Plasmonics*, Feb 2015, DOI 10.1007/s11468-015-9909-2.

## **Laser printing and activation of biosensor surfaces**

**M. Chatzipetrou<sup>1</sup>, M. Massaouti<sup>1</sup>, L. Scheres<sup>2</sup>, A. Trilling<sup>2</sup>,  
M. Smulders, H. Zuilhof<sup>3</sup>, I. Zergioti<sup>1\*</sup>**

*1-National Technical University of Athens, Physics Department, Iroon Polytechniou 9, 15780 Zografou, Athens, Greece*

*2- Surfix BV, 7500 AL Enschede The Netherlands*

*3- Laboratory of Organic Chemistry, Wageningen University, Dreijenplein 8, 6703 HB, Wageningen, The Netherlands*

*email: zergioti@central.ntua.gr*

Laser Induced Forward Transfer is a direct write technique, able to print micropatterns of biomaterials[1, 2] on sensing devices. In this conference we will present a new approach of using LIFT technique for the printing and photo-immobilization of thiol modified aptamers against Ochratoxin A (OTA) on silicon nitride substrates modified with Alkenes and/or Alkynes. Aptamers are oligonucleic acid or peptide molecules that bind to a specific target molecule by modifying their 3D shape.

Following the printing procedure, laser UV illumination of the samples occurred so as to covalently attach the aptamers on the surfaces. The attachment of the aptamers on the surfaces becomes due to a chemical reaction called thiol-ene reaction. The thiol modified aptamers, are able to bond to the alkene/alkyne samples, when the carbon double/triple bond of the alkenes/alkynes breaks due to photo-illumination and carbon molecules react with the hydrogen molecules of the thiol. Light-mediated thiol-ene reactions effectively combine the classical benefits of click reactions with the advantages of a photo-initiated process, which can be activated at specific times and locations, resulting in a powerful method for chemical immobilization of biomaterials.

The printing experiments were carried out, using a pulsed Nd:YAG laser (355 nm, 10 ns) and a high power imaging micromachining system. The laser beam is focused onto a quartz-donor substrate, which is coated

with 10  $\mu$ M aptamers solution. The photo-immobilization experiments occurred with the same laser source, at 355 nm wavelength. The shape and the size of the illumination pulse was specified by a square mask.

Fluorescent microscopy images were taken so as to confirm both the immobilization efficiency of the aptamers and the binding to the target analyte (OTA).

[1] E. Touloupakis, M. Chatzipetrou, C. Boutopoulos, A. Gkouzou, and I. Zergioti, "A polyphenol biosensor realized by laser printing technology," *Sensors Actuators, B Chem.*, vol. 193, pp. 301–305, 2014.

[2] G. Tsekenis, M. K. Filippidou, M. Chatzipetrou, V. Tsouti, I. Zergioti, and S. Chatzandroulis, "Heavy metal ion detection using a capacitive micromechanical biosensor array for environmental monitoring," *Sensors Actuators B Chem.*, vol. 208, pp. 628–635, 2015.

# Planar chiral nanostructures for biosensing

Lingling Huang<sup>1</sup>

*1- School of Optoelectronics, Beijing Institute of Technology, Beijing 100081, China*

*E-mail: huanglingling@bit.edu.cn*

Planar chiral nanostructures (PCSs) are artificial two-dimensional or quasi three-dimensional nanostructures composed of achiral media and patterned with chiral features lacking any spatial inversion or mirror symmetry [1]. PCSs are extensively studied in recent years because they exhibit large chiroptical effects such as optical activity and circular dichroism (CD) much stronger than those in natural chiral media [2]. Based on these effects, PCSs may be developed as, e.g., compact polarization rotators, broadband circular polarizers, circularly polarized light emitting devices, light-driven chiral nanomotors, and negative refractive index metamaterials. In addition, it was reported that PCSs can be developed as novel biosensors for the ultrasensitive detection and characterization of chiral biomolecules [3].

Here, we perform a thorough theoretical investigation on the sensibilities of the PCSs, by comparatively studying two complementary types of PCSs: a hole-type one and a particle-type one. In the chiral sensing operation, a pair of enantiomeric PCSs, i.e., two PCSs with the same geometry but opposite senses of chirality such as right-handed (RH) and left-handed (LH) chiral patterns, are covered with chiral analyte. Their CD spectra, which should be mirror symmetric to each other in an achiral environment, would be blue- or red-shifted depending on the light-matter interactions in the LH- and RH-PCSs. By inspecting the shift (both the direction and magnitude) of the two CD spectra, the conformational and constitutional chirality information of the chiral analyte can be achieved. We further evaluate from the near-field to get the insight physics. We find that the hole-type PCS can exhibit one order of magnitude larger chiral sensitivity than the particle-type counterpart, due to the excitation and coupling of surface plasmon polaritons and localized surface plasmons. The influence of the near-field excitation on the generated superchiral fields in the PCSs is studied, revealing the mechanism of the sensibility improvement.

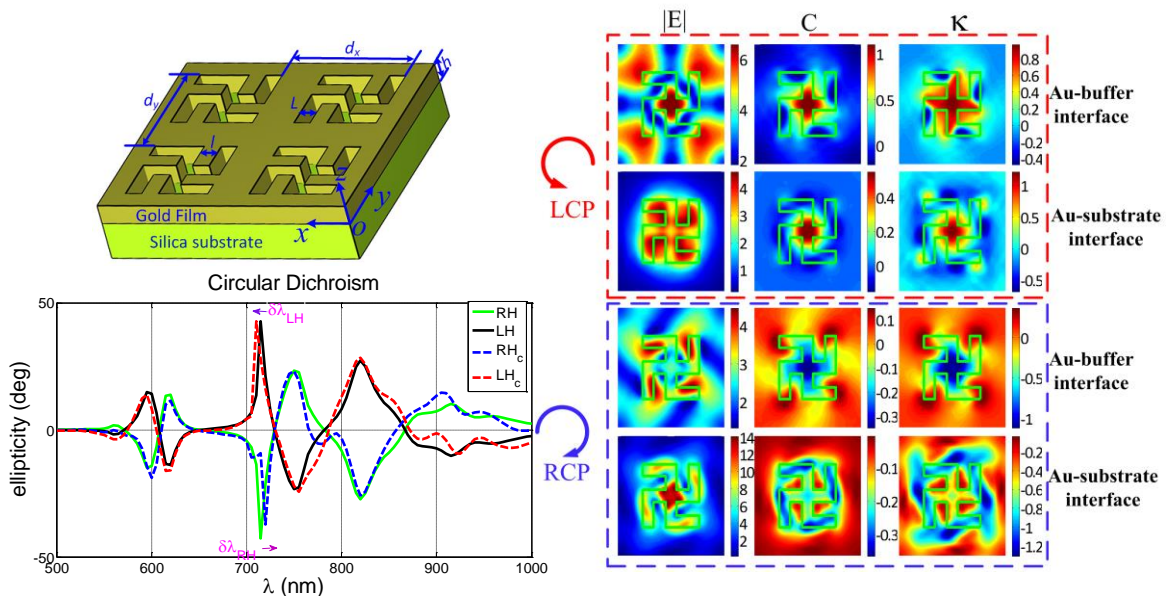


Fig1. Schematic geometries of the investigated hole-type PCSs, calculated CD spectrum shifts in both right-hand and left-hand patterns with chiral solution, and near-field excitation of superchiral fields.

[1] A. V. Rogacheva, V. A. Fedotov, A. S. Schwanecke, and N. I. Zheludev, "Giant gyrotropy due to electromagnetic-field coupling in a bilayered chiral structure," *Phys. Rev. Lett.* 97, 177401 (2006).

[2] M. Decker, M. W. Klein, M. Wegener, and S. Linden, "Circular dichroism of planar chiral magnetic metamaterials," *Opt. Lett.* 32, 856 (2007).

[3] E. Hendry, T. Carpy, J. Johnston, M. Popland, R. V. Mikhaylovskiy, A. J. Laphorn, S. M. Kelly, L.D. Barron, N. Gadegaard and M. Kadodwala, "Ultrasensitive detection and characterization of biomolecules using superchiral fields," *Nature Nanotechnology* 5, 783 (2010).

# Fine spectral interference in Chirped Large-Mode-Area Fiber Bragg Gratings

Reza Poozesh<sup>1,2</sup>, Vahid Vatani<sup>1</sup>, Kamran Hejaz<sup>1</sup>, Ali Roohforouz<sup>1,3</sup>, Amin Babazadeh<sup>1</sup>, S. Naser Tabatabaei Jafari<sup>1</sup>, Reza Rezaei Nasirabad<sup>1</sup>, Amir Heidariazar<sup>1</sup>, Majid Lafouti<sup>1</sup>, Khosro Madanipour<sup>2</sup>

*1-Iranian National Center for Laser Science and Technology, Tehran, Iran*

*2-Optics, Laser and Photonics Institute (OLPI) of Amirkabir University of Technology, Tehran, Iran*

*3-Kharazmi University*

*Email: rpoozesh@aut.ac.ir*

Large Mode Area (LMA) fiber Bragg gratings (FBGs) are widely used in fiber laser systems for different purposes such as fiber laser reflectors, dispersion compensator, spectral filter, etc. Spectral response of LMA FBGs depends on modal content [1,2]. In a work on non-chirped LMA FBGs, it was observed a single fringe of interference in the middle of spectrum because of the overlap of the two modes [3]. However, in all works on LMA FBGs, fine spectral interference has not been observed in the reflection spectrum. We characterized chirped Large-Mode-Area fiber Bragg gratings (CFBGs) spectrum with high resolution in cases of one- and Two-mode operations. We observed a fine spectral interference in the overlapping region of the reflected spectrum of the fiber modes. This interference was appeared in the reflection spectrum because of a large overlapping region of the reflected spectrum of fiber modes in LMA CFBGs. Fig. 1a shows a high resolution reflected spectrum of the CFBG for two cases. In the first one, both  $LP_{01}$  and  $LP_{11}$  modes are present but the  $LP_{01}$  mode is the dominant. As, it is observed, reflected spectrum is modulated by 0.08 nm FSR. In the second one, the CFBG input fiber is coiled at a diameter of 10 cm to remove  $LP_{11}$  mode. We observed that the amplitude of the interference fringes decreased significantly and the reflected spectrum became nearly uniform.

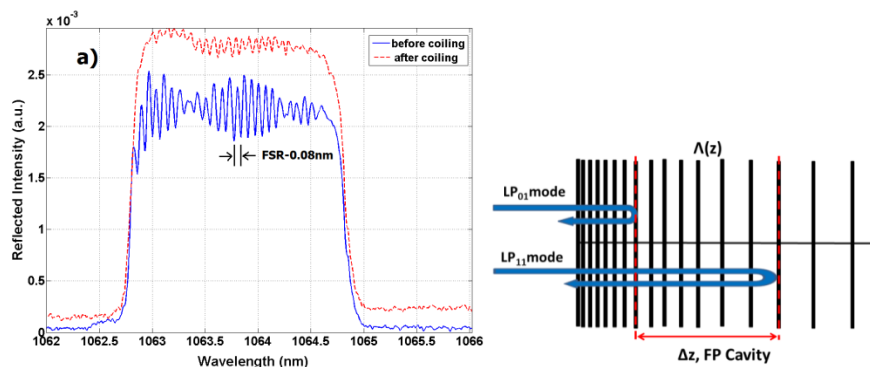


Fig.1a) Reflected spectra of CFBG with high resolution for the two cases: Both modes are present but  $LP_{01}$  mode is dominant (blue line),  $LP_{01}$  mode is present but  $LP_{11}$  mode is removed by coiling (Red line) ; b) Schematic of formed Chirped FBG FP.

To explain spectral interference, it can be assumed that  $LP_{01}$  and  $LP_{11}$  modes are reflected from two given positions in CFBG because of different effective index of modes (Fig. 1b). Therefore, these two positions can be considered as reflector positions of a FP cavity that difference of them is cavity length. We obtained free spectral range by analyzing FP cavity in the two-mode operation. The FSR of the CFBG FP was obtained by calculating FP cavity length [4,5]. The calculated FSR of the CFBG FP is in complete accordance with experimental measurements. The results of this work can be used in bend sensors.

[1]F. Stutzki, C. Jauregui, C. Voigtländer, J. Thomas, S. Nolte, J. Limpert, A. Tünnermann, "Real-Time Monitoring of the Modal Content of Monolithic Large-Mode-Area Fiber Lasers", OSA OFC/NFOEC, (2010)

[2]T. Mizunami, T. Djambova, T. Niiho, and S. Gupta, "Bragg gratings in multimode and few-mode optical fibers," J. Lightw. Technol., vol. 18, no. 2, pp. 230–235, (2000)

[3]W. Mohammed and X. Gu, "Fiber Bragg grating in large-mode-area fiber for high power fiber laser applications," Appl. Opt. vol. 49, p. 5297-5301, (2010)

[4]R. Poozesh, V. Vatani, M. Laffouti, K. Hejaz, R. Rezaei, A. Babazadeh, S.H. Ghasemi, and J. Sabbaghzadeh, "Experimental Study and Simulation of Modular Interference in Two-Mode Fiber Optics and Spectroscopy, vol. 111, no. 2, pp. 284–286, (2011)

[5]R. Kashyap, Fiber Bragg Gratings, Academic, San Diego (1999).

# Catalytic and sensory properties of copper structures obtained by laser-induced deposition from solution

**M. S. Panov, D. I. Gordeychuk, V. V. Mironov, I. I. Tumkin, A. S. Mereshchenko**

*Saint-Petersburg State University, Institute of chemistry, 198504 Russian Federation, Saint-Petersburg, Petrodvorets, Universitetsky pr. 26.*

*mpanov@chem.spbu.ru*

Laser-induced chemical liquid-phase metal deposition (LCLD) is a method based on metal reduction in local volume of solution within the focal point of laser beam resulting in metal deposition on the surface of dielectric substrate. This method allows to produce small-size metal structures with developed surface and high electrical conductivity [1,2]. Moreover, the sensory material in the metal continuous structures obtained by LCLD can be used as a lead-in conductor, i. e. therefore one can avoid the influence of contacts on the analytical signal. Thus it gives an opportunity to apply the aforementioned structures in fabrication of microelectrodes which in turn are a promising basis for biosensors design and production [3]. The surface of the copper electrode fabricated by LCLD was studied by stripping voltammetry. An analytical response of the fabricated copper electrode is 15 times higher than those observed for copper wire with similar geometric parameters which was used as a standard electrode. The sensory characteristics of the copper electrode fabricated by LCLD for hydrogen peroxide detection were studied. It was found that the value of Faraday current at the copper electrode fabricated by LCLD is 2-2.5 orders of magnitude higher than for standard one.

Another unique property of obtained copper structures is their catalytic activity for the process of laser-induced nanoparticles formation in the presence of hydrogen. These particles produced by LCLD can take part in organic catalysis, for example in reforming of alcohols used as the reaction medium. In this work we studied the catalytic decomposition of ethylene diamine tetraacetic acid (EDTA) accompanied by gaseous hydrogen, ethylene and carbon dioxide release. Here, laser initiation of the reaction results in the generation of gas phase and its accumulation but when we shut off the laser beam EDTA containing solution relaxes to the initial state. NMR studies of the observed organic reactions reveal that one of the possible reaction mechanisms is elimination of carboxylic groups and substitution of alpha protons in EDTA molecule.

We acknowledge the Russian Fund for Basic Research (grants 15-03-05139) and Saint-Petersburg State University for a research grants (2015–2017, 12.38.219.2015) and postdoctoral fellowship (No. 12.50.1189.2014). The authors also highly appreciate the Interdisciplinary Resource Center for Nanotechnology St. Petersburg State University.

[1] V. A. Kochemirovsky, L. G. Menchikov, S. V. Safonov, M. D. Bal'makov, I. I. Tumkin, Yu. S. Tver'yanovich, Laser-induced chemical liquid phase deposition of metals: chemical reactions in solution and activation of dielectric surfaces, *Russian Chemical Reviews* (Russ. Chem. Rev.), 80,869-882, (2011).

[2] I. I. Tumkin, V. A. Kochemirovsky, M. D. Bal'makov, S. V. Safonov, E. S. Zhigley, L. S. Logunov, E. V. Shishkova, Laser-induced deposition of nanostructured copper microwires on surfaces of composite materials, *Surf. Coating Tech.*, 264, 187-192, (2015).

[3] J. Wang, Decentralized electrochemical monitoring of trace metals: from disposable strips to remote electrodes, Plenary lecture. *Analyst*, 119,763-766, (1994).

## **Verification of optical frequency references quality - a way to efficient laser standards**

**J. Hrabina<sup>1</sup>, M. Šarbort<sup>1</sup>, M. Zucco<sup>2</sup>, O. Acef<sup>3</sup>, E. Chea<sup>3</sup>, F. Du-Burck<sup>4</sup>, M. Holá<sup>1</sup>,  
J. Oulehla<sup>1</sup>, J. Lazar<sup>1</sup> and O. Číp<sup>1</sup>**

*1- Institute of Scientific Instruments, Academy of Sciences of the Czech Republic, Královopolská 147, 61264 Brno, Czech Republic*

*2- L'Istituto Nazionale di Ricerca Metrologica (INRIM), Strada delle Cacce, 91 - 10135 Torino, Italy*

*3- Systèmes de Référence Temps Espace, SYRTE/CNRS UMR 8630/Observatoire de Paris /LNE/UPMC, 61, avenue de l'Observatoire F-75014 Paris, France*

*4- Laboratoire de Physique des Lasers, CNRS-UMR 7538, Université Paris 13, Sorbonne Paris Cité, 99, avenue Jean-Baptiste Clément, Villetaneuse 93430, Paris, France*

*Email address: hrabina@isibrno.cz*

The optical frequency references - absorption cells - represent an unique tool for a laser frequency stabilization [1]. They have an irreplaceable position in realization of laser standards, sources of light for laser interferometry – in these days the most precise dimensional measurement method [2]. An usage of these references allows not only to obtain stable laser sources, but also ensures the direct traceability of the measurement to fundamental standard. One of the most often used absorption gas is molecular iodine. It covers wide spectral range from green to near IR and it offers a rich atlas of narrow and strong absorption lines. The main disadvantage of this absorption media is its big reactivity with other materials and also its high sensitivity to contamination by other elements. The impurities in iodine cells cause unwanted spectral shifts of absorption spectra and also degradate the frequency stability of realized laser standards. Due to these reasons, the quality of the cells must be precisely controlled during their lifetime. We present a development of new types of iodine absorption cells for frequency stabilization of lasers intended for using in laser interferometry (mainly frequency doubled Nd :YAGs and He-Ne lasers) with simplified design and technology and also cost reduction. These references exploit approaches of using of new materials and technology of filling of absorption media to certain saturation pressure [3]. Technological process is described in detail and performance of these cells is discussed. The research was supplemented with development of novel method for evaluation of quality of the optical frequency references based on molecular iodine. This method is based on hyperfine transition lineshape measurement and we are verifying that it overcomes difficulties and limits of traditionally used laser induced fluorescence and absolute frequency measurement methods. Moreover, the optical setup of these method can be used for another experiments, in our case scanning of unknown part of spectra of molecular iodine. This aspect is also briefly discussed. The comparisons of all of these three methods is presented on a set of several iodine cells of different age, design, and absorption media purity.

[1] J. Lazar, J. Hrabina, P. Jedlička, O. Číp, Absolute frequency shifts of iodine cells for laser stabilization. *Metrolog.*, 46(5), 450-456, (2009)

[2] J. Hrabina, J. Lazar, P. Klapetek, O. Číp, Multidimensional interferometric tool for the local probe microscopy nanometrology, *Meas. Sci. Technol.*, 22(9), (2011).

[3] J. Hrabina, M. Šarbort, O. Acef, F. Du-Burck, N. Chiodo, M. Holá, O. Číp, J. Lazar, Spectral properties of molecular iodine in absorption cells filled to specified saturation pressure. *Appl. Opt.*, 53(31), 7435-7441, (2014).

# High quality LPG fabrication using CO<sub>2</sub> Laser and specially designed electromechanical system

P. Simões, P. Lopes

Dept. of Physics, Univ. of Aveiro, Campus de Santiago, 3810-193 Aveiro, Portugal

paulo@ua.pt

In this work we present a computer controlled high precision yet low cost electromechanical system to produce high quality long period grating sensors (LPG). LPG has shown to have higher sensitivity to strain and temperature than those of Fiber Bragg Grating sensors, and additionally are sensitivity to the refraction index of the surrounding medium [1] making it useful for chemical and environmental applications [2] and other useful behaviors [3]. Its precision, in the nanometric scale with  $31 \text{ nm} \pm 8\%$  per pulse, allows fabrication of LPG with far more quality than those fabricated with the widely used electrical arc method. The fiber inscription process is fully controlled by computer using a *LabView* program. Well formed 25dB peaks were commonly obtained, reaching 30dB.

The experimental setup for LPG fabrication shown in Fig.1 uses a 10W CO<sub>2</sub> Laser, beam expander and two ZnSe lenses. LPG are inscribed in single-mode fiber (SMF-28).

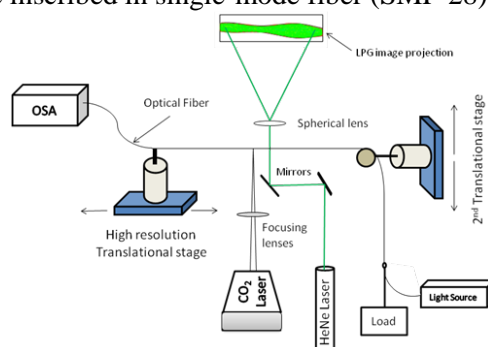


Fig 1. LPG fabrication setup: two translational systems, a 10 W CO<sub>2</sub> Laser, focusing lenses, a light source and the optical spectrum analyzer.

The use of a Michelson interferometer confirmed the expected value of  $33.3 \text{ nm/pulse}$  for the stage:  $31 \text{ nm} \pm 8\%$ . This small value ensures good control of the fabrication process resulting in quality LPG. Fig.2 shows some obtained transmission spectra for different inscription parameters. They are nicely behaved, noise free and have very sharp and pronounced peaks with 25 to 30dB transmission power loss.

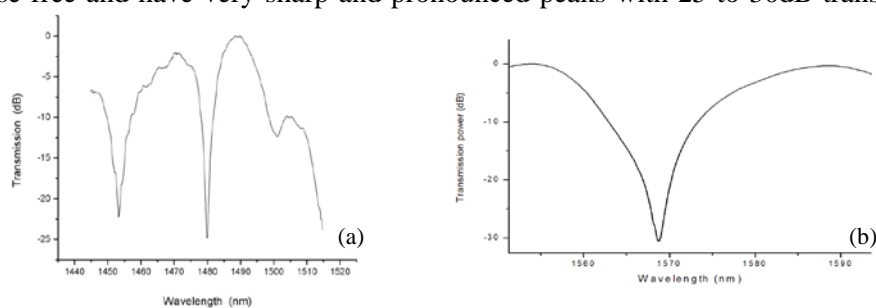


Fig. 2. LPG spectra for two different parameter combinations. (a)  $n=45$ ,  $\Lambda=650\mu\text{m}$ , 25dB. (b)  $n=3$ ,  $\Lambda=650\mu\text{m}$ , 30dB. (although not theoretically predicted,  $n$  showed to have a great influence both in transmissivity and in  $\lambda$ )

All LPG sensors inscribed using this system has shown to have high sensitivity to temperature variations. They reach sensitivities as high as  $125 \text{ pm}/^\circ\text{C}$  which are ten times higher than those of the FBG's and without any fiber coating.

- [1] S. James, R. Tatam, Optical fibre long-period grating sensors: characteristics and application, *Meas. Sci. Technol.*, 14, R49–R61, (2003).  
 [2] E. Simões, I. Abe, J. Oliveira, O. Frazão, P. Caldas, J. Pinto, , Characterization of optical fiber long period grating refractometer with nanocoating, *Sensor Actuat. B-Chem.*, Vol.153, Issue 2, 20th April 2011, pp. 335-339, (2011).  
 [3] P. Simões, P. Lopes, Low-cost temperature measurement using LPG and total transmitted power, *Proc. SPIE 8785*, 8th Iberoamerican Optics Meeting and 11th Latin American Meeting on Optics, Lasers, and Applications, 8785FH, (2013).

# Optimization of Signal to Noise Ratio for an Underwater Laser Range Finder

**F. Almabouada<sup>1</sup>, K.E Aiadi<sup>2</sup>, D. Louhibi<sup>1</sup>**

1- Centre de Développement des Technologies Avancées, Division Milieux Ionisés & Lasers,  
Cité du 20 août 1956, BP n° 17, Baba Hassen, 16303 Algiers, Algeria

2- Université Kasdi Merbah, Département Science de la Matière, Laboratoire LENREZA, Ouargla, Algeria

email address: [falmabouada@cdta.dz](mailto:falmabouada@cdta.dz)

This paper describes the different elements which can affect the signal to noise ratio (SNR) for an underwater laser range finder based on the pulsed time of flight (TOF) measurement technics [1,2]. The SNR optimization includes all the parts of the detection channel, the laser source characteristics and the underwater attenuation coefficient [3]. The detection channel is constituted by the telescope, the detector and the trans-impedance amplifier stage. As the laser beam propagation in a maritime environment is more attenuated than in atmosphere [4] the detector is an avalanche photodiode. The signal to noise ratio include the received optical power and all the noises which can affect the detection process such as the dark current noise, background noise and thermal noise [3]. The detector features (responsivity, dark current, gain), the electronic bandwidth, the efficiency of the optics, the objective diameter and the output laser power are fixed values introduced for the SNR calculation. The attenuation coefficient is a sum of the absorption and the scattering coefficients [4,5] which depend on the compositions and the type of water. For the values of 0.25, 0.5 and 1 m<sup>-1</sup> of the attenuation coefficient and an object reflectivity of 0.1 and 0.9, figure 1 represents the plot of the SNR versus the underwater ranging. Higher is the attenuation coefficient lower is the reflected laser power. This can be observed on the active area of the detector by the use of Zemax software for the optics design. For an object far 20 m from the telescope and an attenuation coefficient of 0.33 m<sup>-1</sup> the peak irradiance obtained by the software on the detector area is done on figure 2. The calculation demonstrated that the SNR is strongly affected by the attenuation coefficient of the underwater environment than other parameters. For a good detection an adequate avalanche photodiode should be selected with a good response at the 532 nm laser wavelength and the gain should be fixed at the right value in order to avoid increasing the noises in the detection channel.

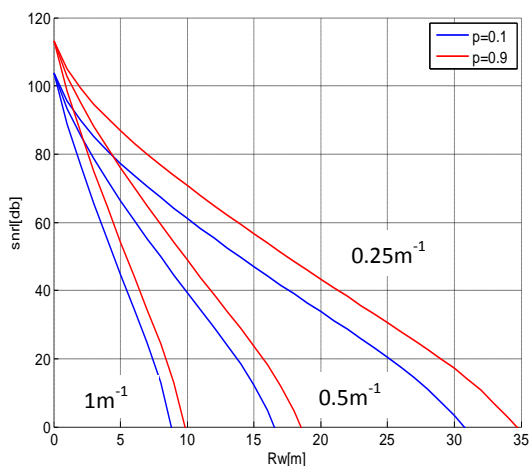


Figure 1: SNR versus underwater ranging

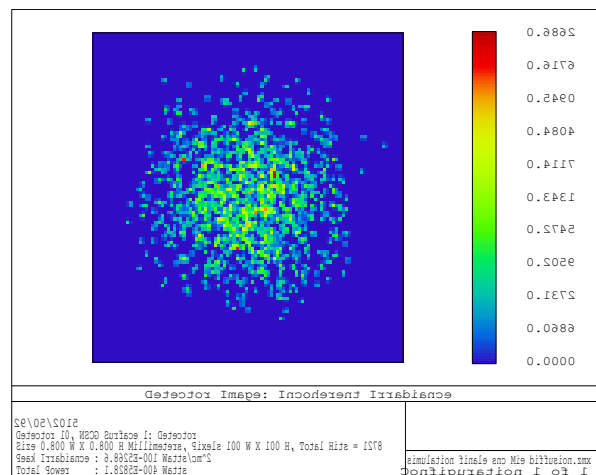


Figure 2: peak irradiance on the detector area

- [1] S. Donati, Electro-Optical Instrumentation: Sensing and Measuring with lasers, Chapter 3 Laser Telemeters (Prentice Hall), (2008).
- [2] M.C. Amann, T. Bosch, M. Lescure, R. Myllyla, M. Rioux, Laser ranging: a critical review of usual techniques for distance measurement, Opt. Eng., vol. 40(1), pp 10–19, (2001).
- [3] G. R. Osche, Optical Detection Theory for Laser Applications (Wiley Series in Pure and Applied Optics), Chapter 2, (2002).
- [4] C. D. Mobley, Handbook of optics Vol. I: Fundamentals, Techniques, & Design, Chapter 43: The Optical properties of water, (1995).
- [5] M. Jonasz and G. R. Fournier, Light Scattering by Particles in Water: Theoretical and Experimental Foundations (Elsevier Inc.), (2007).

## Relative humidity sensing using micro-cavities produced by the catastrophic fuse effect

**N. Alberto<sup>1,2</sup>, C. Tavares<sup>3</sup>, F. Domingues<sup>1</sup>, S. Correia<sup>4</sup>, P. Antunes<sup>1,3</sup>, J.L. Pinto<sup>1,3</sup>, R.A.S. Ferreira<sup>3,4</sup>, P.S. André<sup>5</sup>**

*1- Instituto de Telecomunicações – Pólo de Aveiro and I3N, 3810-193 Aveiro, Portugal*

*2- Center for Mechanical Technology and Automation, Mechanical Engineering Department, University of Aveiro, 3810-193 Aveiro, Portugal*

*3- Physics Department, University of Aveiro, 3810-193 Aveiro, Portugal*

*4- Physics Department and CICECO - Aveiro Institute of Materials, University of Aveiro, 3810-193 Aveiro, Portugal*

*5- Instituto de Telecomunicações and Department of Electrical and Computer Engineering, Instituto Superior Técnico, Technical University of Lisbon, 1049-001 Lisboa, Portugal*

*nelia@ua.pt*

Humidity sensing is of great importance in numerous fields, including food processing and storage, biomedical devices, air conditioning and geotechnical measurements [1]. Within these areas, lowering the production cost and equipment complexity are essential features. Thus, in the last years, the development of humidity sensors gained much attention of scientists aiming to produce compact and lower cost solutions.

Optical fiber based sensors have several advantages over the traditional methods used to monitor this parameter, namely capacitance, electrical resistance, thermal conductivity, wet and dry bulb methods, among others. The advantages of the fiber technology include immunity to electromagnetic interference, feasibility of remote sensing, continuous and real time monitoring in hazardous environments, small size and the possibility of multiplexing information from several sensors onto one optical fiber cable [2].

In this work, a cost effective solution to produce optical fiber relative humidity (RH) sensors based on Fabry-Perot Interferometer (FPI) micro-cavities is proposed. They were created by the recycling of optical fibers destroyed through the catastrophic fuse effect which considerably reduces the manufacturing costs [3]. The micro-cavities were filled with an organo-silica hybrid material, called di-ureasil. Figure 1 Left) shows an optical microscopy image of the sensor head after the RH characterization. Figure 1 Right) presents the dependence of the spectral modulation period ( $\Lambda$ ) with the RH values. The proposed sensor is a cost effective solution when compared with similar sensing approaches, usually produced by expensive and complex methods.

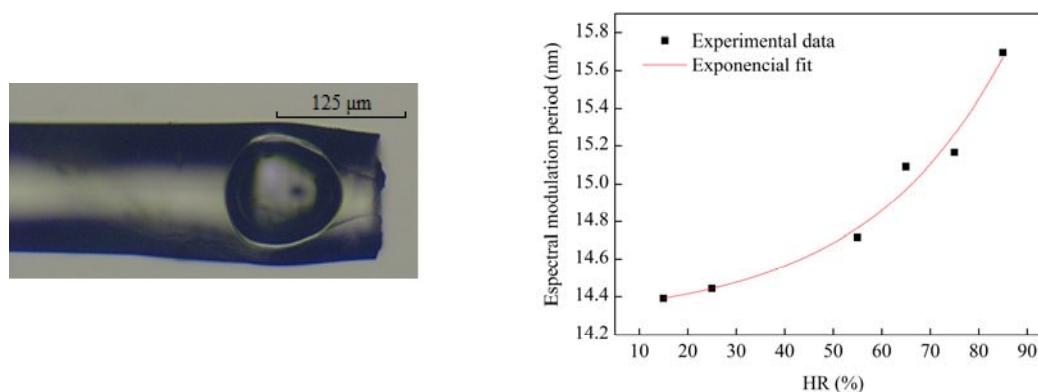


Figure 1. Left) Optical microscopy image of a RH-FPI micro-cavity based sensor; Right) Dependence of the FPI spectral modulation period with the RH values.

[1] D. Bridgeman, J. Corral, A. Quach, X. Xian, E. Forzani, Colorimetric humidity sensor based on liquid composite materials for the monitoring of food and pharmaceuticals, *Langmuir*, vol. 30, pp. 10785-10791, (2014).

[2] L. Alwis, T. Sun, K. Grattan, Optical fibre-based sensor technology for humidity and moisture measurement: Review of recent progress, *Measurement*, vol. 46, pp. 4052-4074, (2013).

[3] P. Antunes, M.F. Domingues, N. Alberto, P. S. André, Optical fiber microcavity strain sensors produced by the catastrophic fuse effect, *Photonics Technology Letters*, vol. 26, pp. 78-81, (2014).

## High temperatures ( $> 1000\text{ }^{\circ}\text{C}$ ) monitoring during the sintering process in microwaves oven using RFBGs

D. Pereira<sup>1</sup>, T. Santos<sup>1,2,3</sup>, R. Nogueira<sup>4</sup>, L. C. Costa<sup>1,2</sup>, N. Alberto<sup>4,5</sup>

1- Physics Department, University of Aveiro, 3810-193 Aveiro, Portugal

2- I3N, University of Aveiro, 3810-193 Aveiro, Portugal

3- CICECO, University of Aveiro, 3810-193 Aveiro

4- Instituto de Telecomunicações, 3810-193 Aveiro, Portugal

5- Center for Mechanical Technology and Automation, Mechanical Engineering Department, University of Aveiro, 3810-193 Aveiro, Portugal

nelia@ua.pt

The sintering of porcelain materials is a process involving temperatures of around  $1400\text{ }^{\circ}\text{C}$  [1]. The monitoring of this parameter is crucial to control the quality of the final product. A deviation from the standard values can be enough for the bloating phenomenon to occur [2], and that information can be used to interrupt/disconnect the process.

The thermal monitoring of the sintering process in the microwave oven requires the use of a high temperature resistant metal (for instance platinum) coated thermocouples and/or pyrometers [3]. These are expensive solutions, becoming the simultaneously monitoring of several points unfeasible, as a result of the associated cost.

Optical fiber Bragg gratings is a technology with advantages over the traditional thermocouples. Among these, it can be highlighted the immunity to electromagnetic interference, small size and feasibility of multiplexing information from several sensors onto one optical fiber cable.

Although the uniform Bragg gratings (FBGs) are only resistant and stable to temperatures below  $500\text{ }^{\circ}\text{C}$ , the regenerated fiber Bragg gratings (RFBGs) proved to be a feasible solution to monitor high temperatures [4].

In this work, results from the thermal monitoring in a resonant cavity microwave during the sintering of porcelain tableware is presented (Figure 1 Left). A mesh of RFBGs was used, being the temperature registered by one of these sensors presented in Figure 1 Right). The technology used in this work can be a suitable alternative to the traditional thermal monitoring methods.

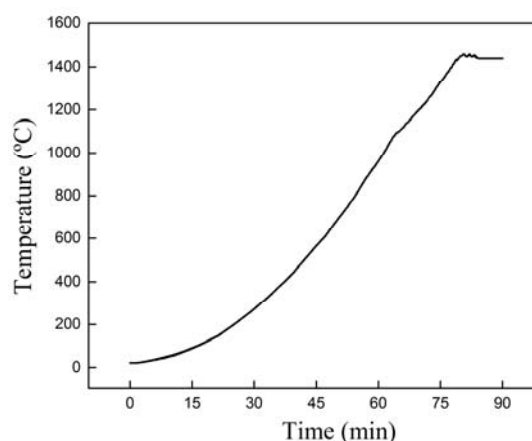
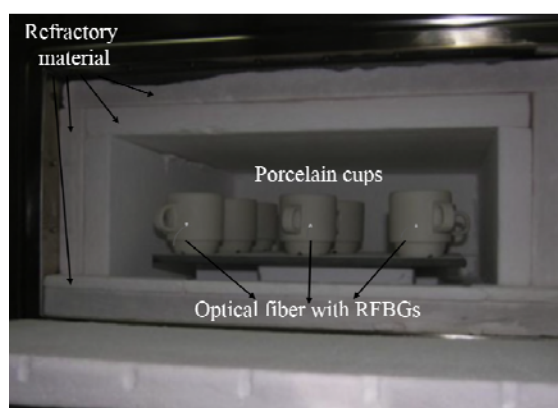


Figure 1. Left) Experimental setup used for the thermal monitoring of the sintering process of porcelain tableware; Right) Temperature evolution during the sintering process in a microwave oven.

[1] T. Santos, L.C. Costa, L. Henriet, M.A. Valente, J. Monteiro, J. Sousa, Microwave processing of porcelain tableware using a multiple generator configuration, *Applied Thermal Engineering*, vol. 50, pp. 677-682, (2013).

[2] S.R. Bragança, C.P. Bergmann, A view of whitewares mechanical strength and microstructure, *Ceramics International*, vol. 29, pp. 801-806, (2003).

[3] T. Santos, L. Henriet, V. A. F. Costa, L. C. Costa, Using microwave radiation for porcelain tableware sintering, *PIERS*, accepted for publication.

[4] N. Alberto, R. Nogueira, V. Neto, Thermal monitoring of the thermoplastic injection molding process with FBGs, *Proc. SPIE*, vol. 9286, pp. 928642-1 - 928642-4, (2014).

---

---

**SECTION TH**

**THz Sources and Applications**

---

---

## **Graphene-based nanostructures: plasmonics in the THz range**

**Yu. V. Bludov<sup>1</sup>, Aires Ferreira<sup>2</sup>, N. M. R. Peres<sup>1</sup>, Jaime E. Santos<sup>1</sup>, M. I. Vasilevskiy<sup>1</sup>**

*1- Centro de Física, Universidade do Minho, Campus de Gualtar 4710-057 Braga, Portugal*

*2- Department of Physics, University of York, Heslington, York, YO10 5DD, UK*

*mikhail@fisica.uminho.pt*

We shall discuss the properties of surface plasmon-polaritons (SPPs) in graphene and describe four possible ways of coupling electromagnetic radiation in the terahertz (THz) spectral range to this type of surface waves: (i) the attenuated total reflection (ATR) method employing a prism, (ii) graphene-based gratings or graphene monolayers with modulated conductivity, (iii) a metal stripe on top of the graphene layer, and (iv) a nanoparticle located above it. Potentially interesting for applications SPP effects, such as switching, modulation and polarization of THz radiation, as well as its enhanced absorption in graphene, will be considered. Depending on the availability of time, the discussion will also include some effects of the non-linear optical conductivity of grapheme, such as optical bistability and solitons.

- [1] Yu. V. Bludov, N. M. R. Peres, and M. I. Vasilevskiy, Graphene-based polaritonic crystal, Phys. Rev. B, vol. 85, pp. 245409 (2012).
- [2] Yu. V. Bludov, M. I. Vasilevskiy and N. M. R. Peres, Mechanism for graphene-based polarizer, J. Appl. Phys., vol. 112, pp. 084320 (2012).
- [3] N. M. R. Peres, Yu. V. Bludov, Aires Ferreira, and M. I. Vasilevskiy, Exact solution for square-wave grating covered with graphene: Surface plasmon-polaritons in the THz range, J. Phys.: Condensed Matter, vol. 25, pp. 125303 (2013).
- [4] Yu. V. Bludov, Aires Ferreira, N. M. R. Peres, and M. I. Vasilevskiy, A Primer on Surface Plasmon-Polaritons in Graphene, Int. J. Mod. Phys. B, vol. 27 pp. 1341001 (2013).
- [5] N. M. R. Peres, Yu. V. Bludov, Jaime E. Santos, Antti-Pekka Jauho, and M. I. Vasilevskiy, Optical bistability of graphene in the terahertz range, Phys. Rev. B, vol. 90, pp. 125425 (2014).
- [6] J. E. Santos, M. I. Vasilevskiy, N. M. R. Peres, G. Smirnov, and Yu. V. Bludov, Renormalization of nanoparticle polarizability in the vicinity of a graphene-covered interface, Phys. Rev. B, vol. 90, pp. 235420 (2014).

## Resonant Tunnelling Diode Terahertz Sources

**E. Wasige<sup>1</sup>, J. Wang<sup>1</sup>, Ata Khalid<sup>1</sup>, A. Kelly<sup>1</sup>, D. Cumming<sup>1</sup>, and José Figueiredo<sup>2</sup>**

*1- High Frequency Electronics Group, School of Engineering, University of Glasgow, Glasgow, UK*

*2 - Center for Electronics, Optoelectronics and Telecommunications (CEOT), Departamento de Física - Faculdade de Ciências e Tecnologia, Universidade do Algarve, Faro, Portugal*

*edward.wasige@glasgow.ac.uk*

The terahertz (THz) frequency range (0.1 THz to 3 THz) has been receiving considerable attention recently because of the inherent advantages it offers, e.g. wider bandwidths, improved spatial resolutions compared to RF electronics, and the new sensing opportunities such as inspection of sealed packages, concealed weapons detection, chemical and biological agents detection, medical diagnostics, etc. The opportunities are clear, but there is a distinct lack of compact, robust, efficient and all solid-state sources offering powers greater than 1mW that operate at room temperature in this frequency range. In this talk we will review such sources that are based on resonant tunnelling diodes (RTDs). RTDs are the fastest purely electronic, solid-state devices and RTD oscillators have achieved record fundamental oscillations at 712 GHz (over 25 years ago) and 1.55 THz recently, though with very low output power, a few micro-Watts. These oscillation frequencies are currently beyond the highest frequency transistor oscillators built to date. Detection experiments have demonstrated that the negative resistance responsible for these oscillations may persist to frequencies as high as 2.5THz, indicating the potential of RTDs as a technology platform for THz electronics. Our work at the University of Glasgow on this topic has achieved record W-band (75 - 100 GHz) and D-band (110 – 170 GHz) oscillators with milli-Watt [1] and sub milli-Watt output powers [2]. This, however, is still significantly well below about the 10 mW that would be desirable at about the 100 GHz range. We will discuss our design approaches to realising milli-Watt RTD-based THz sources. We will also preview work that is being done within the European Commission H2020 project, iBROW - Innovative ultra-BROadband ubiquitous Wireless communications through terahertz transceivers [3]. The project is based on integration of the RTD device technology with laser diodes and photo-detectors to pursue the development of a unified technology that can be integrated into both ends of the wireless link [4], namely consumer portable devices and fibre-optic supported base-stations to enable its deployment in 10 Gbps short-range wireless communication devices in short term and paving the way for 100 Gbps in long term for both the mm-wave and THz frequency bands, seamlessly integrated with optical fibre networks.

[1] J. Wang, L. Wang, C. Li, K. Alharbi, Ata Khalid, and E. Wasige, "W-band InP-based resonant tunnelling diode oscillator with milliwatt output power," 26th International Conference on Indium Phosphide and Related Materials, 11-15 May 2014, Montpellier, France.

[2] J. Wang, A. Alharbi, A. Ofiare, H. Zhou, Ata Khalid, D. Cumming and E. Wasige, "High performance resonant tunnelling diode oscillators for THz applications," Compound Semiconductor IC Symposium, 11-14 October 2015, New Orleans, USA.

[3] <http://ibrow-project.eu/>

[4] T.J. Slight, B. Romeira, L. Wang, J.M.L. Figueiredo, E. Wasige, and C.N. Ironside, "A Liénard oscillator resonant tunnelling diode-laser diode hybrid integrated circuit: model and experiment," IEEE Journal of Quantum Electronics, 44 (12), 2008. pp. 1158-1163.

**Compact laser sources for imaging,  
diagnostics and treatment in biomedicine**

**Edik U. Rafailov**

*Optoelectronics and Biomedical Photonics Group, Aston Institute of Photonic Technologies,  
Aston University, Birmingham, B4 7ET, UK*



In the last decades, progress in the development compact continuous wave and ultrashort pulse lasers has brought to science and industry an enormous number of new applications. Previously, such lasers were mostly utilised in the communication and other industries. However, now such laser systems are becoming adopted in biomedicine and related fields. Here we would like to review some of the most promising applications where compact laser sources in UV/visible and near infrared wavelength ranges are being used in biophotonics, particularly focussing on multi-photon imaging and cancer diagnostics and photo treatment.



**Biography**

Prof. Rafailov received the Ph.D. degrees from the Ioffe Institute. In 2005 he established new group and in 2014 he and his Optoelectronics and Biomedical Photonics Group moved to Aston University. He has authored and co-authored over 350 articles in refereed journals and conference proceedings. Prof. Rafailov coordinated a €14.7M FP7 FAST-DOT project – development of new ultrafast lasers for Biophotonics applications. Currently, he coordinated the €11.8M NEWLED project aims to develop a new generation of white LEDs. He also leads a few others projects funded by FP7 EU and EPSRC. His current research interests include high-power CW, ultrashort-pulse lasers; generation of UV/visible/IR/MIR and THz radiation, nano-structures; nonlinear and integrated optics; Biophotonics.

# Novel Concepts of THz Sources based on the Structural Light Focusing Effect in Photonic Crystals

**Stanislav O. Yurchenko and Kirill I. Zaytsev**

*Bauman Moscow State Technical University, 105005, 2<sup>nd</sup> Baumanskaya str. 5/1, Moscow, Russia*

*E-mail: [st.yurchenko@mail.ru](mailto:st.yurchenko@mail.ru)*

The problems of light generation and non-linear conversion are of high importance in fundamental and applied physics. Novel materials, such as photonic crystals (PCs) [1,2] and quasi-crystalline structures [3], attract considerable interest as a perspective media for solving these problems.

The structural light focusing (SLF) is an effect of electromagnetic wave interaction with PC structures, which is associated with the coherent distortions of the wavefront interacting with 2D and 3D PCs in case of the band-gap pumping,  $\lambda = \lambda_{BG}$  [4,5,6]. SLF leads to strong localization of optical field and to appearance of the vortical structures near the surface of the PC [6]. This effect can dramatically enhance the non-linear optical response of the PC media. In Refs. [4–8] the ability to enhance the second and the third harmonic generation using the SLF in opal-based PCs was demonstrated. One should note, this mechanism of nonlinear conversion enhancement completely differs from the traditional approaches of non-linear generation based on the quasi-phase matching condition in PCs [9–11].

In the present talk we discuss the ability for enhance THz-wave generation in PCs using the SLF. Highly-efficient generation of THz pulses can be performs via the parametric light decay [12] or optical rectification [13] of femtosecond optical pulses in PC media possessing non-zero second order susceptibility,  $\chi^{(2)} \neq 0$ . Moreover, the SLF-enhanced effects of photoswitching and gating [14–15] in semiconductor PC structures can be utilized for THz-wave generation. We consider the results of numerical simulations and propose the concepts of devises for highly-efficient THz-wave generation in PC structures based on the SLF.

- [1] E. Yablonovitch, Inhibited Spontaneous Emission in Solid-State Physics and Electronics, *Physical Review Letters*, vol. 58, no. 20, pp. 2059–2062, (1987).
- [2] S. John, Strong localization of photons in certain disordered dielectric superlattices, *Physical Review Letters*, vol. 58, no. 23, pp. 2486–2489, (1987).
- [3] Z. V. Vardeny et al., Optics of photonic quasicrystals, *Nature Photonics*, vol. 7, pp. 177–187, (2013)
- [4] K. I. Zaytsev et al., Band-gap nonlinear optical generation: The structure of internal optical field and the structural light focusing, *Journal of Applied Physics*, vol. 115, no. 21, p. 213505, (2014).
- [5] K. I. Zaytsev et al., Enhancement of second harmonic generation in NaNO<sub>2</sub>-infiltrated opal photonic crystal using structural light focusing, *Applied Physics Letters*, vol. 105, no. 5, p. 051902, (2014).
- [6] S. O. Yurchenko et al., Structural Light Focusing in Photonic Crystals, *Physical Review Letters* (2015, under review).
- [7] Y. P. Voinov et al., Second optical harmonic near the surface of ferroelectric photonic crystals and photon traps, *Physics of the Solid State*, vol. 57, no. 3, pp. 453-459, (2015).
- [8] V. S. Gorelik et al., Nonlinear optical conversion in synthetic opal, *Inorganic Materials*, vol. 51, no. 5, pp. 419-424, 2015.
- [9] J. Martorell, Scattering of second-harmonic light from small spherical particles ordered in a crystalline lattice, *Physical Review A*, vol. 55, no. 6, pp. 4520–4525, (1997).
- [10] P. P. Markowicz et al., Dramatic Enhancement of Third-Harmonic Generation in Three-Dimensional Photonic Crystals, *Physical Review Letters*, vol. 92, no. 8, p. 083903, (2004).
- [11] A. A. Fedyanin et al., Nonlinear diffraction and second-harmonic generation enhancement in silicon-opal photonic crystals, *Applied Physics Letters*, vol. 87, no. 15, p. 151111, (2005).
- [12] M. A. Pistrup et al., Continuously tunable submillimeter wave source, *Applied Physics Letters*, vol. 26, no. 8, pp. 418–421, (1975).
- [13] D. H. Auston et al., Optical Rectification by Impurities in Polar Crystals, *Physical Review Letters*, vol. 28, no. 14, pp. 897–901, (1972).
- [14] D. H. Auston, Picosecond optoelectronic switching and gating in silicon, *Applied Physics Letters*, vol. 26, no. 3, pp. 101–103, (1975).
- [15] D. H. Auston et al., Picosecond photoconducting Hertzian dipoles, *Applied Physics Letters*, vol. 45, no. 3, pp. 284–286, (1984).

## THz Photonic Devices for Industrial Applications

**Kyung Hyun Park\*, Eui Su Lee, Namje Kim, Il-Min Lee, Kiwon Moon,  
Won-Hui Lee, Hyunsung Ko, Hyun-Soo Kim, and Sang-Pil Han**

*THz Photonics Creative Research Institute, ETRI, Daejeon 305-700, Korea*

*khp@etri.re.kr*

The interests to the terahertz (THz) technologies keep rapidly increasing in the reason of the potential in the wide range of applications such as THz wireless communications, THz spectroscopy, THz sensing, and THz imaging [1]. There are many studies demonstrating THz service scenarios in the laboratory level. However, we are still looking for high performance devices which can open new applications fields. With the well-commercialized photonic technologies in optical communications, the compact, tunable, and low-cost THz photonic devices are envisaged. Since 2009, starting from the monolithically integrated multi-section DML operating at 1.55  $\mu\text{m}$ , we have developed various small compact beating sources based on InP [2]. Recently, our own developed butterfly packaged beating source takes the first step into the THz industrial field. We have also developed the evanescently coupled photodiodes (ECPD) operating at a 1.3  $\mu\text{m}$  wavelength which consists of an optimized absorption length of p-i-n mesa PD section with an extended optical matching layer and a broadband THz antenna. In addition, adopting our THz components into a CW THz spectroscopy system, methods of measuring the thickness or refractive index of a sample have been demonstrated [3].

In this talk, I will discuss the role of the essential components which consist of the main building blocks for the realizations of industrial applications. Fast tuning speed, wide tuning range, low cost, small compact, parallel process, and multi-functional photonic devices will enable THz technologies to open new concept of industrial applications. In addition, our recent progresses in the THz passive device using other novel materials will also be presented.

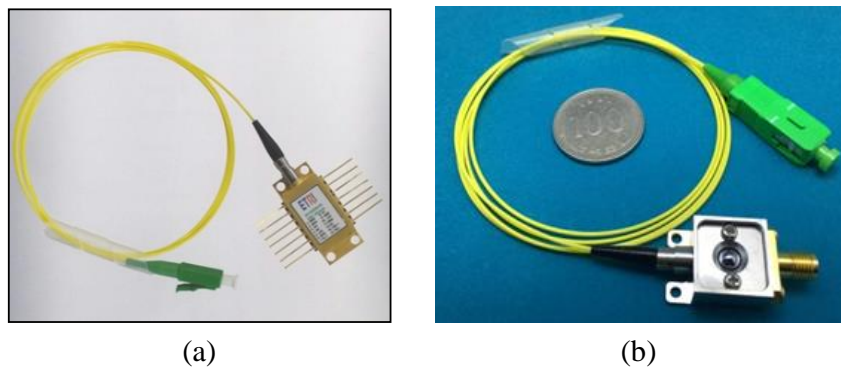


Figure 1. (a) Dual-mode laser module for tunable CW THz wave generation. (b) ECPD module for THz wave generation with high conversion efficiency.

### References

- [1] M. Tonouchi, "Cutting-edge terahertz technology," *Nature Photon.* **1**, 97-105 (2007).
- [2] N. Kim, H.-C. Ryu, D. Lee, S.-P. Han, H. Ko, K. Moon, J.-W. Park, M. Y. Jeon, and K. H. Park, "Monolithically integrated optical beat sources toward a single-chip broadband terahertz emitter," *Laser Phys. Lett.* **10**(8), 085805 (2013).
- [3] I.-M. Lee, N. Kim, E. S. Lee, S.-P. Han, K. Moon, and K. H. Park, "Frequency modulation based continuous-wave terahertz homodyne system," *Opt. Express* **23**(2), 846-858 (2015).

# Simultaneous generation of x-ray and terahertz radiation produced by intense femtosecond laser pulses from atomic cluster plasma

A.V. Balakin<sup>1</sup>, A.V. Borodin<sup>1</sup>, M.S. Dzhidzhoev<sup>1</sup>, M. Evdokimov<sup>1</sup>, M. Esaulkov<sup>2</sup>, V.M. Gordienko<sup>1</sup>, P. Solyankin<sup>1</sup> and A.P. Shkurinov<sup>1</sup>

<sup>1</sup>Department of Physics and International Laser Center, Lomonosov Moscow State University, Moscow, 119992 RUSSIA

<sup>2</sup>Institute on Laser and Information Technologies, Russian Academy of Sciences, Shatura, 140700 RUSSIA

The present paper analyses the main mechanisms and properties of terahertz radiation generated by intense femtosecond laser pulses from gas and nanosize gas clusters. The possibilities of simultaneous generation terahertz and x-ray radiation are discussed and demonstrated experimentally.

The present paper demonstrates the possibility of simultaneous generation of X-ray and THz radiation in a gas cluster jet by intense femtosecond laser pulses. We present the concept of developing of "X-ray-optical-THz" sources of ultrashort pulse duration. We demonstrated that optimal conditions for THz and characteristic X-ray radiation in gas-cluster jets are different. This allows to control the ratio of values and the relative temporal delays of simultaneously generated signals at THz and X-ray frequencies by means of changing the temporal delay between laser pulses and the moment of cluster stream formation, and also when changing chirp parameters of the exciting laser pulses. The diagram showing the direction of the generated THz radiation in the near axial area represents the cone with semiapex angle of  $3.7^\circ$  and the minimal value in the near axial area of the beam. The angular area less than  $15^\circ$  was studied.

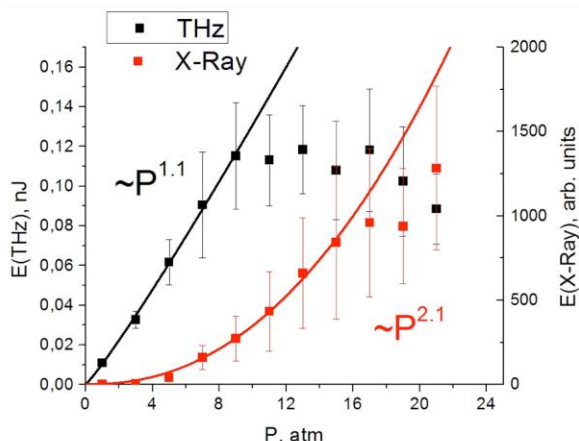


**Fig. 1.** Terahertz and X-ray radiation versus the argon gas cluster pressure.

The THz radiation, generated in the laser-induced cluster plasma excited by linearly polarized optical radiation is also linearly polarized. The dependence of THz signal value on excessive gas pressure, which creates a stream, in the dichromatic system has a nonlinear character and demonstrates saturation in high pressure. The absence of saturation of the volume of THz radiation signal with the growth of energy of exciting pulses at the main frequency observed up to 25 mJ in the pulse, agrees with the published earlier data for both monochromatic and dichromatic systems of optical excitation, and in our experiments up to 80–100 mJ saturation doesn't take place either. Absence of saturation will allow in perspective get THz pulses of higher energy by means of increasing the energies of exciting optical pulses. The comparative analysis of the obtained experimental data

showed that given equal average atom concentrations, THz radiation generation in static gas takes place with a higher optical-THz conversion coefficient than in gas-cluster streams. This effect can be connected with a relatively small volume of plasma waist and accordingly, with a considerably smaller number of atoms/molecules taking part in the interaction in the latter case. The influence of laser plasma transparency on the THz frequency is also discussed. It has been demonstrated that argon clustering leads to the power decrease of THz signal in the near-axial area in the case of dichromatic pumping. One of the possible explanations is the formation of hyper critical cluster plasma. It has been demonstrated experimentally that by means of through changing the ratio of buffer and cluster gases in the gas mixture one can effectively change the value of THz radiation generated in the cluster stream. In the carried out experiments the highest efficiency of THz radiation generation was observed when the gas mixture of Ar (argon) + He (helium) was used with the 1:10 ratio. It seems productive to carry on research in this direction and proceed in the future to mixed clusters, formed at supersonic discharge from the nozzle of double, triple mixtures of multiatomic molecules with inert gases. For the purpose of correct interpretation of the experimental data a model was made which took into consideration the frequency of the cluster own oscillation in the shape of an ellipse. A hypothesis was suggested that widening the resonance in THz radiation observed in a number of experiments of other research groups is connected with the spread in sizes and shapes of clusters. The power of dipole and quadrapole cluster radiation at THz range frequency is the result of action of ponderomotive Miller force and the power of radiation pressure. It has been established that the calculated dependence of the power of THz radiation on the power of laser radiation agrees with the experimental results.

**Novosibirsk FEL terahertz emission for biological application**

**S.E.Peltek**

Institute of Cytology and Genetic SB RAS, Novosibirsk, Russia,

The main goal of this work is: an investigation of a possibility of using terahertz radiation for transfer biomacromolecules and nanoparticles from a solid surface into the aerosol phase. We have show that this process is nondestructive – the ablated molecules conserve primary structure. We applied this technique to standardization of the biochip production and express analysis of nanoparticle's size. We named the process of biomacromolecule and nanoparticle transfer into the aerosol phase the soft nondestructive ablation.

To check the nondestructive character of the soft nondestructive ablation method of biomacromolecules under action of trahertz emission we used three different bioanalytical techniques. First, to monitor a possible loss or retention of the enzymatic activity of a horseradish peroxidase sample we employed histochemical staining. After ablation, horseradish peroxidase particles were collected from the aerosol phase onto the solid filter. By the method developed by BioRad company we checked that the horseradish peroxidase sample retained its enzymatic activity after ablation. Second, by comparison of the electrophoretic mobility of the original and the ablated horseradish peroxidase samples we proved that this complex protein was undamaged. Major part of the enzymatic activity is associated with the high molecular weight fractions. This fraction was very similar to the control sample. Third, we present the experiments proving the nondestructive character of ablation by the MALDI-TOF technique. It was shown a very good correlation of the molecular mass-spectrum of native and ablated horseradish peroxidase samples.

Ablation of the mixture of DNA plasmid pUC18 (2.8 tpb) and lambda phage DNA (48 tpb) was carry out. To prove the nondestructive character of the soft nondestructive ablation method of DNA macromolecules we transformed E. coli competent cells by the ablated plasmid. We compared of the electrophoretic mobility of plasmids extracted from E. coli transformed by native and ablated plasmid samples. The electrophoretic mobility of both samples was the same.

The principle of soft nondestructive ablation of biological macromolecules under terahertz irradiation was applied to the direct analysis of the target DNA from biochip surface. The synthetic DNA-probe of 17 nucleotides was covalently bonded to the surface of a silicone plate. A target DNA from 90 nucleotides was hybridized to the DNA-probe like on the usual biochips. The target DNA on the biochip model is fixed by the hydrogen bonds. By action of terahertz emission we can destroy the hydrogen bonds, left the covalent bonds intact and transfer the target DNA into the aerosol phase. Start of ablation was controlled by the aerosol spectrometer and then the target DNA was collected to the filter for the subsequent analysis by sequencing. After ablation the target DNA was collected by the filter washed out and amplified by PCR. The target and ablated DNA sequences were identical. So we have got the method for the direct analysis of the target DNA.

## **THz beam shaping**

**M. Sypek**

*Faculty of Physics, Warsaw University of Technology, 75 Koszykowa Str. – 00-662 –WARSAW - POLAND*

*maciej.sypek@orteh.pl*

The performance of modern THz systems can be improved by the use of sophisticated optics. Such optical elements can be used for better coupling of the THz radiation into detector as well as for controlling beam profiles from THz emitters. Moreover an advanced THz optics can be used for conventional and unconventional imaging purposes. Many THz sources can emit narrowband, spatially coherent radiation. Due to the application of the heterodyne detection, passive systems (with spatially incoherent radiation) often work also in the narrowband mode. In such cases the use of diffractive optics is feasible. Additionally an application of the diffractive optics can be also expanded for broadband cases.

THz detector systems can work more efficiently with energy concentrators. Focusing of the incoming radiation is crucial for gathering the signal. On the other hand THz sources typically emit very complex beam profiles. Usually, such a source should work together with beam collimator or projection system. The illumination geometry is often defined by user demands. In the case of the imaging systems the THz optics should also provide proper performance. Moreover in certain imaging systems an extended depth of field (or focus) is expected. Such problems can be solved by the utilization of the unconventional imaging systems based on the THz diffractive optics.

The technical aspect of the designing and manufacturing THz optics is also very important. The elements based on the phase retardation coded in the form of the first order kinoform [1] provide almost 100% diffraction efficiency for narrowband illumination case. Moreover an application of the higher order kinoforms [2,3] can suppress chromatic aberration. Optical elements can be easy manufactured of 3D printable [4-6] materials which are transparent enough in the THz range

A several THz diffractive optical elements are described. Specific designs and applications are discusses. Examples of the narrowband and broadband cases are shown. Theoretical considerations, numerical simulations and practical applications are presented.

[1] J. A. Jordan, et al., "Kinoform Lenses", *Appl. Opt.* vol. 9, pp. 1883-1887, (1970)

[2] J. C. Marron, D. K. Angell, and A. M. Tai, "Higher-Order Kinoforms", *Proc. SPIE* 1211, pp. 62-66, (1990)

[3] J. Suszek, et al., "High order kinoforms as a broadband achromatic diffractive optics for terahertz beams", *Optics Express*, Vol. 22, Issue 3, pp. 3137-3144, (2014)

[4] J. Suszek, et al. "Evaluation of the shadow effect in terahertz kinoform gratings". *Optics Letters*, vol. 38, Issue: 9, pp. 1464-1466, (2013)

[5] S. Pandey, et al. "Terahertz plasmonic waveguides created via 3D printing," *Optics Express*, vol. 21, issue 21, pp. 24422-24430, (2013).

[6] A. D. Squires, et al., "3D Printed Terahertz Diffraction Gratings And Lenses," *Journal of Infrared, Millimeter, and Terahertz Waves*, vol. 36, issue 1, pp. 72-80, (2015)

*THz for amplitude and phase characterization of ultrashort laser pulses*

M. Cornet, J. Degert, E. Abraham, E. Freysz  
 Laboratoire Ondes et Matière d'Aquitaine  
 Université de Bordeaux  
 33405 Talence Cedex, France

Electro-optical effect occurring in Zinc-blend crystals is widely used to sample THz pulse generated by pulsed laser sources. The incident THz pulse induces a birefringence in the electro-optic crystal which is proportional to the electric field of the pulse. This varying birefringence can be measured by observing the change in polarization state of a probe near-infrared probe pulse. By measuring the degree of polarization rotation as a function of delay between the terahertz pulse and the near-infrared probe pulse, the terahertz electric field can be mapped. In this presentation, we will demonstrate that if one samples the spectrum of a near-infrared pulse produced during the electro-optical effect versus the delay between the terahertz pulse and the near-infrared probe pulse one can also measure the chirp of the near infrared probe pulses. A simple model accounts for the phenomena. We will demonstrate this technique can easily be implemented to characterize the chirp of ultra-short pulses delivered by a regenerative Ti-Sapphire amplifier.

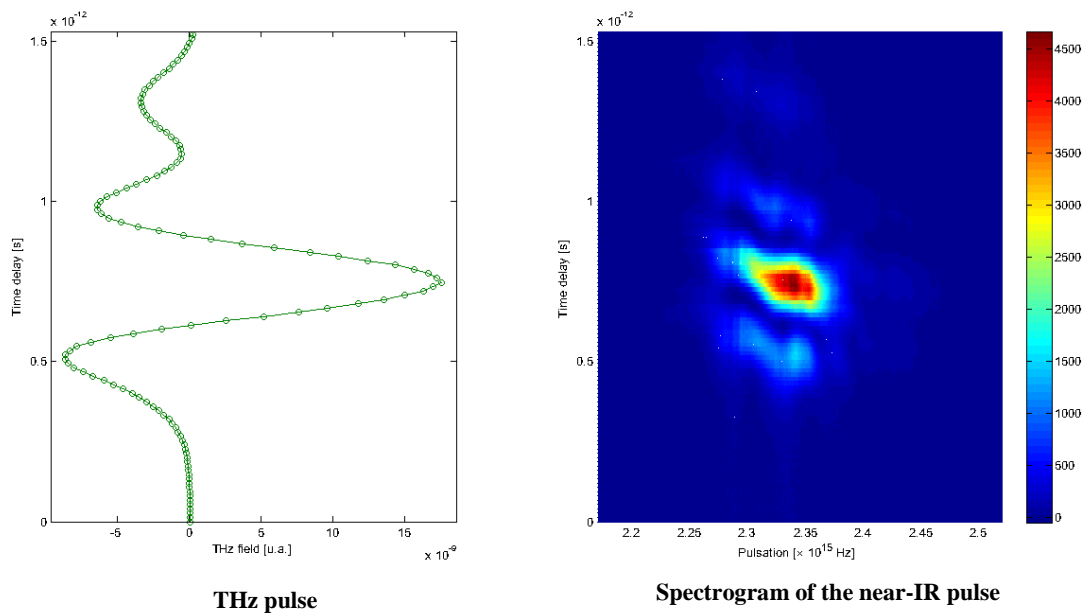


**Figure 1:** Spectrogram of near-infrared pulse generated during THz electro-optical sampling

## Emission of Terahertz pulses from vanadium dioxide films undergoing metal-insulator phase transition

**M. Esaulkov<sup>1</sup>, P. Solyankin<sup>2</sup>, A. Makarevich<sup>3</sup>, L. Parshina<sup>1</sup>, O. Novodvorsky<sup>1</sup>,  
A. Shkurinov<sup>2</sup>, V. Makarov<sup>2</sup>**

*1- Institute on Laser and Information Technologies of the Russian Academy of Sciences (ILIT RAS),  
1 Svyatoozerskaya St., Shatura, Russia, 140700*

*2- Faculty of Physics, M.V. Lomonosov Moscow State University, 1 Leninskie Gory, Moscow, Russia, 119991*

*3 - Faculty of Chemistry, M.V. Lomonosov Moscow State University, 1 Leninskie Gory, Moscow, Russia, 119991*

*Esaulkov\_mich@mail.ru*

Vanadium dioxide (VO<sub>2</sub>) is a substance that exhibits phase transition from insulating VO<sub>2</sub>(M) to conductive VO<sub>2</sub>(R) state at temperature 68°C, which leads to up to 4 orders of magnitude increase in conductivity [1]. High transmission contrast between insulating and conductive phase for THz radiation makes this material attractive for producing active beam guiding elements: controllable attenuators, amplitude and phase screens, mirrors, polarizers, etc [2]. Both metallic and insulating phases of VO<sub>2</sub> belong to centrosymmetric class of materials (semiconductor monoclinic phase has monoclinic structure and space group is P2<sub>1</sub>/c and metallic phase has rutile structure and space group is P4<sub>2</sub>/mmm), thus second-order processes are not expected in the bulk material. Nevertheless, in this work we find that thin (up to 300 nm) VO<sub>2</sub> films can generate broadband THz radiation as a result of interaction with femtosecond optical pulses from Ti:Sapphire regenerative amplifier. The THz emission efficiency shows step-like increase at phase transition temperature. We investigate THz emission in thin VO<sub>2</sub> films grown on sapphire substrates having two different symmetries (C- and R-cut) before and after the insulator-metal phase transition. We focus our attention on polarization of the THz radiation since it gives possibility to define the underlying mechanism of THz emission.

We found that THz emission amplitude for metallic phase of VO<sub>2</sub> follows a linear dependence on pump laser intensity. In the semiconducting phase, the amplitude dependence of the THz pulse on the pump fluence is also linear up to 5 mJ/cm<sup>2</sup>, after which it increases due to light-induced phase transition [3]. The THz emission efficiency in the metallic phase of the film is up to 30 times higher than that for the semiconducting phase. Polarization studies of THz radiation revealed linear polarization for both monoclinic and rutile phase of VO<sub>2</sub> grown on R-cut sapphire substrates. In the high-temperature phase, THz polarization is defined by anisotropic photocurrent influenced by intrinsic electrostatic field which is directed along the preferred [100] direction. Thus the emitted field polarization is linear and almost independent from pump pulse polarization. THz absorption studies show no anisotropy of in-plane conductivity of the VO<sub>2</sub> film. In both the insulating and conductive phase states, the THz radiation is governed by the contribution of the surface displacement current induced by incident optical beam on VO<sub>2</sub>-Al<sub>2</sub>O<sub>3</sub> and VO<sub>2</sub>-air boundaries.

[1] M. M. Qazilbash, M. Brehm, B.-G. Chae *et al*, "Mott transition in VO<sub>2</sub> revealed by infrared spectroscopy and nano-imaging," *Science* **318** (5857), 1750–1753 (2007)

[2] F. Dumas-Bouchiat, C. Champeaux, A. Catherinot *et al*, "RF-microwave switches based on reversible semiconductor-metal transition of VO<sub>2</sub> thin films synthesized by pulsed-laser deposition," *Appl. Phys. Lett.*, **91**, 223505-223505 (2007)

[3] S. Wall, L. Foglia, D. Wegkamp *et al*, "Tracking the evolution of electronic and structural properties of VO<sub>2</sub> during the ultrafast photoinduced insulator-metal transition," *Phys. Rev. B* **87**, 115126 (2003)

# Generation, characterization and application of terahertz “non-diffractive” Bessel beams with orbital angular momentum

**B. A. Knyazev<sup>1,2</sup>, Yu. Yu. Choporova<sup>1,2</sup>, G. N. Kulipanov<sup>1</sup>, M. S. Mitkov<sup>2,5</sup>,  
V. S. Pavelyev<sup>3,4</sup>, V. A. Soifer<sup>3,4</sup>, N. A. Vinokurov<sup>1,2</sup>, B. O. Volodkin<sup>3</sup>**

*1 Budker Institute of Nuclear Physics SB RAS, Novosibirsk, 630090, Russia*

*2 Novosibirsk State University, Novosibirsk, 630090, Russia*

*3 Samara State Aerospace University (SSAU), Samara, 443086, Russia*

*4 Image Processing Systems Institute of the RAS, Samara, 443001, Russia*

*5 Novosibirsk State Technical University, Novosibirsk, 630090, Russia*

ba\_knyazev@phys.nsu.ru

Beams with orbital angular momentum (or vortex beams) are a subject of special interest in modern optics [1] because of many prospective fields of their applications such as particle trapping, micromachining, communications, thick-media imaging, terahertz lidars, *etc.* However, only a few experiments have been performed in the terahertz range in which the Laguerre-Gaussian beams have been formed. In this work, terahertz Bessel vortex beams  $E(r, \varphi, z, t) = J_l(k_r r) \exp[i(l\varphi + k_z z - \omega t)]$  with different topological charges  $l$  were generated via transformation of monochromatic Novosibirsk

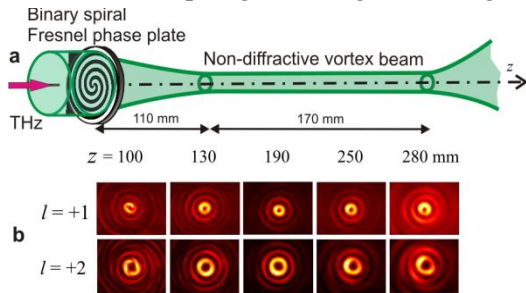


Fig. 1. (a) Generation of vortex beams; (b) beam cross-section vs. distance recorded with a microbolometer array.

free electron laser beam at a wavelength of 141  $\mu\text{m}$  using phase binary silicon spiral Fresnel plates [2], as shown in Fig. 1. To detect the sign and value of the beam topological charge  $l$ , we applied several classical optics experiments. Double-slit diffraction of the vortex beam produced a dogleg-like stripes, from which the  $l$  value was found. Diffraction of the beams on a knife-edge obstacle also gave non-symmetric patterns, which depended on the sign and value of  $l$ .

To study the wavefront characteristics of Bessel-like beams, we recorded interference patterns produced by

a co-axial laser and vortex beams. The patterns were recorded using a Mach-Zender interferometer. While the wavefronts stayed plane (directly after formation of the Bessel beam,  $z = 130$  mm), the interference pattern revealed the linear azimuthal phase distribution  $\Phi = l\varphi = \text{const}(r)$ , and at a distance of 260 mm the interference pattern became a spiral-like one (Fig. 2), which clearly evidenced transformation of the plane vortex beam into a spherical one, albeit the diameters of the beam rings did not change. That made it possible to find the sign and value of  $l$ . Studying intensity spatial distributions behind a lens set in the completely formed vortex beams, we found the wavevector spectra to differ slightly from spectra typical to pure Bessel beams. These results will be discussed in the presentation.

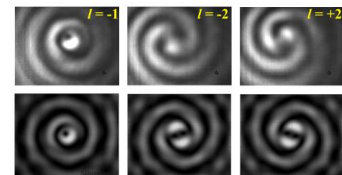


Fig.2. Experimentally observed (above) and calculated interference of plane wavefront of laser radiation and spherical wavefront of vortex beam.

We observed for the first time in the terahertz range the self-healing of Bessel beams after passage of randomly inhomogeneous media. Most unusual results were obtained in the experiments on the application of vortex beams to the generation of surface plasmon polaritons on gold-ZnS-air interfaces. Applying the “end-fire coupling technique” for plasmon generation on the rectangular edge of the samples, we discovered that the plasmons were induced preferably at cross-sections of beam rings with the sample surface in which the azimuthal component of the Poynting vector was aimed into the surface. This phenomenon requires further investigation and explanation of its physical mechanism.

The work was supported by grants RSF (14-50-00080) and RFBR (15-02-06444 and 13-02-97007).

[1] A. M. Yao, M. J. Padgett, Orbital angular momentum: origins, behavior and applications, *Advances in Optics and Photonics*, vol. 3, pp161-204, (2011).

[2] R. N. Heckenberg, R. McDuff, C. P. Smith, A. G. White, Generation of optical phase singularities by computer-generated holograms, *Optics Letters*, vol. 17, pp. 221-223, (1992).

## Classical holography at the terahertz NovoFEL facility: recording and reconstruction techniques

Yu. Yu. Choporova<sup>1,2</sup>, B. A. Knyazev<sup>1,2</sup>, M. S. Mitkov<sup>1,3</sup>

1- Budker Institute of Nuclear Physics, Novosibirsk, 630090, Russia

2- Novosibirsk State University, Novosibirsk, 630090, Russia

3- Novosibirsk State Technical University, Novosibirsk, 630090, Russia

yu.yu.choporova@inp.nsk.su

Imaging is one of the most promising and rapidly developing areas in the terahertz science and technology. Holography is commonly known as an imaging technique in the visible range and still attracts growing attention and gradually expands fields of its application. Nevertheless holography in

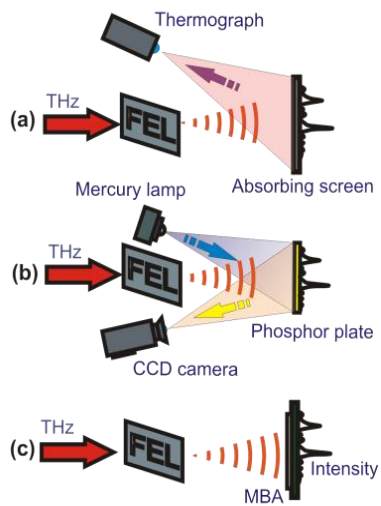


Fig. 1. Configurations for hologram recording (a) with NIR thermograph, (b) with thermal sensitive phosphor plate, and (c) with microbolometer array.

the THz range is still underdeveloped. Methods for pulsed terahertz holography with a time domain spectroscopy technique are different from the methods of classical optics. Appearance of more intense monochromatic terahertz sources (quantum cascade lasers, free electron lasers) and terahertz imaging devices enables the implementation of classical variants of optical techniques in the terahertz range. In this paper we present the results of a decade of research in the field of terahertz holography on the Novosibirsk free electron laser (NovoFEL) facility.

To implement the “classic holography” in the terahertz range, it was necessary to decide on several issues: a hologram recording technique, selection of optical schemes optimal for the THz range and of numerical reconstruction technique. Three imaging devices were applied for hologram recording (Fig. 1). In the THz range any hologram can be only a digital one, which requires numerical reconstruction. Six reconstruction techniques were implemented for hologram reconstruction. Mira images reconstructed using Fresnel convolution, angular spectrum, direct calculation of the Rayleigh-Sommerfeld integral, and the Rayleigh-Sommerfeld convolution methods have reasonable quality (Fig. 2). To improve quality of the images, we applied separately both apodization and extension operations to the digital hologram.

A great advantage of holography is that for an extended object or a group of objects situated along an optical axis only one recorded hologram enables to reconstruct many images. Reconstruction of phase images reconstructed in two planes along the optical axis was shown. Another very prospective application of THz holography in the attenuated total reflection spectrometers was demonstrated.

The work was supported by grants RSF (14-50-00080) and RFBR (15-02-06444 and 13-02-97007).

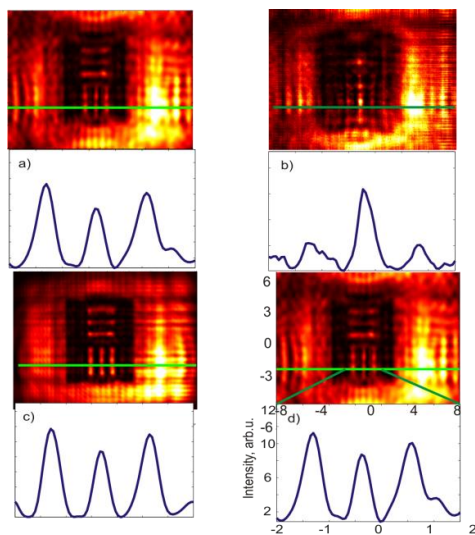


Fig.2. Comparison of different reconstruction methods: (a) Fresnel convolution, (b) angular spectrum (c) direct calculation of the Rayleigh-Sommerfeld integral, and (d) the Rayleigh-Sommerfeld convolution. A hologram of the test pattern was recorded with the microbolometer array

# Electrically Controllable Terahertz Metamaterial based on VO<sub>2</sub> Thin Film

**Han-Cheol Ryu<sup>1</sup>, Jun-Hwan Shin<sup>2</sup>, Kyung Hyun Park<sup>2</sup>**

1- Department of Car Mechatronics, Sahmyook University, Seoul 139-742, Korea

2- THz Photonics Creative Research Center, ETRI, Daejeon 305-700, Korea

hcryu@syu.ac.kr

We propose an electrically controllable terahertz wave modulator based on metamaterial and vanadium dioxide (VO<sub>2</sub>) thin film. Metamaterials have attracted great attentions owing to their unique responses for manipulating electromagnetic resonances that were mostly not founded in natural material. The controllable resonances of the artificially engineered metamaterials can offer the opportunities to realize the new and novel THz devices for a wide variety of THz applications [1]. Numerous researches on the realization of the tunable characteristics for the THz metamaterials have been reported by using semiconductors, graphene, and tunable functional-material [2, 3]. Tunable metamaterial based on vanadium dioxide (VO<sub>2</sub>) which has reversible switching properties caused by insulator-metal transition at a critical temperature at 340 K, is one of promising approach to spatially manipulate the THz wave thanks to easy fabrication and high tunability. There are several researches on the tunable THz metamaterials based on the phase transition of VO<sub>2</sub> by applying temperature, THz-field, or light [4]. However, these methods need external devices such as a heater, a THz or a light source; the external devices make the THz tunable devices more expensive and bulky. Thus, the electrical control for the phase transition of VO<sub>2</sub> is preferred for the practical applications. A square-loop shape is designed to play roles as a resonating metamaterial and a heater to electrically control a conductivity of VO<sub>2</sub> at the same time. A dual-resonant square-loop structure was designed for the stable transmission characteristics in the desired frequency band as shown in Fig. 1. The transmittances of the proposed metamaterial were successfully controlled by applying bias voltage without an external heater. The amplitude modulation depths of the metamaterial fabricated on VO<sub>2</sub> thin films were over 0.82 in the passbands from 0.35 to 0.52 THz.

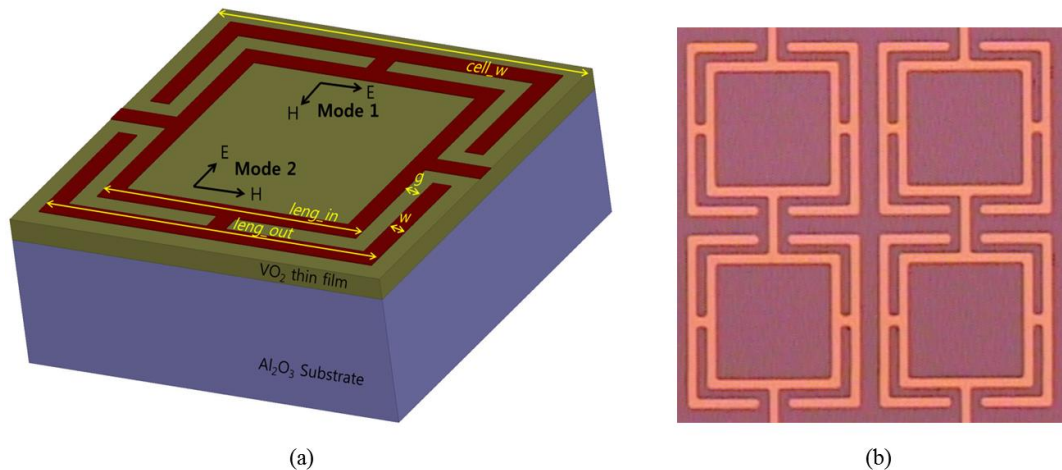


Figure 1. Dual-resonant Square-loop Metamaterial (a) Schematic, (b) Photograph

- [1] H.-T. Chen, W. J. Padilla, J. M. O. Zide, A. C. Gossard, A. J. Taylor, and R. D. Averitt, Active terahertz metamaterial devices, *Nature*, vol. 444, pp. 597-600, (2006).
- [2] L. Ju, B. Geng, J. Horng, C. Girit, M. Martin, Z. Hao, H. A. Bechtel, X. Liang, A. Zettl, Y. R. Shen, and F. Wang, Graphene plasmonics for tunable terahertz metamaterials, *Nat. Nanotech.*, vol. 4, pp. 630-634, (2011).
- [3] B. Sensale-Rodriguez, R. Yan, M. M. Kelly, T. Fang, K. Tahy, W. S. Hwang, D. Jena, L. Liu, and H. G. Xing, Broadband graphene terahertz modulators enabled by intraband transition, *Nat. Comm.*, vol. 3, pp. 1-7, (2012).
- [4] M. Liu, H. Y. Hwang, H. Tao, A. C. Strikwerda, K. Fan, G. R. Keiser, A. J. Sternbach, K. G. West, S. Kittiwatanakul, J. Lu, S. A. Wolf, F. G. Omenetto, X. Zhang, K. A. Nelson, and R. D. Averitt, Terahertz-field-induced insulator-to-metal transition in vanadium dioxide metamaterial, *Nature* vol. 487, pp. 345-348, (2012).

# Novel Applications of THz Pulsed Spectroscopy: from Early Non-Invasive Diagnosis of Dysplastic Skin Nevi to Non-Destructive Evaluation of Composite Structures

**Kirill I. Zaytsev and Stanislav O. Yurchenko**

*Bauman Moscow State Technical University, 105005, 2<sup>nd</sup> Baumanskaya str. 5/1, Moscow, Russia*

*E-mail: [kirzay@gmail.com](mailto:kirzay@gmail.com)*

Terahertz (THz) pulsed spectroscopy (TPS) appeared in 1975 as a result of D. Auston's research on semiconductor photoconductivity under femtosecond optical excitation [1]. It was rapidly developed through novel techniques to generate and detect THz pulses [2–5]. TPS recently attracts considerable interest of scientific community as a perspective instrument of applied physics [6]: It allows solving the problems of remote sensing [7], non-destructive evaluations of materials and constructions [8], studying of picosecond dynamics [9] and phase transitions [10] in media, and non-invasive medical diagnosis [11].

All the TPS applications are related to the methods of TPS signal processing and inverse ill-posed problem solution [12–14]: TPS allows to reconstruct the THz materials parameters of the sample or to study its internal structure (THz time-of-flight tomography [15]). Many factors impact the process of sensing with TPS, including noises in the TPS waveforms and various instabilities of the TPS setup. Thus, all the factors should be considered during the TPS data processing. Development of novel techniques for highly-accurate solution of the TPS inverse ill-posed problems, as well as studying the stability of the TPS inverse problem solution are very important tasks for all the TPS applications.

In our work we consider novel applications of TPS. We show the ability for non-destructive evaluations of composite materials at the stages of material manufacturing [16]. Moreover, we discuss the results of the pilot study of the ability for non-invasive early medical diagnosis of dysplastic skin nevi [17]. Dysplastic nevus of the skin is a precursor of melanoma, which is reported to be the most dangerous cancer of the skin [18]. Finally we consider the problems of TPS signal processing and the TPS inverse problem solution, related to the described TPS applications.

- [1] D. H. Auston, Picosecond optoelectronic switching and gating in silicon, *Applied Physics Letters*, vol. 26, no. 3, pp. 101–103, (1975).
- [2] D. H. Auston, K. P. Cheung, and P. R. Smith, Picosecond photoconducting hertzian dipoles, *Applied Physics Letters*, vol. 45, no. 3, pp. 284–286, (1984).
- [3] L. Xu, X.-C. Zhang, and D. H. Auston, Terahertz beam generation by femtosecond optical pulses in electro-optic materials, *Applied Physics Letters*, vol. 61, no. 15, pp. 1784–1786, (1992).
- [4] C. Winnewisser, P. U. Jepsen, M. Schall, V. Schyja, and H. Helm, Electro-optic detection of THz radiation in LiTaO<sub>3</sub>, LiNbO<sub>3</sub> and ZnTe, *Applied Physics Letters*, vol. 70, no. 23, pp. 3069–3071, (1997).
- [5] X. Lu and X.-C. Zhang, Generation of elliptically polarized terahertz waves from laser-induced plasma with double helix electrodes, *Physical Review Letters*, vol. 108, no. 12, p. 123903, (2012).
- [6] Y.-S. Lee, *Principles of Terahertz Science and Technology* (Springer New York, NY, USA), (2009).
- [7] D. Mittleman (Ed.), *Sensing with Terahertz Radiation* (Springer New York, NY, USA), (2003).
- [8] C. D. Stoik et al., Nondestructive evaluation of aircraft composites using transmissive terahertz time domain spectroscopy, *Optics Express*, vol. 16, no. 21, pp. 17039–17051, (2008).
- [9] J.-Y. Chen et al., Terahertz dielectric assay of solution phase protein binding, *Applied Physics Letters*, vol. 90, no. 24, p. 243901, (2007).
- [10] K. I. Zaytsev et al., Sensing of phase transition in medium with terahertz pulsed spectroscopy, *Journal of Physics: Conference Series*, vol. 486, no. 1, p. 012024, (2014).
- [11] E. Pickwell et al., Biomedical applications of terahertz technology, *Journal of Physics D: Applied Physics*, vol. 39, no. 17, pp. R301–R310, (2006).
- [12] K. I. Zaytsev et al., Invariant embedding technique for medium permittivity profile reconstruction using terahertz time-domain spectroscopy, *Optical Engineering*, vol. 52, no. 6, p. 068203, (2013).
- [13] K. I. Zaytsev et al., Accuracy of sample material parameters reconstruction using terahertz pulsed spectroscopy, *Journal of Applied Physics*, vol. 115, no. 19, p. 193105, (2014).
- [14] K. I. Zaytsev et al., Highly Accurate In Vivo Terahertz Spectroscopy of Healthy Skin: Variation of Refractive Index and Absorption Coefficient along the Human Body, *IEEE Transactions on Terahertz Science and Technology* (2015, under review).
- [15] D. M. Mittleman et al., T-ray tomography, *Optics Letters*, vol. 22, no. 12, pp. 904–906, (1997).
- [16] E. V. Yakovlev et al., Non-Destructive Evaluations of Polymer Composite Materials at the Manufacturing Stage using Terahertz Pulsed Spectroscopy, *IEEE Transactions on Terahertz Science and Technology* (2015, under review).
- [17] K. I. Zaytsev et al., In vivo terahertz spectroscopy of pigmentary skin nevi: Pilot study of non-invasive early diagnosis of dysplasia, *Applied Physics Letters*, vol. 106, no. 5, p. 053702, (2015).
- [18] M. Arumi-Uria et al., Grading of atypia in nevi: Correlation with melanoma risk, *Modern Pathology*, vol. 16, no. 8, pp. 764–771, (2003).

## Spectral characteristics of compact singly-resonant intracavity OPO pumped by a semiconductor disk laser

**Yu. A. Morozov<sup>1</sup>, V. I. Kozlovsky<sup>2,3</sup>**

1 - Kotelnikov Institute of RadioEngineering & Electronics (Saratov Branch), Russian Ac. Sci.  
38 Zeleynaya Str. 410019, Saratov, Russia

2 - P. N. Lebedev Physical Institute, Russian Ac. Sci., 53 Leninsky Ave., 119991, Moscow, Russia

3 - National Research Nuclear University MEPHI (Moscow Engineering Physics Institute)  
31 Kashirskoye shosse, 115409, Moscow, Russia

yuri.mor@rambler.ru

There is a need for sources of coherent radiation which can be applied to spectroscopy in the mid-infrared spectral region between 2.5 and 25  $\mu\text{m}$ . Mid-infrared semiconductor lasers (especially their long-wavelength implementations) are essentially limited to quantum-cascade devices. Despite impressive progress in the last years, quantum-cascade lasers stay as difficult-to-make, expensive and awkward devices because of their need for cryogenic cooling (at wavelengths longer than 16  $\mu\text{m}$ ) in combination with refined optics for beam shaping.

From the other hand, optical parametric oscillators (OPO) are suited almost perfectly to spectroscopic applications [1]. Among the OPOs, continuous-wave singly-resonant oscillators (SROs) are of particular importance. Unfortunately, in order to overcome the threshold of parametric generation these devices need tens-of-watt pumping lasers. The demands to a pump laser may be reduced if a SRO is placed in a high-finesse laser's cavity [2, 3]. Such an intracavity singly-resonant parametric oscillator (ICSRO) has been based on a titanium sapphire laser firstly and subsequently on a neodymium laser [2]. In order to remove long-lived relaxation oscillation appeared to be inherent for the ICSRO [2], D. Stothard *et al.* have proposed to pump an ICSRO with a semiconductor disk laser [3]. In their device, the laser cavity resonating at wavelength of 1.05  $\mu\text{m}$  and the OPO signal cavity (1.6  $\mu\text{m}$ ) had the common part where the nonlinear crystal for parametric interaction was placed. Both cavities were separated from each other with a dichroic beam splitter having a high reflectivity for the signal and transparent for the pump. In our opinion, an application of the approach [3] to the oscillator emitted at longer idler wavelength (i.e. with closer wavelengths of a pump and signal) looks rather problematic because a sophisticated beam splitter is required.

Recently, we have proposed the concept of a truly compact (~15 mm long) continuous-wave ICSRO pumped by GaSb-based semiconductor disk laser and some of its operational characteristics have been simulated [4, 5]. Unlike to the approach [3], single cavity both for the pump laser and signal parametric wave has been used thus avoiding the need for dichroic beam splitter. Moreover, we have used the double-band distributed Bragg reflector grown in the laser's active structure in order to ensure high reflection for both laser and signal radiation.

In this paper, we numerically analyze the spectral characteristics of the proposed ICSRO taking into account the Gaussian profile of generated beams and multimode character of radiation. The mathematical model develops that presented in [6]. We study the stability of steady-state and the conditions of single-mode radiation for all optical fields generated in the ICSRO.

This study was supported by RFBR grant No.13-02-12070-OFI\_M.

- [1] Solid-state mid-infrared laser sources, T. Sorokina, K. L. Vodopyanov, Eds. (Springer-Verlag Berlin Heidelberg), Chapter 11, (2003).
- [2] D. Stothard, M. Ebrahimzadeh, M. Dunn, Low pump threshold, continuous-wave, singly resonant, optical parametric oscillator, *Opt. Lett.*, vol.23, pp. 1895-1897, (1998).
- [3] D. Stothard, J. Hopkins, D. Burns, M. Dunn, Stable, continuous-wave, intracavity, optical parametric oscillator pumped by a semiconductor disk laser (VECSEL), *Opt. Express*, vol.17, pp. 10648-10658, (2009).
- [4] Yu. A. Morozov, M. Yu. Morozov, V. I. Kozlovsky, O. G. Okhotnikov, Intracavity singly-resonant OPO pumped by GaSb-based semiconductor disk laser, *Book of abstr. of Int. Conf. on Adv. Laser Techn. (ALT'2014)*, Cassis, France, Oct. 6-10, p. S1-P28, (2014).
- [5] Yu. A. Morozov, M. Yu. Morozov, V. I. Kozlovsky, O. G. Okhotnikov. Compact intracavity singly-resonant optical parametric oscillator pumped by GaSb-based vertical external cavity surface-emitting laser: Concept and the main operational characteristics. *IEEE Journ. of Sel. Top. in Quantum Electronics*, vol.21, p.1603105-1—1603105-5, (2015).
- [6] G. A. Turnbull, M. H. Dunn, M. Ebrahimzadeh, Continuous-wave, intracavity optical parametric oscillators: an analysis of power characteristics. *Appl. Phys. B*, vol.66, pp.701-710, (1998).

## Noninvasive blood glucose monitoring in the terahertz frequency range

**O. P. Cherkasova<sup>1</sup>, M. M. Nazarov<sup>2</sup>, E. E. Berlovskaya<sup>3</sup>, A. A. Angeluts<sup>3</sup>,  
A. M. Makurenkov<sup>3</sup>, A. P. Shkurinov<sup>2,3</sup>**

*1-Institute of Laser Physics of SB RAS, pr. Lavrentyeva, 13/3, Novosibirsk, 630090 Russia*

*2-Institute on Laser and Information Technologies of RAS, 1 Svyatooserskaya St., Shatura, 142092*

*3-Lomonosov Moscow State University, Leninskie Gory, GSP-1, Moscow, 119991, Russia*

*e-mail: [o.p.cherkasova@gmail.com](mailto:o.p.cherkasova@gmail.com)*

Monitoring of glycemic status of patients with diabetes is considered a cornerstone of their care. Currently, control of this disease involves several times a day finger puncture to obtain a blood sample for chemical analysis of glucose level. This procedure is invasive, painful, non-safe and unpleasant for patients. In the past decades much attention has been paid to the development of spectroscopic methods for noninvasive glucose measuring [1]. For example, it was shown that absorption coefficient of rat ear skin correlates with blood glucose concentration in 27-40 GHz frequency range [2]. In our work studies of human skin reflection spectra were performed in vivo using terahertz (THz) time-domain spectroscopy in 0.1-2.0 THz frequency range.

The experiments were based on the attenuated total internal reflection optical scheme with silicon right angle Dowe prism. The volunteers pushed their palm to the prism base for 3 minutes to obtain reflection spectra. Details of reflection study with our THz time-domain spectrometer have been reported in [3]. The measurements were carried out on 6 volunteers. They were in good health and have a normal blood glucose concentration ( $< 6.1$  mM). A standard oral glucose tolerance test using 75 g glucose was performed in all volunteers. The reflection spectra of palm skin were measured at 0-120 min after intake glucose. The blood glucose concentration was determined by a commercial glucometer "OneTouch Ultra" (USA).

It is shown that the most pronounced difference in the complex reflection spectra  $R$  are observed in the frequency range of 0.1-0.5 THz. Amplitude and phase of the reflection coefficient of human palm skin are changed when the blood glucose concentrations rise above the normal levels. Moreover, changes in the phase of  $R$  are more pronounced. These variations of the optical characteristics of the human skin correlate with the changes in blood glucose level (fig. 1) and can be used as practical biophysical marker of blood state.

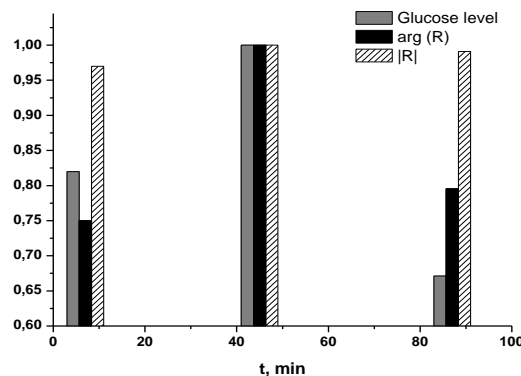


Figure 1. Normalised amplitude  $|R|$ , phase  $\arg(R)$  of the reflection coefficient (at 1.0 THz frequency) and blood glucose concentration versus time  $t$  (min) after intake glucose. For clarity, all parameters are normalized to their maximum value at  $t=45$  min.

Our results demonstrate a possibility of non-invasive real time measurement of blood glucose concentration. This work has been supported by RFBR (grant № 13-02-01364).

- [1] R. He, H. Wei, H. Gu, Z. Zhu, Y. Zhang, X. Guo, T. Cai "Effects of optical clearing agents on noninvasive blood glucose monitoring with optical coherence tomography: a pilot study", *Journal of Biomedical Optics*, vol. 17(10), pp. 101513-1 (2012).  
 [2] P.H. Sigel, Y. Lee, V. Pikov, "Millimeter-Wave Non-Invasive Monitoring of Glucose in Anesthetized Rats", 39th International Conference on Infrared, Millimeter, and Terahertz Waves (IRMMW-THz 2014): proceedings, T2/D-8 (2014).  
 [3] M. M. Nazarov, A. P. Shkurinov, E. A. Kuleshov, V. V. Tuchin, "Terahertz time-domain spectroscopy of biological tissues", *Quantum Electronics*, vol. 38, pp. 647-654 (2008).

## KEY FOR AUTHORS/CHAIRS

<i>Name</i>	<i>Number</i>	<i>Page</i>	<i>Name</i>	<i>Number</i>	<i>Page</i>
Abraham E.	TH-I-9	217	Bakhtinov P.I.	D-P-9	74
Acef O.	S-P-1	205	Balakin A.V.	TH-I-6	214
Achim (Popa) C.	D-I-11	60	Balling P.	LM-O-8	115
Achim C.	D-P-2, D-P-3	67, 68	Bañas A.	B-O-6	36
Afanasev D.	LM-P-17	141	Banchelli M.	B-I-8	21
Agrba P.D.	B-O-5	35	Banita S.	D-I-10, D-O-1, D-P-2, D-P-3	60, 62, 67, 68
Aguiló M.	LS-I-1, LS-P-6	151, 180	Bashkatov A.N.	B-I-5, B-P-1	18, 39
Aiadi K.E.	S-P-3	207	Bashouti M.	D-I-2	52
Alberto N.	S-P-4, S-P-5	207A, 207B	Bastos J.M.	S-I-3	199
Allakhverdiev K.R.	LS-O-8	174	Batentschuk M.	D-P-1	66
Allen W.M.	B-I-9	22	Batomonkuev A.	B-I-3	16
Almabouada F.	S-P-3	207	Baum O.	B-I-7	20
Almeida A.	LM-I-18	97	Bayer L.	LM-O-2, LM-P-11	109, 135
Alves E.	D-I-4	54	Beiler B.	D-P-11	76
Alves E.P.	LS-I-12	162	Belghachem N.	LS-O-1	167
Alves J.	LS-I-13	163	Bercu M.	D-P-2	67
Alves L.	NL-O-2	186	Berlovskaya E.E.	TH-O-7	224
Alyshev S.V.	OC-O-1	193	Besley M.	NL-O-2	186
Amado S.B.	NL-I-3	184	Bessonov D.	LM-P-7	131
Ammar M.R.	D-I-1	51	Bibikova O.	B-P-4	42
André P.	NL-P-2, OC-O-2, S-I-3, S-I-4, S-P-4	189, 194, 199, 200, 207A	Bigi A.	B-O-8	38
Andrijauskas D.	LM-O-10	117	Bimberg D.	PI-2	7
Angelis M.	B-I-8	21	Bingham R.	LS-I-12	162
Angelov I.	B-P-7	45	Birukov V.P.	LM-P-2	126
Angeluts A.A.	TH-O-7	224	Bludov Yu.V.	TH-I-1	209
Anisimov S.	LM-O-17	124	Bo Xia	LM-I-8	87
Antipov A.	LM-P-25	149	Bockowski M.	D-I-4	54
Antoniou Ch.	D-P-7	72	Bogomolov A.	D-P-12	77
Antunes P.	S-I-3, S-I-4, S-P-4	199, 200, 207A	Bolshunov A.	B-I-7	20
Arakelian S.	LM-I-14, LM-O-9, LM-P-25	93, 116, 149	Borisova E.	B-I-4, B-P-7	17, 45
Arenal R.A.	D-P-4	69	Borodin A.V.	TH-I-6	214
Aronov A.N.	LM-P-9	133	Boulanger B.	LS-I-5	155
Aronzon B.A.	LM-P-9, LM-P-13	133, 137	Boursier E.	LS-I-5	155
Artemyev D.	D-O-4, D-P-8, D-P-9	65, 73, 74	Boutou V.	LS-I-5	155
Aryshev A.	LM-P-22	146	Brabec Ch.	D-P-1	66
Ascencio S.M.	B-I-13	26	Bratchenko I.	D-O-4	65
Ashikkalieva K.	LM-P-21	145	Bratu A.-M.	D-I-10, D-O-1, D-P-2, D-P-3	60, 62, 67, 68
Ashmarov V.	B-I-3	16	Breckenfeld E.	PI-5	10
Astapovich M.S.	LS-I-15	165	Brekhov K.	LM-P-17	141
Auyeung R. C. Y.	PI-5	10	Bruns Th.	B-I-10	23
Avramenko V.	D-P-4	69	Bucharskaya A.	B-P-1	39
Avramopoulos H.	LS-P-5	179	Buchta Z.	D-P-10, LS-O-3	75, 169
Avramov L.	B-I-4, B-P-7	17, 45	Budriūnas R.	LS-P-4	178
Axente E.	B-O-8	38	Bueno J.M.	B-I-1	14
Azamoum Y.	LM-O-3	110	Bulgakov A.V.	LM-I-22	101
Babazadeh A.	S-O-3	203	Bulgakova N.M.	LM-I-13, LM-I-22	92, 101
Bacopoulos P.	LS-P-5	179	Bulgakova N.N.	B-I-3	16
Bagratashvili V.	B-I-14	27	Burck F.D.	S-P-1	205
			Burdonov K.	LS-I-10	160

<i>Name</i>	<i>Number</i>	<i>Page</i>
Buyanova N.	B-P-6	44
Buzanov O.	LS-P-3	177
Búzás A.	LM-I-24	103
Bykov A.	B-P-4	42
Bykov D.	LS-O-5	171
Bykovskiy D.P.	LM-P-3	127
Byoung Yoon Kim	PI-1	6
Bystrova A.	B-I-14	27
<hr/>		
Campbell E.E.B.	LM-I-22	101
Canalias C.	LS-I-8	158
Canizarès A.	D-I-1	51
Carlos L.D.	NL-P-2	189
Carvalho M.I.B.	B-O-7, B-P-3	37, 41
Carvalho R.G.	LM-I-7	85
Castellani C.E.S.	S-I-4	200
Cavigli L.	B-I-8	21
Centi S.	B-I-8	21
Charipar N. A.	PI-5	10
Charmasson L.	LM-O-3	110
Chatzipetrou M.	S-O-1	201
Chea E.	S-P-1	205
Cherebilo E.A.	LS-P-2	176
Cherepenin V.A.	LM-O-16	123
Cherkasova E.	B-I-14	27
Cherkasova O.	TH-O-7	224
Chernoglazov K.Yu.	LM-P-10	134
Chesnokov Ju.M.	LM-P-13	137
Chia-Liang Cheng	B-P-4	42
Chichkov B.	LM-I-21	100
Chin L.	B-I-9	22
Chistyakov A.	NL-P-1	188
Chizhikov S.	LS-O-6	172
Choe C.-S.	B-I-13	26
Chomchik O.	B-I-7	20
Choporova Yu.Yu.	TH-O-2, TH-O-3	219, 220
Christiansen S.	D-I-2	52
Christofidou E.	D-P-7	72
Chunlei Guo	LM-I-9	88
Churlyayeva O.N.	LM-P-2	126
Čip O.	LS-O-3, S-P-1	169, 205
Čížek M.	LS-O-3	169
Clady R.	LM-I-1, LM-O-3	79, 110
Cornet M.	TH-I-9	217
Correia M.R.	D-I-4	54
Correia S.	S-P-4	207A
Costa F.M.	LM-I-7	85
Costa L.C.	S-P-5	207B
Costa S.	NL-O-2	186
Csíkvári P.	LM-P-14	138
Cumming D.	TH-I-2	210
Cunha A.	LM-I-18	97

<i>Name</i>	<i>Number</i>	<i>Page</i>
Cunha A.D. da	OC-O-2	194
Cyras V.	LM-O-10	117
Czitrovsky A.	D-I-8	58
<hr/>		
Danilevičius R.	LS-P-4	178
Darvin M.	B-I-13	26
Daue S.	B-I-3	16
Davydkin I.L.	D-P-8, D-P-9	73, 74
Davydov A.B.	LM-P-13	137
Debray J.	LS-I-5	155
Deev S.M.	B-O-1	31
Degert J.	TH-I-9	217
Demin M.M.	LM-P-19	143
Denker B.I.	LS-I-9, LS-I-15	159, 165
Deryagin A.G.	LS-I-11	161
Desgranges L.	D-I-1	51
Dessinioti C.	D-P-7	72
Dholakia K.	B-I-11	24
Di Jianke	LM-I-25	104
Dianov E.M.	LS-I-15, OC-O-1	165, 193
Dias João M.	LS-I-13	163
Díaz F.	LS-I-1, LS-P-6	151, 180
Didenko I.	LS-P-3	177
Diez J.C.	LM-I-7	85
Dolotov L.E.	B-I-5	18
Domingues F.	S-P-4	207A
Dong Wu	LM-I-10	89
Doroshenko M.E.	LS-I-2	152
Doskolovich L.	LS-O-5	171
Drakaki E.	D-P-7	72
Dubinina T.	NL-P-1	188
Dubrov A.	LM-O-13, LM-P-20	120, 144
Dubrov V.	LM-O-13	120
Dudelev V.V.	LS-I-11	161
Dudenkova V.	B-I-14	27
Dumitras D.C.	D-I-10, D-O-1, D-P-2, D-P-3	60, 62, 67, 68
Dutreilh-Colas M.	D-I-1	51
Duval F.	D-I-1	51
Dzhidzhoev M.S.	TH-I-6	214
Dzhumaev P.S.	LM-P-3	127
<hr/>		
Edwards P.R.	D-I-4	54
Efimova A.	D-I-5	55
Egorova O.N.	LS-I-15	165
Ehrhardt M.	LM-O-2, LM-P-11	109, 135
Elagin V.	B-P-6	44
Eliseev A.	D-I-5	55
Elshin A.	LM-O-11	118
Emel'yanov V.	LM-I-14, LM-O-11	93, 118
Es' Haghian S.	B-I-9	22
Esaulkov M.	TH-I-6, TH-O-1	214, 218
Esenaliev R.	D-I-9	59

<i>Name</i>	<i>Number</i>	<i>Page</i>
Eui Su Lee	TH-I-5	213
Evdokimov M.	TH-I-6	214
<b>Fadeev V.</b>	<b>B-O-3, B-P-9, B-P-11</b>	<b>33, 47, 49</b>
Fadyukova O.	B-I-12, B-O-2	25, 32
Fajardo M.	LS-I-13	163
Farsari M.	LS-I-11	161
Fedorchenko I.V.	LM-P-13	137
Feichtner Th.	D-I-2	52
Feldchtein F.	B-P-6	44
Félix C.	LS-I-5	155
Felix Sima	LM-I-10	89
Fernandes A.J.S.	LM-I-7	85
Fernández-Pradas J.M.	LM-I-11	90
Ferreira A.	TH-I-1	209
Ferreira Mário F.S.	NL-I-2, NL-O-3	183, 187
Ferreira N.M.	LM-I-7	85
Ferreira R.A.S.	NL-P-2, S-P-4	189, 207A
Ferreira R.C.M.	NL-O-2	186
Figueira G.	LS-I-13, OC-O-2	163, 194
Figueiredo F.M.	LM-I-7	85
Figueiredo J.M.L.	OC-I-2, TH-I-2	192, 210
Firsova N.	LM-O-11	118
Firstov S.V.	OC-O-1	193
Florian C.	LM-I-11	90
Fogel O.	LM-O-7	114
Fokin V.B.	LM-O-15	122
Forsh P.A.	B-O-5	35
Fotso Gueutue E.S.	D-I-1	51
Freysz E.	TH-I-9	217
Frolov S.V.	B-P-2	40
Frolov V.D.	LM-O-4	111
Fu L.	NL-P-2	189
Fürjes P.	LM-P-23	147
<b>Galagan B.</b>	<b>LS-I-9, LS-I-15</b>	<b>159, 165</b>
Gamayunov S.	B-I-3, B-P-5	16, 43
Garcia-Lechuga M.	LM-O-8	115
Garliauskas M.	LM-O-5	112
Gaskov A.M.	LM-P-8	132
Gelikonov G.	B-P-6	44
Generalova A.N.	B-O-1, LM-P-16	31, 140
Genina E.	B-I-5, B-P-1	18, 39
Genova Ts.	B-I-4	17
Gerasimenko A.S.	LS-I-2	152
Geretovszky Z.	LM-I-24	103
Gladkova N.	B-P-6	44
Glückstad J.	B-O-6	36
Golovan L.A.	B-O-5, D-I-5, LM-P-6	35, 55, 130
Golovastikov N.	LS-O-5	171
Gomes N.	LS-I-13	163
Gonçalves H.	NL-O-2	186
Gong P.	B-I-9	22

<i>Name</i>	<i>Number</i>	<i>Page</i>
Goodfriend N.	LM-I-22	101
Gordeychuk D.I.	LM-O-12, S-O-4	119, 204
Gordienko V.M.	TH-I-6	214
Gorin D.A.	B-I-5	18
Gouveia N.S.	OC-P-1	195
Griebner U.	LS-I-1, LS-P-6	151, 180
Grigorenko A.N.	LM-O-4	111
Grigoriev K.S.	NL-I-1, NL-O-1	182, 185
Grishin M.	LS-O-7	173
Grishunin K.	LM-P-17	141
Grüner Ch.	LM-O-2	109
Guimbretière G.	D-I-1	51
Guiomar F.P.	NL-I-3	184
Guizard S.	LM-O-8	115
Guk I.V.	LM-P-15	139
Gulyaev P.Yu.	B-P-8	46
Gurfinkel Yu.	B-I-12	25
<b>Haahr-Lillevang L.</b>	<b>LM-O-8</b>	<b>115</b>
Han-Cheol Ryu	TH-O-4	221
Haohai Yu	LS-P-6	180
Hariton V.	LS-I-13	163
Harmand J.C.	D-I-4	54
Hashemi A.	D-P-1	66
Heidariazar A.	S-O-3	203
Heilmann M.	D-I-2	52
Hejaz K.	S-O-3	203
Henriques M.	OC-P-1	195
Hideki Gotoh	LM-I-17	96
Hidetoshi Nakano	LM-I-17	96
Himics L.	D-I-8, D-P-11, LM-P-14, LM-P-23	58, 76, 138, 147
Höflich K.	D-I-2	52
Holá M.	D-P-10, S-P-1	75, 205
Holz T.	LM-I-7	85
Honghui He	B-I-16	29
Horbaciauskas D.	LM-O-10	117
Hrabina J.	S-P-1	205
Hristu R.	B-I-1	14
Huaijin Zhang	LS-P-6	180
Hucl V.	LS-O-3	169
Hui Ma	B-I-16	29
Huseyinoglu M.F.	LS-O-8	174
Hyun-Soo Kim	TH-I-5	213
Hyunsung Ko	TH-I-5	213
<b>Iliadis N.</b>	<b>LS-P-5</b>	<b>179</b>
Il-Min Lee	TH-I-5	213
Imran Tayyab	LS-I-13	163
Inogamov N.	LM-O-17	124
Ionin A.	LS-I-4	154
Isamai Takade	LM-I-3	81
Istratov A.	LM-P-25	149

<i>Name</i>	<i>Number</i>	<i>Page</i>
Itina T.	LM-P-25	149
Ivleva L.I.	LS-I-6	156
Jäckle S.	D-I-2	52
Jaeggi B.	LM-I-16	95
Jafari S.N.T.	S-O-3	203
Jancu J.-M.	D-I-4	54
Jang H.	LS-I-8	158
Javaloyes J.	LS-I-16, OC-I-2	166, 192
Jégou C.	D-I-1	51
Jegouso D.	LS-I-5	155
Jelinek M.	LS-I-2	152
Jelinkova H.	LS-I-2	152
Jian Xu	LM-I-10	89
Jiang Jiasheng	LS-I-13	163
Jintao Chang	B-I-16	29
João Celso P.	LS-I-13	163
Jovicic G.	D-P-1	66
Junhai Liu	LS-P-6	180
Jun-Hwan Shin	TH-O-4	221
Kabashin A.V.	LM-I-19	98
Kamenskikh I.A.	B-O-5	35
Kaminskaya T.P.	LM-P-6	130
Kamynin V.A.	LS-O-2	168
Kanakis J.	LS-P-5	179
Karabut M.	B-P-6	44
Karapuzikov A.A.	D-O-2	63
Karasik A.Ya.	LS-O-2	168
Karmenyan A.	B-P-4	42
Kashaev F.V.	B-O-5, LM-P-6	35, 130
Kashkarov P.K.	B-O-5, D-I-5, D-P-6	35, 55, 71
Katsambas A.D.	D-P-7	72
Katsumi Midorikawa	LM-I-10	89
Katsuya Oguri	LM-I-17	96
Keiko Kato	LM-I-17	96
Kelly A.	TH-I-2	210
Kennedy B.F.	B-I-9	22
Kerekes A.	D-I-8	58
Khalid A.	TH-I-2	210
Khaydukov E.V.	B-O-1, B-O-4, LM-P-16	31, 34, 140
Khazanov E.	LS-I-10	160
Khlebtsov N.G.	B-P-1	39
Khochenkov D.A.	B-O-1	31
Khokhlov V.	LM-O-17	124
Kholodov M.	D-I-5	55
Khomenko M.D.	LM-O-14	121
Khomich A.A.	LM-O-4, LM-P-21	111, 145
Khomich V.	D-O-3	64
Khomich V.Yu.	LS-P-1	175
Khramova O.D.	LM-P-4, LM-P-8, LM-P-9, LM-P-13	128, 132, 133, 137
Khristoforova J.A.	D-P-8	73

<i>Name</i>	<i>Number</i>	<i>Page</i>
Khristoforova J.	D-O-4	65
Kim H.	PI-5	10
Kimel A.	LM-P-17	141
Kinnunen M.	B-P-4	42
Kirillin M.	B-I-3, B-O-5, B-P-5	16, 35, 43
Kisung Lee	B-I-12	25
Kiwon Moon	TH-I-5	213
Klimentov S.	LM-O-8	115
Klöppel M.	LM-O-2	109
Klyen B.R.	B-I-9	22
Knize R.J.	LS-I-14	164
Knyazev B.	TH-O-2, TH-O-3	219, 220
Kochemirovsky V.	LM-O-12	119
Koji Miyazaki	LM-I-12	91
Koji Sugioka	LM-I-10	89
Kolesnikova E.A.	B-I-5	18
Kolker D.	D-O-2	63
Kononenko T.	LM-P-21	145
Konov V.I.	LM-O-4, LM-P-21	111, 145
Konyukhov V.N.	D-P-8, D-P-9	73, 74
Konyushkin V.A.	LS-O-2	168
Koós M.	D-I-8, D-P-11, LM-P-14, LM-P-23	58, 76, 138, 147
Kopczynski K.	LS-O-1	167
Kornienko V.N.	LM-O-16	123
Koshelev V.	B-I-12, B-O-2	25, 32
Kostyukova N.Yu.	D-O-2	63
Kotaro Okamura	LM-I-12	91
Kotler Z.	LM-O-7	114
Kotvanova M.K.	B-P-8	46
Kouta Tateno	LM-I-17	96
Kovalenko N.O.	LS-I-2	152
Kozlov A.	LS-I-4	154
Kozlov S.	D-O-4	65
Kozlova A.	LS-P-3	177
Kozlova N.S.	D-P-9, LS-P-3	74, 177
Kozlovskii V.F.	LM-P-8	132
Kozlovsky V.I.	TH-O-6	223
Krasovskii V.	NL-P-1	188
Krokhin O.	PI-3	8
Kucherik A.	LM-I-14, LM-O-9, LM-P-25	93, 116, 149
Kuchinskii V.I.	LS-I-11	161
Kugler Sz.	D-I-8	58
Kulagin V.V.	LM-O-16	123
Kulchin Yu.N.	LM-I-27	106
Kulipanov G.N.	TH-O-2	219
Kulmas M.	D-I-2	52
Kunzel S.	LS-I-13	163
Kussovski V.	B-P-7	45
Kutrovskaya S.	LM-I-14, LM-O-9, LM-P-25	93, 116, 149

<i>Name</i>	<i>Number</i>	<i>Page</i>
Kuz'micheva G.M.	LS-I-6	156
Kuzmina T.P.	D-P-8	73
Kuzminov F.	B-P-9	47
Kuznetsova D.	B-I-14	27
Kyung Hyun Park	TH-I-5, TH-O-4	213, 221
Lademann J.	B-I-13	26
Lafouti M.	S-O-3	203
Laguta O.	LS-I-9	159
Lan Jiang	LM-I-8	87
Larin K.	B-I-6	19
Larina I.	B-I-15	28
Latas S.C.V.	NL-O-3	187
Latzel M.	D-I-2	52
Lazar J.	D-P-10, LS-O-3, S-P-1	75, 169, 205
Leahy M.	PI-4	9
Lebedev O.	B-O-1	31
Leitão C.	S-I-3	199
Leitão J.P.	D-I-3	53
Levashov P.R.	LM-O-15	122
Levshov D.I.	D-P-4	69
Lin M.	B-O-2	32
Lingling Huang	S-O-2	202
Linkov K.G.	D-P-5	70
Linn M.	B-I-12	25
Loginov A.	LM-P-22	146
Logunov L.	LM-O-12	119
Lohmüller T.	LM-I-28	107
Loiko P.	LS-I-1, LS-P-6	151, 180
Loor R. de	LM-I-16	95
Lopes N.C.	LS-I-13	163
Lopes P.	S-P-2	206
Lorenz K.	D-I-4	54
Lorenz P.	LM-O-2, LM-P-11	109, 135
Loschenov V.B.	D-P-5	70
Losev S.N.	LS-I-11	161
Lotin A.A.	LM-P-12, LS-P-2	136, 176
Louchev O.A.	LM-I-12	91
Louhibi D.	S-P-3	207
Lugovtsov A.	B-I-12, B-O-2	25, 32
Lukstaraupis T.	LM-O-10	117
Lykina A.A.	D-P-8	73
Lykov P.A.	LS-I-6	156
Madanipour K.	S-O-3	203
Madre M.A.	LM-I-7	85
Magnin M.	D-I-1	51
Makarevich A.Yu.	TH-O-1	218
Makarov V.A.	NL-I-1, NL-O-1, TH-O-1	182, 185, 218
Makropoulou M.	D-P-7	72
Maksimov E.	B-P-9	47
Makurenkov A.M.	TH-O-7	224

<i>Name</i>	<i>Number</i>	<i>Page</i>
Malinskiy T.	D-O-3	64
Manshina A.	LM-O-9	116
Mantareva V.	B-P-7	45
Marenkin S.F.	LM-P-9, LM-P-13	133, 137
Markovic V.	LM-I-16	95
Marques C.A.F.	S-I-2	198
Marques R.S.	S-I-4	200
Martin C.S.	NL-I-3	184
Masaharu Tsuji	LM-I-3	81
Masahiko Iwasaki	LM-I-12	91
Maslova O.A.	D-I-1	51
Maslyakova G.N.	B-P-1	39
Massaouti M.	S-O-1	201
Matei C.	D-O-1, D-P-2, D-P-3	62, 67, 68
Mateos X.	LS-I-1, LS-P-6	151, 180
Mathews S.	PI-5	10
Matos Gomes E. de	NL-O-2	186
Matsui H.	LM-I-15	94
Matteini P.	B-I-8	21
Matuzin E.I.	LM-P-1	125
Matveev L.	B-P-6	44
Mauguin O.	D-I-4	54
Mazhukin A.V.	LM-P-19	143
Mazhukin V.I.	LM-P-18, LM-P-19	142, 143
McLaughlin R.A.	B-I-9	22
Medvedkov O.I.	LS-I-15	165
Meglinski I.	B-I-17, B-P-4	30, 42
Meleshina A.	B-I-14	27
Melissinaki V.	LS-I-11	161
Meller A.	B-P-5	43
Melnikov I.V.	LM-I-5	83
Ménaert B.	LS-I-5	155
Mendonça J.T.	PI-7, LS-I-12	12, 162
Mereshchenko A.S.	S-O-4	204
Meshcheryakov Yu.P.	LM-I-13	92
Michailovas A.	LS-O-7, LS-P-4	173, 178
Michel Th.	D-P-4	69
Mihailescu I.N.	LM-I-20, B-O-8	99, 38
Mihailescu N.	B-O-8	38
Mikhalevskiy V.A.	LM-P-4, LM-P-9, LM-P-12, LM-P-13	128, 133, 136, 137
Mikio Higuchi	LS-O-4	170
Min Yong Jeon	S-I-1	197
Mironov V.	S-O-4	204
Mironova K.E.	B-O-1, LM-P-16	31, 140
Mirzade F.Kh.	LM-O-14, LM-P-5, LM-P-20	121, 129, 144
Mishina E.	LM-O-11, LM-P-17	118, 141
Mitkov M.S.	TH-O-2, TH-O-3	219, 220
Mlynczak J.	LS-O-1	167
Model S.S.	D-P-5	70
Mohun R.	D-I-1	51
Molchanov V.	LS-O-6	172

<i>Name</i>	<i>Number</i>	<i>Page</i>
Molchkov E.V.	D-P-9	74
Monteiro T.	D-I-4, LM-I-7	54, 85
Morenza J.L.	LM-I-11	90
Morozov Yu.A.	TH-O-6	223
Moryatov A.	D-O-4	65
Mouskeftaras A.	LM-O-8	115
Muga N.J.	NL-I-3	184
Mulenko S.	LM-I-23	102
Murzakov M.F.	LM-P-2	126
Myakinin O.O.	D-O-4	65
Myeong Ock Ko	S-I-1	197
<hr/>		
Nagy A.	D-I-8	58
Nakajima T.	LM-I-15	94
Nakamura T.	LM-I-15	94
Namje Kim	TH-I-5	213
Naoto Koshizaki	LM-I-3	81
Nasirabad R.R.	S-O-3	203
Navolokin N.A.	B-P-1	39
Nazarov M.M.	TH-O-7	224
Nebogatkin S.V.	LS-P-1	175
Nechaev A.V.	B-O-1, LM-P-16	31, 140
Negut I.	B-O-8	38
Nemec M.	LS-I-2	152
Nerushev O.	LM-I-22	101
Neto A.F.	S-I-4	200
Neuenschwander B.	LM-I-16	95
Neves A. J.	D-I-4	54
Nikitin S.	B-I-12	25
Nikolaev I.V.	D-I-6	56
Nikolaev S.N.	LM-P-10	134
Niziev V.G.	LM-O-14, LM-P-20	121, 144
Nogueira E.M.S.M.	B-O-7, B-P-3	37, 41
Nogueira R.	S-P-5	207B
Norihito Saito	LM-I-12	91
Novodvorsky O.A.	LM-P-4, LM-P-8, LM-P-9, LM-P-10, LM-P-12, LM-P-13, LS-P-2, TH-O-1	128, 132, 133, 134, 136, 137, 176, 218
<hr/>		
O'Donnell K.P.	D-I-4	54
Obraztsova E.	LM-P-21	145
Ochkin V.N.	D-I-6	56
Okhrimchuk A.G.	LS-I-15	165
Oliveira L.M.C.	B-O-7, B-P-3	37, 41
Oliveira V.	LM-I-18, LM-O-1	97, 108
Omelchenko A.I.	B-P-8, LM-P-24	46, 148
Oner E.T.	B-O-8	38
Osiko V.V.	LS-I-6	156
Osipov A.	LM-O-9	116
Oszetzky D.	D-I-8	58
Oulehla J.	S-P-1	205
<hr/>		
Paillet M.	D-P-4	69

<i>Name</i>	<i>Number</i>	<i>Page</i>
Palianov P.	LM-O-8	115
Palima D.	B-O-6	36
Panchenko V.Ya.	B-O-1	31
Panov M.S.	S-O-4	204
Panova O.	B-I-3	16
Parshina L.S.	LM-P-4, LM-P-9, LM-P-12, LM-P-13	128, 133, 136, 137
Parshina L.V.	TH-O-1	218
Pasiskevicius V.	LS-I-8	158
Pasquier C.	LM-I-1	79
Patachia M.	D-I-10, D-O-1, D-P-2, D-P-3	60, 62, 67, 68
Patimisco P.	D-I-11	61
Patrascioiu A.	LM-I-11	90
Pavelyev V.S.	TH-O-2	219
Peltek S.E.	TH-I-7	215
Pena A.	LS-I-5	155
Penkov N.	B-I-4	17
Penning L.	LM-I-16	95
Pereira D.	S-P-5	207B
Peres N.M.R.	TH-I-1	209
Perevedentseva E.	B-P-4	42
Perezhogin I.A.	NL-I-1, NL-O-1	182, 185
Perminov P.A.	LM-P-6	130
Petrov V.	LS-I-1, LS-P-6	151, 180
Petrov Yu.	LM-O-17	124
Petrovskiy V.N.	LM-P-2, LM-P-3	126, 127
Petrus M.	D-I-10, D-O-1, D-P-3	60, 62, 68
Petukhov I.A.	LM-P-4, LM-P-8	128, 132
Pinho P.	OC-P-1	195
Pini R.	B-I-8	21
Pinto A.N.	NL-I-3	184
Pinto J.L.	S-I-3, S-P-4	199, 207A
Piqué A.	PI-5	10
Pires H.	LS-I-13	163
Pivovarov P.A.	LM-O-4, LM-P-18	111, 142
Pol'skiy V.I.	LM-P-3	127
Pontes M.J.	S-I-4	200
Poozesh R.	S-O-3	203
Popa C.	D-O-1	62
Potlov A.Yu.	B-P-2	40
Povarnitsyn M.E.	LM-O-15	122
Povolotckaia A.	LM-O-9	116
Povolotskiy A.	LM-O-9	116
Prado A.R.	S-I-4	200
Presnov D.	D-I-5	55
Priezzhev A.	B-I-12, B-O-2, B-P-11	25, 32, 49
Prokopova N.M.	LM-P-2, LM-P-3	126, 127
Proskurin S.G.	B-P-2	40
Proskurina O.	B-P-10	48
Prunskaitė-Hyyryläinen R.	B-P-4	42
Pustovoit V.	D-I-7	57
Putilin F.N.	LM-P-4, LM-P-8	128, 132

<i>Name</i>	<i>Number</i>	<i>Page</i>
Qiang Cao	LM-I-8	87
Račiukaitis G.	LM-O-5	112
Rafailov E U.	LS-I-11, TH-I-3	161, 211
Raimboux N.	D-I-1	51
Raposo M.	NL-O-2	186
Rasekh Sh.	LM-I-7	85
Ratto F.	B-I-8	21
Razdobreev I.	LS-I-9	159
Rebrov I.E.	LS-P-1	175
Rech B.	D-I-2	52
Resan B.	LM-I-16	95
Ribeiro M.R.N.	S-I-4	200
Richter V.	B-I-10	23
Rigó I.	D-I-8, D-P-11, LM-P-23	58, 76, 147
Rino L.	D-I-4	54
Ristoscu C.	LM-I-20, B-O-8	99, 38
Rocheva V.	LM-P-16	140
Rodin A.M.	LS-O-7	173
Rodrigues J.	D-I-4, LM-I-7	54, 85
Romeira B.	OC-I-2	192
Roohforouz A.	S-O-3	203
Rossi F.	B-I-8	21
Rotermund F.	LS-I-3	153
Rotondaro M.D.	LS-I-14	164
Rovnyagina N.	B-O-3	33
Ruão F.	LS-I-13	163
Rumyantseva M.N.	LM-P-8	132
Rusteika N.	LS-P-4	178
Rylkin Yu.	B-P-5	43
Rylkov V.V.	LM-P-10	134
Sáfrány Á.	D-P-11	76
Salgado H.M.	OC-I-1	191
Samokhin A.A.	LM-P-18, LM-P-19	142, 143
Samokhvalov A.	LM-P-22	146
Sampaolo A.	D-I-11	61
Sampson D.D.	B-I-9	22
Sanches E.	B-I-3	16
Sang-Pil Han	TH-I-5	212
Sanner N.	LM-I-1, LM-O-3	79, 110
Santos J.E.	TH-I-1	209
Santos N.F.	LM-I-7	85
Santos T.	S-P-5	207B
Sapunov D.	B-P-5	43
Sarau G.	D-I-2	52
Šarbort M.	D-P-10, LS-O-3, S-P-1	75, 169, 205
Sarnet T.	LM-O-6	113
Satoshi Wada	LM-I-12, LS-O-4	91, 170
Sauvajol J.-L.	D-P-4	69
Savelieva T.A.	D-P-5	70
Savelyev A.G.	B-O-4	34
Scamarcio G.	D-I-11	61

<i>Name</i>	<i>Number</i>	<i>Page</i>
Scheres L.	S-O-1	201
Schickinger S.	B-I-10	23
Schmitt S.	D-I-2	52
Schneckenburger H.	B-I-10	23
Sedrine N.B.	D-I-4	54
Segonds P.	LS-I-5	155
Semchishen V.A.	B-O-1, B-O-4, LM-P-16	31, 34, 140
Semin S.	LM-P-17	141
Semjonov S.L.	LS-I-15	165
Sentis M.	LM-I-1, LM-O-6, LM-O-3	79, 113, 110
Sequeir M.C.	D-I-4	54
Serafetinides A.A.	D-P-7	72
Seregin V.F.	LS-O-2	168
Sergeev M.M.	LM-I-6, LM-P-1	84, 125
Sergeeva O.	D-P-12	77
Serra P.	LM-I-11	90
Serres J.M.	LS-I-1, LS-P-6	151, 180
Shakhov A.	B-P-5	43
Shakhova M.	B-P-5	43
Shakhova N.	B-I-3	16
Shandybina G.D.	LM-P-15	139
Shapranov A.V.	LM-P-18, LM-P-19	142, 143
Sharma S.	LM-O-1	108
Shaykin A.	LS-I-10	160
Shcherbakov I.A.	LS-I-7	157
Sherstyuk N.	LM-P-17	141
Shesterkin V.	LM-P-7	131
Shirshin E.	B-I-12, B-O-3, B-P-9, B-P-10, B-P-11	25, 33, 47, 48, 49
Shkurinov A.P.	TH-I-6, TH-O-1, TH-O-7	214, 218, 224
Shorokhova A.V.	LM-P-4, LM-P-8, LM-P-10, LM-P-12, LM-P-13	128, 132, 134, 136, 137
Shukhov Yu.G.	LM-I-22	101
Shuleiko D.V.	D-P-6	71
Sianoudis I.A.	D-P-7	72
Sibbett W.	LS-I-11	161
Siegel J.	LM-O-8	115
Sikora A.	LM-O-6	113
Silva L.O.	LS-I-12	162
Silva R.F.	LM-I-7	85
Sima F.	B-O-8	38
Sima L.	B-O-8	38
Siminel N.	LS-P-3	177
Simões P.	S-P-2	206
Simon P.	D-I-1	51
Sinitsyn D.	LS-I-4	154
Sirotkina M.	B-P-6	44
Skovorodkin I.	B-P-4	42
Smikhovskaia A.A.	LM-O-12	119
Smulders M.	S-O-1	201
Soares M.R.	LM-I-7	85

<i>Name</i>	<i>Number</i>	<i>Page</i>
Sobol E.	B-I-7, B-P-8	20, 46
Soboleva K.K.	LS-I-11	161
Soifer V.A.	TH-O-2	219
Sokolova T.	LM-P-7	131
Sokolovskii G.S.	LS-I-11	161
Solis J.	LM-O-8	115
Solnyskin A.	D-P-12	77
Solyankin P.	TH-I-6, TH-O-1	214, 218
Sotelo A.	LM-I-7	85
Spagnolo V.	D-I-11	61
Sperandio V.M.	S-I-4	200
Stanciu G.A.	B-I-1	14
Stanciu S.G.	B-I-1	14
Stankevičius E.	LM-O-5	112
Starikova M.K.	D-O-2	63
Starinskiy S.V.	LM-I-22	101
Stefanaki I.	D-P-7	72
Stepanova E.V.	B-O-1	31
Stratigos A.J.	D-P-7	72
Sukhorukov G.B.	B-I-5	18
Sulinskas K.	LM-O-10	117
Surmenko E.	LM-P-7	131
Svenskaya Yu.I.	B-I-5	18
Sverchkov S.	LS-I-9, LS-I-15	159, 165
Sypek M.	TH-I-8	216
<hr/>		
Tadashi Nishikawa	LM-I-17	96
Takanobu Tsunoi	LM-I-17	96
Takayo Ogawa	LS-O-4	170
Takeshi Tsuji	LM-I-3	81
Tatini F.	B-I-8	21
Tavares C.	S-P-4	207A
Tcheremiskine V.	LM-O-3	110
Terentyuk G.S.	B-I-5, B-P-1	18, 39
Tessarek Ch.	D-I-2	52
Tetsuomi Sogawa	LM-I-17	96
Tiguntseva E.Y.	LM-P-1	125
Tikhonova T.	B-I-12, B-O-3	25, 33
Timashev P.	B-I-14	27
Tittel F.K.	D-I-11	61
Tkachev A.	D-I-5	55
Tobon Y.	D-I-1	51
Tomilova L.	NL-P-1	188
Tóth S.	D-I-8, D-P-11, LM-P-14, LM-P-23	58, 76, 138, 147
Tranca D.E.	B-I-1	14
Tribelsky M.I.	LM-I-26	105
Trikshev A.I.	LS-O-2	168
Trilling A.	S-O-1	201
Trines R.	LS-I-12	162
Troyanova P.	B-I-4	17
Tskhai S.N.	D-I-6	56
Tsuchiya T.	LM-I-15	94

<i>Name</i>	<i>Number</i>	<i>Page</i>
Tsvetkov V.B.	LS-I-7, LS-O-2	157, 168
<hr/>		
Tuchin V.V.	B-I-2, B-I-5, B-O-7, B-P-1, B-P-3	15, 18, 37, 39, 41
Tumkin I.	LM-O-12, S-O-4	119, 204
<hr/>		
Ustinov V.	B-O-2	32
Uteza O.	LM-I-1, LM-O-3	79, 110
Vainio S.	B-P-4	42
Vartanyan T.	LM-P-25	149
Vasilevskiy M.I.	TH-I-1	209
Vasiliev A.L.	LM-P-13	137
Vatani V.	S-O-3	203
Veiko V.P.	LM-I-6, LM-P-1, LM-P-22	84, 125, 146
Verebély T.	D-I-8, D-P-11	58, 76
Veres M.	D-I-8, D-P-11, LM-P-14, LM-P-23	58, 76, 138, 147
Vettenburg T.	B-I-11	24
Vetter A.	D-P-1	66
Vicente C.M.S.	NL-P-2	189
Vieira J.	LS-I-12	162
Vilar R.	LM-I-18, LM-O-1	97, 108
Villangca M.	B-O-6	36
Vinokurov N.A.	TH-O-2	219
Visan A.	B-O-8	38
Vitkin A.	B-P-6	44
Vladimirov B.	B-I-4	17
Voisin P.	D-I-4	54
Volodkin B.O.	TH-O-2	219
<hr/>		
Wagner M.	B-I-10	23
Wang J.	TH-I-2	210
Wasige E.	TH-I-2	210
Webb D.J.	S-I-2	198
Weber P.	B-I-10	23
Weingarten K.	LM-I-16	95
Wijesinghe P.	B-I-9	22
Williams G.	LS-I-13	163
Won-Hui Lee	TH-I-5	213
<hr/>		
Xiaowei Li	LM-I-8	87
Xueliang Yan	LM-I-8	87
<hr/>		
Yakovlev E.B.	LM-P-15	139
Yamaguchi I.	LM-I-15	94
Yamshchikov V.A.	LS-P-1	175
Yang Liu	LM-I-8	87
Yanina I.Yu.	B-I-5	18
Ye Wang	B-I-16	29
Yong Feng Lu	LM-I-8	87
Yong Seok Kwon	S-I-1	197
Yongfeng Lu	LM-I-2	80

<i>Name</i>	<i>Number</i>	<i>Page</i>
Yoshie Ishimawa	LM-I-3	81
Yu Oishi	LM-I-12	91
Yumashev K.	LS-I-1, LS-P-6	151, 180
Yurchenko S.	TH-I-4, TH-O-5	212, 222
Yushkov K.	LS-O-6	172
Yuuma Higashi	LM-I-3	81
Yuzyuk Y.I.	D-I-1, D-P-4	51, 69
Zabelina E.	LS-P-3	177
Zabotnov S.V.	B-O-5, D-I-5, D-P-6, LM-P-6	35, 55, 71, 130
Zaccaro J.	LS-I-5	155
Zacharatos F.	LS-P-5	179
Zagaynova E.	B-I-14, B-P-6	27, 44
Zagaynova E.	B-P-6	44
Zaitsev V.	B-P-6	44
Zakharov V.	D-O-4, D-P-8, D-P-9	65, 73, 74
Zasedatelev A.	NL-P-1	188
Zavalov Yu.	LM-O-13	120
Zavedeev E.V.	LM-O-4, LM-P-21	111, 145
Zavestovskaya I.	LM-I-4	82
Zaytsev A.A.	D-I-6	56
Zaytsev K.	TH-I-4, TH-O-5	212, 222
Zelenina A.	D-P-6	71

<i>Name</i>	<i>Number</i>	<i>Page</i>
Zenou M.	LM-O-7	114
Zenov K.	D-O-2	63
Zergioti I.	LS-P-5, S-O-1	179, 201
Zhakhovsky V.	LM-O-17	124
Zhang Hongyu	LM-I-25	104
Zhdanov B.	LS-I-14	164
Zhdanova N.	B-P-11	49
Zheltikov A.	PI-6	11
Zhelyazkova Al.	B-I-4	17
Zhigalina O.	LM-O-11	118
Zhigunov D.M.	B-O-5, D-P-6	35, 71
Zhou Ming	LM-I-25	104
Zhukov V.P.	LM-I-13	92
Ziaie S.	NL-I-3	184
Zimin S.	LM-I-14	93
Zimmer K.	LM-O-2, LM-P-11	109, 135
Zimmermann M.	LM-I-16	95
Zucco M.	S-P-1	205
Zuev D.A.	LM-P-8, LM-P-10, LM-P-12	132, 134, 136
Zuilhof H.	S-O-1	201
Zukauskas A.	LS-I-8	158
Zverev P.G.	LS-I-6	156
Zvyagin A.V.	B-O-1	31